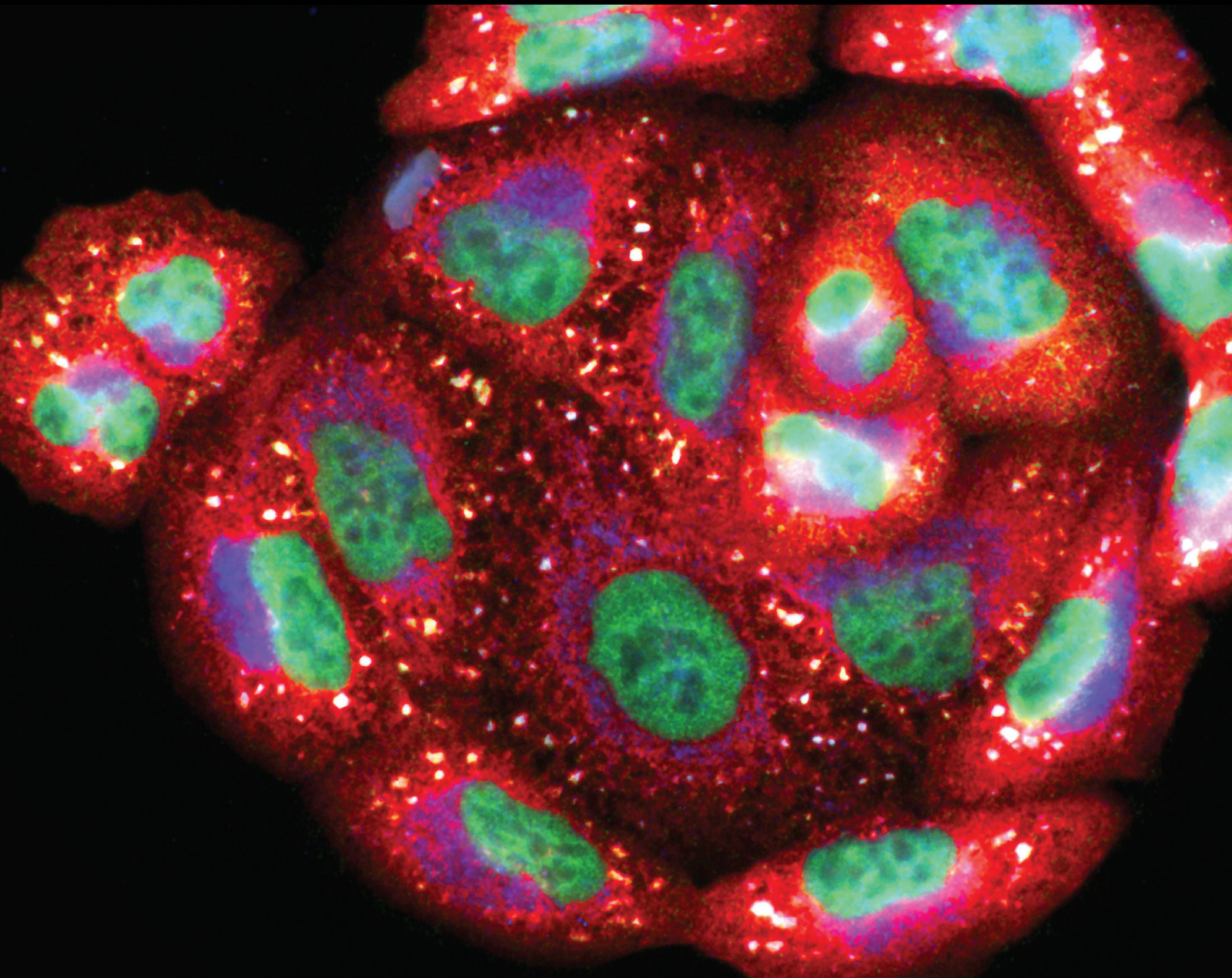


Gaseous Signalling Molecules in Aging and Age-Related Pathologies

Lead Guest Editor: Vitor Fernandes

Guest Editors: Michael De Silva and Andrea Berenyiova





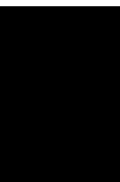
Gaseous Signalling Molecules in Aging and Age-Related Pathologies

Oxidative Medicine and Cellular Longevity

Gaseous Signalling Molecules in Aging and Age-Related Pathologies

Lead Guest Editor: Vitor Fernandes

Guest Editors: Michael De Silva and Andrea
Berenyiova



Copyright © 2022 Hindawi Limited. All rights reserved.

This is a special issue published in "Oxidative Medicine and Cellular Longevity" All articles are open access articles distributed under the Creative Commons Attribution License, which permits unrestricted use, distribution, and reproduction in any medium, provided the original work is properly cited.

Chief Editor

Jeannette Vasquez-Vivar, USA

Associate Editors

Amjad Islam Aqib, Pakistan
Angel Catalá , Argentina
Cinzia Domenicotti , Italy
Janusz Gebicki , Australia
Aldrin V. Gomes , USA
Vladimir Jakovljevic , Serbia
Thomas Kietzmann , Finland
Juan C. Mayo , Spain
Ryuichi Morishita , Japan
Claudia Penna , Italy
Sachchida Nand Rai , India
Paola Rizzo , Italy
Mithun Sinha , USA
Daniele Vergara , Italy
Victor M. Victor , Spain

Academic Editors

Ammar AL-Farga , Saudi Arabia
Mohd Adnan , Saudi Arabia
Ivanov Alexander , Russia
Fabio Altieri , Italy
Daniel Dias Rufino Arcanjo , Brazil
Peter Backx, Canada
Amira Badr , Egypt
Damian Bailey, United Kingdom
Rengasamy Balakrishnan , Republic of Korea
Jiaolin Bao, China
Ji C. Bihl , USA
Hareram Birla, India
Abdelhakim Bouyahya, Morocco
Ralf Braun , Austria
Laura Bravo , Spain
Matt Brody , USA
Amadou Camara , USA
Marcio Carochio , Portugal
Peter Celec , Slovakia
Giselle Cerchiaro , Brazil
Arpita Chatterjee , USA
Shao-Yu Chen , USA
Yujie Chen, China
Deepak Chhangani , USA
Ferdinando Chiaradonna , Italy

Zhao Zhong Chong, USA
Fabio Ciccarone, Italy
Alin Ciobica , Romania
Ana Cipak Gasparovic , Croatia
Giuseppe Cirillo , Italy
Maria R. Ciriolo , Italy
Massimo Collino , Italy
Manuela Corte-Real , Portugal
Manuela Curcio, Italy
Domenico D'Arca , Italy
Francesca Danesi , Italy
Claudio De Lucia , USA
Damião De Sousa , Brazil
Enrico Desideri, Italy
Francesca Diomede , Italy
Raul Dominguez-Perles, Spain
Joël R. Drevet , France
Grégory Durand , France
Alessandra Durazzo , Italy
Javier Egea , Spain
Pablo A. Evelson , Argentina
Mohd Farhan, USA
Ioannis G. Fatouros , Greece
Gianna Ferretti , Italy
Swaran J. S. Flora , India
Maurizio Forte , Italy
Teresa I. Fortoul, Mexico
Anna Fracassi , USA
Rodrigo Franco , USA
Juan Gambini , Spain
Gerardo García-Rivas , Mexico
Husam Ghanim, USA
Jayeeta Ghose , USA
Rajeshwary Ghosh , USA
Lucia Gimeno-Mallench, Spain
Anna M. Giudetti , Italy
Daniela Giustarini , Italy
José Rodrigo Godoy, USA
Saeid Golbidi , Canada
Guohua Gong , China
Tilman Grune, Germany
Solomon Habtemariam , United Kingdom
Eva-Maria Hanschmann , Germany
Md Saquib Hasnain , India
Md Hassan , India







Tim Hofer , Norway
John D. Horowitz, Australia
Silvana Hrelia , Italy
Dragan Hrnčić, Serbia
Zebo Huang , China
Zhao Huang , China
Tarique Hussain , Pakistan
Stephan Immenschuh , Germany
Norsharina Ismail, Malaysia
Franco J. L. , Brazil
Sedat Kacar , USA
Andleeb Khan , Saudi Arabia
Kum Kum Khanna, Australia
Neelam Khaper , Canada
Ramoji Kosuru , USA
Demetrios Kouretas , Greece
Andrey V. Kozlov , Austria
Chan-Yen Kuo, Taiwan
Gaocai Li , China
Guoping Li , USA
Jin-Long Li , China
Qiangqiang Li , China
Xin-Feng Li , China
Jialiang Liang , China
Adam Lightfoot, United Kingdom
Christopher Horst Lillig , Germany
Paloma B. Liton , USA
Ana Lloret , Spain
Lorenzo Loffredo , Italy
Camilo López-Alarcón , Chile
Daniel Lopez-Malo , Spain
Massimo Lucarini , Italy
Hai-Chun Ma, China
Nageswara Madamanchi , USA
Kenneth Maiese , USA
Marco Malaguti , Italy
Steven McAnulty, USA
Antonio Desmond McCarthy , Argentina
Sonia Medina-Escudero , Spain
Pedro Mena , Italy
V́ctor M. Mendoza-Núñez , Mexico
Lidija Milkovic , Croatia
Alexandra Miller, USA
Sara Missaglia , Italy

Premysl Mladenka , Czech Republic
Sandra Moreno , Italy
Trevor A. Mori , Australia
Fabiana Morroni , Italy
Ange Mouithys-Mickalad, Belgium
Iordanis Mourouzis , Greece
Ryoji Nagai , Japan
Amit Kumar Nayak , India
Abderrahim Nemmar , United Arab Emirates
Xing Niu , China
Cristina Nocella, Italy
Susana Novella , Spain
Hassan Obied , Australia
Pál Pacher, USA
Pasquale Pagliaro , Italy
Dilipkumar Pal , India
Valentina Pallottini , Italy
Swapnil Pandey , USA
Mayur Parmar , USA
Vassilis Paschalis , Greece
Keshav Raj Paudel, Australia
Ilaria Peluso , Italy
Tiziana Persichini , Italy
Shazib Pervaiz , Singapore
Abdul Rehman Phull, Republic of Korea
Vincent Pialoux , France
Alessandro Poggi , Italy
Zsolt Radak , Hungary
Dario C. Ramirez , Argentina
Erika Ramos-Tovar , Mexico
Sid D. Ray , USA
Muneeb Rehman , Saudi Arabia
Hamid Reza Rezvani , France
Alessandra Ricelli, Italy
Francisco J. Romero , Spain
Joan Roselló-Catafau, Spain
Subhadeep Roy , India
Josep V. Rubert , The Netherlands
Sumbal Saba , Brazil
Kunihiro Sakuma, Japan
Gabriele Saretzki , United Kingdom
Luciano Saso , Italy
Nadja Schroder , Brazil

Anwen Shao , China
Iman Sherif, Egypt
Salah A Sheweita, Saudi Arabia
Xiaolei Shi, China
Manjari Singh, India
Giulia Sita , Italy
Ramachandran Srinivasan , India
Adrian Sturza , Romania
Kuo-hui Su , United Kingdom
Eisa Tahmasbpour Marzouni , Iran
Hailiang Tang, China
Carla Tatone , Italy
Shane Thomas , Australia
Carlo Gabriele Tocchetti , Italy
Angela Trovato Salinaro, Italy
Rosa Tundis , Italy
Kai Wang , China
Min-qi Wang , China
Natalie Ward , Australia
Grzegorz Wegrzyn, Poland
Philip Wenzel , Germany
Guangzhen Wu , China
Jianbo Xiao , Spain
Qiongming Xu , China
Liang-Jun Yan , USA
Guillermo Zalba , Spain
Jia Zhang , China
Junmin Zhang , China
Junli Zhao , USA
Chen-he Zhou , China
Yong Zhou , China
Mario Zoratti , Italy










Contents

Age- and Hypertension-Related Changes in NOS/NO/sGC-Derived Vasoactive Control of Rat Thoracic Aortae

Andrea Berenyiova , Peter Balis , Michal Kluknavsky , Iveta Bernatova , Sona Cacanyiova , and Angelika Puzserova 











Research Article (13 pages), Article ID 7742509, Volume 2022 (2022)

Gasotransmitters: Potential Therapeutic Molecules of Fibrotic Diseases

Yingqing Chen , Shuo Yuan , Yuying Cao , Guangyao Kong , Feng Jiang , You Li , Qi Wang , Minli Tang , Qinggao Zhang , Qianqian Wang , and Liping Liu 

Review Article (18 pages), Article ID 3206982, Volume 2021 (2021)

Vascular Ageing Features Caused by Selective DNA Damage in Smooth Muscle Cell

Ehsan Ataei Ataabadi , Keivan Golshiri , Janette van der Linden, Martine de Boer, Dirk J. Duncker , Annika Jüttner , René de Vries, Richard Van Veghel , Ingrid van der Pluijm , Sophie Dutheil, Suman Chalgeri, Lei Zhang, Amy Lin, Robert E. Davis , Gretchen L. Snyder , A. H. Jan Danser , and Anton J. M. Roks 




Research Article (13 pages), Article ID 2308317, Volume 2021 (2021)

Gasotransmitter CO Attenuates Bleomycin-Induced Fibroblast Senescence via Induction of Stress Granule Formation

Yingqing Chen , Feng Jiang , Guangyao Kong , Shuo Yuan , Yuying Cao , Qinggao Zhang , Qianqian Wang , and Liping Liu 

Research Article (21 pages), Article ID 9926284, Volume 2021 (2021)

Endothelial Cell-Derived SO₂ Controls Endothelial Cell Inflammation, Smooth Muscle Cell Proliferation, and Collagen Synthesis to Inhibit Hypoxic Pulmonary Vascular Remodelling

Xin Liu, Shangyue Zhang, Xiuli Wang, Yuanyuan Wang, Jingyuan Song, Chufan Sun, Guozhen Chen, Guosheng Yang, Yinghong Tao, Yongyan Hu, Dingfang Bu, Yaqian Huang , Junbao Du , and Hongfang Jin 

Research Article (14 pages), Article ID 5577634, Volume 2021 (2021)

Research Article

Age- and Hypertension-Related Changes in NOS/NO/sGC-Derived Vasoactive Control of Rat Thoracic Aortae

Andrea Berenyiova , **Peter Balis** , **Michal Kluknavsky** , **Iveta Bernatova** ,
Sona Cacanyiova , and **Angelika Puzserova** 

Institute of Normal and Pathological Physiology, Centre of Experimental Medicine Slovak Academy of Sciences, Bratislava 84104, Slovakia

Correspondence should be addressed to Andrea Berenyiova; andrea.berenyiova@savba.sk

Received 2 July 2021; Revised 21 October 2021; Accepted 15 February 2022; Published 9 March 2022

Academic Editor: Colin Murdoch

Copyright © 2022 Andrea Berenyiova et al. This is an open access article distributed under the Creative Commons Attribution License, which permits unrestricted use, distribution, and reproduction in any medium, provided the original work is properly cited.

This study was aimed at examining the role of the NOS/NO/sGC signaling pathway in the vasoactive control of the thoracic aorta (TA) from the early to late ontogenetic stages (7 weeks, 20 weeks, and 52 weeks old) of normotensive Wistar-Kyoto (WKY) rats and spontaneously hypertensive rats (SHRs). Systolic blood pressure (SBP) and heart rate (HR) were significantly increased in SHRs compared to age-matched WKYs, which was associated with left heart ventricle hypertrophy in all age groups of rats. The plasma urea level was increased in 20-week-old and 52-week-old SHRs compared with WKYs without increasing creatinine and uric acid. The total cholesterol levels were lower in 20-week-old and 52-week-old SHRs than in WKYs, but triglycerides were higher in 7-week-old SHRs. The fructosamine level was increased in 52-week-old SHRs compared with age-matched WKYs and unchanged in other age groups. Superoxide production was increased only in 7-week-old SHRs compared to age-matched WKYs. The endothelium-dependent relaxation (EDR) of the TA deteriorated in both rat strains during aging; however, endothelial dysfunction already occurred in 20-week-old SHRs and was even more enhanced in 52-week-old rats. Our results also demonstrated increased activity of NOS in 52-week-old WKYs. Moreover, 7-week-old and 52-week-old WKY rats displayed an enhanced residual EDR after L-NMMA (NOS inhibitor) incubation compared with 20-week-old rats. Our results showed that in 7-week-old SHRs, the residual EDR after L-NMMA incubation was increased compared to that in other age groups. The activity of NOS in the TA was comparable in 7-week-old and 20-week-old SHRs, but it was reduced in 52-week-old SHRs compared to younger SHRs and 52-week-old WKYs. Thus, it seems that, in contrast to SHRs, the NOS/NO system in WKYs is probably able to respond to age-related pathologies to maintain endothelial functions and thus optimal BP levels even in later periods of life.

1. Introduction

Aging and age-related processes have become important issues in recent cardiovascular studies since they significantly deteriorate the quality of life of older populations [1]. There is an obvious correlation between cardiovascular outcomes and aging. Several structural, functional, and molecular changes in the cardiovascular system have been reported in aged individuals. The process of aging involves, among others, an increased production of free radicals and fluid shear stress, endothelial dysfunction, and vascular remodeling. These pathological mechanisms lead to

enhanced vasoconstriction, reduced vasorelaxation, vascular hypertrophy, and rigidity of the vessel wall [2].

Alterations similar to aging were confirmed under conditions of elevated arterial blood pressure (BP)—hypertension. Previous studies using an animal model of arterial hypertension, spontaneously hypertensive rats (SHRs), demonstrated an increased contractile response after stimulation of adrenergic receptors in both conduit and resistant arteries [3] mainly as a consequence of hyperactivity of the sympathetic nervous system [4]. Moreover, morphological studies revealed that along with BP elevation, the arterial wall area increased and was hypertrophied in all parts of the arterial

tree, in the thoracic aorta (TA), carotid artery, and iliac artery in adult SHR [5].

Endothelial dysfunction is a common hallmark of age- and hypertension-related pathologies. This is a term that covers the imbalance between the vasoconstrictor and vasorelaxant agents produced by endothelial cells [6]; moreover, it is associated with reduction of their anticoagulant and anti-thrombotic properties, acceleration of vascular growth, and remodeling [7]. Nitric oxide (NO) is a crucial molecule of the arterial wall with a significant vasorelaxant effect. It has also been shown that NO represents the dominant mediator of endothelium-dependent vasorelaxation in TA [8]. Endothelial NO rapidly diffuses to vascular smooth muscle cells (VSMCs) and initiates the production of cyclic guanosine monophosphate (cGMP) due to the activity of soluble guanylate cyclase (sGC). Recently, sGC has proven to be a key enzyme in the treatment of various cardiovascular pathologies since sGC stimulators and activators are in preclinical and clinical development for the treatment of pulmonary hypertension, which has been reported as a new and promising milestone in the field of NO/sGC/cGMP pharmacology [9].

Our previously performed studies related to the participation of endogenous NO in the vasoregulatory mechanism in the early stage of SHR ontogenesis revealed that the NO-dependent vasorelaxant component of the TA in 4-week-old SHRs was enhanced compared with that in age-matched normotensive controls. We also speculated that TA could be endowed with a unique predisposition to decreased contractility and strengthened endothelium-regulated vasorelaxant mechanisms that serve as adaptive mechanisms during the fully developed phase of hypertension [10]. On the other hand, in 7-week-old SHRs, we showed reduced endothelium-dependent relaxation associated with a reduction in NO-independent mechanisms in femoral arteries accompanied by increased systolic BP. However, the contribution of NO to vasorelaxation was significant and comparable to that in normotensive rats [11]. In young adult SHRs (18-week-old), we found reduced maximal endothelium-dependent vasorelaxation and NO synthase (NOS) activity in the aorta compared with 4-week-old SHRs [12]. Similar findings of NOS activity were seen in 22-week-old SHR aortae compared with 7-week-old SHRs [10].

Based on this, it seems that the endogenous NOS/NO/sGC system and its involvement in the regulation of arterial tone are highly influenced by age. Therefore, the main aim of this study was to investigate the importance of NO and its participation in the vasomotor control of TA during aging and BP increase. The paper may offer a complex overview of the position of NO in endothelium-derived vasorelaxation and pathophysiology of essential hypertension focusing on three different age groups: young juvenile (7-week-old), young adult (20-week-old), and old (52-week-old) normotensive Wistar-Kyoto (WKY) rats and SHRs. In addition, we evaluated the levels of selected plasma parameters that could affect the function of vessels and superoxide production in TA as an important scavenger of vascular NO. We hypothesized that the reduced NO synthesis and/or bioavailability with altered oxidative status would produce reduced

endothelium-dependent vasorelaxation and BP increases in the course of aging.

2. Materials and Methods

2.1. Guide for the Use and Care of Laboratory Animals. Procedures were performed in accordance with institutional guidelines and were approved by the State Veterinary and Food Administration of the Slovak Republic (decision no. Ro-3095/14-221 and decision no. Ro-1087/17-221) and by the Ethics Committee (project code EK/vekhyp/2014, approved 24 June 2014, and EK/1/17, approved 6 February 2017) according to the European Convention for the Protection of Vertebrate Animals Used for Experimental and Other Scientific Purposes, Directive 2010/63/EU of the European Parliament. All rats used in the study were born in an accredited breeding establishment of the Institute of Normal and Pathological Physiology, Centre of Experimental Medicine Slovak Academy of Sciences (INPP CEM SAS), and were housed in groups of 2 to 4 animals, each strain separately, under a 12 h light-12 h dark cycle (06:00–18:00 light phase), at a constant humidity (45–60%) and temperature (22–24°C), with free access to standard laboratory rat chow and drinking water. INPP CEM SAS provided veterinary care. 7-week-old (young juvenile rats), 20-week-old (young adult rats), and 52-week-old (old rats) males of normotensive Wistar-Kyoto (WKY, sublines WKY/NHsd, HARLAN UK) and spontaneously hypertensive rats (SHR, sublines SHR/NHsd, HARLAN UK) were included in the present study. Every phenotype was divided into three groups: 7-week-old (WKY-7, $n = 10$; SHR-7, $n = 11$), 20-week-old (WKY-20, $n = 9$; SHR-20, $n = 10$), and 52-week-old (WKY-52, $n = 9$; SHR-52, $n = 14$). The rats were killed by decapitation after brief CO₂ anesthesia.

2.2. General Biometric and Cardiovascular Parameters. The systolic blood pressure (SBP) and heart rate (HR) were measured in prewarmed rats by noninvasive plethysmography on rat tail arteries before the beginning of the in vitro study (except handling); the body weight (BW) of the animal was also measured [13]. The weight of the left heart ventricle (free wall) (LV) and the length of the tibia (TL) were measured to evaluate organ hypertrophy [14, 15].

2.3. Basic Plasma Parameters. Trunk blood was collected just after decapitation in heparinized test tubes, and blood was immediately centrifuged (850 g, 10 min, 4°C). Plasma samples were frozen in aliquots for biochemical determinations and stored at -80°C until analysis. The basic levels of urea, creatinine, uric acid, total cholesterol, triglycerides (TAG), and fructosamines were commercially determined in the accredited veterinary laboratory Laboklin GMBH (Bratislava, Slovakia) using standard laboratory methods.

2.4. Measurement of Superoxide Production in Aortic Tissue. The assay was performed as described previously [16] with some modifications. The aortic rings were cut (10–15 mg), cleaned of connective tissue, and placed into cold modified physiological salt solution (PSS, in mmol/L: NaCl 118.99, KCl 4.69, NaHCO₃ 25, MgSO₄·7H₂O 1.17, KH₂PO₄ 1.18,

CaCl₂·2H₂O 2.5, Na₂EDTA 0.03, and glucose 5.5, pH 7.4). Lucigenin (50 μmol/L), as well as tissue samples alone, was added to PSS bubbled with pneumoxide (5% CO₂ and 95% O₂) at pH 7.4 and 37°C and preincubated in the dark for 20 min. After preincubation, either background chemiluminescence or chemiluminescence produced by the aortic rings was measured for 6 min using a TriCarb 2910TR liquid scintillation analyzer (PerkinElmer, Waltham, USA). Background counts were subtracted from values obtained from the samples. The results are expressed as counts per minute per mg of tissue (cpm/mg).

2.5. Functional Study. The isolated TA was cleaned of connective tissue using a microscope and cut into 5 mm length rings. The rings were vertically fixed between 2 stainless wire triangles and immersed in a 20 mL incubation organ bath with PSS. This solution was oxygenated with a mixture of 95% O₂ and 5% CO₂ and kept at 37°C. The upper triangles were connected to sensors of isometric tension (FSG-01, MDE, Budapest, Hungary), the changes in tension were registered by an AD converter NI USB-6221 (National Instruments, Austin, USA, MDE, Budapest, Hungary), and the changes in isometric tension were registered by using DEWEsoft (Dewetron, Prague, Czech Republic) and SPEL Advanced Kymograph (MDE, Budapest, Hungary) software. A resting tension of 1 g was applied to each ring and maintained throughout a 45- to 60 min equilibration period until stress relaxation no longer occurred.

The relaxant responses were followed on rings precontracted with phenylephrine (Phe; 10⁻⁶ mol/L) after achieving a stable plateau of contraction. The isolated TA rings were then exposed to cumulative concentrations of acetylcholine (ACh; 10⁻⁹–3×10⁻⁵ mol/L). The rate of relaxation was expressed as a percentage of the Phe-induced contraction.

The participation of the endogenous NO system in the vasomotor responses of TA was followed before and 30 minutes after pretreatment with a nonspecific inhibitor of NOS, N^G-methyl-L-arginine acetate salt (L-NMMA; 10⁻⁴ mol/L), to block basal and receptor-induced endogenous NO production. To confirm the involvement of the soluble guanylate cyclase (sGC) signaling pathway in ACh-induced relaxation, a sGC inhibitor, 1H-[1,2,4]oxadiazole[4,3-a]quinoxalin-1-one (ODQ, 10⁻⁵ mol/L), was applied 30 min before the addition of the contractile agonist.

All drugs were dissolved in distilled water, except ODQ, which was dissolved in dimethylsulfoxide. All concentrations are expressed as the final concentrations in the organ chamber.

The effect of the age and hypertension on the endothelium-dependent relaxation (EDR) is expressed separately using the same concentration-dependent ACh curves from all animals in each group, before and after application of inhibitors, respectively.

2.6. Nitric Oxide Synthase Activity. The aortae were carefully dissected, and connective tissue was removed. NOS activity was determined in 20% fresh tissue homogenates (*w:v*) as described in detail previously [17]. Briefly, the aortic tissue was immersed in ice-cold buffer (0.05 mol/L Tris-HCl,

pH 7.4) containing 1% protease inhibitor cocktail. After homogenization at 4°C (Ultra-Turrax homogenizer) and centrifugation of homogenates (4°C, 10 min, 3000 g), NOS activity was determined in the supernatants by the conversion of [3H]-L-arginine (specific activity 5 GBq/mmol, ~100,000 dpm, ARC, St. Louis, USA) to [3H]-L-citrulline in the presence of 50 mmol/L Tris/HCl (pH 7.4), containing NOS cofactors in a total volume of 100 μL. The reaction was stopped after 20 min of incubation by adding 1 mL of ice-cold stop solution containing 20 mmol/L 4-(2-hydroxyethyl)-1-piperazineethanesulfonic acid (pH 5.5) and NOS inhibitors. One milliliter of the final mixture was applied to Dowex 50 WX-8 columns (Na⁺-form), and [3H]-L-citrulline was eluted by adding deionized water. The results were determined by liquid scintillation counting (TriCarb 2910TR, PerkinElmer, Waltham, USA). NOS activity was expressed as pkat per gram of protein. The protein concentration was determined using the Lowry method [18].

2.7. Statistical Analysis. The data were expressed as means ± SEM. For the statistical evaluation of differences between groups, a two- and three-way analysis of variance (ANOVA) with the Bonferroni post hoc test was used. The differences between means were considered significant at *p* < 0.05. OriginPro2019b (OriginLab, Northampton, USA), GraphPad Prism 5.0 (GraphPad Software; San Diego, USA), and Statistica 13.5 (StatSoft; Hamburg, Germany) were used for the statistical analyses.

2.8. Drugs. All drugs were purchased from Sigma-Aldrich (Bratislava, Slovakia) unless otherwise stated.

3. Results

3.1. General Biometric and Cardiovascular Parameters. Table 1 summarizes the differences in SBP and other basic biometric and cardiovascular parameters among the experimental groups. The BW of the animals increased with age in both WKYs and SHR; however, the 52-week-old SHR had a significantly lower BW than the age-matched WKYs. On the other hand, SHR revealed an elevated SBP compared to WKYs in all ontogenetic stages. In SHR, the SBP was comparable between the young adult and old rats, but it was significantly higher compared to young juvenile 7-week-old animals. There was also an age-dependent increase in SBP in WKY rats; in 52-week-old rats, we observed significantly higher SBP than the other age groups of this strain. The HR of SHR was higher than that of WKYs in all age groups, but there were no changes in this parameter during ontogenesis in either SHR or WKYs. By age, the weight of LV was increased in both strains; moreover, in SHR, the weight of LV was higher than that in age-matched WKY rats, except in the 7-week groups. An age-dependent increase was also observed in TL in both WKYs and SHR. The length of the tibia was decreased in 20-week-old SHR compared to WKYs of the same age; in 52-week-old rats, there were no differences between the strains in TL. Generally, in SHR, the LV/BW ratio and LV/TL were increased compared to those in WKYs.

TABLE 1: General biometric and cardiovascular parameters.

	WKY-7	SHR-7	WKY-20	SHR-20	WKY-52	SHR-52
BW (g)	144 ± 4	145 ± 5	359 ± 5 ⁺	350 ± 6 ⁺	447 ± 8 ^{+x}	426 ± 3 ^{+xx}
SBP (mmHg)	117 ± 1	160 ± 3 [*]	119 ± 3	204 ± 6 ^{**}	126 ± 1 ^{+x}	198 ± 3 ^{**}
HR (bpm)	479 ± 14	547 ± 9 [*]	463 ± 16	561 ± 13 [*]	483 ± 12	559 ± 17 [*]
LV (mg)	265 ± 11	308 ± 15	596 ± 16 ⁺	745 ± 25 ^{**}	691 ± 16 ^{+x}	883 ± 19 ^{+xx}
TL (mm)	25.88 ± 0.24	25.81 ± 0.23	37.06 ± 0.16 ⁺	36.46 ± 0.14 ^{**}	39.44 ± 0.20 ^{+x}	39.06 ± 0.09 ^{+xx}
LV/TL (mg/mm)	10.21 ± 0.39	11.91 ± 0.50 [*]	16.09 ± 0.45 ⁺	20.42 ± 0.62 ^{**}	17.52 ± 0.38 ^{+x}	22.60 ± 0.50 ^{+xx}
LV/BW (mg/g)	1.84 ± 0.08	2.08 ± 0.08 [*]	1.66 ± 0.05	2.13 ± 0.07 [*]	1.55 ± 0.05 ⁺	2.07 ± 0.05 [*]

BW: body weight; SBP: systolic blood pressure; HR: heart rate; LV: weight of the left heart ventricle; TL: tibia length; LV/TL: ratio of weight of the left heart ventricle to tibia length; LV/BW: ratio of weight of the left heart ventricle to body weight; WKY-7, WKY-20, and WKY-52: 7-week-old, 20-week-old, and 52-week-old Wistar-Kyoto rats; SHR-7, SHR-20, and SHR-52: 7-week-old, 20-week-old, and 52-week-old spontaneously hypertensive rats. The results are presented as the mean ± SEM of $n=9-14$ rats, and differences between groups were analyzed by two-way analysis of variance (ANOVA) with the Bonferroni post hoc test on ranks. ^{*} $p < 0.05$ vs. WKY at the same age (WKY-7 vs. SHR-7, WKY-20 vs. SHR-20, and WKY-52 vs. SHR-52), ⁺ $p < 0.05$ vs. 7-week group of the same phenotype (WKY-20 vs. WKY-7, SHR-20 vs. SHR-7, WKY-52 vs. WKY-7, and SHR-52 vs. SHR-7), ^x $p < 0.05$ vs. 20-week group of the same phenotype (WKY-52 vs. WKY-20 and SHR-52 vs. SHR-20).

3.2. Selected Plasma Parameters. In WKY rats, the highest urea level was measured in 20-week-old rats, which decreased with age. The plasma levels of creatinine were similarly increased from the 20th week of age, and there was a significant reduction in uric acid in 52-week-old WKY rats compared with 20-week-old rats. The total cholesterol in plasma was increased only in 52-week-old WKY rats, and the levels of fructosamines were also increased in young adult and old normotensive rats compared to young juvenile rats. In SHRs, the plasma level of urea was increased in 20-week-old rats compared to young juveniles, and it was reduced in 52-week-old rats compared with young adults but not with young juvenile rats. Creatinine in plasma increased with age, and uric acid was reduced in 20-week-old and 52-week-old SHRs. The results demonstrated significantly reduced plasma levels of total cholesterol and TAG in young adult and old SHRs, and the levels of fructosamines increased with the age of the animals (Figure 1).

Our results revealed a significantly increased urea level in 20-week-old and 52-week-old SHRs compared with age-matched WKYs; on the other hand, there were no differences between the strains in terms of plasma levels of creatinine and uric acid (Figure 1). Moreover, the levels of total cholesterol were significantly lower in 20-week-old and 52-week-old SHRs than in WKYs; however, we recorded an increased TAG level in 7-week-old SHRs. The fructosamine level was increased in 52-week-old SHRs compared with age-matched WKYs and unchanged in other age groups.

3.3. Superoxide Production in the Aortic Tissue. While the production of superoxide in WKY rats was unchanged by age, in SHRs, the superoxide levels were decreased in 20- and 52-week-old rats. Superoxide production was increased in 7-week-old SHRs compared to age-matched WKYs, and there was no significant difference in the other age groups (Figure 2).

3.4. Vasoactive Responses of Isolated Aortic Rings

3.4.1. Age-Related Differences in Endothelium-Dependent Vasorelaxation in WKYs and SHRs. The EDR amplitude was significantly age-dependent in both strains (WKY: $F_{(2,268)} = 149.77$, $p < 0.0001$, SHR: $F_{(2,288)} = 449.56$, $p < 0.0001$). The EDR was comparable between the 7-week and 20-week WKYs. In 52-week-old WKYs, the EDR was significantly reduced compared to the other age groups (Figure 3(a)). On the other hand, reduced vasorelaxation of the TA in SHRs was observed in 20-week-old rats (compared to 7-week-old SHRs), which was more pronounced in 52-week-old SHRs than in both 7-week-old and 20-week-old SHRs (Figure 3(b)).

3.4.2. Hypertension-Related Differences in Endothelium-Dependent Vasorelaxation between Age-Matched WKYs and SHRs. In 7-week-old SHRs, the EDR was significantly enhanced ($F_{(1,218)} = 52.37$, $p < 0.0001$; Figure 4(a)) compared with that in the WKY. However, a deterioration of the vasorelaxant ability of the TA in SHRs already appeared in 20-week-old rats ($F_{(1,138)} = 23.69$, $p < 0.0001$; Figure 4(b)), and we also observed significant endothelial dysfunction in 52-week-old SHRs ($F_{(1,198)} = 18.95$, $p < 0.0001$; Figure 4(c)).

3.4.3. Age-Related Changes in NO Synthase and Soluble Guanylate Cyclase Participation in Endothelium-Dependent Vasorelaxation in WKYs and SHRs. To test the participation of the NO/NOS and sGC systems in EDR, we incubated the aortic rings with L-NMMA and ODQ. In normotensive rats, acute NOS inhibition reduced the EDR to the greatest extent in 20-week-old rats compared to 7-week-old and 52-week-old rats; however, there were no differences in the EDR after L-NMMA incubation between young (7-week-old) and old (52-week-old) rats ($F_{(2,138)} = 77.69$, $p < 0.0001$; Figure 5(a)). The inhibition of sGC significantly blocked the EDR, similarly in every age group (Figure 5(b)). Our results demonstrated that the participation of the NO/NOS system in the EDR was affected by the age of SHRs. While

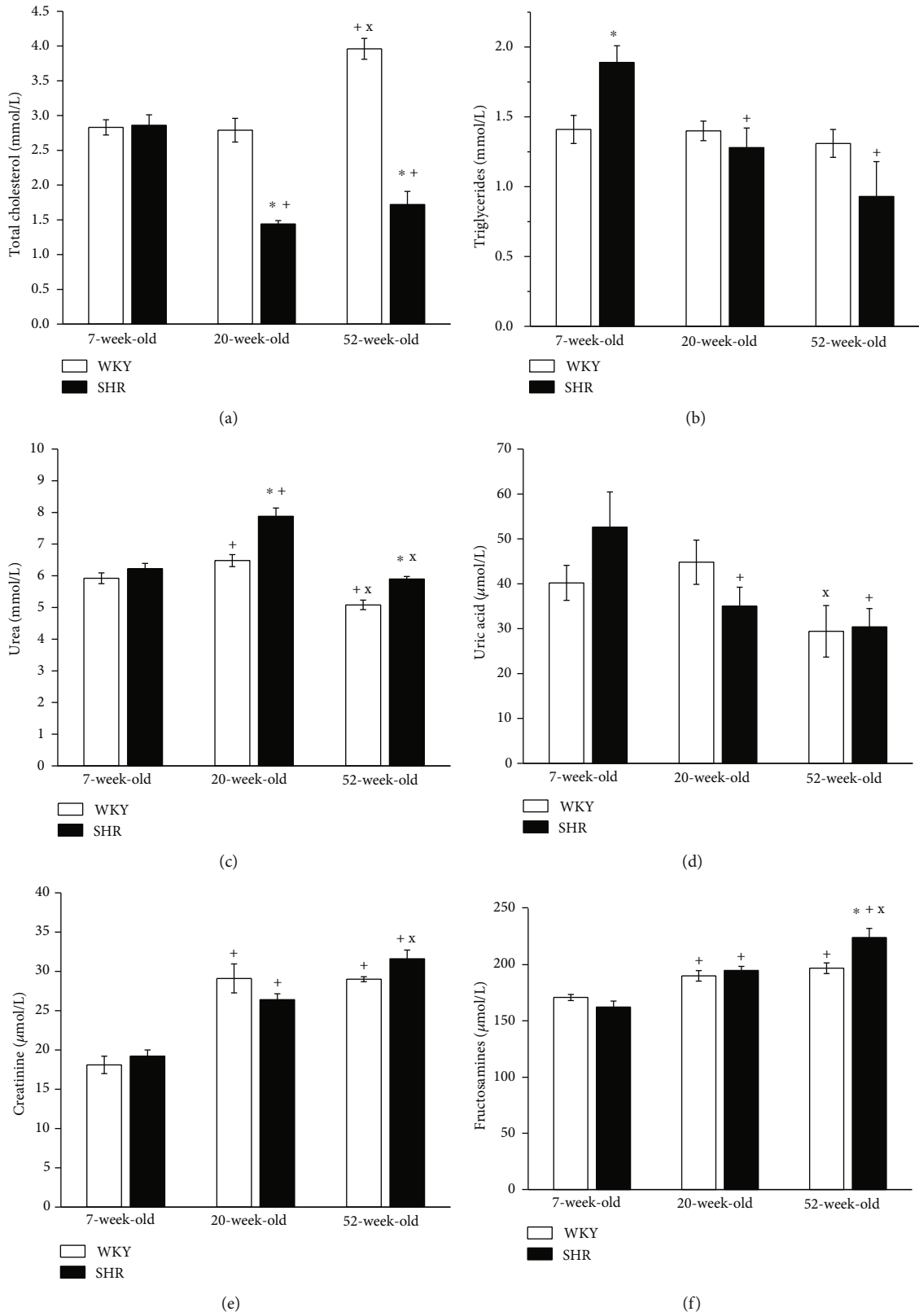


FIGURE 1: The effect of the age and phenotype on selected plasma parameters. WKY: Wistar-Kyoto rats; SHR: spontaneously hypertensive rats. The results are presented as the mean \pm SEM of $n = 5-10$ rats, and differences between groups were analyzed by two-way analysis of variance (ANOVA) with the Bonferroni post hoc test on ranks. * $p < 0.05$ vs. WKY at the same age (WKY-7 vs. SHR-7, WKY-20 vs. SHR-20, and WKY-52 vs. SHR-52), + $p < 0.05$ vs. 7-week group of the same phenotype (WKY-20 vs. WKY-7, SHR-20 vs. SHR-7, WKY-52 vs. WKY-7, and SHR-52 vs. SHR-7), x $p < 0.05$ vs. 20-week group of the same phenotype (WKY-52 vs. WKY-20 and SHR-52 vs. SHR-20).

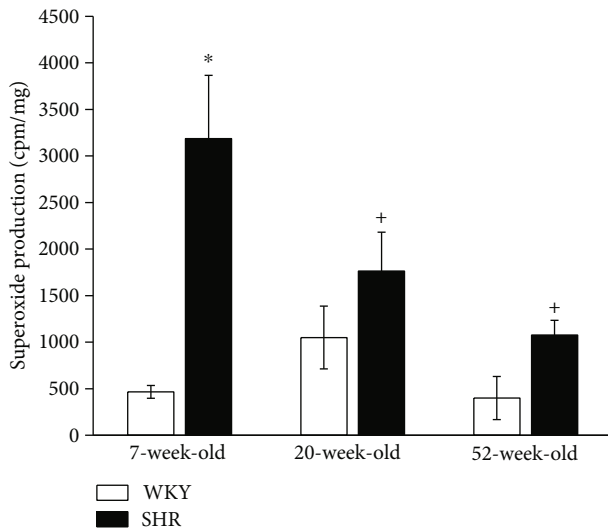


FIGURE 2: The effect of the age and phenotype on the production of superoxide in the aorta. WKY: Wistar-Kyoto rats; SHR: spontaneously hypertensive rats. The results are presented as the mean \pm SEM of $n = 5-9$ rats, and differences between groups were analyzed by two-way analysis of variance (ANOVA) with the Bonferroni post hoc test on ranks. * $p < 0.05$ vs. WKY at the same age (WKY-7 vs. SHR-7), + $p < 0.05$ vs. 7-week group of the same phenotype (SHR-20 vs. SHR-7 and SHR-52 vs. SHR-7).

in young adults and old SHRs, L-NMMA incubation significantly inhibited the EDR, in young juvenile rats, we observed a significant residual EDR despite NOS inhibition ($F_{(2,148)} = 114.62$, $p < 0.0001$; Figure 5(c)). Incubation with ODQ significantly inhibited the EDR regardless of age (Figure 5(d)).

3.4.4. Hypertension-Related Differences in NO Synthase and Soluble Guanylate Cyclase Participation in Endothelium-Dependent Vasorelaxation between Age-Matched WKYs and SHRs. We observed a relatively well-preserved EDR in 7-week-old rats after L-NMMA incubation in both strains; however, in SHRs, this residual relaxation was significantly larger than in age-matched WKYs (phenotype: $F_{(1,228)} = 57.28$, $p = 0.0001$; inhibition: $F_{(1,228)} = 1934.32$, $p < 0.0001$; concentration \times phenotype \times inhibition: $F_{(9,228)} = 3.26$, $p = 0.001$; Figure 6(a)). Although endothelial dysfunction appeared in 20-week-old rats, the effect of acute NOS inhibition on the EDR was comparable between the two phenotypes (Figure 6(b)). In 52-week-old rats, there was a significant effect of the phenotype \times inhibition interaction on the EDR ($F_{(1,118)} = 6.79$, $p = 0.01$); in old SHRs, the residual EDR after acute L-NMMA application was smaller than that in WKYs (Figure 6(c)). Our results demonstrated that sGC is significantly involved in the EDR regardless of the phenotype and age (Figures 7(a)–7(c)).

3.4.5. Nitric Oxide Synthase Activity. The activity of NOS in the aorta was comparable between the 7-week-old and 20-week-old WKY rats, but it was significantly increased in 52-week-old normotensive rats. On the other hand, in SHRs,

NOS activity was decreased in 52-week-old rats compared with the other age groups. In 7-week-old and 20-week-old SHRs, NOS activity was significantly increased compared with that in WKYs; however, in 52-week-old rats, reduced NOS activity was observed (Figure 8).

4. Discussion

The present study provides an overview of the vasoactive manifestation of the NOS/NO/sGC signaling pathway in the TA from the early to late ontogenetic stages of normotensive WKYs and SHRs. Moreover, the effect of aging and increased blood pressure on selected plasma parameters and superoxide production in these rat strains was investigated. The main limitation of the present study is the lack of the morphological confirmation of the physiological/biochemical analyses. There is clear evidence that the structural remodeling of the arterial wall significantly modifies the vasoactive properties of the vessels, including their vasorelaxant abilities [12], which has to be kept in mind.

SHRs are a widely used experimental model of human arterial hypertension. According to the literature, BP in SHRs starts to increase from 6 weeks of age, and the continual increase in SBP stops at approximately 36 weeks of age [19]. Our results are in agreement with these data, since we observed a significantly increased SBP in all investigated age groups of SHRs compared with age-matched WKYs; nevertheless, the SBP values were comparable in 20- and 52-week-old SHRs. The increased SBP in SHRs was also associated with increased HR and left heart ventricle hypertrophy in all age groups investigated. The main morphological alterations in SHRs, such as changes in the heart and arterial wall trophicity, start from approximately the 5th week of life. Our previous morphological analysis revealed hypotrophy of the TA wall in 4-week-old SHRs compared to Wistar rats. On the other hand, in adulthood, together with a rapid BP increase, the TA was hypertrophied compared to normotensive rats [12].

In SHRs, the total cholesterol and TAG levels decreased with age; moreover, in 20- and 52-week-old SHRs, the level of total cholesterol was significantly lower than that in age-matched WKYs. In SHRs, an enhanced lipolysis has been suggested as a result of increased sympathetic outflow; moreover, an increased secretion of cholesterol combined with deficiencies in enteric capture and molecular transport of cholesterol was also demonstrated [20, 21]. In addition, it has been shown that the levels of cholesterol-related steroid hormones, such as corticosterone, were elevated already in 7-week-old female SHRs compared to age-matched WKYs, and in 10-week-old SHRs, the serum levels of progesterone, corticosterone, and cortisol were significantly elevated compared to those in 5-week-old SHRs and 10-week-old WKYs [16, 22], which may also contribute to the reduction in total cholesterol in our experimental group.

Indeed, it is known that a high plasmatic uric acid level is associated with an increased risk of cardiovascular diseases (CVDs), and endothelial dysfunction has been suggested as a potential mechanism involved in hyperuricemia-induced CVDs. In this study, we did not find increased uric acid

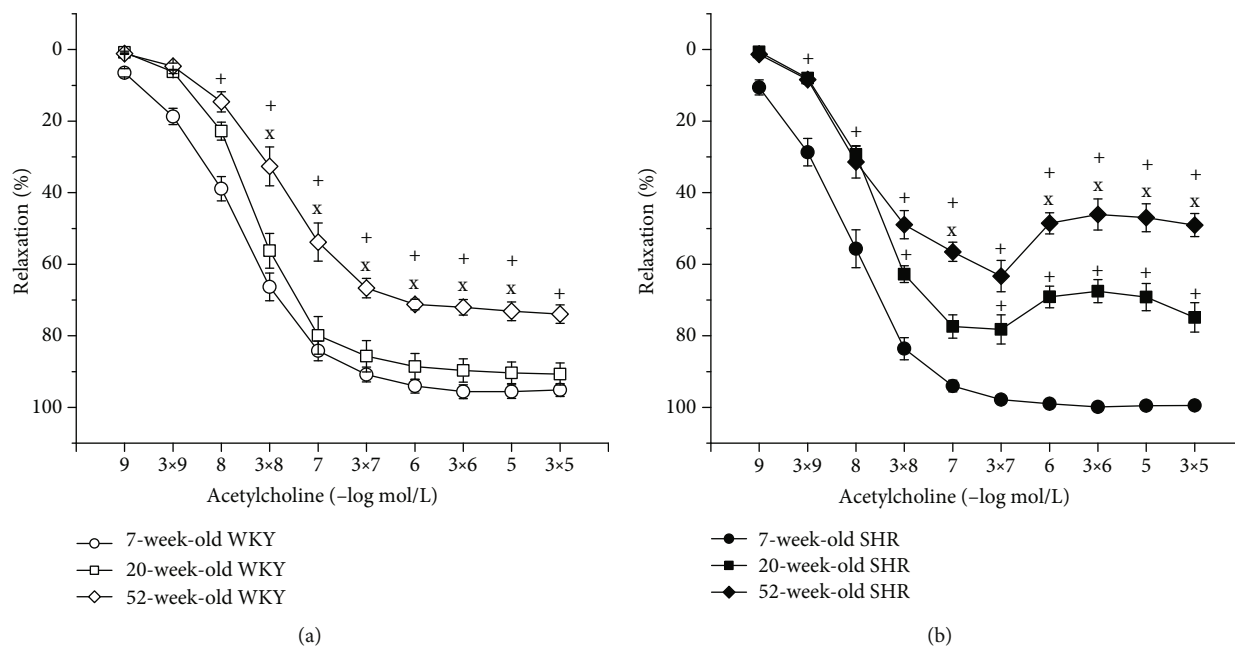


FIGURE 3: The effect of the age on the endothelium-dependent vasorelaxation of the thoracic aorta in Wistar-Kyoto (WKY) (a) and spontaneously hypertensive rats (SHR) (b). The results are presented as the mean \pm SEM of $n=8-10$ rats, and differences between groups were analyzed by two-way analysis of variance (ANOVA) with the Bonferroni post hoc test on ranks. $^+p < 0.05$ vs. 7-week-old rats, $^x p < 0.05$ vs. 20-week-old rats.

levels in SHRs compared to age-matched WKYs. In our previous study, acute exposure of resistant mesenteric arteries, femoral arteries, and aortae isolated from aged WKY rats to a high concentration of uric acid did not provoke changes in endothelial function in these arteries [23]. We observed a decreasing uric acid concentration and EDR with age. Thus, the role of hyperuricemia in endothelial dysfunction in aged rats is not supported by our data.

Fructosamine concentration is often used as a marker of carbonyl stress. In our recent study, we reported that the plasma concentration of advanced glycation end-products (AGEs) was stably decreased in 20- and 52-week-old WKYs compared to 7-week-old WKYs; however, in SHRs, it was decreased only in 20-week-old SHRs, and there was no difference between the strains. We also reported that fructosamine concentrations were not significantly different between these individual age groups when expressed in molar concentration to gram of proteins [24]. On the other hand, we found a decreased superoxide production with age in SHRs, while in WKYs, superoxide production was comparable between the age groups. We surprisingly recorded significantly enhanced superoxide production only in young juvenile SHRs. Gomes et al. [25] reported increased H_2O_2 production in the renal cortex, although no differences were detected in urinary lipid peroxidation in 12-week-old SHRs. This finding was associated with an upregulation of NADPH oxidase and downregulation of antioxidant superoxide dismutase (SOD) 1 and SOD3 enzymes. However, 48-week-old WKYs and SHRs displayed comparable oxidant and antioxidant profiles. The authors suggested that this conflict with the current view that hypertension is a state of oxidative stress might arise from the fact that normotensive WKY

developed obesity with aging, which could operate as a confounding factor of oxidative stress. In agreement, in our study, 52-week-old SHRs had a significantly lower BW (and comparable TL) than age-matched WKYs.

In the other part of our experiment, we examined the impact of age and hypertension on the EDR of TA. We incubated the aortic rings with a nonselective NOS inhibitor (L-NMMA) to assess the participation of NO in EDR during aging. The degree of EDR inhibition after L-NMMA is in agreement with the degree of NO participation in EDR; in general, the more enhanced inhibition is, the more significant NO participation. The vasorelaxant abilities of the TA deteriorated in both rat strains during aging; however, endothelial dysfunction already occurred in 20-week-old SHRs and was even more enhanced in 52-week-old rats. Similar results were reported by Matz et al. [26] in Wistar rats, who demonstrated an unchanged EDR between 12- to 14-old and 32-week-old normotensive rats, but a significant reduction was reported at 70-100 weeks of age. They also found increased endothelial NOS protein expression and a significant involvement of endothelial NO in the EDR, since N^G -nitro-L-arginine (L-NA) abolished the response to ACh in the aorta. Our results also demonstrated a significantly increased total activity of NOS in 52-week-old WKYs compared to the other age groups. The increased NOS activity and the unchanged superoxide production during the aging indicated a high NO bioavailability in old WKY which was not, however, manifested in the vasoactive responses of TA, since we observed a reduced EDR in these rats. We assume that this fact could be associated with the prevalence of other negative impacts such as enhanced production of contractile agents, advanced structural remodeling that

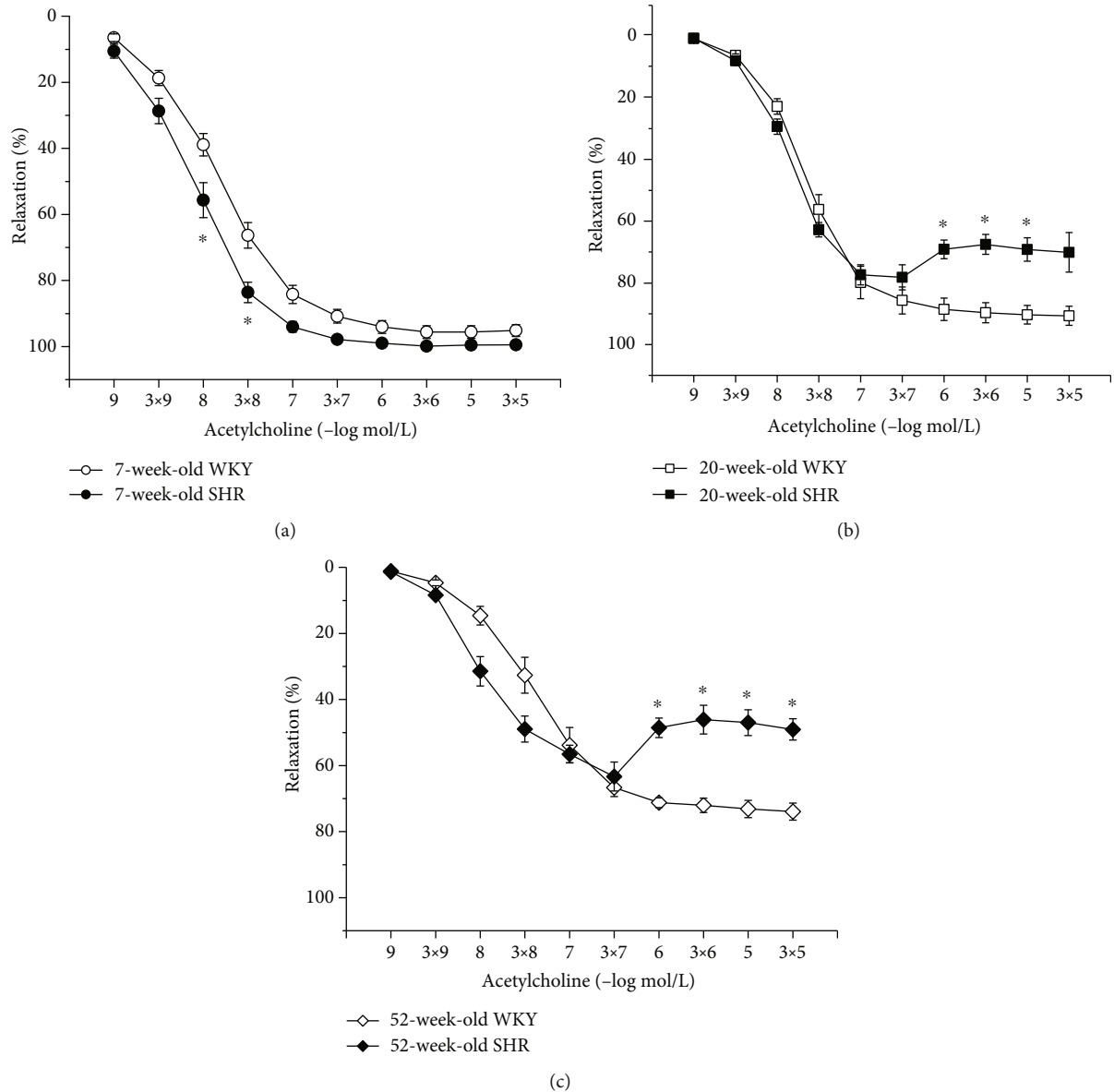


FIGURE 4: The effect of hypertension on the endothelium-dependent vasorelaxation of the thoracic aorta in 7-week-old (a), 20-week-old (b), and 52-week-old (c) rats. WKY: Wistar-Kyoto rats; SHR: spontaneously hypertensive rats. The results are presented as the mean \pm SEM of $n = 8-10$ rats, and differences between groups were analyzed by two-way analysis of variance (ANOVA) with the Bonferroni post hoc test on ranks. * $p < 0.05$ vs. WKY.

could eliminate the vasoactive manifestation of the preserved NO sources. Moreover, we showed that 7-week-old and 52-week-old WKY rats displayed an enhanced residual EDR after L-NMMA incubation compared with 20-week-old rats. Our results suggested that the greatest L-NMMA-sensitive component of EDR was present in 20-week-old WKY rats and the smallest in 52-week-old WKY rats. Incomplete inhibition of EDR after L-NMMA could be caused by a concentration of L-NMMA that only partly inhibited NOS and therefore was not maximally effective in reducing the total NO-dependent vasorelaxation or due to compensatory increased NO-independent vasodilator mechanisms [27]. On the other hand, the inhibition of sGC significantly blocked the EDR in all age groups, indicating important sGC involvement in these vasoactive

responses. Recent studies implicated nitroxyl (HNO) as another possible activator of sGC whose action is independent of NO formation [28, 29]. Andrews et al. [30] demonstrated that HNO is produced endogenously and serves as an endothelium-derived relaxing and hyperpolarizing factor in both mouse and rat isolated small mesenteric resistance-like arteries. However, information about the age-related changes in HNO production and its vasoactive properties is limited. According to this, we assume that aging in the WKY could probably be associated with enhanced NO production (increased NOS activity in the old WKY) and bioavailability (comparable superoxide concentrations among age groups); indeed, the smallest L-NMMA-sensitive component of EDR was confirmed in aged WKY; in order to prevent the additional deterioration of EDR and SBP increase.

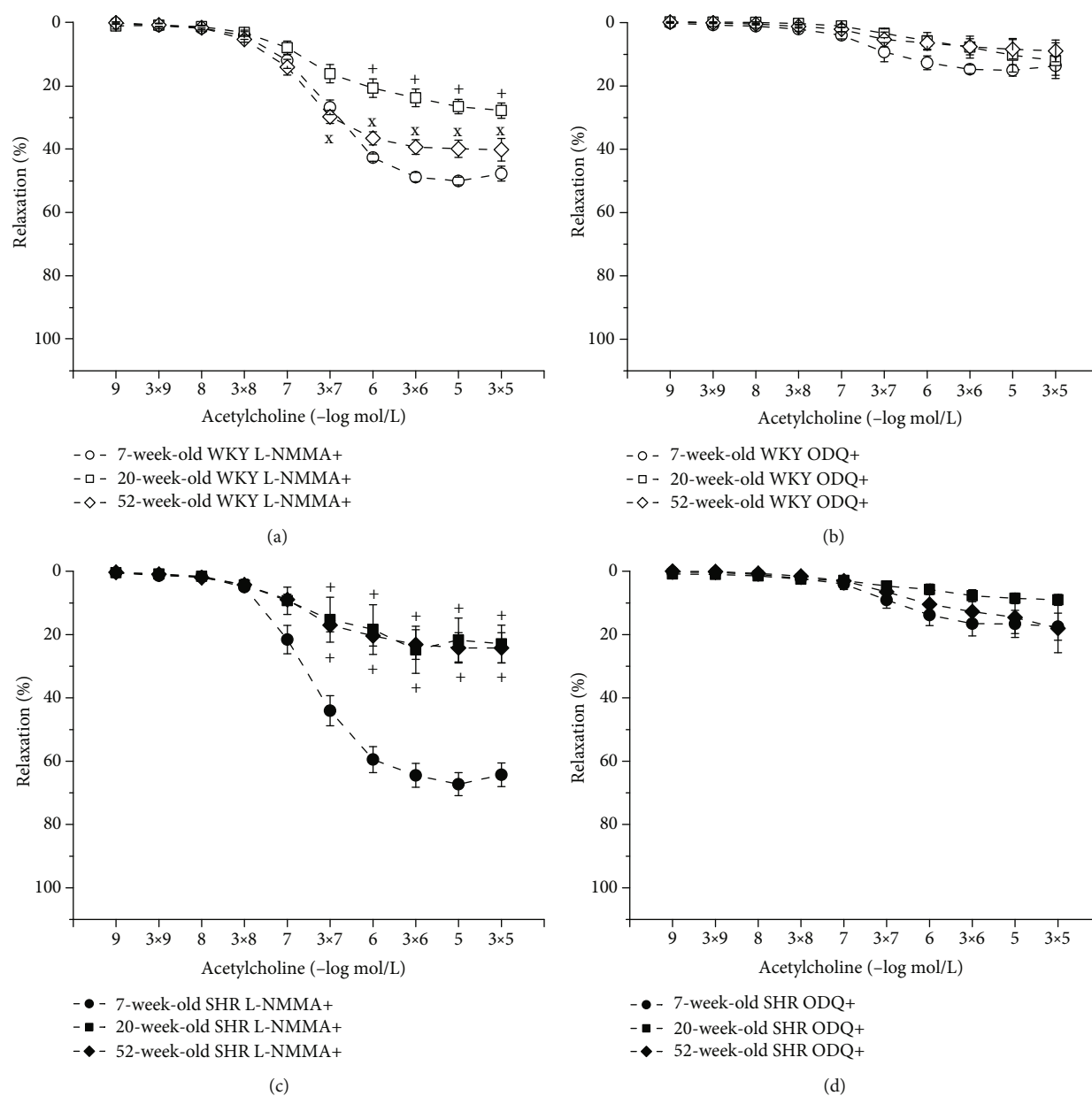


FIGURE 5: The effect of the age on participation of NO synthase (a, c) and soluble guanylate cyclase (b, d) in the endothelium-dependent vasorelaxation of the thoracic aorta in Wistar-Kyoto (WKY) and spontaneously hypertensive rats (SHR). The results are presented as the mean \pm SEM of $n = 8-10$ rats, and differences between groups were analyzed by two-way analysis of variance (ANOVA) with the Bonferroni post hoc test on ranks. $^+p < 0.05$ vs. 7-week-old, $^*p < 0.05$ vs. 20-week-old rats.

Interestingly, in the young SHRs, the EDR was increased compared to the age-matched WKYs, while in the other age groups, a significantly reduced EDR was observed. Since endothelial dysfunction resulted in a shift of endothelium-derived vasoactive agents toward vasoconstrictors, our previous studies were aimed at testing the effect of cyclooxygenase (COX) inhibition on EDR in SHRs. We confirmed that specific COX-2 inhibition recovered the reduced EDR in 20-week-old and 52-week-old SHRs [31, 32]. Thus, COX-2-derived vasoconstrictor prostaglandins are significantly involved in the development of endothelial dysfunction in SHRs. Apart from this, a reduced bioavailability of NO has often been reported as a main factor of impaired EDR in

SHRs. Our present results showed that in 7-week-old SHRs, the residual EDR after L-NMMA incubation was increased compared to that of rats in other age groups, but rats at 20 weeks and 52 weeks had similar residual EDRs. The activity of NOS in the TA was comparable in 7-week-old and 20-week-old SHRs, but it was significantly reduced in 52-week-old hypertensive rats compared to younger animals and 52-week-old WKYs. According to these data, it seems that in SHRs, the lowest aortic NO bioavailability was in the 52-week-old group.

A comparison of these responses between the strains revealed that the 7-week-old SHRs had significantly enhanced residual relaxation after L-NMMA incubation

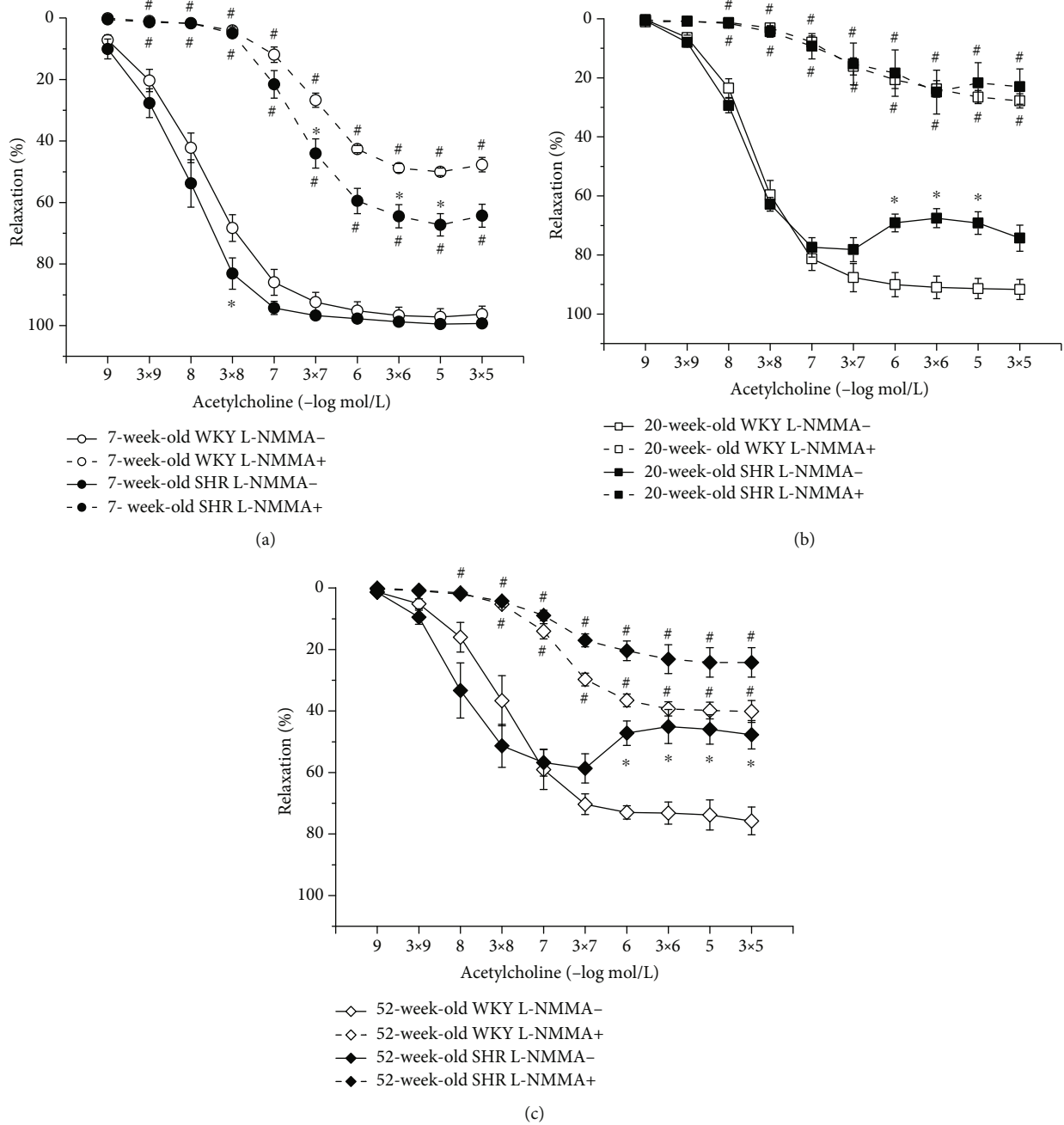


FIGURE 6: The effect of hypertension on NO synthase participation in endothelium-dependent vasorelaxation of the thoracic aorta in 7-week-old (a), 20-week-old (b), and 52-week-old (c) rats. WKY: Wistar-Kyoto rats; SHR: spontaneously hypertensive rats. The results are presented as the mean \pm SEM of $n = 8-10$ rats, and differences between groups were analyzed by three-way analysis of variance (ANOVA) with the Bonferroni post hoc test on ranks. * $p < 0.05$ vs. WKY, # $p < 0.05$ vs. EDR without L-NMMA.

compared with the age-matched WKYs, indicating a decreased L-NMMA-sensitive component of the EDR in SHRs. On the other hand, NOS activity and superoxide production were significantly increased in the 7-week-old SHRs compared to age-matched WKY rats. In our previous study, we confirmed that maximal acetylcholine-induced vasorelaxation was inhibited by a nonspecific NOS inhibitor (L-NAME) to a higher extent in 4-week-old SHRs than in age-matched normotensive rats. Moreover, a higher concentration of L-NAME induced a significant increase in TA

basal tone in SHRs, which was comparable with submaximal noradrenaline-induced vasoconstriction [10]. These findings indicate the prevalent participation of NO in vasoactive control of prehypertensive and early hypertensive stages of SHRs and support the existence of adaptation mechanisms involving abundant endogenous vascular NO production [12]. This was also observed previously in the femoral arteries, in which endothelial dysfunction in SHRs was NO-independent, while there was a significant negative correlation between BP and the L-NAME-resistant component of

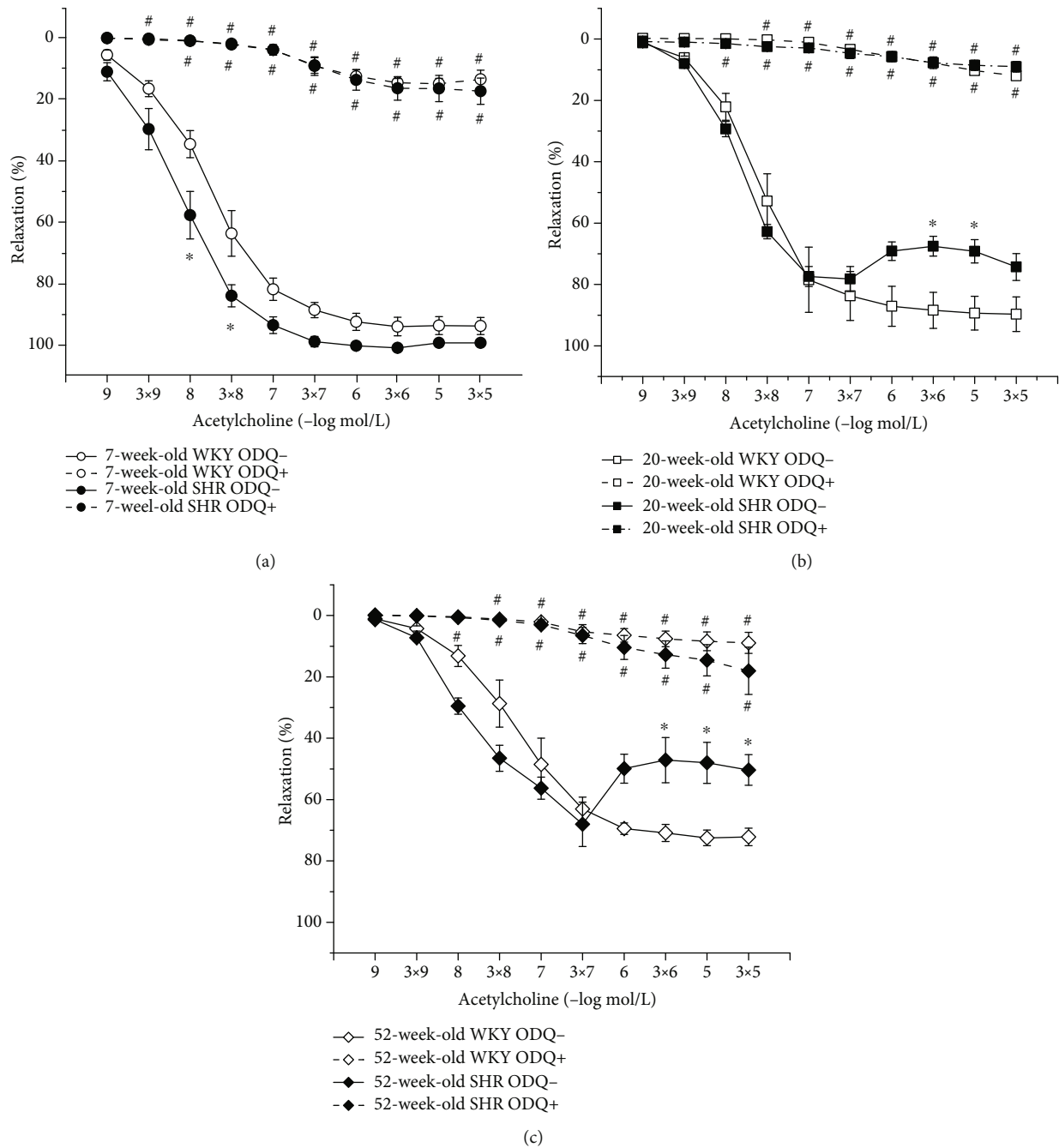


FIGURE 7: The effect of hypertension on sGC participation in endothelium-dependent vasorelaxation of the thoracic aorta in 7-week-old (a), 20-week-old (b), and 52-week-old (c) rats. WKY: Wistar-Kyoto rats; SHR: spontaneously hypertensive rats. The results are presented as the mean \pm SEM of $n = 8-10$ rats, and differences between groups were analyzed by three-way analysis of variance (ANOVA) with the Bonferroni post hoc test on ranks. * $p < 0.05$ vs. WKY, # $p < 0.05$ vs. EDR without ODQ.

ACh-induced relaxation in young adult rats with various genetic predispositions to hypertension [33]. These adaptation mechanisms are functional in 7-week-old SHRs, since we also found enhanced NOS activity in the aorta compared to 7-week-old male WKYs in this study and previously in age-matched female SHRs [16]. In the present study, the increased NOS activity persisted in 20-week-old SHRs; how-

ever, the EDR was reduced, and the residual EDR after L-NMMA was the same as that in age-matched WKYs. Therefore, it seems that in young adult SHR there is a sufficient amount of vasoactively relevant NO in TA. However, in aged SHRs, the activity of the L-arginine/NO pathway in TA decreased, which was not observed in WKY rats. Thus, it seems that in contrast to SHRs, in WKYs, the NOS/NO

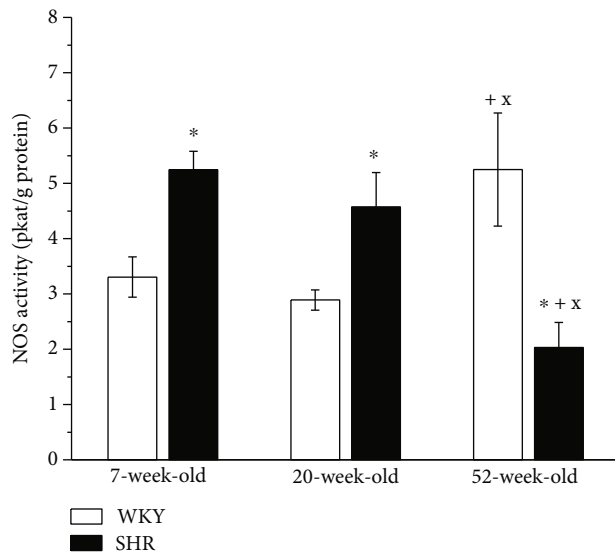


FIGURE 8: The effect of the age and phenotype on the NO synthase activity in the aorta. WKY: Wistar-Kyoto rats; SHR: spontaneously hypertensive rats. The results are presented as the mean \pm SEM of $n = 6$ rats, and differences between groups were analyzed by two-way analysis of variance (ANOVA) with the Bonferroni post hoc test on ranks. * $p < 0.05$ vs. WKY at the same age, + $p < 0.05$ vs. 7-week-old of the same phenotype, x $p < 0.05$ vs. 20-week-old rats of the same phenotype.

system is probably able to respond to age-related pathologies to maintain endothelial functions and thus optimal BP levels even in later periods of life.

5. Conclusions

In summary, our results demonstrated that sGC is the dominant target of endogenous NO in both normotensive and hypertensive conditions and that age did not alter its importance in the EDR of TA. However, the production and participation of vascular NO in EDR is clearly affected not only by hypertension but also by age. While young juvenile SHRs revealed enhanced NOS activity and vasomotor manifestations of NO compared with age-matched WKYs, these benefits partially disappeared in young adult rats (enhanced NOS activity but EDR reduction). Moreover, in old SHRs, there was an obvious reduction in the activity of the L-arginine/NO pathway in the TA, which was not found in the WKY rats. We can conclude that in WKYs, the NOS/NO system is probably able to respond to age-related pathologies in an effort to maintain endothelial functions and normotension, which is missing in aged hypertensive rats.

Data Availability

The data used to support the findings of this study are available from the corresponding author upon request.

Conflicts of Interest

The authors declare that there is no conflict of interest regarding the publication of this paper.

Acknowledgments

This study was supported by the Scientific Grant Agency of the Ministry of Education, Science, Research and Sport of the Slovak Republic and Slovak Academy of Sciences (VEGA 2/0153/21, VEGA 2/0111/19) and Slovak Research and Development Agency (APVV-16-0263) and by the grant of the Slovak Society of Cardiology. Peter Balis was supported by the Schwarz fund of the Slovak Academy of Sciences. The authors thank Mrs. Jana Petova and Mrs. Branislava Bolgacova for providing technical assistance with housing the animals.

References

- [1] M. Noale, F. Limongi, and S. Maggi, "Epidemiology of cardiovascular diseases in the elderly," in *In Veronese N. (eds) Frailty and Cardiovascular Diseases. Advances in Experimental Medicine and Biology*, vol. 1216, pp. 29–38, Springer, Cham, 2020.
- [2] O. Arishe, J. McKenzie, F. Priviero, A. B. Ebeigbe, and R. C. Webb, "L-Arginase induces vascular dysfunction in old spontaneously hypertensive rats," *Journal of African Association of Physiological Sciences*, vol. 7, no. 2, pp. 119–127, 2019.
- [3] A. Zemancikova and J. Torok, "Diminished contractile responses of isolated conduit arteries in two rat models of hypertension," *The Chinese Journal of Physiology*, vol. 56, no. 4, pp. 230–235, 2013.
- [4] M. Toledo-Durand, J. A. Castania, and F. J. Rubens, "Hemodynamic responses to aortic depressor nerve stimulation in conscious L-NAME-induced hypertensive rats," *American Journal of Physiology-Regulatory, Integrative and Comparative Physiology*, vol. 300, no. 2, pp. 418–427, 2010.
- [5] F. Kristek, M. Drobna, and S. Cacanyiova, "Different structural alterations in individual conduit arteries of SHRs compared to Wistar rats from the prehypertensive period to late adulthood," *Physiological Research*, vol. 66, no. 5, pp. 769–780, 2017.
- [6] D. Konukoglu and H. Uzun, "Endothelial dysfunction and hypertension," in: *Islam M.S. (eds) Hypertension: From Basic Research to Clinical Practice*, vol. 956, pp. 511–540, 2016.
- [7] I. Bernatova, "Endothelial dysfunction in experimental models of arterial hypertension: cause or consequence?," *BioMed Research International*, vol. 2014, 14 pages, 2014.
- [8] S. Cacanyiova, A. Berenyiova, M. Malekova et al., "Different vasoactive effects of chronic endothelial and neuronal NO-synthase inhibition in young Wistar rats," *Journal of Physiology and Biochemistry*, vol. 70, no. 3, pp. 749–760, 2014.
- [9] P. Sandner, D. P. Zimmer, G. T. Milne, M. Follmann, A. Hobbs, and J. P. Stasch, "Soluble guanylate cyclase stimulators and activators," *Handbook of Experimental Pharmacology*, vol. 264, pp. 355–394, 2021.
- [10] S. Cacanyiova, A. Berenyiova, F. Kristek, M. Drobna, K. Ondrias, and M. Grman, "The adaptive role of nitric oxide and hydrogen sulphide in vasoactive responses of thoracic aorta is triggered already in young spontaneously hypertensive

- rats," *Journal of Physiology and Pharmacology*, vol. 67, no. 4, pp. 501–512, 2016.
- [11] A. Puzserova, V. Ilovská, P. Balis, P. Slezak, and I. Bernatova, "Age-related alterations in endothelial function of femoral artery in young SHR and WKY rats," *BioMed Research International*, vol. 2014, Article ID 658479, 12 pages, 2014.
- [12] A. Berenyiova, M. Drobna, M. Cebova, F. Kristek, and S. Cacanyiova, "Changes in the vasoactive effects of nitric oxide, hydrogen sulfide and the structure of the rat thoracic aorta: the role of age and essential hypertension," *Journal of Physiology and Pharmacology*, vol. 69, no. 4, 2018.
- [13] A. Puzserova, P. Slezak, P. Balis, and I. Bernatova, "Long-term social stress induces nitric oxide-independent endothelial dysfunction in normotensive rats," *Stress*, vol. 16, no. 3, pp. 331–339, 2013.
- [14] P. Balis, A. Puzserova, P. Slezak, N. Sestakova, O. Pechanova, and I. Bernatova, "Short-term administration of alibernet red wine extract failed to affect blood pressure and to improve endothelial function in young normotensive and spontaneously hypertensive rats," *Physiological Research*, vol. 62, no. 6, pp. 631–641, 2013.
- [15] F. C. Yin, H. A. Spurgeon, K. Rakusan, M. L. Weisfeldt, and E. G. Lakatta, "Use of tibial length to quantify cardiac hypertrophy: application in the aging rat," *The American Journal of Physiology*, vol. 243, no. 6, pp. H941–H947, 1982.
- [16] P. Slezak, A. Puzserova, P. Balis et al., "Genotype-related effect of crowding stress on blood pressure and vascular function in young female rats," *BioMed Research International*, vol. 2014, Article ID 413629, 11 pages, 2014.
- [17] S. Liskova, P. Balis, A. Micurova et al., "Effect of iron oxide nanoparticles on vascular function and nitric oxide production in acute stress-exposed rats," *Physiological Research*, vol. 69, no. 6, pp. 1067–1083, 2020.
- [18] O. H. Lowry, N. J. Rosebrough, A. L. Farr, and R. J. Randall, "Protein measurement with the Folin phenol reagent," *The Journal of Biological Chemistry*, vol. 193, no. 1, pp. 265–275, 1951.
- [19] M. Cebova and F. Kristek, "Age-dependent ultrastructural changes of coronary artery in spontaneously hypertensive rats," *General Physiology and Biophysics*, vol. 30, no. 4, pp. 364–372, 2011.
- [20] B. Galvez, J. De Castro, D. Herold et al., "Perivascular adipose tissue and mesenteric vascular function in spontaneously hypertensive rats," *Arteriosclerosis, Thrombosis, and Vascular Biology*, vol. 26, no. 6, pp. 1297–1302, 2006.
- [21] S. A. Oliveira Junior, K. Okoshi, A. P. Lima-Leopoldo et al., "Nutritional and cardiovascular profiles of normotensive and hypertensive rats kept on a high fat diet," *Arquivos Brasileiros de Cardiologia*, vol. 93, no. 5, pp. 526–533, 2009.
- [22] A. Kozłowska, P. Wojtacha, M. Rowniak, M. Kolenkiewicz, and M. L. Tsai, "Differences in serum steroid hormones concentrations in spontaneously hypertensive rats (SHR) – an animal model of attention-deficit/hyperactivity disorder (ADHD)," *Physiological Research*, vol. 68, no. 1, pp. 25–36, 2019.
- [23] P. Balis, A. Berenyiova, J. Radosinska, M. Kvandova, I. Bernatova, and A. Puzserova, "High concentration of uric acid failed to affect endothelial function of small mesenteric arteries, femoral arteries and aortas from aged Wistar-Kyoto rats," *Journal of Physiology and Pharmacology*, vol. 71, no. 3, 2020.
- [24] M. Kollarova, A. Puzserova, P. Balis et al., "Age- and phenotype-dependent changes in circulating MMP-2 and MMP-9 activities in normotensive and hypertensive rats," *International Journal of Molecular Sciences*, vol. 21, no. 19, article 7286, 2020.
- [25] S. Simão, P. Gomes, V. Pinto et al., "Age-related changes in renal expression of oxidant and antioxidant enzymes and oxidative stress markers in male SHR and WKY rats," *Experimental Gerontology*, vol. 46, no. 6, pp. 468–474, 2011.
- [26] R. L. Matz, M. A. de Sotomayor, C. Schott, C. Stoclet, and R. Andriantsitohaina, "Vascular bed heterogeneity in age-related endothelial dysfunction with respect to NO and eicosanoids," *British Journal of Pharmacology*, vol. 131, no. 2, pp. 303–311, 2000.
- [27] M. Dawes, P. J. Chowienczyk, and J. M. Ritter, "Quantitative aspects of the inhibition by N(G)-monomethyl-L-arginine of responses to endothelium-dependent vasodilators in human forearm vasculature," *British Journal of Pharmacology*, vol. 134, no. 5, pp. 939–944, 2001.
- [28] N. Paolucci, M. I. Jackson, B. E. Lopez et al., "The pharmacology of nitroxyl (HNO) and its therapeutic potential: not just the Janus face of NO¹," *Pharmacology & Therapeutics*, vol. 113, no. 2, pp. 442–458, 2007.
- [29] T. W. Miller, M. M. Cherney, A. J. Lee et al., "The effects of nitroxyl (HNO) on soluble guanylate cyclase activity: interactions at ferrous heme and cysteine thiols," *The Journal of Biological Chemistry*, vol. 284, no. 33, pp. 21788–21796, 2009.
- [30] K. L. Andrews, J. C. Irvine, M. Tare et al., "A role for nitroxyl (HNO) as an endothelium-derived relaxing and hyperpolarizing factor in resistance arteries," *British Journal of Pharmacology*, vol. 157, no. 4, pp. 540–550, 2009.
- [31] A. Berenyiova, A. Puzserova, M. Grman, F. Kristek, and S. Cacanyiova, "The participation of nitric oxide and hydrogen sulphide signalisation in vasoactive responses of rat thoracic aorta in condition of developed spontaneous hypertension," *Artery Research*, vol. 20, no. C, p. 64, 2017.
- [32] A. Berenyiova, S. Cacanyiova, P. Balis, and A. Puzserova, "Impact of hypertension and age on the NO and COX signaling pathways in vasoactive responses of thoracic aorta in normotensive Wistar-Kyoto and spontaneously hypertensive rats," *Cardiology Letters*, vol. 26, article 12S, suppl, 2017.
- [33] A. Puzserova, J. Kopincova, P. Slezak, P. Balis, and I. Bernatova, "Endothelial dysfunction in femoral artery of the hypertensive rats is nitric oxide independent," *Physiological Research*, vol. 62, no. 6, pp. 615–629, 2013.

Review Article

Gasotransmitters: Potential Therapeutic Molecules of Fibrotic Diseases

Yingqing Chen ^{1,2}, **Shuo Yuan** ³, **Yuying Cao** ^{1,2}, **Guangyao Kong** ^{1,2}, **Feng Jiang** ^{1,2},
You Li ^{1,2}, **Qi Wang** ^{1,2}, **Minli Tang** ^{1,2}, **Qinggao Zhang** ^{1,2,3}, **Qianqian Wang** ^{1,2}
and **Liping Liu** ^{1,2}

¹Chronic Disease Research Center, Medical College, Dalian University, Dalian, 116622 Liaoning, China

²Engineering Technology Research Center for the Utilization of Functional Components of Organic Natural Products, Dalian University, Dalian, 116622 Liaoning, China

³Key Laboratory of Natural Medicines of the Changbai Mountain, Ministry of Education, College of Pharmacy, Yanbian University, Yanji, 133002 Jilin Province, China

Correspondence should be addressed to Qinggao Zhang; zhangqinggao@dlu.edu.cn, Qianqian Wang; wangqianqian@dlu.edu.cn, and Liping Liu; liuliping@dlu.edu.cn

Received 28 May 2021; Accepted 31 August 2021; Published 21 September 2021

Academic Editor: Vítor Fernandes

Copyright © 2021 Yingqing Chen et al. This is an open access article distributed under the Creative Commons Attribution License, which permits unrestricted use, distribution, and reproduction in any medium, provided the original work is properly cited.

Fibrosis is defined as the pathological progress of excessive extracellular matrix (ECM), such as collagen, fibronectin, and elastin deposition, as the regenerative capacity of cells cannot satisfy the dynamic repair of chronic damage. The well-known features of tissue fibrosis are characterized as the presence of excessive activated and proliferated fibroblasts and the differentiation of fibroblasts into myofibroblasts, and epithelial cells undergo the epithelial-mesenchymal transition (EMT) to expand the number of fibroblasts and myofibroblasts thereby driving fibrogenesis. In terms of mechanism, during the process of fibrosis, the activations of the TGF- β signaling pathway, oxidative stress, cellular senescence, and inflammatory response play crucial roles in the activation and proliferation of fibroblasts to generate ECM. The deaths due to severe fibrosis account for almost half of the total deaths from various diseases, and few treatment strategies are available for the prevention of fibrosis as yet. Recently, numerous studies demonstrated that three well-defined bioactive gasotransmitters, including nitric oxide (NO), carbon monoxide (CO), and hydrogen sulfide (H₂S), generally exhibited anti-inflammatory, antioxidative, antiapoptotic, and antiproliferative properties. Besides these effects, a number of studies have reported that low-dose exogenous and endogenous gasotransmitters can delay and interfere with the occurrence and development of fibrotic diseases, including myocardial fibrosis, idiopathic pulmonary fibrosis, liver fibrosis, renal fibrosis, diabetic diaphragm fibrosis, and peritoneal fibrosis. Furthermore, in animal and clinical experiments, the inhalation of low-dose exogenous gas and intraperitoneal injection of gaseous donors, such as SNAP, CINOD, CORM, SAC, and NaHS, showed a significant therapeutic effect on the inhibition of fibrosis through modulating the TGF- β signaling pathway, attenuating oxidative stress and inflammatory response, and delaying the cellular senescence, while promoting the process of autophagy. In this review, we first demonstrate and summarize the therapeutic effects of gasotransmitters on diverse fibrotic diseases and highlight their molecular mechanisms in the process and development of fibrosis.

1. Introduction

Fibrosis is a well-known pathological process in which several extracellular matrixes (ECMs), such as collagen, fibronectin,

and elastin, accumulate abnormally in chronic inflamed and damaged tissues. Excessive fibrosis, in chronic inflammation, can cause permanent scars, multiple organ sclerosis, and dysfunction [1]. Tissue fibrosis will be the main cause of disability

and death in many diseases and which affects various organs such as the cardiovascular, lung, liver, and kidney [2].

Although the mechanisms of various fibrotic diseases are different, the common feature of tissues affected by fibrosis is the presence of excessive activated fibroblasts and transformed myofibroblasts [3]. These cells have unique biological functions, including the secretion of fibrous type I and type III collagen and the expression of α -smooth muscle actin (α -SMA) [3]. In the occurrence and development of fibrosis, the activation of fibroblast and transformation into myofibroblasts are two very important factors. Once fibroblasts are activated by tissue damage and chronic inflammation, it will secrete a variety of ECM and promote the conversion of fibroblasts to myofibroblasts. The critical molecules and signaling pathways involved in fibrosis mainly consist of transforming growth factor β (TGF- β), connective tissue growth factor (CTGF/CCN2), platelet-derived growth factor (PDGF), endothelin 1 (ET-1), and the Wnt, Hedgehog, and Notch signaling pathways [4–10]. Therefore, the strategies for the treatment of fibrosis, to date, mainly include the inhibition of fibroblast activity and the myofibroblast transformation, interfering TGF- β expression and its signaling pathways, decreasing the homing of fibroblasts into the tissues, and the inhibition of other profibrosis signaling pathways [11].

Gasotransmitters are small molecules with a short half-life and play crucial roles in cellular homeostasis [12]. Nitrogen monoxide (NO), carbon monoxide (CO), and hydrogen sulfide (H₂S) are three best-known gasotransmitters, and all these three gases have been demonstrated to possess antioxidative, anti-inflammatory, antiapoptotic, and antiproliferative properties [12]. Besides that, these gasotransmitters are gradually being known by many researchers for exploring their molecular mechanisms in fibrotic diseases. In this review, we first try to discuss and summarize the therapeutic mechanisms of gasotransmitters in diverse fibrotic diseases.

2. Molecular and Cellular Mechanisms of Fibrosis

2.1. TGF- β and Fibrosis. TGF- β has a dimeric structure and is expressed in all cells. It is important for regulating cell growth, migration, immunosuppression, and endothelial-mesenchymal transition (EMT) [13]. TGF- β 1 is the most abundant subtype of the TGF- β family. It plays a critical role in promoting fibrotic cell proliferation, collagen secretion, protease inhibitor production, and extracellular matrix (ECM) deposition in tissues [13]. After its receptors are bound, the signal can be further transmitted to the downstream Smads protein family [13, 14]. First, TGF- β 1 recognizes and combines with TGF- β RII dimer and then forms a heterotetraploid with the TGF- β R1 dimer successively, so that the glycine-serine- (GS-) rich region of TGF- β R1 starts to phosphorylate and activate TGF- β R1 kinase. Then, the activated Smad2/3 components bind with Smad4 to form oligomeric complex and which translocate into the nucleus and participate in the transcription of target genes associated with the process of cell apoptosis, proliferation, and differentiation [15]. Besides that, Smad2/3 phosphorylation can increase the expression of fibrosis relative genes and enhances the activity of fibroblasts to facilitate the progression

of fibrosis [15]. However, Smad7, as an inhibitory Smad (I-Smad), may block the TGF- β 1/Smads signaling pathway by interfering with the activated TGF- β R1. This also means that the phosphorylation of Smad2/3 is hindered from the root cause, thereby delaying or improving the process of fibrosis [16, 17]. Moreover, the screening of targets related to the TGF- β signaling pathway has become a novel method to provide theoretical support for the development of therapeutic drugs of fibrotic diseases [13–15, 18].

More recently, several studies have found that galectin-3 is a key signal molecule in the TGF- β pathway and which mediates fibroblast activation to provoke TGF- β expression and to activate its downstream profibrosis-related pathways [18]. Galectin-3 is expressed and secreted by inflammatory cells and that can bind to glycoproteins and glycolipids on cell surface to participate in a variety of physiological and pathological processes [19]. Galectin-3 has the function of accelerating the proliferation and differentiation of cardiac fibroblasts and which plays an important role in the pathophysiological process such as cardiac fibrosis. It is also an emerging marker used to diagnose and predict congenital hepatic fibrosis (CHF) in recent years [19].

2.2. Oxidative Stress and Fibrosis. Oxidative stress is referred as the excessive free radicals that are produced under the stimulation of harmful factors in vitro and in vivo. The excessive accumulation of oxygen free radicals and related metabolites can cause the cell to produce a variety of toxic effects [20]. Glutathione (GSH) and superoxide dismutase (SOD) are the main players in antioxidant defense system, which can eliminate harmful peroxidation metabolites, block lipid peroxidation, and protect the integrity of cellular membrane [21].

NADPH oxidase (NOX) is a transmembrane complex composing multiple protein subunits which are the main regulators of reactive oxygen species (ROS) production in cells. There are 7 subtypes of NOX, namely, NOX1, NOX2, NOX3, NOX4, NOX5, DUOX1, and DUOX2 [22]. Hepatic stellate cells (HSCs) and Kupffer cells are the key effectors for liver NOX expression. Kupffer cells mainly participate in the generation of ROS in the early stage of liver fibrosis by expressing NOX2 [23]. The increase of NOX2 can induce HSC activation by releasing ROS to mediate liver damage and fibrosis through activating the platelet-derived growth factor (PDGF) signal pathway [24].

Oxidative stress and the antioxidant system appear to be crucial modulators in regulating the TGF- β 1 signaling, metabolic homeostasis, and chronic inflammation, all of which are associated with the development and persistence of fibrosis [25]. The TGF- β 1/p38 MAPK signaling pathway is activated in response to various inflammations, oxidative stress, and other stimuli. Inhibiting the activity of this pathway can slow down the progression of fibrosis [26]. TGF- β 1 is activated after receiving various stimuli, including oxidative stress, which further affects the activation of the downstream factor apoptosis signal-regulating kinase 1 (ASK-1). Overexpression of ASK-1 can promote MKK3/6 phosphorylation and which subsequently activate p38 MAPK and phosphorylation of cyclic AMP-dependent transcription

factor 2 (ATF2), thereby producing a series of biological reactions [27]. ATF2 is a member of the leucine zipper family of DNA-binding proteins. It is mainly involved in the regulation of cellular stress response. Phosphorylated ATF2 plays a key role in inflammation, apoptosis, and fibrosis [28–31]. JNK-dependent phosphorylation of ATF2/c-Jun transcription factors can result in TGF- β transcription to promote oral submucous fibrosis [30]. In addition, anti-ATF2 antibody, as a novel autoantibody, can serve as a serological marker for inflammation and lung involvement in systemic sclerosis [31].

ROS production can activate the p38 MAPK pathway and that in turn aggravates the oxidative stress state, resulting in oxidative damage and tissue fibrosis [32]. Moreover, oxidative stress interacts with other pathophysiological mechanisms to promote the occurrence and development of fibrosis [33]. Therefore, the role of oxidative stress in fibrotic diseases has been attracted more attention by researchers. Only clarifying the complex mechanism can we discover the effective antioxidative stress drugs to treat fibrosis.

2.3. Cellular Senescence and Fibrosis. Numerous studies have strongly suggested that the progression of fibrotic diseases is highly correlated with age. The accumulation of senescent cells caused by aging is proved as a key factor to the development of fibrosis [34]. With the aging of the body, the increase of damaged cells and the decline in immune monitoring capabilities can reduce the clearance rate of senescent cells and which subsequently result in the secretion of various senescence-associated secretory phenotypes (SASPs), such as proinflammatory cytokines, chemokines, and metalloproteinases (MMPs), to accelerate the development of fibrosis [35, 36].

The activation of p53, after the senescence occurred in type II alveolar epithelial cells, can participate in the development of pulmonary fibrosis by upregulating miR-34 and downregulating key target genes of the cell cycle [37]. Moreover, p21 can maintain the survival of senescent HSCs by inhibiting caspase and c-Jun N-terminal kinase (JNK) signals [38]. Lehmann et al. proved that the type II alveolar epithelial cells from mice with pulmonary fibrosis could secrete higher levels of SASP, especially insulin-like growth factor-binding protein- (IGFBP-) 3, 4, 7 and matrix metalloproteinase- (MMP-) 3, 12, 14 [39]. Therefore, prevention of cellular senescence is of great significance for attenuating the pathogenesis of fibrosis and which can provide novel antifibrotic treatment strategies.

Recent studies have found that the TGF- β pathway is also involved in the aging process. Tasanarong et al. suggested that TGF- β could trigger stress-induced senescence via the p16^{INK4a} and Smad3 pathways, and the loss of Smad3 will reduce the formation of senescent cells [40, 41]. Furthermore, in the process of cellular senescence, senescent cells are resistant to cell apoptosis, and whose accumulation over time can secrete a variety of SASP and which subsequently stimulate fibroblasts into damaged tissues, as well as accelerate the activation of fibroblasts [40]. Fang et al. demonstrated that advanced glycation end-products (AGE) are an important factor for cardiac aging and fibrosis, and AGE-

induced cardiac aging might be the crucial factor for TGF- β -mediated fibrosis [42].

Conversely, studies have shown that after knocking out p53, HSCs could continuously promote the expression of ECM and α -SMA to accelerate the process of liver fibrosis [43]. This indicated that the senescent HSCs could interfere with the development of liver fibrosis [43]. In addition, insulin-like growth factors (IGF-I) can induce HSC senescence. IGF-I can increase the expression of senescence-associated proteins, such as p21 and p53, to reduce ECM deposition and prevent liver fibrosis [43, 44]. Kong et al. found that IL-22 can induce HSC senescence through the p53 pathway and which can eventually reverse liver fibrosis in mice [45]. These studies indicate that senescent HSCs can inhibit the development of liver fibrosis through activating the p53 signaling pathway and which are expected to realize the reversal of liver fibrosis [43–45].

2.4. Inflammation and Fibrosis. In most chronic inflammatory diseases, fibrosis has increasingly become the main cause of morbidity and mortality [46]. Many immune-related elements are involved in the occurrence and development of fibrotic diseases [47, 48].

Nuclear factor- κ B (NF- κ B) is a transcriptional regulatory factor that has been studied extensively in recent years [49]. Translocation of activated NF- κ B into the nucleus can promote the expression of related genes, such as TNF- α , IL-6, IL1 β , and NLRP3 [49]. These substances are reported to play an important role in the occurrence and development of fibrosis [50–55]. Research showed that Krüppel-like factor 4 (KLF4), a zinc finger transcription factor, can ameliorate chronic kidney disease through mitigating TNF-mediated tissue injury and fibrosis [50]. Moreover, TNF- α can stimulate IL-33 secretion via interaction with TNFR2 and which promotes myofibroblast development to accelerate the process of myocardial fibrosis [51]. NOD-like receptor protein 3 (NLRP3) inflammasome inhibitor, MCC950, is first demonstrated to ameliorate nonalcoholic fatty liver disease (NAFLD) and fibrosis in obese diabetic mice, and the targeting of NLRP3 is a logical direction in pharmacotherapy for liver fibrosis [54].

Signal transducers and activators of transcription 6 (STAT6) is mainly activated by IL-4 and IL-13 and plays an important role in immune regulation, involving the development of fibrosis [56, 57]. STAT6 is mainly activated by cytokines, including IL-4 and IL-13, which are secreted by Th2 cells (Figure 1). IL-13 is an important fibrotic factor. The profibrosis effect of IL-13 may be closely related to the upregulation of many fibrosis-related proteins in HSC and HSC activation. IL-13 can regulate liver fibrosis by activating macrophages. Both the upregulation of miR-142-5p and the downregulation of miR-130a-3p in macrophages can promote fibrosis [56]. The upregulated miR-142-5p promotes the phosphorylation of STAT6 by targeting SOCS1, and the downregulated miR-130a-3p reduces its inhibition of peroxisome proliferator-activated receptor γ (PPAR γ) to promote fibrosis [56]. In the bleomycin-induced mouse pulmonary fibrosis model, IL-4 and IL-13 levels were significantly increased, but after blocking the IL-4/IL-13 signaling

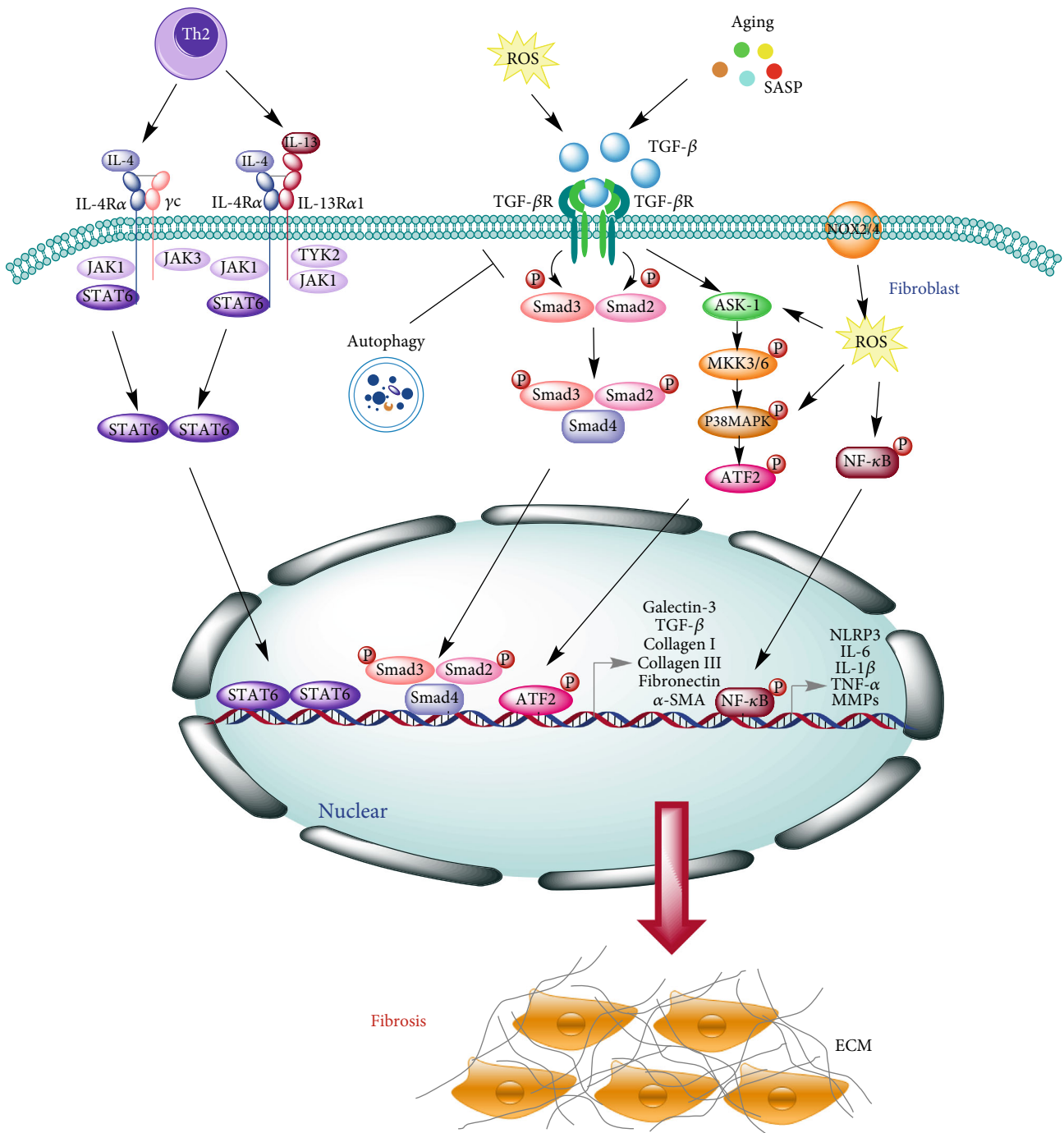


FIGURE 1: Molecular and cellular mechanisms of fibrosis. TGF- β recognizes and combines with TGF- β R II and TGF- β R I successively, and then, the glycine-serine- (GS-) rich region of TGF- β R I phosphorylates Smad2/3 to facilitate the formation of oligomeric complex with Smad4 and which translocates into the nucleus and participates in the transcription of fibrotic genes, such as galectin 3, collagen I, collagen III, α -SMA, and TGF- β . Besides that, the TGF- β signaling pathway can be activated by oxidative stress and cellular senescence, which further affects the activation of the downstream factors ASK-1. ASK-1 can promote MKK3/6 phosphorylation and which subsequently activates p38 MAPK and phosphorylates ATF2, thereby promoting the transcription of fibrosis-associated genes. NOX2/4 can stimulate ROS production and provoke the NF- κ B signaling pathway to upregulate inflammatory-associated genes, such as NLRP3, IL-6, IL-1 β , TNF- α , and MMPs, to promote the development of fibrosis. IL-4 and IL-13 secreted by Th2 cells can activate STAT6 and which can promote the expression of fibrotic genes and inflammatory cytokines to accelerate the process of fibrosis. Autophagy exerts a protective role in fibrotic diseases by downregulating the TGF- β /Smad4 pathway and NLRP3 inflammasome.

pathway, the activation of STAT6 was reduced and which could significantly ameliorate pulmonary fibrosis [57].

Autophagy is a highly conservative cell degradation and recycling process that can regulate cell death and proliferation. Previous studies have shown that autophagy has an inhibitory effect in fibrosis (Figure 1) [58]. Conditionally knocking out the autophagy-related protein 7 (Atg7) gene in the distal renal tubular epithelial cells from unilateral ureteral obstruction (UUO) mouse model can promote the activation of the TGF- β /Smad4 pathway and the NLRP3 inflammasome, as well as aggravate renal interstitial fibrosis [58]. This suggests that autophagy can play a protective role in renal interstitial fibrosis by regulating the TGF- β /Smad4 pathway and NLRP3 inflammasome.

Hypoxia can induce an increase of NLRP3 inflammasome. NLRP3 gene knockout renal tubular cells can reduce the production of ROS under hypoxic conditions. ROS scavengers can downregulate the expression of NLRP3 and reduce renal fibrosis [59]. Although the NLRP3 inflammasome has been reported to associate with the process of fibrosis, the exact mechanisms have not been fully clarified, and further studies are required to identify and provide novel possibilities for the treatment of fibrosis.

The abnormal expression of various inflammatory components in fibrotic diseases suggests that the inflammation is an important link in the occurrence and development of fibrosis in various organs. Therefore, the increasing understanding of inflammation-related signaling pathways will provide new therapeutic ideas and support more direct and effective drug targets for the treatment of fibrotic diseases.

3. Protective Effects of Gasotransmitters in Fibrotic Diseases

3.1. The Interference Role of NO in Fibrotic Diseases. Nitric oxide has been studied in many medical areas and which is defined as an important player in most physiological systems, such as nervous, cardiovascular, and conventional outflow physiology [60–63]. Endogenous NO is mainly produced intracellularly by the enzymatic action of NO synthase (NOS) from amino acid L-arginine. The three different types of NOS mainly include neuronal NOS (nNOS or NOS₁), inducible NOS (iNOS or NOS₂), and endothelial NOS (eNOS or NOS₃) [64]. NO has a short half-life and is rapidly transformed into stable final products in the body, such as nitrate (NO₃) and nitrite (NO₂) [64]. NO has a variety of biological functions, including relaxing smooth muscle, lowering blood pressure, inhibiting the proliferation of vascular smooth muscle cells, preventing the aggregation of platelets, and enhancing nonspecific immune defense [65]. Recently, increasing studies demonstrated that the endogenous and exogenous of NO showed protective effects on diverse fibrotic diseases via multiple antifibrotic mechanisms (Figure 2) [66–75].

3.1.1. NO and Liver Fibrosis. Liver fibrosis is a dynamic response process to various stimuli, such as alcoholism, viral infection, and toxins, which can lead to the destruction of liver parenchymal structure and excessive deposition of the extracellular matrix, thereby promoting the formation of

liver fibrosis [76]. Long-term lack of treatment can further cause liver cirrhosis and hepatocellular carcinoma. Liver fibrosis is characterized by sustained activation of hepatic stellate cells (HSCs) and the excessive accumulation of ECM [76].

ROS is widely known to play a critical role in the development of liver fibrosis, and NO can react with ROS to produce peroxynitrite, which is normally recognized as a very reactive, toxic, and strongly oxidizing compound [66]. However, the relative amounts of peroxynitrite can act as a scavenger of ROS and which depend on the exact conditions of the local microenvironment. Svegliati-Baroni et al. [66] have demonstrated that the supplementation of exogenous NO donor, S-nitroso-N-acetylpenicillamine (SNAP), could prevent liver cirrhosis by scavenging the production of ROS, thus inhibiting HSCs activation and proliferation.

NO derived from eNOS in liver sinusoidal endothelial cells (LSECs) is demonstrated to possess a protective effect on the development of fibrotic disease. In pathological conditions, LSECs become dysfunctional, and the level of NO produced by eNOS showed a significant decrease followed by the activation of quiescent HSCs, and leading to the deposition of the ECM, fibrogenesis, and further cirrhosis [67, 77]. Simvastatin, one kind of lipid-lowering medication, was reported to provoke a conversion of activated HSCs into quiescent cells via enhancement of eNOS mediated by transcription factor Krüppel-like factor 2 (KLF2) [78]. Langer DA suggested that NO could limit the activation of HSCs by promoting the apoptosis of HSCs and which was conferred by mitochondrial membrane depolarization but not the caspase-dependent pathway [79].

As opposed to the protective effect of eNOS on fibrogenesis, iNOS exerts an inducing effect in the occurrence and development of liver fibrosis [68, 69]. The deletion or mutation of the iNOS can reduce the development of liver fibrosis [68]. Anavi et al. showed that as iNOS gene knockout mice were fed with a high-cholesterol diet for 6 weeks, the liver fibrosis was significantly attenuated compared with that in wild-type mice, and the expressions of inflammatory cytokines and fibrogenic genes were all remarkably decreased. However, the paradoxical mechanisms of NOS in liver fibrosis remain unclear [68].

3.1.2. NO and Renal Fibrosis. Renal fibrosis is the buildup of scar within renal parenchyma and which commonly occurs in all chronic and progressive nephropathies, including glomerular hyperfiltration, hyperperfusion, high pressure, and ischemia-reperfusion injury [80]. The basic pathological features of renal fibrosis are composed of the injury and death of renal parenchymal cells, the infiltration of interstitial inflammatory cells, the proliferation of fibroblasts, the transformation of myofibroblasts, the excessive deposition of the ECM, and the formation of interstitial fibrosis [80].

Glomerulonephritis is a type of kidney disease in which there is inflammation of the glomeruli and progresses through the accumulation of ECM and results in loss of the glomerular architecture and scarring [81]. The pathogenesis of glomerulonephritis is incompletely understood; however, increasing studies indicated that the immunological injuries of resident

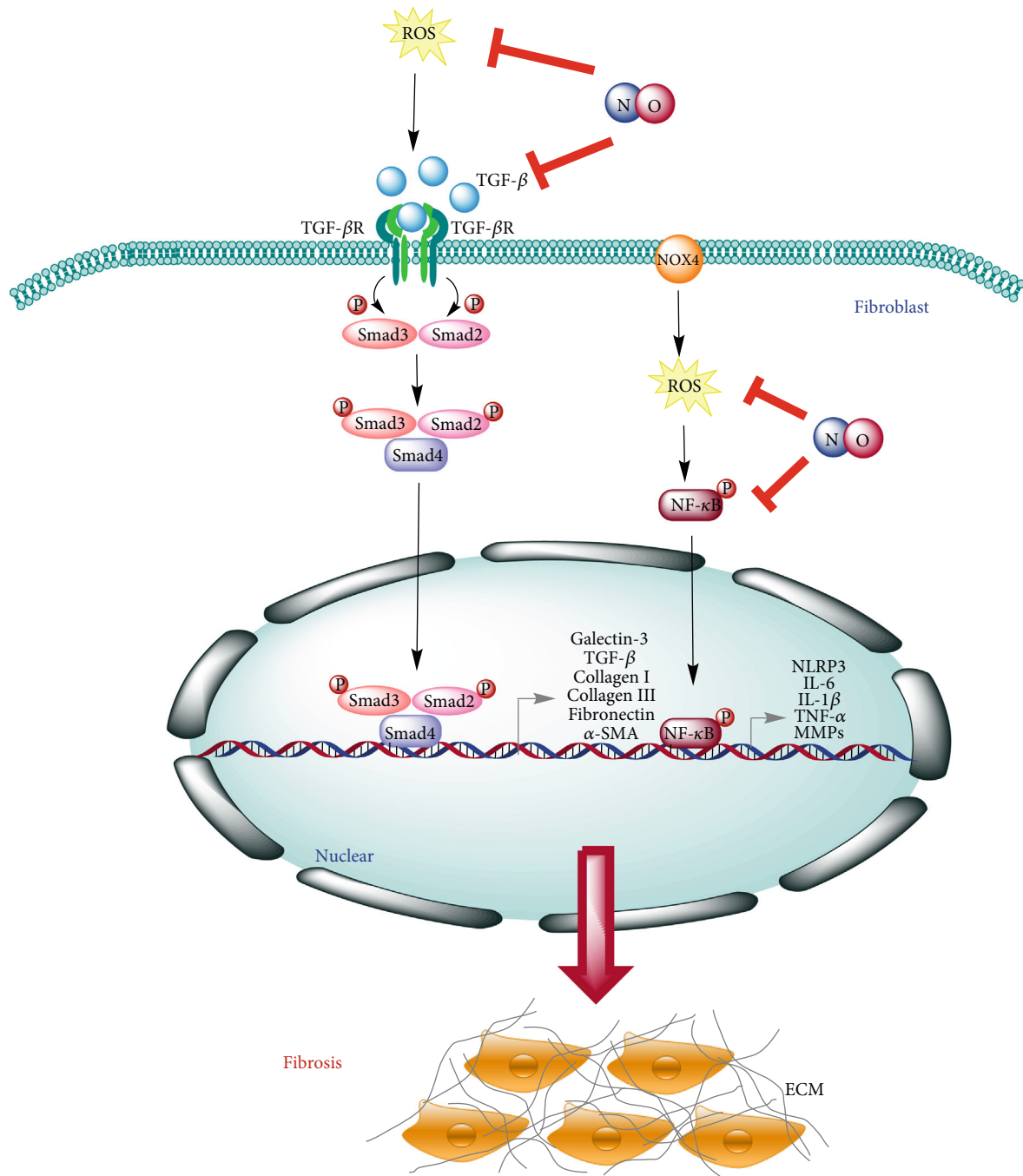


FIGURE 2: The interference mechanisms of NO in fibrotic diseases. NO can reduce the amount of ROS by peroxynitrite formation and which subsequently attenuates the activation of the NF- κ B signaling pathway to inhibit the expression of fibrosis and inflammatory-related genes. Moreover, NO can also downregulate the expression of TGF- β to attenuate its downstream signaling pathway.

cells in glomeruli, such as mesangial cells and podocytes, were associated with the focal glomerulosclerosis [82]. In the process of cultured rat glomerular mesangial cells (MCs), the administration of NO donors, such as spermine NONOate, NOC-18, and SNAP, can suppress the expression of fibrogenic genes at the transcriptional level [70]. This study revealed a complex role of NO in regulating gene expression in mesangial cells and suggests an antifibrotic potential of NO. Additionally, Peters et al. revealed that the supplementation of L-

arginine can reduce the fibrotic disease in antithymocyte serum- (ATS-) glomerulonephritis animal model and which is mediated by multiple pathways, including the suppression of TGF- β expression, while further studies are required to reveal the therapeutic potential of L-arginine supplementation in humans [72, 73].

MMP-9 is an essential matrix metalloproteinase involved in the process of renal fibrosis, which can be regulated in different levels, and finally, the endogenous MMP-9

inhibitor TIMP-1 inhibits the enzyme activity. In the kidney, glomerular mesangial cells are the main source for the synthesis of MMP-9 and its endogenous inhibitor TIMP-1. In renal MCs, NO can modulate the expression of several ECM-degrading proteases and intrinsic inhibitors, including MMP-9, MMP-13, plasminogen activator inhibitor-1 (PAI-1), and TIMP-1 [83, 84]. In addition, NO donor SNAP can amplify the expression of TIMP-1 in a TGF- β -dependent manner and thereby may play a critical role in the regulation of the proteinase-antiproteinase homeostasis in renal MCs [71].

3.1.3. NO and Idiopathic Pulmonary Fibrosis. Idiopathic pulmonary fibrosis (IPF) is a chronic and progressive interstitial lung disease, which can be triggered by various harmful factors like toxic chemicals, radiation, inorganic particles, and microbial infections. Its basic pathological process is the activation of lung fibroblasts and the transformation into myofibroblasts and which can cause the excessive deposition of ECM and ultimately destruct the lung parenchymal structure. The typical pathological features of idiopathic pulmonary fibrosis are the proliferation and accumulation of lung parenchymal fibers and their structural destruction [85].

Patients with pulmonary fibrosis showed a significant enhancement of NOS expression and plasma nitrite and nitrate (NO_x) levels, indicating that NO might play an important role in the process of lung fibrosis [86–88]. The use of bleomycin can induce pulmonary fibrosis in mice. In the lack of all three NOS isoforms, including iNOS, eNOS, and nNOS, bleomycin-treated mice showed a deterioration of pulmonary fibrosis, suggesting the entire endogenous NO and NOS systems exert an important protective role in the pathogenesis of pulmonary fibrosis [74].

Cyclooxygenase-inhibiting NO donors (CINODs) are designed to inhibit COX1 and COX2 while releasing NO, which exhibits anti-inflammatory, pain-relieving, and antioxidant effects [75]. In bleomycin-induced lung fibrosis model, one prototype CINOD compound, (S)-(5S)-5,6-bis(nitrooxy)hexyl-2-(6-methoxynaphthalen-2-yl) propanoate (NCX466), has shown a significant efficacy in reducing lung inflammation, the TGF- β signaling pathway, and the collagen accumulation, suggesting that COX inhibition along with NO donation may exhibit therapeutic potential in pulmonary fibrosis [75].

3.1.4. NO and Peyronie's Disease. In normal condition, myofibroblasts share both phenotypic characteristics of fibroblasts and smooth muscle cells. It plays a key role in collagen deposition and wound healing and disappears through apoptosis when the wound is healed. However, its abnormal persistence can be observed in the fibrotic plaque of the tunica albuginea (TA) of the penis in men with Peyronie's disease (PD) [89, 90]. Vernet demonstrated that the enhancement of iNOS via the administration of cytokine cocktail plus NO donor, SNAP, can inhibit the process of fibrosis by the reduction of myofibroblast abundance and lead to a reduction in collagen 1 synthesis and the inhibition of ROS production [91].

3.2. The Interference Role of CO in Fibrotic Diseases. Carbon monoxide (CO) is generated by the action of heme oxygenase (HO), which is involved in the degradation of heme [92]. Although the toxic effects of CO are well documented, it was only discovered in the last decade that low concentration of CO can exert numerous biological effects, such as anti-inflammation, antiapoptosis, and antioxidation [93]. As the sudden surge in research of CO and its beneficial biological effects, several novel compounds termed carbon monoxide-releasing molecules (CORMs) have been developed, and their biochemical properties have been characterized [94, 95]. The two most recently developed CORM are tricarbonylchloro(glycinato)ruthenium (II) (CORM-3) and sodium boranocarbonate (CORM-A1), both of which are fully water-soluble and thus easy to handle. Upon incubation in a physiological medium, both CORM-3 and CORM-A1 can liberate CO gas [95].

Aki et al. demonstrated that the application of 1 mM CORM3 to mouse embryonic fibroblasts (MEFs) resulted in the reduction of collagen I and III within 24 h, which confirmed an antifibrotic effect of CO [96]. CORM3 also caused a rapid dissociation of cell-associated plasma fibronectin (FN) from MEFs within 1 h, and which is associated with the formation of a reduction-resistant oligomer of plasma FN, suggesting FN is a CORM-3-interactive plasma protein, and the CORM-3-FN interaction is involved in the death of fibroblasts [96].

3.2.1. CO and Idiopathic Pulmonary Fibrosis. Zhou et al. reported that in bleomycin-induced IPF mouse model, inhaling low-dose exogenous 250 ppm CO gas into mice showed a significant therapeutic effect on the development of lung fibrosis [97]. This study revealed that CO could inhibit the formation of pulmonary fibrosis by inhibiting the synthesis and the deposition of extracellular matrix, as well as the proliferation of fibroblasts through increasing p21Cip1 expression while decreasing cyclin A and D levels. Furthermore, CO-exposed cells significantly downregulated fibronectin (FN) and collagen-1 via the regulation of transcriptional regulator, an inhibitor of DNA binding 1 (Id1) [97]. Besides that, one recent study also demonstrated that a nanotechnology-based CO donor, CO-bound hemoglobin vesicles (CO-HbV), showed a therapeutic effect on IPF and which was attributed to a decrease in ROS production by the NOX4 signaling pathway, as well as the production of inflammatory cytokines and TGF- β in the lung [98]. Rosas et al. have demonstrated that inhaled low-dose CO gas was well tolerated and can be safely administered to patients with IPF in phase II clinical trials [99]. Overall, exogenous and endogenous CO exert an antifibrotic effect in the lung, and this effect can ameliorate bleomycin-mediated IPF.

3.2.2. CO and Renal Fibrosis. Wang and his colleagues reported that the exogenous administration of CO can ameliorate UO-induced renal fibrosis and protect against kidney injury [100]. As mice were exposed to CO, the deposition of ECM and the expression of α -SMA, type I collagen, and FN in the kidneys were significantly decreased. In addition, the beneficial effect of CO is mainly associated with the MKK3 pathway. These findings suggest that low-dose CO

exerts protective effects on inhibition of renal fibrosis in obstructive nephropathy [99].

3.2.3. CO and Myocardial Fibrosis. Myocardial fibrosis refers to the pathological process in which various harmful stimuli, such as myocardial injury, mechanical stretching, and myocardial inflammation, trigger the proliferation of fibroblasts in heart tissue. This process leads to excessive ECM deposition and disorganization of cardiac structure and function, such as cardiac hypertrophy, heart failure, and arrhythmia [101].

Human immunodeficiency virus (HIV) protease inhibitor-induced cardiac dysfunction is characterized as a pathologic fibrosis related to the activation of TGF- β_1 [102, 103]. Laurence et al. have demonstrated that inhalation of low-dose CO (250 ppm) can suppress ritonavir-induced cardiac fibrosis and which is modulated by the canonical (Smad2) and noncanonical TGF- β_1 signaling pathways. In addition, CO treatment can also suppress the M1 proinflammatory subset of macrophages, while increase M2c subset of macrophages in the hearts of ritonavir-treated mice and which is also associated with CO-induced autophagy [104]. Taken together, the antifibrotic effects of CO are linked to the inhibition of the TGF- β signaling and the stimulation of autophagy as shown in Figure 3.

3.3. The Interference Role of H₂S in Fibrotic Diseases. Hydrogen sulfide is a widely known gas with a malodorous smell and which is the most recently recognized member of gaseous signaling molecules, as well as exhibits remarkable therapeutic characteristics in several pathologies [105]. H₂S is produced endogenously in the cytoplasm and mitochondria of mammalian cells by utilizing L-cysteine and D-cysteine as substrates catalyzed cystathionine- β -synthase (CBS), cystathionine- γ -lyase (CSE), 3-mercaptopyruvate sulfurtransferase (3-MST), and D-amino acid oxidase (DAO) [106–108]. Besides its endogenous production, H₂S can also be produced via its exogenous sources such as sodium hydrosulfide (NaHS), sodium sulfide (Na₂S), S-allyl-cysteine (SAC), GYY4137, AP39, and AP123, SG1002, S-propargyl-cysteine, sodium thiosulfate, sulfurous mineral water, garlic-derived polysulfide, diallyl disulfide, and diallyl sulfide [109]. Numerous studies have shown that low-dose exogenous and endogenous H₂S have therapeutic and protective effects on common organ fibroproliferative diseases and syndromes and which are mainly due to its anti-inflammatory, antioxidant, and antifibrotic properties (Figure 4) [110]. Furthermore, the deficiency in endogenous CBS/H₂S or CSE/H₂S system is involved in the development of fibrosis [111], while the supplementation of exogenous H₂S can significantly inhibit the progression of fibrosis [112–115].

3.3.1. H₂S and Renal Fibrosis. In normal condition, the expression of CBS is predominantly located in proximal renal tubules, while a small amount of CSE is expressed in the renal glomeruli, interstitium, and interlobular arterioles. Moreover, MST is mainly expressed in the proximal tubular epithelium in the kidney [116, 117].

In unilateral ureteral obstruction- (UUO-) induced renal injury and fibrosis mouse model, treatment with H₂S donor NaHS can significantly reduce kidney damage and fibrosis

through the inhibition of M1 and M2 macrophages' infiltration and downregulation of fibrogenic genes [118]. These beneficial effects of NaHS might be contributed to the inactivation of NLRP3, as well as to its downstream signaling pathways and the phosphorylation of the NF- κ B and IL-4/STAT6 signaling pathways [118]. Additionally, in the recovery of the kidney following ischemia/reperfusion (I/R) injury, the levels of CSE, CBS, and H₂S were significantly decreased and which did not recover in eight days as fibrotic lesions were observed. However, the administration of NaHS can accelerate tubular cell proliferation and delay the progression of renal fibrosis by attenuating oxidative stress and inflammation in a mouse model with ureteral obstruction [119].

Angiotensin II (Ang II) and TGF- β can induce renal tubular epithelial-to-mesenchymal (EMT), and the abnormal activation of EMT can lead to the tubular interstitial fibrosis. In the presence of H₂S donor NaHS, the TGF- β signaling pathway and the EMT-promoting effect of Ang II were all decreased and which were contributed to the reduction of TGF- β activity [120]. NaHS can cleave the disulfide bond in the dimeric active TGF- β_1 and subsequently promote to form inactive TGF- β monomer form [120]. This study provides a novel antifibrotic mechanism of H₂S and suggests that H₂S can be used to treat renal sclerotic diseases (Figure 4) [120]. Besides that, NaHS can also affect TGF- β_1 -induced EMT in renal tubular epithelial (HK-2) cells and which might be associated with suppression of both the ERK- and β -catenin-dependent signaling pathways to ameliorate renal fibrosis [121].

3.3.2. H₂S and Myocardial Fibrosis. In mammals, CSE is abundant in the heart, vascular smooth muscle, and vascular endothelial cells. It is the most relevant enzyme in the cardiovascular system to produce H₂S. Increasing evidence demonstrates that endogenous H₂S can participate in attenuating the development of myocardial fibrosis [122]. The decline of H₂S content in heart tissues was significantly correlated with the severity of myocardial fibrosis [122–124]. Ma et al. have demonstrated that chronic aerobic exercise training can upregulate CSE and 3-MST expression. Furthermore, as aged rats were given moderate-intensity exercise or treated with NaHS (intraperitoneal injection of 0.1 mL/kg per day of 0.28 mol/L NaHS), the myocardial hydroxyproline level and fibrotic area in the heart could be declined dramatically, suggesting that exercise could restore bioavailability of H₂S in the heart of aged rats and which partly explained the benefits of exercise against myocardial fibrosis of aged population [125].

Nicotinamide adenine dinucleotide phosphate II (NADPH) oxidase 2 (NOX2) and NADPH oxidase 4 (NOX4) are the main sources of reactive oxygen species (ROS), which play a key role in the fibrotic reaction of cardiac fibroblasts and ischemic myocardium. The exogenous treatment of NaHS and sodium thiosulfate (STS) can remarkably decrease NOX2/4, phosphorylation of ERK1/2, and the generation of ROS to ameliorate oxidative stress-mediated myocardial fibrosis [115, 122]. Moreover, the slow-releasing water-soluble H₂S donor, GYY4137, can reduce adverse remodeling and play postischemic cardioprotective effects through the enhancement of early

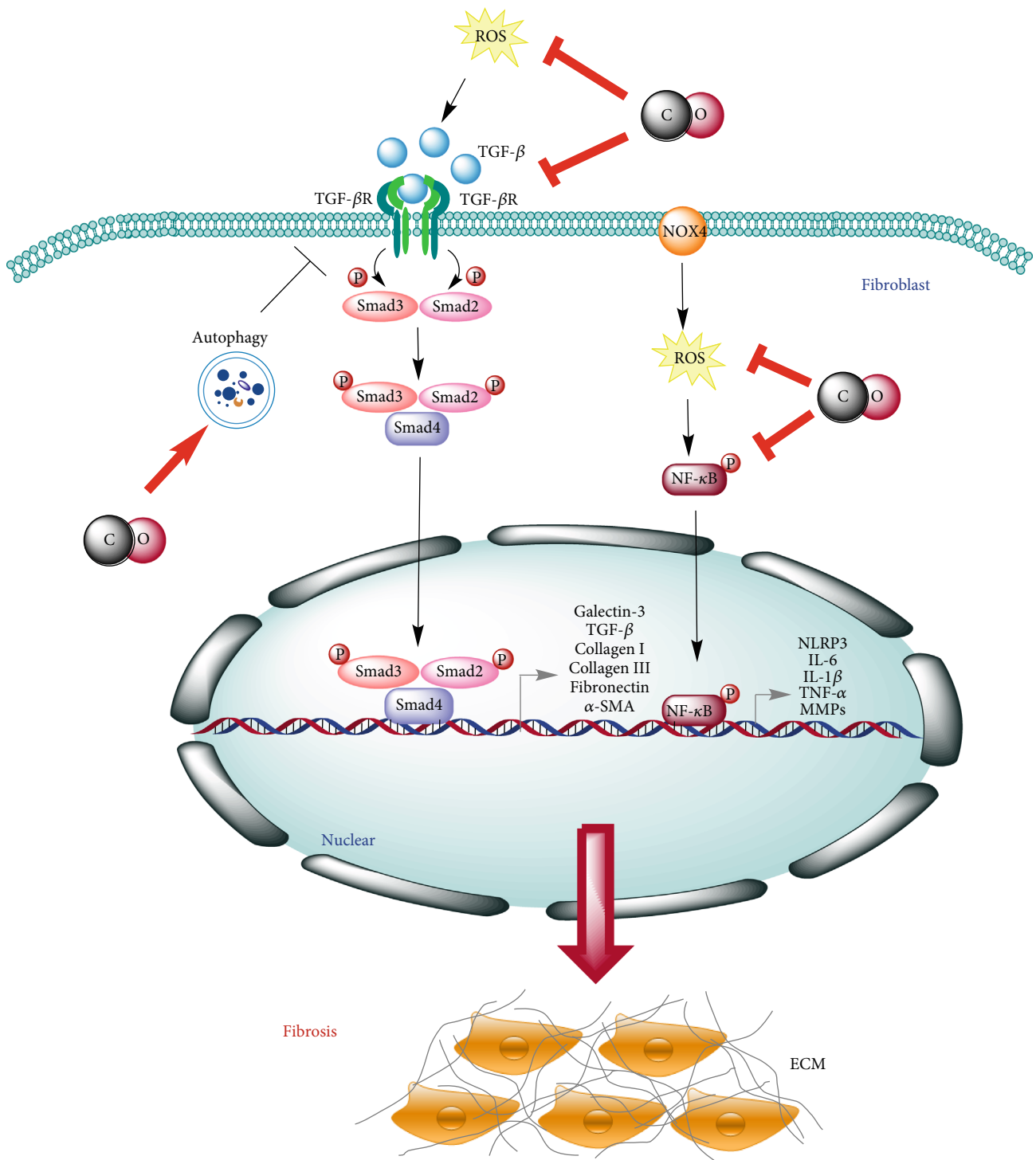


FIGURE 3: The interference mechanisms of CO in fibrotic diseases. Low-dose exogenous and endogenous CO can interfere with the TGF- β and NF- κ B signaling pathway via reducing the expression of fibrosis and inflammatory-related genes. In addition, CO can also inhibit the TGF- β signaling by the stimulation of autophagy.

postischemic endogenous natriuretic peptide activation [123]. Similarly, the administration of GYY4137 can also prevent myocardial infarction-induced adverse cardiac remodeling in both wild type- and CSE-deficient mice [126]. One recent study

reported that after the administration of NaHS, the area of myocardial fibrosis in myocardial infarction (MI) rats is reduced, and the level of type I collagen, type III collagen, and MMP-9 is reduced, and the heart function is improved. This study

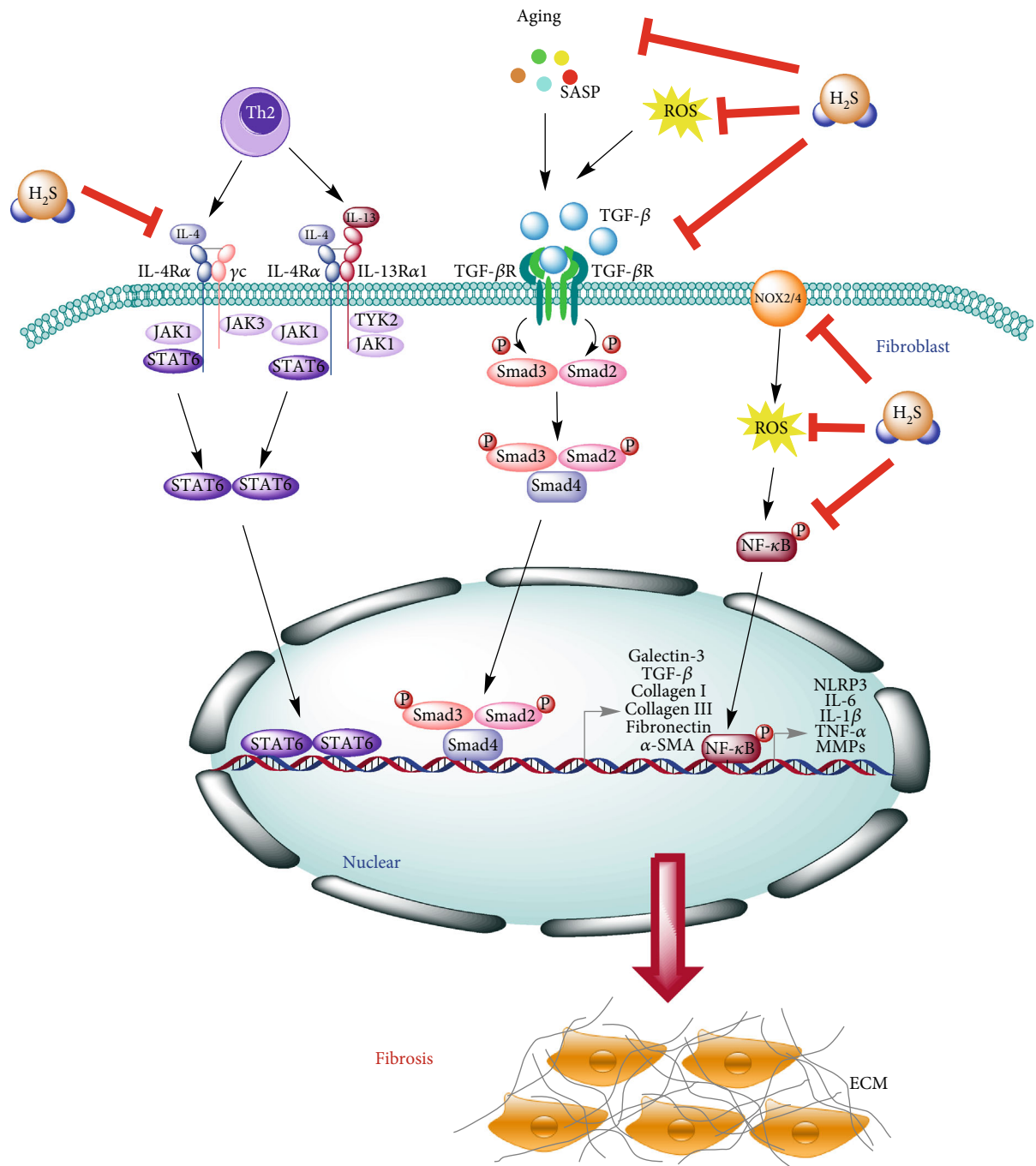


FIGURE 4: The interference mechanisms of H_2S in fibrotic diseases. H_2S can effectively slow down the process of fibrosis through inhibiting the $NF-\kappa B$, $TGF-\beta$, and $IL-4/STAT6$ signaling pathways, as well as attenuating the production of ROS via downregulation of NOX2/4. Moreover, H_2S can also inhibit the formation of NLRP3 inflammasome and the process of aging to control the occurrence and development of fibrosis.

demonstrated that exogenous H_2S potentially prevents heart remodeling by inhibition of extracellular matrix accumulation and increasing blood vessel density [124].

3.3.3. H_2S and Liver Fibrosis. In the combination of carbon tetrachloride (CCl_4) and olive oil-induced liver fibrosis model, the treatment of S-allyl-cysteine (SAC, 50 mg/kg/day), one endogenous donor of H_2S , could significantly reduce the

mRNA expression of inflammatory and fibrotic cytokines, as well as increased the levels of antioxidant relative genes, including superoxide dismutase, catalase, and glutathione peroxidase [127]. Moreover, the treatment of SAC can also decrease the phosphorylation of Smad3 and STAT3, as well as further inhibit their ability to bind to transcription promoters. Therefore, the exogenous donor of H_2S , SAC, can reduce CCl_4 and olive oil-induced liver fibrosis through its

TABLE 1: Related mechanisms of gasotransmitters in fibrotic diseases.

Gasotransmitters	Diseases	Mechanisms	References
NO	Liver fibrosis	SNAP can eliminate the generation of ROS, inhibit the activation and proliferation of HSC, and inhibit the generation of fibrosis.	[66]
	Renal fibrosis	SNAP can amplify the expression of TIMP-1 in a TGF- β -dependent manner and reduce fibrosis.	[71]
	Peyronie's disease	SNAP can inhibit fibrosis by inhibiting the production of ROS, decreasing the expression of collagen 1, and reducing the abundance of myofibroblasts.	[91]
	Liver fibrosis	eNOS can reduce fibrosis by promoting HSC apoptosis and ROS-mediated mitochondrial membrane depolarization to inhibit HSC activation.	[77-79]
	Renal fibrosis	L-arginine can be mediated through a variety of pathways, including inhibiting the expression of TGF- β to reduce fibrosis.	[73]
CO	Idiopathic pulmonary fibrosis	CINOD can inhibit the expression of COX1 and COX2, showing anti-inflammatory and antioxidant effects to resist fibrosis.	[75]
	Activation of mouse embryonic fibroblasts	1 mM CORM3 can reduce the production of collagen I and III and interact with plasma fibronectin to prevent fibrosis.	[96]
	Idiopathic pulmonary fibrosis	CO-HbV reduces the production of ROS by inhibiting the NOX4 signaling and attenuating the TGF- β signaling pathway.	[98]
CO	Idiopathic pulmonary fibrosis	Exogenous 250 ppm CO gas inhibits the synthesis of deposition of ECM and interferes with the proliferation of fibroblasts through the regulation of Id1 expression.	[97]
	Renal fibrosis	250 ppm CO can ameliorate UUO-induced renal fibrosis and protect against kidney injury.	[100]
H ₂ S	Myocardial fibrosis	250 ppm CO can play an antifibrosis effect by inhibiting the TGF- β signaling and stimulating autophagy.	[103, 104]
	Idiopathic pulmonary fibrosis	NaHS can reduce the deposition of collagen and reduce pulmonary fibrosis.	[113]
	Renal fibrosis	NaHS can significantly reduce fibrosis through phosphorylation of the NF- κ B and IL-4/STAT6 signaling pathway and inactivation of NLRP3 and its downstream signaling pathways, inhibiting the infiltration of M1 and M2 macrophages and downregulating fibrogenic genes.	[118]
	Renal fibrosis	NaHS can accelerate the proliferation of renal tubular cells and delay renal fibrosis by reducing oxidative stress and inflammation.	[119]
	Renal fibrosis	NaHS can prevent the formation of fibrosis by reducing the expression of TGF- β .	[120]
	Renal fibrosis	NaHS can inhibit the ERK- and β -catenin-dependent signaling pathways to improve renal fibrosis.	[121]
	Myocardial fibrosis	The chronic aerobic exercise or NaHS administration can downregulate myocardial hydroxyproline level and fibrotic area.	[125]
	Myocardial fibrosis	NaHS can reduce the content of Nox2/4, the phosphorylation of ERK1/2, and ROS, thereby reducing the myocardial fibrosis mediated by oxidative stress.	[115, 122]
	Myocardial fibrosis	NaHS inhibits the accumulation of extracellular matrix and increases blood vessel density to reduce myocardial fibrosis.	[124]
	Liver fibrosis	NaHS can elevate serum H ₂ S level, decrease hyaluronic acid, and reduce the number of activated HSCs.	[131-133]
GYY4137	Diabetic diaphragm fibrosis	NaHS can inhibit the inflammatory response mediated by NLRP3 inflammasome and reduce collagen deposition.	[137]
	Myocardial fibrosis	GYY4137 exerts antifibrosis and cardioprotective effects by enhancing the activation of endogenous natriuretic peptides after early ischemia.	[123, 126]
	Liver fibrosis	SAC can reduce liver fibrosis through its antioxidant and anti-inflammatory properties, as well as inhibiting the STAT3/SMAD3 signaling pathway.	[127]
	Idiopathic pulmonary fibrosis	H2S can inhibit the expression of NF- κ B p65 and downregulate Th2 cells to reduce fibrosis.	[135]

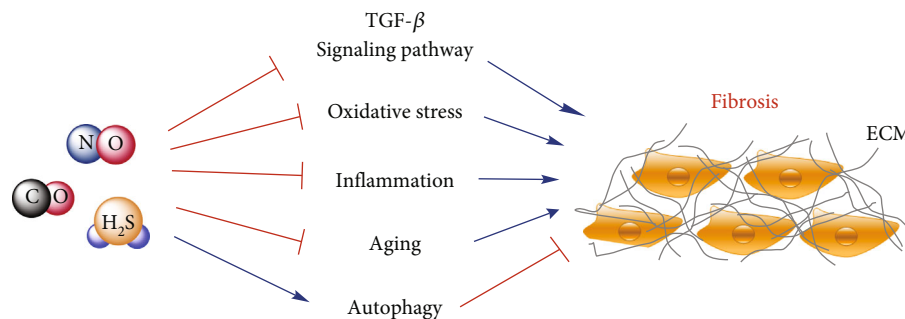


FIGURE 5: Three gasotransmitters, NO, CO, and H₂S, can prevent the development of organ fibrosis through interfering with the TGF- β signaling pathway, oxidative stress, inflammation, and aging and provoking autophagy.

antioxidant and anti-inflammatory features, as well as the inhibition of the STAT3/SMAD3 signaling pathway to control fibrotic gene expression [127].

Several studies indicated that plasma levels of H₂S exhibited a dramatic decline during the progression of hepatic fibrosis [128, 129], and the expression of H₂S produced by CBS and CSE was significantly decreased in patients with cirrhosis-induced portal hypertension [130]. These reports suggested that the inhibition of endogenous H₂S might be associated with the development of human and animal liver fibrosis. For that, the supplementation of NaHS could significantly elevate serum H₂S level, prevent portal pressure, decrease hyaluronic acid and hepatic hydroxyproline levels, and reduce the number of activated HSCs by induction of G1 phase cell cycle arrest [131–133]. Conversely, one recent study found that the exogenous and endogenous H₂S can increase the proliferation and activation of HSCs, and inhibitors of H₂S can decrease the proliferation and fibrotic marks of HSCs, and which is mediated by the cellular bioenergetics [134]. These paradoxical reports suggested that the protective effect and the molecular mechanisms of H₂S in hepatic fibrosis should be proved in further animal and cellular studies.

3.3.4. H₂S and Idiopathic Pulmonary Fibrosis. In one recent study, bleomycin-induced IPF mouse model revealed that the plasma concentration of H₂S and CSE activity in lung tissues was significantly downregulated on day 7, while the injection of sodium hydrosulfide (NaHS, 1.4 and 7 μ mol/kg body weight) could significantly decrease the collagen deposition and the severity of pulmonary fibrosis [113]. The therapeutic effect of H₂S in bleomycin-induced IPF could be attributed to the inhibition of NF- κ B p65 expression and downregulation of Th2 cells [135]. Conversely, a high level of H₂S (50~500 ppm) can lead to bronchiolitis obliterans and pulmonary edema, ultimately leading to chronic inflammation and idiopathic pulmonary fibrosis [136]. These studies clearly suggested that H₂S exhibits two faces of the same coin and the mechanisms by which the excessive administration of H₂S in the promotion of IPF is still not uncovered.

3.3.5. H₂S and Diabetic Diaphragm Fibrosis. Diabetes is related to the failure of multiple organs and can lead to respiratory dysfunction by reducing the endurance of respiratory muscles and lung capacity. The diaphragm is an

important skeletal muscle in the mammalian breathing process [137]. Excessive inflammation of diabetes often leads to collagen deposition and muscle fibrosis. However, one recent study demonstrated that administration of NaHS could ameliorate hyperglycemia-induced diaphragm muscle fibrosis and improved the diaphragmatic biomechanical properties in diabetes mellitus, which might be associated with the alleviation of collagen deposition through the suppression of NLRP3 inflammasome-mediated inflammatory reaction [137]. This report confirmed that the therapeutic strategies aimed at inhibiting NLRP3 inflammasome-mediated fibrosis by utilizing exogenous H₂S might serve as efficient targeted therapy in diabetes mellitus.

3.3.6. H₂S and Peritoneal Fibrosis. Peritoneal fibrosis is one of the long-term complications of peritoneal dialysis (PD) patients [138]. Peritoneal fibrosis model was constructed in Sprague-Dawley rats through intraperitoneally injecting 4.25% glucose PD fluids and lipopolysaccharide. After daily injection of 56 μ g/kg NaHS, this can significantly decrease the biomarkers of inflammation, fibrosis, and angiogenesis in the peritoneum, although the exact molecular mechanisms have not been discovered [139]. The evidence suggests again that the exogenous H₂S possess a strong antifibrotic property and which can be a potential therapy against peritoneal fibrosis during chronic PD.

4. Conclusion and Perspectives

According to these reports, many stress responses and molecular targets are involved in the formation and development of fibrosis. Among them, the activations of the TGF- β signaling pathway, oxidative stress, chronic inflammation, and aging are considered as key regulatory targets (Figure 1). Three well-known gasotransmitters, NO, CO, and H₂S, are demonstrated to regulate the development of fibrotic diseases mainly through anti-inflammation, antioxidation, antiapoptosis, and the induction of autophagy (Table 1). To date, although a great number of animal experiments have reported that these gasotransmitters exhibited various beneficial effects (Figure 5) on delaying the process of fibrotic disease, more clinical trials are necessary to be applied for proving their therapeutic effects on fibrotic diseases. In addition, to support more evidence about their preventive effects, the detailed molecular and

cellular mechanisms are also needed to be further clarified. In the future study, given the synergistic effect of these gasotransmitters on fibrotic diseases, the combinatorial treatment of exogenous NO, CO, and H₂S donors can be applied for delaying the process of fibrosis. Moreover, it is necessary to develop and utilize more effective gas donors as important components of health products for the prevention and treatment of fibrotic diseases.

Abbreviations

3-MST:	3-Mercaptopyruvate sulfurtransferase
α -SMA:	α -Smooth muscle actin
ATF2:	Cyclic AMP-dependent transcription factor 2
ASK-1:	Apoptosis signal-regulating kinase 1
AGE:	Advanced glycation end-products
Atg7:	Autophagy-related protein 7
CO:	Carbon monoxide
CORMs:	Carbon monoxide-releasing molecules
CCl ₄ :	Carbon tetrachloride
JNK:	c-Jun N-terminal kinase
CO-HbV:	CO-bound hemoglobin vesicles
CHF:	Congenital hepatic fibrosis
CTGF/CCN2:	Connective tissue growth factor
CINODs:	Cyclooxygenase-inhibiting NO donors
CBS:	Cystathionine- β -synthase
CSE:	Cystathionine- γ -lyase
DAO:	D-Amino acid oxidase
ET-1:	Endothelin 1
EMT:	Endothelial-mesenchymal transition
ECM:	Extracellular matrix
FN:	Fibronectin
GMCs:	Glomerular mesangial cells
GSH:	Glutathione
GS:	Glycine-serine
HO:	Heme oxygenase
HSCs:	Hepatic stellate cells
HIV:	Human immunodeficiency virus
H ₂ S:	Hydrogen sulfide
IPF:	Idiopathic pulmonary fibrosis
Id1:	Inhibitor of DNA binding 1
IGFBP:	Insulin-like growth factor-binding proteins
KLF4:	Krüppel-like factor 4
KLF2:	Krüppel-like factor 2
LSECs:	Liver sinusoidal endothelial cells
MMP:	Matrix metalloproteinase
MEFs:	Mouse embryonic fibroblasts
MI:	Myocardial infarction
NOX:	Nicotinamide adenine dinucleotide phosphate II (NADPH) oxidase
NLRP3:	NOD-like receptor protein 3
NO:	Nitric oxide
NOS:	NO synthase
NF- κ B:	Nuclear factor- κ B
PD:	Peyronie's disease
PAI-1:	Plasminogen activator inhibitor-1
PDGF:	Platelet-derived growth factor
ROS:	Reactive oxygen species

SAC:	S-Allyl-cysteine
SASP:	Senescence-associated secretory phenotype
STAT6:	Signal transducers and activators of transcription 6
SNAP:	S-Nitroso-N-acetylpenicillamine
NaHS:	Sodium hydrosulfide
Na ₂ S:	Sodium sulfide
SOD:	Superoxide dismutase
TIMP1:	Tissue inhibitor matrix metalloproteinase 1
TGF- β :	Transforming growth factor β
TA:	Tunica albuginea
UUO:	Unilateral ureteral obstruction.

Data Availability

The data used to support this study are included within the article.

Conflicts of Interest

All authors have disclosed that they do not have any conflicts of interest.

Authors' Contributions

Yingqing Chen, Shuo Yuan, Yuying Cao, Guangyao Kong, Feng Jiang, You Li, Qi Wang, and Minli Tang contributed to the collection of reference. Yingqing Chen, Shuo Yuan, and Yuying Cao contributed to the analysis of reference and writing of the manuscript. Liping Liu, Yingqing Chen, and Qianqian Wang contributed to the topic conception, manuscript revision, and decision to submit for publication. Liping Liu, Qianqian Wang, and Qinggao Zhang contributed to reference analysis (corresponding authors). Yingqing Chen, Shuo Yuan, and Yuying Cao contributed equally to this work (co-first authors).

Acknowledgments

This work was supported by the National Natural Science Foundation of China (82000074 and 61671098), the Scientific Research Funding Project of Education Department of Liaoning Province (jyt-dldxjc202005), the Natural Science Fund of the Science and Technology Department of Liaoning Province (20180550388), the Science and Technology Innovation Fund Project of Dalian (2020JJ27SN071), and the Dalian Youth Science and Technology Star Research Project (2020RQ080).

References

- [1] T. A. Wynn and T. R. Ramalingam, "Mechanisms of fibrosis: therapeutic translation for fibrotic disease," *Nature Medicine*, vol. 18, no. 7, pp. 1028–1040, 2012.
- [2] P. J. Wermuth and S. A. Jimenez, "The significance of macrophage polarization subtypes for animal models of tissue fibrosis and human fibrotic diseases," *Clinical and Translational Medicine*, vol. 4, no. 1, p. 2, 2015.
- [3] T. Krieg, D. Abraham, and R. Lafyatis, "Fibrosis in connective tissue disease: the role of the myofibroblast and fibroblast-

- epithelial cell interactions,” *rthritis Research & Therapy*, vol. 9, Supplement 2, p. S4, 2007.
- [4] L. Zhang, C. Liu, X. M. Meng, C. Huang, F. Xu, and J. Li, “Smad2 protects against TGF- β 1/Smad3-mediated collagen synthesis in human hepatic stellate cells during hepatic fibrosis,” *Molecular and Cellular Biochemistry*, vol. 400, no. 1-2, pp. 17–28, 2015.
 - [5] Y. E. Zhang, “Non-Smad signaling pathways of the TGF- β family,” *Cold Spring Harbor Perspectives in Biology*, vol. 9, no. 2, 2017.
 - [6] J. Jiang, N. L. Leong, U. Khaliq, T. M. Phan, K. M. Lyons, and J. V. Luck Jr., “Connective tissue growth factor (CTGF/CCN2) in haemophilic arthropathy and arthrofibrosis: a histological analysis,” *Haemophilia*, vol. 22, no. 6, pp. e527–e536, 2016.
 - [7] B. M. Klinkhammer, J. Floege, and P. Boor, “PDGF in organ fibrosis,” *Molecular Aspects of Medicine*, vol. 62, pp. 44–62, 2018.
 - [8] R. Rohatgi, L. Milenkovic, R. B. Corcoran, and M. P. Scott, “Hedgehog signal transduction by Smoothed: pharmacologic evidence for a 2-step activation process,” *Proceedings of the National Academy of Sciences of the United States of America*, vol. 106, no. 9, pp. 3196–3201, 2009.
 - [9] Y. Bai, Y. Bai, J. Dong et al., “Hedgehog signaling in pancreatic fibrosis and cancer,” *Medicine*, vol. 95, no. 10, article e2996, 2016.
 - [10] A. Engler, R. Zhang, and V. Taylor, “Notch and neurogenesis,” *Advances in Experimental Medicine and Biology*, vol. 1066, pp. 223–234, 2018.
 - [11] R. Santoro and A. Mangia, “Progress in promising anti-fibrotic therapies,” *Expert Review of Gastroenterology & Hepatology*, vol. 13, no. 12, pp. 1145–1152, 2019.
 - [12] K. D. Hendriks, H. Maassen, P. R. van Dijk, R. H. Henning, H. van Goor, and J. L. Hillebrands, “Gasotransmitters in health and disease: a mitochondria-centered view,” *Current Opinion in Pharmacology*, vol. 45, pp. 87–93, 2019.
 - [13] Y. Itatani, K. Kawada, and Y. Sakai, “Transforming growth factor- β signaling pathway in colorectal cancer and its tumor microenvironment,” *International Journal of Molecular Sciences*, vol. 20, no. 23, p. 5822, 2019.
 - [14] L. Zhao, Y. Zou, and F. Liu, “Transforming growth factor-beta1 in diabetic kidney disease,” *Frontiers in Cell and Development Biology*, vol. 8, p. 187, 2020.
 - [15] H. Wu, Y. Sun, W. L. Wong et al., “The development of a novel transforming growth factor- β (TGF- β) inhibitor that disrupts ligand-receptor interactions,” *European Journal of Medicinal Chemistry*, vol. 189, article 112042, 2020.
 - [16] X. Zhang, H. Xie, P. Chang et al., “Glycoprotein M6B interacts with T β RI to activate TGF- β -Smad2/3 signaling and promote smooth muscle cell differentiation,” *Stem Cells*, vol. 37, no. 2, pp. 190–201, 2019.
 - [17] R. M. Hussein, M. M. Anwar, H. S. Farghaly, and M. A. Kandil, “Gallic acid and ferulic acid protect the liver from thioacetamide-induced fibrosis in rats via differential expression of miR-21, miR-30 and miR-200 and impact on TGF- β 1/Smad3 signaling,” *Chemico-Biological Interactions*, vol. 324, article 109098, 2020.
 - [18] C. Shimizu, T. Oharaseki, K. Takahashi, A. Kottek, A. Franco, and J. C. Burns, “The role of TGF- β and myofibroblasts in the arteritis of Kawasaki disease,” *Human Pathology*, vol. 44, no. 2, pp. 189–198, 2013.
 - [19] C. Gehlken, N. Suthahar, W. C. Meijers, and R. A. de Boer, “Galectin-3 in heart failure: an update of the last 3 years,” *Heart Failure Clinics*, vol. 14, no. 1, pp. 75–92, 2018.
 - [20] K. Daenen, A. Andries, D. Mekahli, A. Van Schepdael, F. Jouret, and B. Bammens, “Oxidative stress in chronic kidney disease,” *Pediatric Nephrology*, vol. 34, no. 6, pp. 975–991, 2019.
 - [21] K. Richter and T. Kietzmann, “Reactive oxygen species and fibrosis: further evidence of a significant liaison,” *Cell and Tissue Research*, vol. 365, no. 3, pp. 591–605, 2016.
 - [22] K. Mortezaee, “Nicotinamide adenine dinucleotide phosphate (NADPH) oxidase (NOX) and liver fibrosis: a review,” *Cell Biochemistry and Function*, vol. 36, no. 6, pp. 292–302, 2018.
 - [23] T. Luangmonkong, S. Suriguga, H. A. M. Mutsaers, G. M. M. Groothuis, P. Olinga, and M. Boersema, “Targeting oxidative stress for the treatment of liver fibrosis,” *Reviews of Physiology, Biochemistry and Pharmacology*, vol. 175, pp. 71–102, 2018.
 - [24] L. J. Dixon, M. Barnes, H. Tang, M. T. Pritchard, and L. E. Nagy, “Kupffer cells in the liver,” *Comprehensive Physiology*, vol. 3, no. 2, pp. 785–797, 2013.
 - [25] W. C. Lee, S. S. Mokhtar, S. Munisamy, S. Yahaya, and A. H. G. Rasool, “Vitamin D status and oxidative stress in diabetes mellitus,” *Cellular and Molecular Biology*, vol. 64, no. 7, 2018.
 - [26] Y. L. Lee, C. W. Chen, F. H. Liu, Y. W. Huang, and H. M. Huang, “Aclacinomycin A sensitizes K562 chronic myeloid leukemia cells to imatinib through p38MAPK-mediated erythroid differentiation,” *PLoS One*, vol. 8, no. 4, article e61939, 2013.
 - [27] H. M. Kang, S. H. Ahn, P. Choi et al., “Defective fatty acid oxidation in renal tubular epithelial cells has a key role in kidney fibrosis development,” *Nature Medicine*, vol. 21, no. 1, pp. 37–46, 2015.
 - [28] K. Sinha, J. Das, P. B. Pal, and P. C. Sil, “Oxidative stress: the mitochondria-dependent and mitochondria-independent pathways of apoptosis,” *Archives of Toxicology*, vol. 87, no. 7, pp. 1157–1180, 2013.
 - [29] T. Yu, Y. J. Li, A. H. Bian et al., “The regulatory role of activating transcription factor 2 in inflammation,” *Mediators of Inflammation*, vol. 2014, Article ID 950472, 10 pages, 2014.
 - [30] I. Pant, S. G. Rao, and P. Kondaiah, “Role of arca nut induced JNK/ATF2/Jun axis in the activation of TGF- β pathway in precancerous oral submucous fibrosis,” *Scientific Reports*, vol. 6, no. 1, article 34314, 2016.
 - [31] Y. Akiyama, F. Ogawa, Y. Iwata et al., “Autoantibody against activating transcription factor-2 in patients with systemic sclerosis,” *Clinical and Experimental Rheumatology*, vol. 27, no. 5, pp. 751–757, 2009.
 - [32] W. Y. Liu, S. S. Liou, T. Y. Hong, and I. M. Liu, “Protective effects of hesperidin (citrus flavonone) on high glucose induced oxidative stress and apoptosis in a cellular model for diabetic retinopathy,” *Nutrients*, vol. 9, no. 12, p. 1312, 2017.
 - [33] X. Chen, J. Li, M. Li et al., “KH902 suppresses high glucose-induced migration and sprouting of human retinal endothelial cells by blocking VEGF and PIGF,” *Diabetes Obesity & Metabolism*, vol. 15, no. 3, pp. 224–233, 2013.
 - [34] M. S. Dzeshka, F. Shahid, A. Shantsila, and G. Y. H. Lip, “Hypertension and atrial fibrillation: an intimate association

- of epidemiology, pathophysiology, and outcomes,” *American Journal of Hypertension*, vol. 30, no. 8, pp. 733–755, 2017.
- [35] C. López-Otín, M. A. Blasco, L. Partridge, M. Serrano, and G. Kroemer, “The hallmarks of aging,” *Cell*, vol. 153, no. 6, pp. 1194–1217, 2013.
- [36] D. Muñoz-Espín and M. Serrano, “Cellular senescence: from physiology to pathology,” *Nature Reviews. Molecular Cell Biology*, vol. 15, no. 7, pp. 482–496, 2014.
- [37] S. Disayabutr, E. K. Kim, S. I. Cha et al., “miR-34 miRNAs regulate cellular senescence in type II alveolar epithelial cells of patients with idiopathic pulmonary fibrosis,” *PLoS One*, vol. 11, no. 6, article e0158367, 2016.
- [38] R. Yosef, N. Pilpel, N. Papismadov et al., “p21 maintains senescent cell viability under persistent DNA damage response by restraining JNK and caspase signaling,” *The EMBO Journal*, vol. 36, no. 15, pp. 2280–2295, 2017.
- [39] M. Lehmann, M. Korfei, K. Mutze et al., “Senolytic drugs target alveolar epithelial cell function and attenuate experimental lung fibrosis *in vivo*,” *European Respiratory Journal*, vol. 50, no. 2, article 1602367, 2017.
- [40] A. Tasanarong, S. Kongkham, and S. Khositseth, “Dual inhibiting senescence and epithelial-to-mesenchymal transition by erythropoietin preserve tubular epithelial cell regeneration and ameliorate renal fibrosis in unilateral ureteral obstruction,” *BioMed Research International*, vol. 2013, Article ID 308130, 12 pages, 2013.
- [41] C. le Maitre, A. J. Freemont, and J. A. Hoyland, “Accelerated cellular senescence in degenerate intervertebral discs: a possible role in the pathogenesis of intervertebral disc degeneration,” *Arthritis Research & Therapy*, vol. 9, no. 3, p. R45, 2007.
- [42] M. Fang, J. Wang, S. Li, and Y. Guo, “Advanced glycation end-products accelerate the cardiac aging process through the receptor for advanced glycation end-products/transforming growth factor- β -Smad signaling pathway in cardiac fibroblasts,” *Geriatrics & Gerontology International*, vol. 16, no. 4, pp. 522–527, 2016.
- [43] H. Nishizawa, G. Iguchi, H. Fukuoka et al., “IGF-I induces senescence of hepatic stellate cells and limits fibrosis in a p53-dependent manner,” *Scientific Reports*, vol. 6, no. 1, article 34605, 2016.
- [44] A. E. Handayaningsih, M. Takahashi, H. Fukuoka et al., “IGF-I enhances cellular senescence via the reactive oxygen species-p53 pathway,” *Biochemical and Biophysical Research Communications*, vol. 425, no. 2, pp. 478–484, 2012.
- [45] X. Kong, D. Feng, H. Wang et al., “Interleukin-22 induces hepatic stellate cell senescence and restricts liver fibrosis in mice,” *Hepatology*, vol. 56, no. 3, pp. 1150–1159, 2012.
- [46] M. Mack, “Inflammation and fibrosis,” *Matrix Biology*, vol. 68–69, pp. 106–121, 2018.
- [47] M. Jeljeli, L. G. C. Riccio, L. Doridot et al., “Trained immunity modulates inflammation-induced fibrosis,” *Nature Communications*, vol. 10, no. 1, p. 5670, 2019.
- [48] S. Kolahian, I. E. Fernandez, O. Eickelberg, and D. Hartl, “Immune mechanisms in pulmonary fibrosis,” *American Journal of Respiratory Cell and Molecular Biology*, vol. 55, no. 3, pp. 309–322, 2016.
- [49] S. C. Sun, “The noncanonical NF- κ B pathway,” *Immunological Reviews*, vol. 246, no. 1, pp. 125–140, 2012.
- [50] Y. Wen, X. Lu, J. Ren et al., “KLF4 in macrophages attenuates TNF α -mediated kidney injury and fibrosis,” *Journal of the American Society of Nephrology*, vol. 30, no. 10, pp. 1925–1938, 2019.
- [51] D. Izadi, T. B. Layton, L. Williams et al., “Identification of TNFR2 and IL-33 as therapeutic targets in localized fibrosis,” *Science Advances*, vol. 5, no. 12, article eaay0370, 2019.
- [52] C. Yu-Wai-Man, A. D. Tagalakakis, J. Meng et al., “Genotype-phenotype associations of IL6 and PRG4 with conjunctival fibrosis after glaucoma surgery,” *JAMA Ophthalmology*, vol. 135, no. 11, pp. 1147–1155, 2017.
- [53] L. Forcina, C. Miano, B. M. Scicchitano, and A. Musarò, “Signals from the niche: insights into the role of IGF-1 and IL-6 in modulating skeletal muscle fibrosis,” *Cells*, vol. 8, no. 3, p. 232, 2019.
- [54] A. R. Mridha, A. Wree, A. A. B. Robertson et al., “NLRP3 inflammasome blockade reduces liver inflammation and fibrosis in experimental NASH in mice,” *Journal of Hepatology*, vol. 66, no. 5, pp. 1037–1046, 2017.
- [55] H. Zhang and Z. Wang, “Effect and regulation of the NLRP3 inflammasome during renal fibrosis,” *Frontiers in Cell and Development Biology*, vol. 7, p. 379, 2020.
- [56] S. Su, Q. Zhao, C. He et al., “miR-142-5p and miR-130a-3p are regulated by IL-4 and IL-13 and control profibrogenic macrophage program,” *Nature Communications*, vol. 6, no. 1, article 8523, 2015.
- [57] C. Jakubzick, E. S. Choi, B. H. Joshi et al., “Therapeutic attenuation of pulmonary fibrosis via targeting of IL-4- and IL-13-responsive cells,” *The Journal of Immunology*, vol. 171, no. 5, pp. 2684–2693, 2003.
- [58] S. A. Nam, W. Y. Kim, J. W. Kim et al., “Autophagy attenuates tubulointerstitial fibrosis through regulating transforming growth factor- β and NLRP3 inflammasome signaling pathway,” *Cell Death & Disease*, vol. 10, no. 2, p. 78, 2019.
- [59] S. M. Kim, Y. G. Kim, D. J. Kim et al., “Inflammasome-independent role of NLRP3 mediates mitochondrial regulation in renal injury,” *Frontiers in Immunology*, vol. 9, article 2563, 2018.
- [60] A. T. J. Maria, P. Rozier, G. Fonteneau et al., “iNOS activity is required for the therapeutic effect of mesenchymal stem cells in experimental systemic sclerosis,” *Frontiers in Immunology*, vol. 9, article 3056, 2018.
- [61] J. O. Lundberg, M. T. Gladwin, and E. Weitzberg, “Strategies to increase nitric oxide signalling in cardiovascular disease,” *Nature Reviews. Drug Discovery*, vol. 14, no. 9, pp. 623–641, 2015.
- [62] C. Bogdan, “Nitric oxide and the immune response,” *Nature Immunology*, vol. 2, no. 10, pp. 907–916, 2001.
- [63] J. Y. Chang, W. D. Stamer, J. Bertrand et al., “Role of nitric oxide in murine conventional outflow physiology,” *American Journal of Physiology-Cell Physiology*, vol. 309, no. 4, pp. C205–C214, 2015.
- [64] T. Yang, A. N. Zelikin, and R. Chandrawati, “Progress and promise of nitric oxide-releasing platforms,” *Advanced Science*, vol. 5, no. 6, article 1701043, 2018.
- [65] P. Vallance, “Nitric oxide: therapeutic opportunities,” *Fundamental & Clinical Pharmacology*, vol. 17, no. 1, pp. 1–10, 2003.
- [66] G. Svegliati-Baroni, S. Saccomanno, H. van Goor, P. Jansen, A. Benedetti, and H. Moshage, “Involvement of reactive oxygen species and nitric oxide radicals in activation and proliferation of rat hepatic stellate cells,” *Liver*, vol. 21, no. 1, pp. 1–12, 2001.









- [67] Y. Iwakiri and M. Y. Kim, "Nitric oxide in liver diseases," *Trends in Pharmacological Sciences*, vol. 36, no. 8, pp. 524–536, 2015.
- [68] S. Anavi, M. Eisenberg-Bord, M. Hahn-Obercyger, O. Genin, M. Pines, and O. Tirosh, "The role of iNOS in cholesterol-induced liver fibrosis," *Laboratory Investigation*, vol. 95, no. 8, pp. 914–924, 2015.
- [69] D. C. Rockey and J. J. Chung, "Reduced nitric oxide production by endothelial cells in cirrhotic rat liver: endothelial dysfunction in portal hypertension," *Gastroenterology*, vol. 114, no. 2, pp. 344–351, 1998.
- [70] J. Wani, M. Carl, A. Henger, P. J. Nelson, and H. Rupperecht, "Nitric oxide modulates expression of extracellular matrix genes linked to fibrosis in kidney mesangial cells," *Biological Chemistry*, vol. 388, no. 5, pp. 497–506, 2007.
- [71] E.-S. Akool, A. Doller, R. Müller et al., "Nitric Oxide Induces TIMP-1 Expression by Activating the Transforming Growth Factor β -Smad Signaling Pathway," *Journal of Biological Chemistry*, vol. 280, no. 47, pp. 39403–39416, 2005.
- [72] Y. H. Chuang, W. L. Chuang, S. P. Huang, and C. H. Huang, "Roles of nitric oxide and nitric oxide synthases in tissue damage of obstructed ureters in rats," *Scandinavian Journal of Urology and Nephrology*, vol. 39, no. 3, pp. 187–193, 2005.
- [73] H. Peters, W. A. Border, and N. A. Noble, "Tandem antifibrotic actions of L-arginine supplementation and low protein diet during the repair phase of experimental glomerulonephritis," *Kidney International*, vol. 57, no. 3, pp. 992–1001, 2000.
- [74] S. Noguchi, K. Yatera, K. Y. Wang et al., "Nitric oxide exerts protective effects against bleomycin-induced pulmonary fibrosis in mice," *Respiratory Research*, vol. 15, no. 1, p. 92, 2014.
- [75] A. Pini, S. Viappiani, M. Bolla, E. Masini, and D. Bani, "Prevention of bleomycin-induced lung fibrosis in mice by a novel approach of parallel inhibition of cyclooxygenase and nitric-oxide donation using NCX 466, a prototype cyclooxygenase inhibitor and nitric-oxide donor," *The Journal of Pharmacology and Experimental Therapeutics*, vol. 341, no. 2, pp. 493–499, 2012.
- [76] V. Hernandez-Gea and S. L. Friedman, "Pathogenesis of liver fibrosis," *Annual Review of Pathology*, vol. 6, no. 1, pp. 425–456, 2011.
- [77] L. D. Deleve, X. Wang, and Y. Guo, "Sinusoidal endothelial cells prevent rat stellate cell activation and promote reversion to quiescence," *Hepatology*, vol. 48, no. 3, pp. 920–930, 2008.
- [78] G. Marrone, L. Russo, E. Rosado et al., "The transcription factor KLF2 mediates hepatic endothelial protection and paracrine endothelial-stellate cell deactivation induced by statins," *Journal of Hepatology*, vol. 58, no. 1, pp. 98–103, 2013.
- [79] D. A. Langer, A. Das, D. Semela et al., "Nitric oxide promotes caspase-independent hepatic stellate cell apoptosis through the generation of reactive oxygen species," *Hepatology*, vol. 47, no. 6, pp. 1983–1993, 2008.
- [80] M. V. Nastase, J. Zeng-Brouwers, M. Wygrecka, and L. Schaefer, "Targeting renal fibrosis: mechanisms and drug delivery systems," *Advanced Drug Delivery Reviews*, vol. 129, pp. 295–307, 2018.
- [81] P. Delanaye, R. J. Glasscock, and M. E. De Broe, "Epidemiology of chronic kidney disease: think (at least) twice!," *Clinical Kidney Journal*, vol. 10, no. 3, pp. 370–374, 2017.
- [82] S. J. Chadban and R. C. Atkins, "Glomerulonephritis," *The Lancet*, vol. 365, no. 9473, pp. 1797–1806, 2005.
- [83] W. Eberhardt, T. Beeg, K. F. Beck et al., "Nitric oxide modulates expression of matrix metalloproteinase-9 in rat mesangial cells," *Kidney International*, vol. 57, no. 1, pp. 59–69, 2000.
- [84] W. Eberhardt, K. F. Beck, and J. Pfeilschifter, "Cytokine-induced expression of tPA is differentially modulated by NO and ROS in rat mesangial cells," *Kidney International*, vol. 61, no. 1, pp. 20–30, 2002.
- [85] L. Richeldi, H. R. Collard, and M. G. Jones, "Idiopathic pulmonary fibrosis," *The Lancet*, vol. 389, no. 10082, pp. 1941–1952, 2017.
- [86] D. Saleh, P. J. Barnes, and A. Giaid, "Increased production of the potent oxidant peroxynitrite in the lungs of patients with idiopathic pulmonary fibrosis," *American Journal of Respiratory and Critical Care Medicine*, vol. 155, no. 5, pp. 1763–1769, 1997.
- [87] E. Lakari, Y. Soini, M. Säily, P. Koistinen, P. Pääkkö, and V. L. Kinnula, "Inducible nitric oxide synthase, but not xanthine oxidase, is highly expressed in interstitial pneumonias and granulomatous diseases of human lung," *American Journal of Clinical Pathology*, vol. 117, no. 1, pp. 132–142, 2002.
- [88] P. Almodéver, J. Milara, A. De Diego et al., "Role of tetrahydrobiopterin in pulmonary vascular remodelling associated with pulmonary fibrosis," *Thorax*, vol. 68, no. 10, pp. 938–948, 2013.
- [89] W. J. Hellstrom and T. J. Bivalacqua, "Peyronie's disease: etiology, medical, and surgical therapy," *Journal of Andrology*, vol. 21, no. 3, pp. 347–354, 2000.
- [90] N. F. Gonzalez-Cadavid, T. R. Magee, M. Ferrini, A. Qian, D. Vernet, and J. Rajfer, "Gene expression in Peyronie's disease," *International Journal of Impotence Research*, vol. 14, no. 5, pp. 361–374, 2002.
- [91] D. Vernet, M. G. Ferrini, E. G. Valente et al., "Effect of nitric oxide on the differentiation of fibroblasts into myofibroblasts in the Peyronie's fibrotic plaque and in its rat model," *Nitric Oxide*, vol. 7, no. 4, pp. 262–276, 2002.
- [92] M. D. Maines, "The heme oxygenase system: a regulator of second messenger gases," *Annual Review of Pharmacology and Toxicology*, vol. 37, no. 1, pp. 517–554, 1997.
- [93] D. Stucki and W. Stahl, "Carbon monoxide - beyond toxicity?," *Toxicology Letters*, vol. 333, pp. 251–260, 2020.
- [94] R. Motterlini, B. E. Mann, T. R. Johnson, J. E. Clark, R. Foresti, and C. J. Green, "Bioactivity and pharmacological actions of carbon monoxide-releasing molecules," *Current Pharmaceutical Design*, vol. 9, no. 30, pp. 2525–2539, 2003.
- [95] R. Motterlini, P. Sawle, J. Hammad et al., "CORM-A1: a new pharmacologically active carbon monoxide-releasing molecule," *The FASEB Journal*, vol. 19, no. 2, pp. 284–286, 2005.
- [96] T. Aki, K. Unuma, K. Noritake, H. Kurahashi, T. Funakoshi, and K. Uemura, "Interaction of carbon monoxide-releasing ruthenium carbonyl CORM-3 with plasma fibronectin," *Toxicology In Vitro*, vol. 50, pp. 201–209, 2018.
- [97] Z. Zhou, R. Song, C. L. Fattman et al., "Carbon monoxide suppresses bleomycin-induced lung fibrosis," *The American Journal of Pathology*, vol. 166, no. 1, pp. 27–37, 2005.
- [98] S. Nagao, K. Taguchi, H. Sakai et al., "Carbon monoxide-bound hemoglobin-vesicles for the treatment of bleomycin-induced pulmonary fibrosis," *Biomaterials*, vol. 35, no. 24, pp. 6553–6562, 2014.

- [99] I. O. Rosas, H. J. Goldberg, H. R. Collard et al., "A phase II clinical trial of low-dose inhaled carbon monoxide in idiopathic pulmonary fibrosis," *Chest*, vol. 153, no. 1, pp. 94–104, 2018.
- [100] L. Wang, J. Y. Lee, J. H. Kwak, Y. He, S. I. Kim, and M. E. Choi, "Protective effects of low-dose carbon monoxide against renal fibrosis induced by unilateral ureteral obstruction," *American Journal of Physiology Renal Physiology*, vol. 294, no. 3, pp. F508–F517, 2008.
- [101] L. Yue, J. Xie, and S. Nattel, "Molecular determinants of cardiac fibroblast electrical function and therapeutic implications for atrial fibrillation," *Cardiovascular Research*, vol. 89, no. 4, pp. 744–753, 2011.
- [102] R. P. Shannon, M. A. Simon, M. A. Mathier, Y. J. Geng, S. Mankad, and A. A. Lackner, "Dilated cardiomyopathy associated with simian AIDS in nonhuman primates," *Circulation*, vol. 101, no. 2, pp. 185–193, 2000.
- [103] J. A. Walker, M. L. Sulciner, K. D. Nowicki, A. D. Miller, T. H. Burdo, and K. C. Williams, "Elevated numbers of CD163+ macrophages in hearts of simian immunodeficiency virus-infected monkeys correlate with cardiac pathology and fibrosis," *AIDS Research and Human Retroviruses*, vol. 30, no. 7, pp. 685–694, 2014.
- [104] J. Laurence, S. Elhadad, T. Robison et al., "HIV protease inhibitor-induced cardiac dysfunction and fibrosis is mediated by platelet-derived TGF- β 1 and can be suppressed by exogenous carbon monoxide," *PLoS One*, vol. 12, no. 10, article e0187185, 2017.
- [105] G. J. Dugbartey, "H₂S as a possible therapeutic alternative for the treatment of hypertensive kidney injury," *Nitric Oxide*, vol. 64, pp. 52–60, 2017.
- [106] Y. Mikami, N. Shibuya, Y. Kimura, N. Nagahara, Y. Ogasawara, and H. Kimura, "Thioredoxin and dihydroliipoic acid are required for 3-mercaptopyruvate sulfurtransferase to produce hydrogen sulfide," *Biochemical Journal*, vol. 439, no. 3, pp. 479–485, 2011.
- [107] M. Xia, L. Chen, R. W. Muh, P. L. Li, and N. Li, "Production and actions of hydrogen sulfide, a novel gaseous bioactive substance, in the kidneys," *The Journal of Pharmacology and Experimental Therapeutics*, vol. 329, no. 3, pp. 1056–1062, 2009.
- [108] N. Shibuya, S. Koike, M. Tanaka et al., "A novel pathway for the production of hydrogen sulfide from D-cysteine in mammalian cells," *Nature Communications*, vol. 4, no. 1, p. 1366, 2013.
- [109] C. R. Powell, K. M. Dillon, and J. B. Matson, "A review of hydrogen sulfide (H₂S) donors: Chemistry and potential therapeutic applications," *Biochemical Pharmacology*, vol. 149, pp. 110–123, 2018.
- [110] S. Zhang, C. Pan, F. Zhou et al., "Hydrogen sulfide as a potential therapeutic target in fibrosis," *Oxidative Medicine and Cellular Longevity*, vol. 2015, Article ID 593407, 12 pages, 2015.
- [111] L. P. Fang, Q. Lin, C. S. Tang, and X. M. Liu, "Hydrogen sulfide attenuates epithelial-mesenchymal transition of human alveolar epithelial cells," *Pharmacological Research*, vol. 61, no. 4, pp. 298–305, 2010.
- [112] K. J. Jung, H. S. Jang, J. I. Kim, S. J. Han, J. W. Park, and K. M. Park, "Involvement of hydrogen sulfide and homocysteine transsulfuration pathway in the progression of kidney fibrosis after ureteral obstruction," *Biochimica et Biophysica Acta*, vol. 1832, no. 12, pp. 1989–1997, 2013.
- [113] L. Fang, H. Li, C. Tang, B. Geng, Y. Qi, and X. Liu, "Hydrogen sulfide attenuates the pathogenesis of pulmonary fibrosis induced by bleomycin in rats," *Canadian Journal of Physiology and Pharmacology*, vol. 87, no. 7, pp. 531–538, 2009.
- [114] G. Tan, S. Pan, J. Li et al., "Hydrogen sulfide attenuates carbon tetrachloride-induced hepatotoxicity, liver cirrhosis and portal hypertension in rats," *PLoS One*, vol. 6, no. 10, article e25943, 2011.
- [115] L. L. Pan, X. H. Liu, Y. Q. Shen et al., "Inhibition of NADPH oxidase 4-related signaling by sodium hydrosulfide attenuates myocardial fibrotic response," *International Journal of Cardiology*, vol. 168, no. 4, pp. 3770–3778, 2013.
- [116] K. Song, F. Wang, Q. Li et al., "Hydrogen sulfide inhibits the renal fibrosis of obstructive nephropathy," *Kidney International*, vol. 85, no. 6, pp. 1318–1329, 2014.
- [117] E. M. Bos, R. Wang, P. M. Snijder et al., "Cystathionine γ -lyase protects against renal ischemia/reperfusion by modulating oxidative stress," *Journal of the American Society of Nephrology*, vol. 24, no. 5, pp. 759–770, 2013.
- [118] Y. Zhou, X. Zhu, X. Wang et al., "H₂S alleviates renal injury and fibrosis in response to unilateral ureteral obstruction by regulating macrophage infiltration via inhibition of NLRP3 signaling," *Experimental Cell Research*, vol. 387, no. 1, article 111779, 2020.
- [119] S. J. Han, J. I. Kim, J. W. Park, and K. M. Park, "Hydrogen sulfide accelerates the recovery of kidney tubules after renal ischemia/reperfusion injury," *Nephrology Dialysis Transplantation*, vol. 30, no. 9, pp. 1497–1506, 2015.
- [120] Y. Huang, Z. Zhang, Y. Huang et al., "Induction of inactive TGF- β 1 monomer formation by hydrogen sulfide contributes to its suppressive effects on Ang II- and TGF- β 1-induced EMT in renal tubular epithelial cells," *Biochemical and Biophysical Research Communications*, vol. 501, no. 2, pp. 534–540, 2018.
- [121] L. Guo, W. Peng, J. Tao et al., "Hydrogen sulfide inhibits transforming growth factor- β 1-induced EMT via Wnt/catenin pathway," *PLoS One*, vol. 11, no. 1, article e0147018, 2016.
- [122] P. M. Snijder, A. R. Frenay, R. A. de Boer et al., "Exogenous administration of thiosulfate, a donor of hydrogen sulfide, attenuates angiotensin II-induced hypertensive heart disease in rats," *British Journal of Pharmacology*, vol. 172, no. 6, pp. 1494–1504, 2015.
- [123] S. Lilyanna, M. T. Peh, O. W. Liew et al., "GYY4137 attenuates remodeling, preserves cardiac function and modulates the natriuretic peptide response to ischemia," *Journal of Molecular and Cellular Cardiology*, vol. 87, pp. 27–37, 2015.
- [124] L. L. Pan, X. L. Wang, X. L. Wang, and Y. Z. Zhu, "Sodium hydrosulfide prevents myocardial dysfunction through modulation of extracellular matrix accumulation and vascular density," *International Journal of Molecular Sciences*, vol. 15, no. 12, pp. 23212–23226, 2014.
- [125] N. Ma, H. M. Liu, T. Xia, J. D. Liu, and X. Z. Wang, "Chronic aerobic exercise training alleviates myocardial fibrosis in aged rats through restoring bioavailability of hydrogen sulfide," *Canadian Journal of Physiology and Pharmacology*, vol. 96, no. 9, pp. 902–908, 2018.
- [126] L. J. Ellmers, E. M. Templeton, A. P. Pilbrow et al., "Hydrogen sulfide treatment improves post-infarct remodeling and long-term cardiac function in CSE knockout and wild-type mice," *International Journal of Molecular Sciences*, vol. 21, no. 12, p. 4284, 2020.

- [127] Z. Gong, H. Ye, Y. Huo et al., "S-allyl-cysteine attenuates carbon tetrachloride-induced liver fibrosis in rats by targeting STAT3/SMAD3 pathway," *American Journal of Translational Research*, vol. 10, no. 5, pp. 1337–1346, 2018.
- [128] C. Wang, J. Han, L. Xiao, C. E. Jin, D. J. Li, and Z. Yang, "Role of hydrogen sulfide in portal hypertension and esophagogastric junction vascular disease," *World Journal of Gastroenterology*, vol. 20, no. 4, p. 1079, 2014.
- [129] Y. Zhang, J. Gao, W. Sun et al., "H₂S restores the cardioprotective effects of ischemic post-conditioning by upregulating HB-EGF/EGFR signaling," *Aging*, vol. 11, no. 6, pp. 1745–1758, 2019.
- [130] S. Fiorucci, E. Distrutti, G. Cirino, and J. L. Wallace, "The emerging roles of hydrogen sulfide in the gastrointestinal tract and liver," *Gastroenterology*, vol. 131, no. 1, pp. 259–271, 2006.
- [131] H. N. Fan, H. J. Wang, C. R. Yang-Dan et al., "Protective effects of hydrogen sulfide on oxidative stress and fibrosis in hepatic stellate cells," *Molecular Medicine Reports*, vol. 7, no. 1, pp. 247–253, 2013.
- [132] H. N. Fan, H. J. Wang, L. Ren et al., "Decreased expression of p38 MAPK mediates protective effects of hydrogen sulfide on hepatic fibrosis," *European Review for Medical and Pharmaceutical Sciences*, vol. 17, no. 5, pp. 644–652, 2013.
- [133] S. Fiorucci, E. Antonelli, A. Mencarelli et al., "The third gas: H₂S regulates perfusion pressure in both the isolated and perfused normal rat liver and in cirrhosis," *Hepatology*, vol. 42, no. 3, pp. 539–548, 2005.
- [134] T. Damba, M. Zhang, M. Buist-Homan, H. van Goor, K. N. Faber, and H. Moshage, "Hydrogen sulfide stimulates activation of hepatic stellate cells through increased cellular bioenergetics," *Nitric Oxide*, vol. 92, pp. 26–33, 2019.
- [135] H. Cao, X. Zhou, J. Zhang et al., "Hydrogen sulfide protects against bleomycin-induced pulmonary fibrosis in rats by inhibiting NF- κ B expression and regulating Th1/Th2 balance," *Toxicology Letters*, vol. 224, no. 3, pp. 387–394, 2014.
- [136] R. Wang, "Physiological implications of hydrogen sulfide: a whiff exploration that blossomed," *Physiological Reviews*, vol. 92, no. 2, pp. 791–896, 2012.
- [137] R. Yang, Q. Jia, Y. Li, and S. Mehmood, "Protective effect of exogenous hydrogen sulfide on diaphragm muscle fibrosis in streptozotocin-induced diabetic rats," *Experimental Biology and Medicine*, vol. 245, no. 14, pp. 1280–1289, 2020.
- [138] M. S. Balzer, "Molecular pathways in peritoneal fibrosis," *Cellular Signalling*, vol. 75, article 109778, 2020.
- [139] Y. Lu, L. Gao, L. Li et al., "Hydrogen sulfide alleviates peritoneal fibrosis via attenuating inflammation and TGF- β 1 synthesis," *Nephron*, vol. 131, no. 3, pp. 210–219, 2015.

Research Article

Vascular Ageing Features Caused by Selective DNA Damage in Smooth Muscle Cell

Ehsan Ataei Ataabadi ¹, Keivan Golshiri ¹, Janette van der Linden,^{1,2,3} Martine de Boer,² Dirk J. Duncker ², Annika Jüttner ¹, René de Vries,¹ Richard Van Veghel ¹, Ingrid van der Pluijm ^{3,4}, Sophie Duthel,⁵ Suman Chalgeri,⁵ Lei Zhang,⁵ Amy Lin,⁵ Robert E. Davis ⁵, Gretchen L. Snyder ⁵, A. H. Jan Danser ¹, and Anton J. M. Roks ¹

¹Division of Pharmacology and Vascular Medicine, Department of Internal Medicine, Erasmus MC, Rotterdam, Netherlands

²Division of Experimental Cardiology, Department of Cardiology, Thorax Center, Erasmus MC, Rotterdam, Netherlands

³Department of Molecular Genetics, Erasmus MC, Rotterdam, Netherlands

⁴Department of Vascular Surgery, Erasmus MC, Rotterdam, Netherlands

⁵Intra-Cellular Therapies Inc, 430 R 29th Street, Suite 900, New York, NY 10016, USA

Correspondence should be addressed to Anton J. M. Roks; a.roks@erasmusmc.nl

Received 2 June 2021; Revised 16 July 2021; Accepted 16 August 2021; Published 31 August 2021

Academic Editor: Andrea Berenyiova

Copyright © 2021 Ehsan Ataei Ataabadi et al. This is an open access article distributed under the Creative Commons Attribution License, which permits unrestricted use, distribution, and reproduction in any medium, provided the original work is properly cited.

Persistently unrepaired DNA damage has been identified as a causative factor for vascular ageing. We have previously shown that a defect in the function or expression of the DNA repair endonuclease ERCC1 (excision repair cross complement 1) in mice leads to accelerated, nonatherosclerotic ageing of the vascular system from as early as 8 weeks after birth. Removal of ERCC1 from endothelial alone partly explains this ageing, as shown in endothelial-specific *Ercc1* knockout mice. In this study, we determined vascular ageing due to DNA damage in vascular smooth muscle cells, as achieved by smooth muscle-selective genetic removal of ERCC1 DNA repair in mice (SMC-KO: SM22aCre+ *Ercc1fl/-*). Vascular ageing features in SMC-KO and their wild-type littermates (WT: SM22aCre+ *Ercc1fl/+*) were examined at the age of 14 weeks and 25 weeks. Both SMC-KO and WT mice were normotensive. Compared to WT, SMC-KO showed a reduced heart rate, fractional shortening, and cardiac output. SMC-KO showed progressive features of nonatherosclerotic vascular ageing as they aged from 14 to 25 weeks. Decreased subcutaneous microvascular dilatation and increased carotid artery stiffness were observed. Vasodilator responses measured in aortic rings in organ baths showed decreased endothelium-dependent and endothelium-independent responses, mostly due to decreased NO-cGMP signaling. NADPH oxidase 2 and phosphodiesterase 1 inhibition improved dilations. SMC-KO mice showed elevated levels of various cytokines that indicate a balance shift in pro- and anti-inflammatory pathways. In conclusion, SMC-KO mice showed a progressive vascular ageing phenotype in resistant and conduit arteries that is associated with cardiac remodeling and contractile dysfunction. The changes induced by DNA damage might be limited to VSMC but eventually affect EC-mediated responses. The fact that NADPH oxidase 2 as well as phosphodiesterase 1 inhibition restores vasodilation suggests that both decreased NO bioavailability and cGMP degradation play a role in local vascular smooth muscle cell ageing induced by DNA damage.

1. Introduction

Cardiovascular disease (CVD) remains a leading cause of morbidity and mortality worldwide and has an enormous economic burden on healthcare systems [1]. Even with developments controlling the classical risk factors, such as

smoking, high cholesterol, diabetes, or hypertension, cardiovascular problems remain a chief health issue. Ageing remains the largest risk factor for cardiovascular disease [2]. Ageing is defined as a time-dependent functional deterioration that affects most living organisms and causes advanced loss of physiological integrity, impaired organ function, and

larger risk of premature death [3]. There are different factors that are associated with ageing or accelerate ageing of which accumulating DNA damage is a major one [1, 4, 5]. DNA damage can be induced by different sources like endogenous (e.g., generation of reactive oxygen species (ROS) and other oxidative reactions) or exogenous (e.g., UV and ionizing radiations) reactive agents that may cause hundreds thousands of DNA lesions per cell per day [3, 6]. Because of the intricate network of DNA repair systems in our body, most of those lesions will be eliminated. However, some lesions are not repaired, and these persistent lesions can induce transcription problems, metabolic and signaling changes, and cellular senescence that cumulate with age. Depending on the mediator, extent of exposure, target cell, and individual differences in repair capacity, ageing shows different interindividual and organ-specific (segmental) rates of development, as observed in daily human life and animal models of ageing [7, 8].

Several genetically modified mouse strains have been generated that model accelerated ageing. These are based on a specific deficiency in DNA repair. Different DNA repair systems and components can be targeted to accelerate ageing, and among them, excision repair cross-complementation group 1 (ERCC1) is a protein that, when defective, affects several main DNA repair systems [9]. ERCC1-xeroderma pigmentosum (XP) F is a structure-specific protein complex which acts as an endonuclease enzyme involved in the repair of several types of DNA lesions, mainly bulky, helix-distorting lesions that are repaired by the nucleotide excision repair pathway, but also double-strand breaks and interstrand cross-links [10–12]. *Ercc1*-deficient mice have been used repeatedly by diverse groups to study human-like ageing features [13–16]. The *Ercc1*^{Δ/Δ} mouse is a convenient model to study vascular ageing and potential therapies. The Δ allele is a truncation of the *Ercc1* gene by 7 amino acids of its C-terminus that disrupts the interaction between ERCC1 and XPF proteins and subsequently causes accumulation of DNA lesions in a progressive manner [7].

Ercc1^{Δ/Δ} mice have a short life span of around 24–28 weeks and display many human-like ageing features like neurodegeneration, osteoporosis, and liver, kidney, heart, and muscle dysfunctions that mostly start from the age of about 12 weeks [15, 17]. With regard to cardiovascular ageing, *Ercc1*^{Δ/Δ} mice show increased vascular stiffness and vascular wall thickness, increased blood pressure, and diminished macro- and microvascular relaxation that is mainly explained by reduced NO-cGMP pathway signaling, a major player in dysfunction of the aged cardiovascular system [17]. *Ercc1*^{Δ/Δ} mice display segmental progeria [18], which suggests that affected organs could be influenced by a local DNA damage process rather than a systemic one. Indeed, we have demonstrated that *Ercc1* knockout specifically in vascular endothelial cells (EC-KO) selectively affects endothelium-derived nitric oxide (NO) and leads to decreased end-organ perfusion, vascular leakage, and increased wall thickness [7]. However, vascular smooth muscle cells (VSMC) in *Ercc1*^{Δ/Δ} mice displayed an additional hyporesponsiveness to NO as compared to EC-KO mice [17]. Moreover, there is a rapid development of carotid artery stiffness in *Ercc1*^{Δ/Δ} mice

which is absent in EC-KO [17]. These differences suggest that some of the ageing features in the *Ercc1*^{Δ/Δ} mice can be induced by DNA damage in VSMC [7, 17]. To address the question if a local VSMC DNA repair defect is critical for the specific changes in vascular function as observed in *Ercc1*^{Δ/Δ} mice, we investigated cardiovascular function in a mouse model with specific loss of *Ercc1* function in smooth muscle cells (SMCs). We focused on changes of NO-cGMP responsiveness since this is a major hallmark of ageing and DNA damage-related vascular dysfunction.

2. Methods

2.1. Animals. We evaluated the effect of SMC genomic instability on cardiovascular function in a mouse model with SMC-targeted deletion of *Ercc1*, based on crossbreeding of mice with floxed *Ercc1* gene with the B6.129S6-*Tagln*^{tm2(cre)Yec/J} strain (SM22^{acreKI}, Jackson Labs USA, stock no. 006878) [19]. SM22^{acreKI} harbours a Cre recombinase-coding sequence under control of the endogenous transgelin, or smooth muscle 22 α -actin, promoter, which is the best-studied smooth muscle promoter. Expression of Cre recombinase in embryonal SMC and cardiac myocytes, a drawback of other SM22^{Cre} strains, is absent in this model [19, 20]. Apart from expression in vascular smooth muscle cells, there are reports suggesting promoter activation in platelets, adipocytes, and myeloid cells, and fully specific promoters for smooth muscle have hitherto not been identified [20]. To target the smooth muscle cells, various Cre recombinase models can be used. SM22^{Cre} models have been used in this study. SM22 α is an actin-binding regulatory protein involved in SMC contraction and serves as a marker to study a SMC-specific expression model [20].

As the *Ercc1* flox strain, we have used the FVB/N background-based transgenic mice generated by Melton et al. (Edinburgh, United Kingdom) [21]. SM22^{Cre}+/- female mice were crossed with *Ercc1*+/- male mice to generate SM22^{Cre}+/-::*Ercc1*+/- mice in a pure C57BL/6J background. This offspring was then crossed with *Ercc1*fl/fl mice in a pure FVB/N background to produce SM22^{Cre}+ *Ercc1*fl/- mice knockout mice (SMC-KO) in a C57BL6/FVB F1 hybrid background [22]. Thus, the *Ercc1* gene is fully inactivated for both alleles. Littermates (genotypes: SM22^{Cre}+ *Ercc1*fl/+) were used as controls. We also selected SM22^{Cre} mice to exclude potential effects of Cre on vascular function.

Male and female mice were housed in individually ventilated cages, in a 12 h light/dark cycle, and fed normal chow and water *ad libitum*. SMC-KO developed weight difference compared with WT controls that at 6 months reached the threshold for termination of experiments on ethical requirements of the EU directive. Consequently, we decided to measure cardiac and vascular phenotyping features at 12–13 (early time-point: ET) and 22–23 weeks of age (late time-point: LT), when no visible clinical signs (except for the body weight loss) were evident. At the end of the experiment, mice were euthanized under deep anesthesia by exsanguination from the portal vein. We sacrificed the mice at the age of 14 and 25 weeks. Mice that were sacrificed at the age of 14 and 25 weeks old are referred to as earlier

time-point (ET) and later time-point (LT), respectively, throughout this article. In total, for ET, 14 SMC-KO and 14 WT and for LT, 16 SMC-KO and 21 WT were included into the study. For each group, both genders were included with quite equal number and all the methods were performed with both genders. All animal procedures were performed at the Erasmus MC facility for animal experiments following the guidelines from Directive 2010/63/EU of the European Parliament on the protection of animals used for scientific purposes. All animal studies were approved by the National Animal Care Committee and the local administration within Erasmus University Medical Center Rotterdam.

2.2. Blood Pressure Measurement. Blood pressure (BP) was measured with a noninvasive method in conscious mice at both time-points using the tail cuff technique (CODA High-Throughput device, Kent Scientific). BP was measured on 5 consecutive days, and each session consisted of 30 measurement cycles per mouse. Acclimatization sessions were performed on the first 4 days, and the 5th day was used as the main measurement for each mouse. BP values are reported as the average of all valid cycles recorded at day 5 [17].

2.3. Microvascular Vasodilator Function In Vivo. We assessed *in vivo* vasodilator function using Laser Doppler perfusion imaging (LDPI, Perimed, PeriScan PIM 3 System). Reactive hyperemia, defined as the hindleg perfusion that increases after temporary occlusion of the blood flow, was calculated. One day prior to LDPI in the left hindleg, hair was removed by hair-removal cream. The hindleg was kept still with the aid of a fixation device. After recording baseline perfusion for 5 minutes, blood flow was occluded for 2 minutes with a tourniquet. After releasing the tourniquet, blood flow was monitored for 10 minutes to observe its return to the postocclusion baseline and to record hyperemia. During all measurements, mice were under 2.8% isoflurane anesthesia, and body temperature was kept at 36.4–37.0°C by means of a heating pad with rectal temperature probe feedback. For each mouse, the maximum response to occlusion and the area under the curve (AUC) relative to the postocclusion baseline were calculated. Only the area above the baseline was considered, and values below the baseline were set to 0.

2.4. Mechanical Properties and Dimensions of the Vascular Wall. After removing the surrounding tissues, carotid arteries explanted from ET and LT mice were mounted in a pressure myograph (Danish Myograph Technology (DMT), Aarhus, Denmark) in calcium-free buffer (in mmol/L: NaCl 120, KCl 5.9, EGTA 2, MgCl₂ 3.6, NaH₂PO₄ 1.2, glucose 11.4, and NaHCO₃ 26.3; pH 7.4), thus excluding measurements of both strain-induced contraction and an acute effect of PDE1 inhibition (PDE1 is relatively inactive in the absence of Ca²⁺). The intraluminal pressure of the carotid artery was increased stepwise by 10 mmHg starting at 0 mmHg and reaching 120 mmHg. Following each step, the vessels were allowed to equilibrate and then lumen and ves-

sel diameters were measured and used to calculate strain and stress [23].

2.5. Cardiac Function. Mice were sedated with 4% isoflurane, intubated, and connected to a pressure-controlled ventilator. Anesthesia was maintained with 2.5% isoflurane, and body temperature was kept at 37°C [24]. Cardiac geometry and function were evaluated by performing 2-D-guided short-axis M-mode transthoracic echocardiography (Vevo 770 High-Resolution Imaging System, VisualSonics) equipped with a 35 MHz probe. Left ventricular (LV) external and internal diameters were traced, and subsequently, heart rate, fractional shortening, cardiac output, LV mass, and LV wall thickness were calculated using the Visual Sonics Cardiac Measurements Package. Cardiac volume was calculated from the measured diameters assuming a spheric shape. Echocardiography was performed at 13 and 24 weeks of age in mice that were sacrificed at LT, allowing us to obtain echocardiographic parameters for the same animal at two different time-points (corresponding to ET and LT). After completing echocardiography, mice were sacrificed and hearts were quickly excised and rinsed in ice-cold saline. Subsequently, LV was dissected from the right ventricle and atria and LV was weighed and stored for further analyses.

2.6. Histology in the Heart. Paraffin-embedded LV samples were cut into 4 μm sections, deparaffinized, and stained to determine free wall myocardial collagen content and cardiomyocyte size. Collagen content was measured using picosirius red staining according to the standard protocol. Images were analyzed using a quantitative image analysis system (BioPix iQ software, BioPix AB). Cardiomyocyte size was quantified by performing Gomori staining using the standard protocol. Images were analyzed using a quantitative image analysis software (Leica Qwin Plus V3).

2.7. Ex Vivo Vascular Function Assessment. Immediately after sacrificing the mice, the thoracic aorta and iliac arteries were carefully isolated from mice and kept in cold Krebs-Henseleit buffer (in mmol/L: NaCl 118, KCl 4.7, CaCl₂ 2.5, MgSO₄ 1.2, KH₂PO₄ 1.2, NaHCO₃ 25, and glucose 8.3 in distilled water; pH 7.4). After removing the surrounding tissues, vessel segments of 1.5–2 mm length were mounted in small wire myograph organ baths (Danish Myograph Technology, Aarhus, Denmark) containing 6 mL of Krebs-Henseleit buffer oxygenated with 95% O₂ and 5% CO₂ at 37°C. The tension was normalized by stretching the vessels in steps until 90% of the estimated diameter at which the effective transmural pressure of 100 mmHg is reached [25]. Thereafter, the viability of the vessels was checked by inducing contractions with 30 and 100 mmol/L KCl. After reaching the maximum contraction induced by KCl, vessels were washed 4 times with a 5-minute interval. To evaluate vasodilatory responses, aortic and iliac segments were precontracted with either 30 nmol/L of U46619 (a thromboxane A₂ analogue) or 30 mmol/L KCl, resulting in a precontraction corresponding with 50–100% of the response to 100 mmol/L KCl.

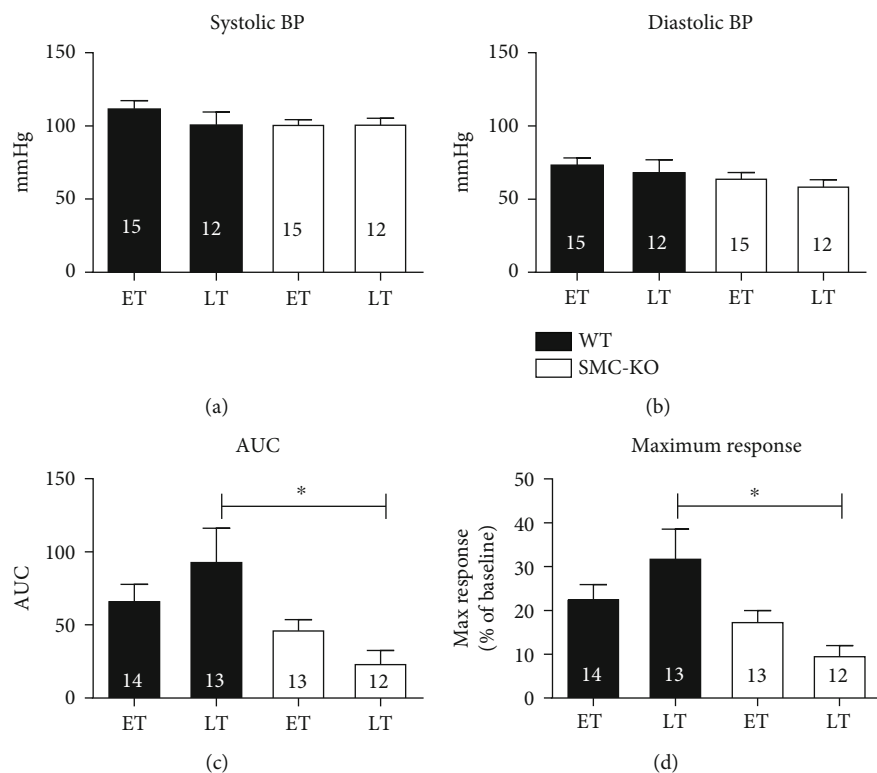


FIGURE 1: Systolic BP (a) and diastolic BP (b) and functional differences between skin reperfusion after 2 minutes of occlusion in the calculated area under the curve (c) and average maximum response (d) between WT and SMC-KO at ET and LT. The number in each column represents the number of animals in the corresponding group. Statistical differences were analyzed two-way ANOVA followed by Bonferroni's post hoc test (* $p < 0.05$).

After reaching a contraction plateau on U46619, concentration-response curves (CRCs) were constructed with the endothelium-dependent vasodilator acetylcholine (ACh) at cumulative doses (10^{-9} - 10^{-5} mol/L). When the CRC of ACh was completed, the endothelium-independent vasodilator sodium nitroprusside (SNP, 0.1 mmol/L) was added. To evaluate the involvement of the NO-cGMP pathway, one segment was preincubated with NG-nitro-L-arginine methyl ester salt (L-NAME, 10^{-4} mol/L), an endothelial nitric oxide synthase inhibitor. To investigate the role of endothelium-dependent hyperpolarization (EDH), the small conductance Ca^{2+} -activated K^{+} (SKCa) channel inhibitor apamin (100 nmol/L) and the intermediate conductance Ca^{2+} -activated K^{+} (IKCa) channel inhibitor TRAM34 (10 μ mol/L) were added on top of L-NAME. We also evaluated the role of NADPH oxidase- (Nox-) dependent reactive oxygen species generation, in parallel rings, preincubated either with no inhibitor, apocynin (a broad spectrum Nox inhibitor, 10^{-4} mol/L), or GSK279503 (a selective Nox2 inhibitor, 6 μ mol/L). Inhibitors were given 10 minutes before U46619 except for apocynin (30 minutes) and GSK279503 (60 minutes).

In parallel rings, CRCs to NO-donor SNP (10^{-11} - 10^{-4} mol/L) were constructed. Rings were precontracted with 30 mmol/L KCl to avoid bias of NO-cGMP responses by EDH. To avoid bias by intrinsic release of NO, segments were preincubated with L-NAME 10^{-4} mol/L added 20 minutes before precontraction. To explore the contribution of

PDE1 and PDE5, the most abundant cGMP-degrading PDEs in VSMC [1], segments were preincubated either with sildenafil 100 nmol/L (a selective PDE5 inhibitor) [16] or lenrispodun 100 nmol/L (a selective PDE1 inhibitor) [26] on top of L-NAME. Inhibitors were given 10 minutes before inducing precontraction.

2.8. Molecular Analysis: Analysis of Plasma Cytokine Levels. For mouse plasma, protein levels of IL-1 β , IL-2, IL-4, IL-6, IL-10, TNF- α , and IFN- γ were measured using a V-Plex Meso Scale Discovery (MSD) multiplex spot assay mouse neuroinflammation 1 panel. All samples were diluted at a ratio of 1:4 with diluent 41—provided in the MSD kit. Samples and standards were run in duplicate or triplicate according to manufacturer's instructions and analyzed with MSD Discovery Workbench software (Meso Scale Discovery, Gaithersburg, MD) at ITCI.

2.9. Quantitative Real-Time PCR. Total RNA was isolated from the abdominal aorta, heart, and kidney of LT mice using the RNeasy Mini Kit (Qiagen). The cDNA was synthesized from the total RNA using SuperScript IV First-Strand Synthesis System (ThermoFisher Scientific) according to the manufacturer's protocol. The cDNA was then amplified by quantitative real-time PCR on a QuantStudio 7 Flex Real-time PCR system (Applied Biosystems). Each reaction was performed in duplicate with TaqMan Universal Master Mix II (Applied Biosystems). The TaqMan Assay IDs and

context probe sequences used for *Pde1a*, *Il-6*, and *Gapdh* are mentioned in Table S1. PCR cycling conditions were 50°C for 2 min, 95°C for 10 min, followed by 40 cycles of 95°C for 15 s and 60°C for 1 min.

To measure mRNA expression of *Ercc1*, *p16*, and *p21* in the abdominal aorta, each reaction was performed in duplicate with SYBR Green PCR Master Mix (UK, Applied Biosystems). PCR cycling conditions were 50°C for 2 min, 95°C for 2 min, followed by 40 cycles of 95°C for 15 s and 60°C for 1 min. β -Actin and *Hprt1* were used as household genes. Results from unreliable duplicates or melting curves were discarded. The relative amount of genomic DNA in DNA samples was determined as follows: relative quantification = $2(-\Delta\Delta Ct)$. The sense and antisense mouse primer sequences are mentioned in Table S2.

2.10. Statistical Methods. Data are presented as mean and standard error of the mean, unless otherwise indicated. Statistical analysis between the groups of single values was performed by unpaired, two-tailed *t*-test. Differences among the groups, depending on the number of variables, were analyzed by either one-way or two-way or three-way ANOVA followed by Bonferroni's post hoc test. Differences between CRCs were tested by general linear model for repeated measures (sphericity assumed). *p* values below 0.05 were considered as significant. Initial analysis was performed separately in male and female mice. However, since alterations, if present, occurred in a gender-independent manner (not shown), it was decided to pool all data in male and female mice.

3. Results

3.1. General Health Features. There were no visible signs of decline in SMC-KO mice until the age of 20 to 22 weeks. At 23 to 25 weeks, the mice exhibited a mean body weight decrease of 20% compared to WT mice (Supplemental Table S3) and were sacrificed according to the ethical requirements of the EU directive.

3.2. Blood Pressure. Blood pressure measurements showed no significant difference between WT and SMC-KO mice for both ET and LT, neither within the groups of WT and SMC-KO mice nor at different time-points (Figures 1(a) and 1(b)).

3.3. Microvascular Vasodilator Function In Vivo. At ET, there was no significant difference in reactive hyperemia (indicated by AUC and maximum response) in the hind limb skin between SMC-KO and WT mice (Figures 1(c) and 1(d)). At LT, SMC-KO mice showed significant decreased reactive hyperemia compared to WT mice (Figures 1(c) and 1(d)). When passing from ET to LT, reactive hyperemia tended to increase in WT mice, whereas it tended to decrease in SMC-KO mice.

3.4. Mechanical Properties and Dimensions of the Vascular Wall. At LT, SMC-KO mice displayed significantly declined media strain versus WT mice (Figure 2(b)) at comparable media stress (Figures 2(c) and 2(d)), indicat-

ing higher stiffness. This was not observed at ET (Figure 2(a)).

3.5. Cardiac Function. Heart rate was lower in SMC-KO mice, both at ET and LT (Figure 3(a)). This was also true for cardiac output (Figure 3(c)). Fractional shortening was significantly lower at LT in SMC-KO mice (Figure 3(b)). At LT, LV wall thickness in SMC-KO mice was significantly smaller compared to WT mice (Figure 3(d)), and the same was true for LV mass (Figure 3(e)). Yet, there were no significant differences for LV mass (Figure 3(e)) and wall thickness at ET (Figure 3(d)) between WT and SMC-KO mice. There were no significant gender differences between males and females in terms of the abovementioned parameters using three-way ANOVA.

Echocardiographic software predicted SMC-KO mice to have a different heart volume and weight as compared to WT. This was confirmed when measuring relative LV weight (=LV weight/body weight) at the age of 25 weeks (Figure 3(f)). Sirius red and Gomori staining (Supplemental Figure S1 A–D) revealed elevated interstitial collagen levels and an increased cardiomyocyte size, respectively, at LT in SMC-KO vs. WT mice (Figures 3(g) and 3(h)). There were no gender differences in both collagen content and cardiomyocyte size using two-way ANOVA.

3.6. Ex Vivo Vascular Function Assessment

3.6.1. Endothelium-Dependent and Endothelium-Independent Response in SMC-KO Mice versus WT. Iliac U46619 precontraction values in WT vs. SMC-KO for ET and LT were 3.67 ± 0.25 vs. 3.01 ± 0.31 and 3.28 ± 0.3 vs. 2.32 ± 0.2 , respectively. Aortic U46619 precontraction values in WT vs. SMC-KO for ET and LT were 5.58 ± 1.12 vs. 6.87 ± 0.61 and 7.71 ± 0.85 vs. 7.27 ± 0.86 , respectively. Aortic KCl 30 mmol/L precontraction values in WT vs. SMC-KO for ET and LT were 3.25 ± 0.65 vs. 3.76 ± 0.27 and 3.99 ± 0.45 vs. 3.20 ± 0.22 , respectively. All the precontraction values are in millinewton.

Cre recombinase expression alone did not alter aortic responses to ACh and SNP (Supplemental Figures S2A and S2B). In contrast, the aortic ACh response showed a decline in SMC-KO mice for both time-points, and at LT, a major part of this response was lost compared to WT littermates (Figure 4(a)). In iliac arteries, a similar decline was observed at LT but not at ET (Supplemental Figure S3A). Inhibition of NOS and EDH in aortic segments revealed that the majority of the response to ACh in WT mice is mediated by NO, while the contribution of EDH was modest (Figures 4(b) and 4(c)). In the SMC-KO mice, EDH was absent at ET already, while the NO-cGMP response showed a less robust decline (Figures 4(d) and 4(e)).

There was a reduction in SNP response for the SMC-KO mice at ET which was further decreased at LT compared with the corresponding WT littermates (Figure 4(f)). When studying the relaxation to a single SNP dose after the ACh CRC, both in aortic (Figure 4(g)) and iliac rings (Figure S3B), the same observation was made.

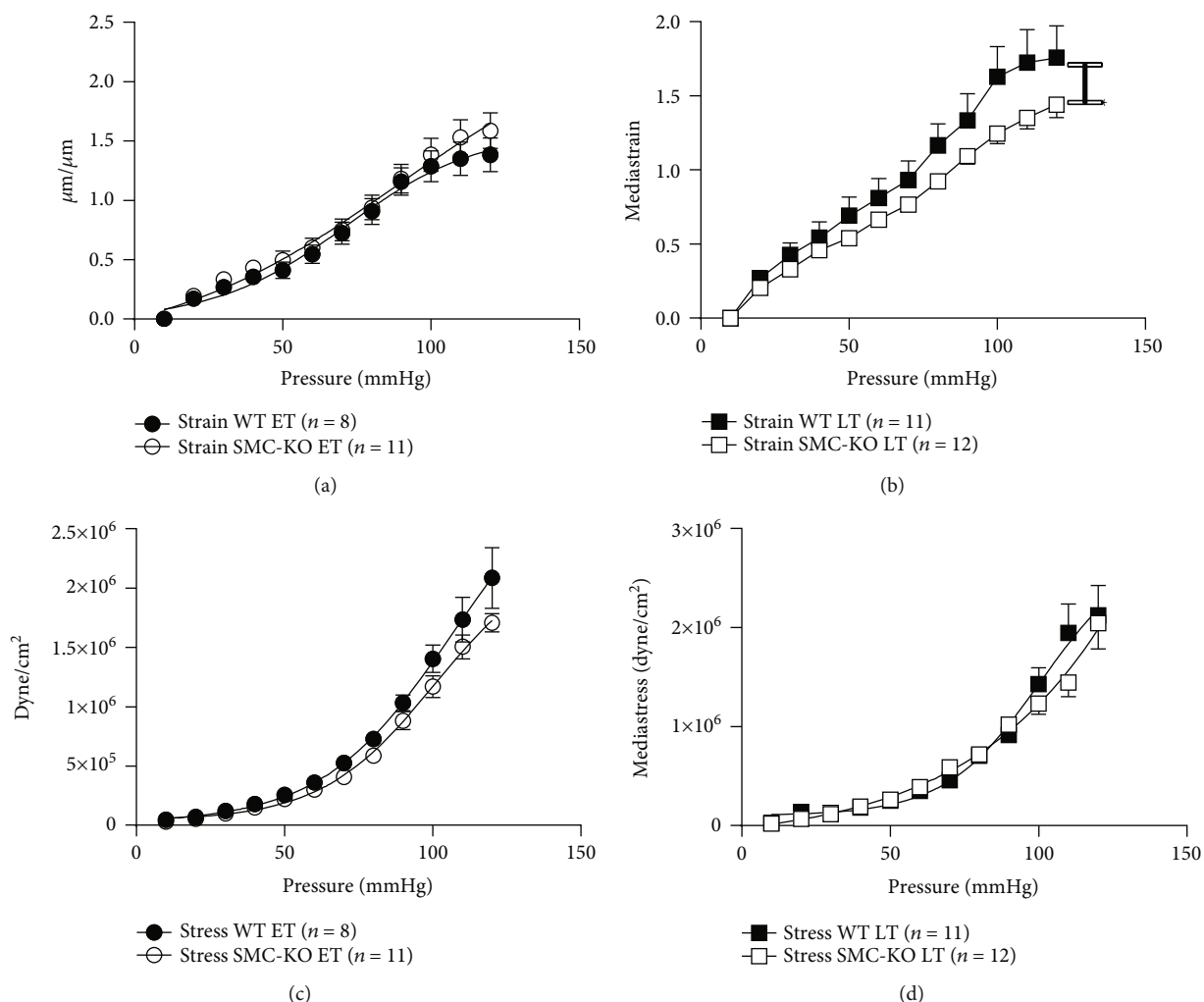


FIGURE 2: Strain difference at ET (a) and LT (b) and stress differences at ET (c) and LT (d) of the carotid arteries of SMC-KO vs. WT. Statistical difference was analyzed by general linear model repeated measures ($*p < 0.05$).

To explore whether the decline in vasorelaxation is VSMC-dependent, we corrected the ACh results in nonpretreated rings for the response to SNP (0.1 mmol/L) administered after the ACh CRC. In both the aorta and iliac artery, the ACh response in SMC-KO mice was decreased only at LT when correcting for SNP (Figure 4(h) and Figure S3C).

Apocynin and GSK279503 comparably improved ACh and SNP aortic responses in LT SMC-KO mice (Figures 5(a), 5(c), and 5(d)). There was no effect on aortic responses in LT WT mouse rings (Figures 5(b)–5(d)).

After preincubation with lenrispodun in aortic rings, the difference in SNP responses in SMC-KO control vs. lenrispodun at ET and LT was at the borderline to be significant (ET: $p = 0.1$, LT: $p = 0.08$). Moreover, the SNP responses in SMC-KO were identical to those in WT, both in ET and LT mice (Figures 5(e) and 5(f)). No such effects were observed for sildenafil (Figures 5(e) and 5(f)). Neither PDE inhibitor affected SNP responses in WT mice at any time-point (data not shown).

3.7. Molecular Analysis. One of the major changes that occur during ageing is the dysregulation in inflammatory status of

cells; thus, we measured certain pro- and anti-inflammatory cytokines in LT SMC-KO mice and the corresponding WT [27]. The plasma protein levels of IL-6 and IL-10 at LT were increased in SMC-KO versus LT mice, and the opposite was true for IFN- γ (Figures 6(a)–6(c)). No changes were observed in plasma IL-1 β , TNF- α , IL-2, and IL-4 (data not shown; $n = 12$ for both WT and SMC-KO mice). *Il-6* mRNA expression was upregulated in both the heart (Figure 6(d)) and kidney (Figure 6(e)), and the same was true for *Pde1a* in the aorta (Figure 6(f)). *Pde1a* mRNA expression in the heart and kidney was unaltered (data not shown; $n = 12$ for both WT and SMC-KO mice). *Ercc1* mRNA expression was significantly lower in the abdominal aorta of SMC-KO vs. WT at LT (Figure S4A). DNA damage response and senescent marker *p16* and *p21* expressions were significantly higher in the abdominal aorta of SMC-KO vs. WT at LT (Figures S4B and S4C).

4. Discussion

We investigated the role of smooth muscle cell-specific DNA repair deficiency on cardiovascular function in a mouse

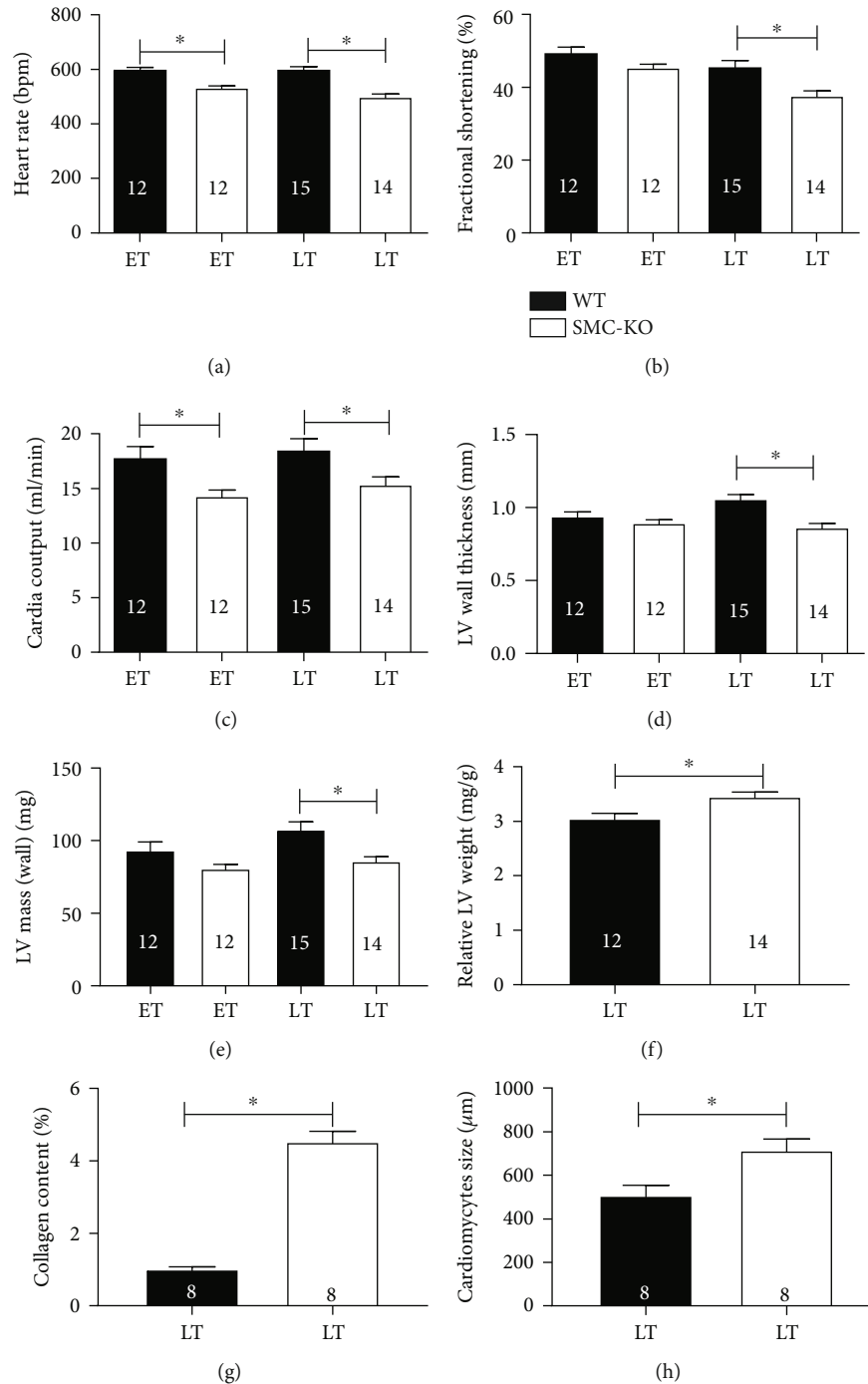


FIGURE 3: Cardiac function comparison between WT and SMC-KO at ET and LT for heart rate (a), fractional shortening (b), cardiac output (c), LV wall thickness (d), LV mass (e), relative LV weight to body weight at LT (f), LV free wall collagen content (g), and LT free wall cardiomyocyte size (h). The number in each column represents the number of animals in the corresponding group. Statistical differences were analyzed by two-way ANOVA followed by Bonferroni's post hoc test for (a–e) and two-tailed *t*-test for (f–h) ($*p < 0.05$).

model with specific loss of *Ercc1* in smooth muscle cells. We found that there was no BP differences between SMC-KO and WT mice nor within SMC-KO mice tested at different time-points. However, LDPI microvascular perfusion imaging showed a progressive decline in reactive hyperemia between ET and LT in SMC-KO mice. Moreover, we evaluated the mechanical properties of carotid arteries and found

a significantly diminished compliance between these two groups. Another well-known vascular ageing feature of SMC-KO mice was decreased NO-mediated vasodilation. The latter appeared to be due, at least in part, to upregulation of *Pde1* and *Nox2*. The fact that these vascular alterations did not result in a rise in blood pressure is suggestive of an adaptive response, most likely at the level

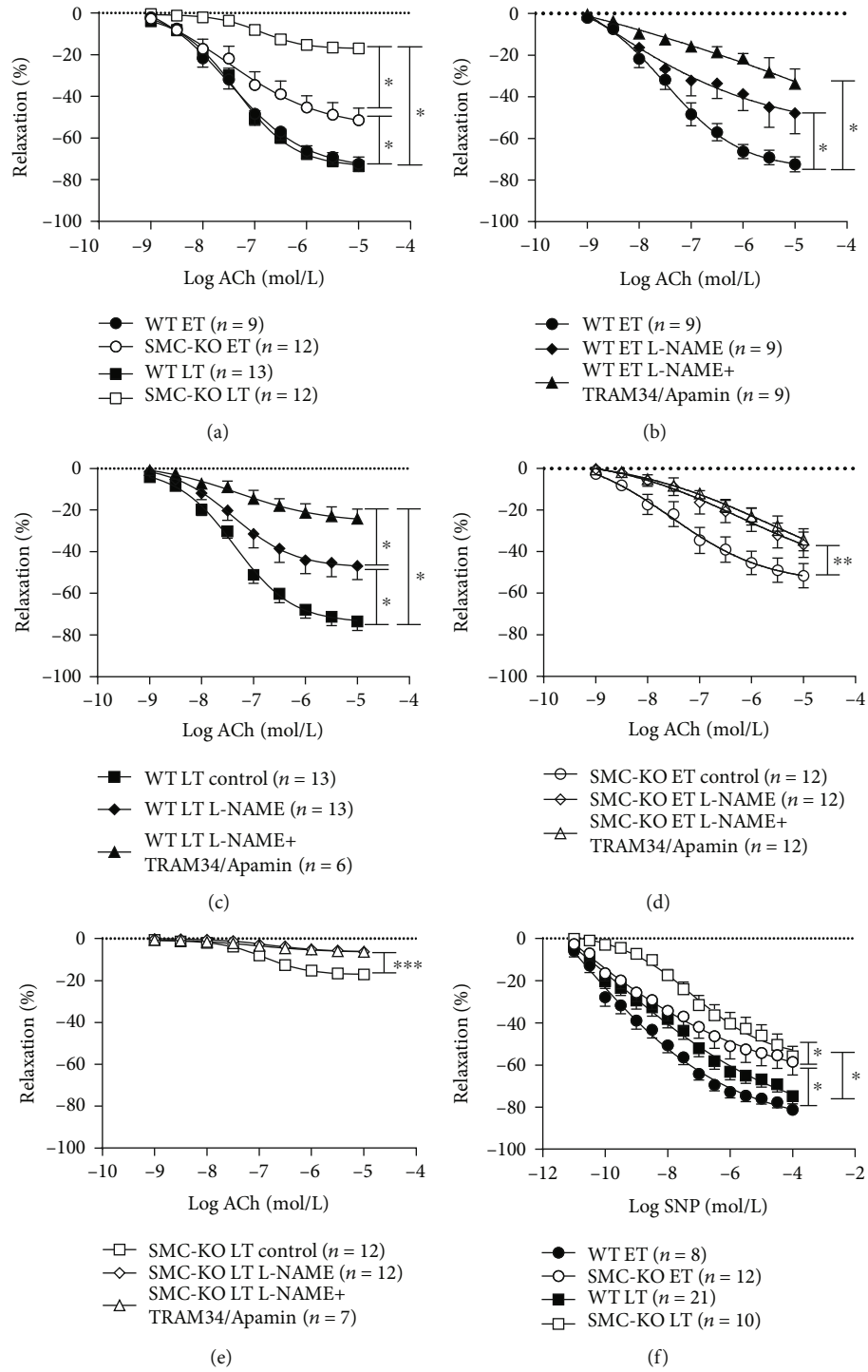


FIGURE 4: Continued.

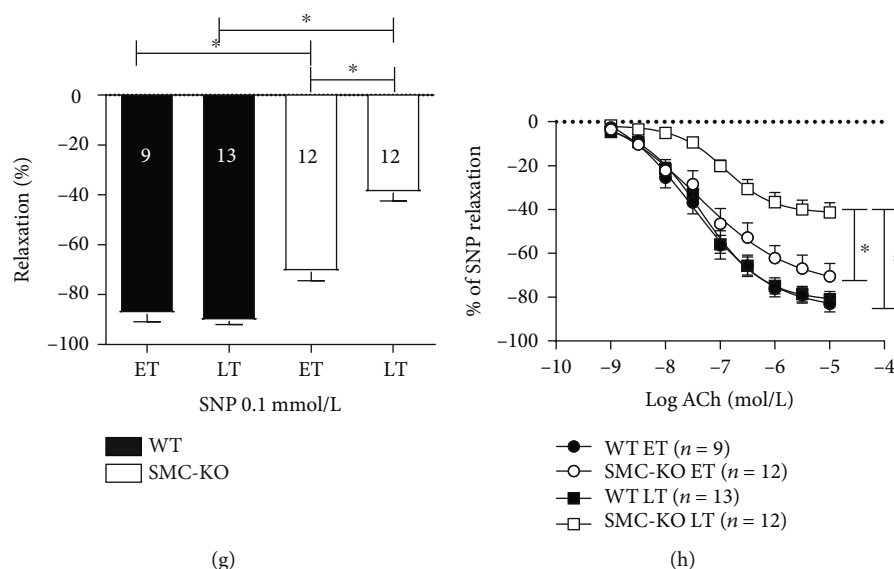


FIGURE 4: Vasorelaxation in aortic rings of SMC-KO and WT mice for both time-points in response to ACh (10^{-9} to 10^{-5} mol/L) (a). The contribution of NO-cGMP and EDH pathway in WT ET (b), WT LT (c), SMC-KO ET (d), and SMC-KO LT (e). Vasorelaxation in aortic rings of SMC-KO and WT mice for both time-points in response to SNP (10^{-11} to 10^{-4} mol/L) (f), SNP (0.1 mmol/L) after ACh CRC (g), and ACh (10^{-9} to 10^{-5} mol/L) corrected to SNP (0.1 mmol/L) (h). The number in each column represents the number of animals in the corresponding group. Statistical differences were analyzed by general linear model repeated measures for (a–f) and (h) and two-way ANOVA followed by Bonferroni's post hoc test for (g) (* $p < 0.05$).

of the heart. Indeed, at ET, heart rate and cardiac output are lower in the absence of contractile cardiac dysfunction, suggesting an adaptation in autonomic regulation. At LT, however, fractional shortening is reduced, and this was associated with aberrant cardiac remodeling, characterized by an increased collagen content and cardiomyocyte size. Such changes rather point at a malignant cardiac remodeling. This ageing-like phenotype was accompanied by an altered inflammatory status. No gender-specific effects were detected in any of the variables.

As we found a markedly diminished vascular function *in vivo* by LDPI, we suspected impaired vasodilator responses. We demonstrated this in *ex vivo* organ bath experiments and explored the underlying mechanisms. NO signaling was found to be decreased, evidenced by a reduced response to the NO donor SNP. This reduction was already maximal at ET, and no further decrease was observed thereafter (Figure 4). Importantly, correction of the ACh response to SNP did not normalize the disturbed endothelium-dependent responses in SMC-KO mice to the level of WT (Figure 4; Figure S3). This is indicative of a residual loss of endothelial function. Indeed, no IKCa/SKCa-mediated EDH-dependent response could be observed at both ET and LT in the SMC-KO mice (Figure 4), while the endothelial NO-mediated response additionally diminished over time. Taken together, SMC-KO mice display EDH loss and reduced responsiveness to NO released by the endothelium at ET and LT. Other EDH mechanisms, like BKCa or connexin-mediated effects [28], might also play a role. Therefore, the further unraveling of EDH changes in this accelerated SMC ageing model is warranted.

Decreased NO signaling is a commonly observed feature of mouse models of accelerated ageing caused by reduced functioning of DNA repair proteins [1]. Whole body *Ercc1*^{Δ/Δ} mice are characterized by a combination of a reduced ageing vasodilator response to NO and endothelial dysfunction [29], while in endothelium-specific *Ercc1* KO mice (EC-KO), only the latter was the case [7]. We observed a reduced vasodilator response of VSMC to exogenous NO and to endothelium-derived NO in SMC-KO mice.

The lost NO responsiveness in SMC-KO mice in all likelihood indicates that DNA damage in VSMC leads to decreased bioavailability of NO. The observation that the PDE1 inhibitor, lenrispodun, fully restored the SNP responses in the aorta (Figures 5) suggests that lost NO responsiveness involves *Pde1* upregulation. The aortic *Pde1A* mRNA expression data confirms this view, while a similar *Pde1A* upregulation was observed earlier in whole body *Ercc1*^{Δ/Δ} mice and ageing human VSMC [30]. PDE5 inhibition with sildenafil was without effect in SMC-KO mouse vessels, arguing against a role for *Pde5* upregulation. The reduced endothelial NO release might be explained on the basis of NO inactivation by oxygen radicals, given our finding that Nox inhibition additionally restored the effects of NO. Since selective Nox2 inhibition and nonselective Nox inhibition yielded the same effect, the most likely contributor to the NO-inactivating radicals is Nox2. *Nox2* upregulation is a well-known consequence of cytokine dysregulation [31], evidenced in this model by *Il-6* upregulation that may induce *Nox2* upregulation and ROS production. This process would be expected to eventually lead to reduced NO availability [32]. More general in cardiovascular ageing,

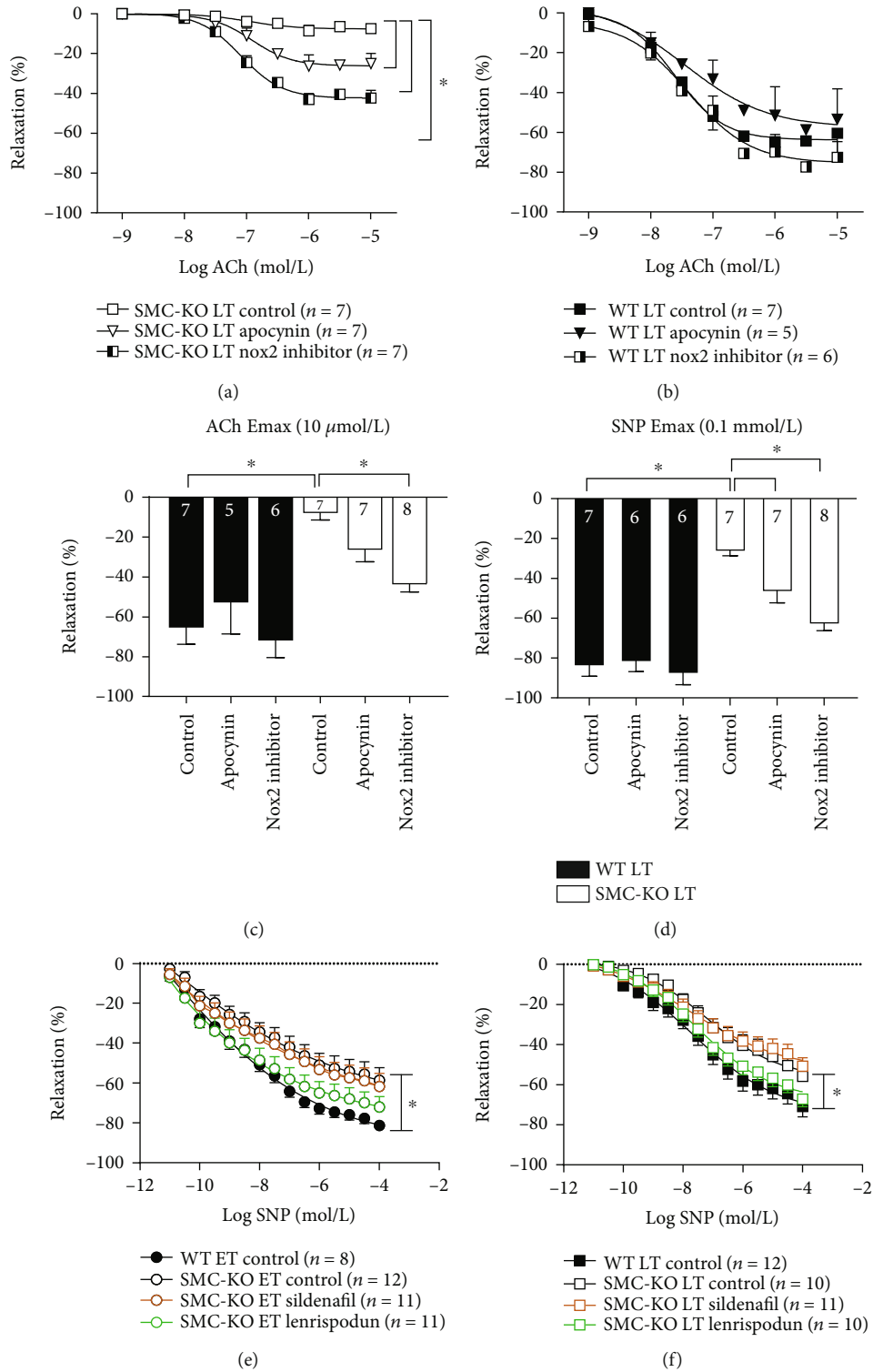


FIGURE 5: Vasorelaxation response to ACh (10^{-9} to 10^{-5} mol/L) in aortic rings either without inhibitor or with apocynin or GSK279503 preincubation in WT LT (a), SMC-KO LT (b), ACh (10 μ mol/L) Emax (c), and SNP (0.1 mmol/L) Emax (d) at LT. Vasorelaxation response to SNP (10^{-11} to 10^{-4} mol/L) in aortic rings either without inhibitor or with sildenafil or lenrispodun preincubation at ET (e) and LT (f). The number in each column represents the number of animals in the corresponding group. Statistical differences were analyzed by general linear model repeated measures for (a), (b), (e), and (f) and one-way ANOVA followed by Bonferroni's post hoc test for (c) and (d) ($*p < 0.05$).

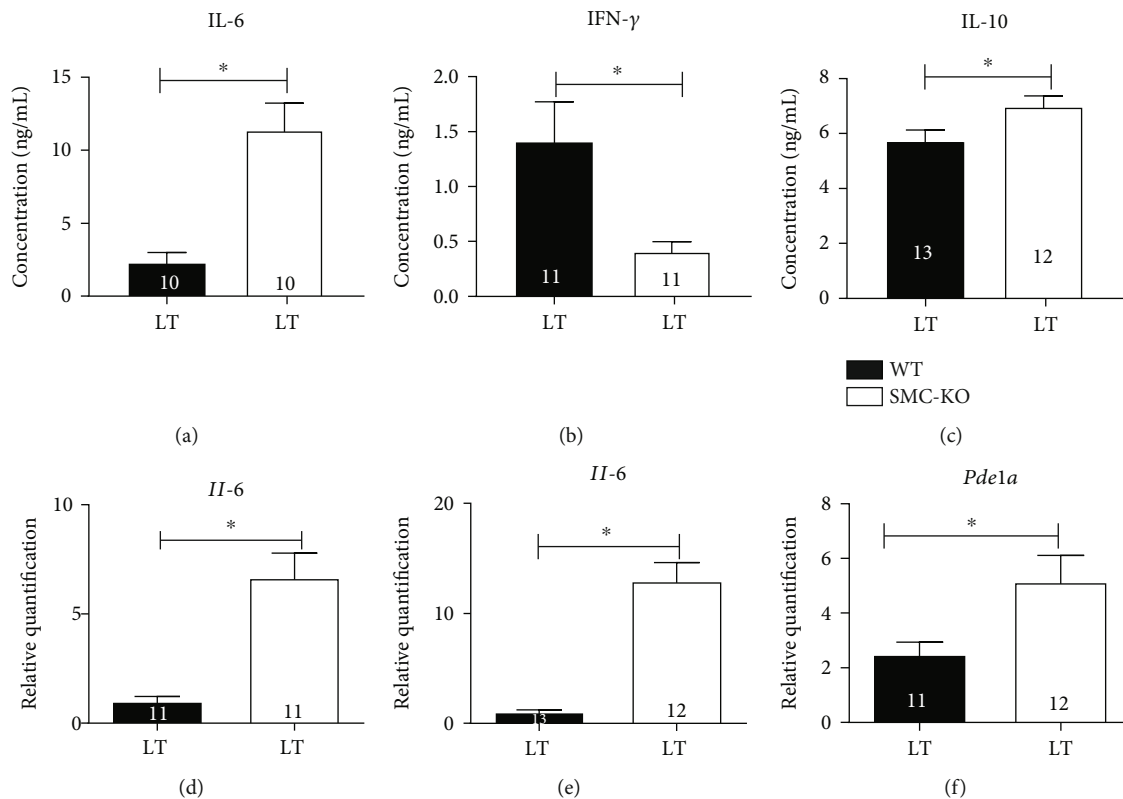


FIGURE 6: MSD analysis of plasma samples in LT WT and SMC-KO for IL-6 (a), IFN- γ (b), and IL-10 (c). qPCR analysis in WT and SMC-KO for Il-6 in LV (d), Il-6 in kidney (e), and Pde1a in the abdominal aorta (f). The number in each column represents the number of animals in the corresponding group. Statistical differences were analyzed by two-tailed *t*-test (**p* < 0.05).

Song et al. measured the inflammatory response in cultured aortic vascular smooth muscle cells of aged (16-18 month) vs. young (2-4 months) mice in a nonstimulatory condition and found that aged mice exhibited elevation of basal IL-6. Elevated IL-6 functions in an autocrine manner to further accelerate inflammatory responses in VSMC, thereby making the vasculature prone to atherosclerosis and a less contractile phenotype [33, 34].

Cytokines are known to be altered in *Ercc1*-mutant mice, with specificity for the target cell in which the DNA repair was affected [13, 35, 36]. In SMC-KO mice, circulating IL-10 was found to be increased, while circulating IFN- γ was decreased. This might reflect an anti-inflammatory feedback response to the increased plasma IL-6 levels. The IFN- γ reduction is in agreement with changes in aged VSMC of *Macaca mulatta* [37], although IL-10 was also reduced in this model. An intricate shift in inflammatory factors has been observed in *Ercc1*-mutant mice and other DNA repair mutants. Therefore, the specific meaning of cytokine shifts is to be interpreted with caution, although a general assumption is that *Ercc1*-mutant mice display primarily a proinflammatory phenotype [38]. In conclusion, the inflammatory status in SMC-KO might be involved in the vascular dysfunction that was observed, and our current observations warrant further inspection in future studies, which would require the development of proper tools for this purpose.

Blood pressure was normal in SMC-KO mice, and at first glance, this is in contradiction with the reduced vasodilation

capacity. However, there was a decrease in heart rate and fractional shortening, and cardiac output was decreased by 20% on average in SMC-KO vs. WT mice. At an equal level of vascular resistance in the two mouse strains, this should translate to a 20% lower blood pressure in the SMC-KO mice (blood pressure = cardiac output \times vascular resistance). Yet, the blood pressure was identical in both strains. Reasoning backward to how this translates to vascular resistance, the Hagen-Poiseuille equation can be applied. It states that pressure or flow is changed with blood vessel length, blood viscosity, and radius⁴. Vessel length and blood viscosity being similar and with blood flow (=cardiac output) being reduced by 20%, the vascular diameter of SMC-KO should on average be 0.95x that of WT mice. Since this requires a state of vasoconstriction relative to WT, SMC-KO might be able to sustain a normal blood pressure despite the strongly reduced vasodilation capacity, e.g., by reducing sympathetic neurohormonal input. The reduced cardiac output, if due to such regulation (or due to pathological remodeling or a combination of both), therefore accommodates normalization of blood pressure in SMC-KO mice. Like in the vasculature, the IL-6 increase might be involved in cardiac changes. Interestingly, Meléndez et al. showed in rats that IL-6 infusion resulted in concentric LV remodeling, a significant increase in collagen volume fraction and relative increases in cardiomyocyte width and length that all were independent of blood pressure changes [39]. Despite the remodeling, no overt heart failure was observed in SMC-

KO mice. It seems likely that apart from pathological remodeling, adaptation of hemodynamic function by neurohormonal mechanisms accounts for the observed hemodynamic changes. However, the possibility of heart failure like phenotype cannot be excluded and needs further investigation.

In conclusion, SMC-KO mice show a progressive ageing phenotype in resistant and conduit arteries. The changes induced by DNA damage might be limited to VSMC, although it seems that dysfunction in VSMC eventually has an impact on EC function as well, affecting the bioavailability of endothelium-derived NO through Nox2-mediated ROS production. PDE1 inhibition restores vasodilator function, whereas PDE5 seems to play a minor role in progressed VSMC dysfunction. As a future perspective, it might be of interest to study the effect of chronic treatment with PDE1 specific inhibitors on progression of vascular dysfunction, inflammation, and cardiac remodeling. Currently, lenrispodun is under clinical development for treatment of neurodegenerative disease and has been shown to be a safe and well-tolerated drug in heart failure patients [40].

Data Availability

Data is available on request.

Conflicts of Interest

Sophie Dutheil, Suman Chalgeri, Lei Zhang, Amy Lin, Robert E Davis, and Gretchen L Snyder are employees of Intracellular Therapies Inc. New York, U.S.A.

Authors' Contributions

Ehsan Ataei Ataabadi and Keivan Golshiri contributed equally.

Acknowledgments

We thank Ilona Krabbendam-Peters for her technical support. This work has been supported by a grant from Stichting Lijf en Leven project 60 and Technologie en Kennis Instituut–Life Sciences and Health Holland project EMCLSH 19-0913 and a grant from Intracellular Therapies Inc. New York to A.J.M. Roks.

Supplementary Materials

Supplementary 1. Table S1: TaqMan ID assay and probe context sequence that were used for *Pde1a*, *Il-6*, and *Gapdh* qPCR measurements. Table S2: sense and antisense sequence of primers that were used for *p16*, *p21*, *Ercc1*, β -*actin*, and *Hprt1* qPCR measurements. Supplementary 2. Table S3: body weight of SMC-KO and WT mice stratified by age and gender. Supplementary 3. Figure S1: photographs of collagen staining for WT (A) and SMC-KO (B) and cardiomyocyte staining for WT (C) and SMC-KO (D) at LT. Supplementary 4. Figure S2: vasorelaxation response to ACh (10^{-9} to 10^{-5} mol/L) (A) and SNP (10^{-11} to 10^{-4} mol/L) (B) in aortic rings of WT mice with and without Cre. Statis-

tical differences were analyzed by general linear model repeated measures. Supplementary 5. Figure S3: vasorelaxation response to ACh (10^{-9} to 10^{-5} mol/L) (A), SNP (0.1 mmol/L) after ACh (B), and ACh (10^{-9} to 10^{-5} mol/L) corrected for SNP (0.1 mmol/L) in iliac rings of SMC-KO and WT mice for both time-points. The number in each column represents the number of animals in the corresponding group. Statistical differences were analyzed by general linear model repeated measures for A and C and two-way ANOVA followed by Bonferroni's post hoc test for B ($*p < 0.05$). Supplementary 6. Figure S4: qPCR analysis in WT and SMC-KO in abdominal aorta at LT for *Ercc1* (A), *p16* (B), and *p21* (C). The number in each column represents the number of animals in the corresponding group. Statistical differences were analyzed by two-tailed *t*-test ($*p < 0.05$). (Supplementary Materials)









References

- [1] K. Golshiri, E. Ataei Ataabadi, E. C. Portilla Fernandez, A. Jan Danser, and A. J. Roks, "The importance of the nitric oxide-cGMP pathway in age-related cardiovascular disease: focus on phosphodiesterase-1 and soluble guanylate cyclase," *Basic & Clinical Pharmacology & Toxicology*, vol. 127, no. 2, pp. 67–80, 2020.
- [2] E. G. Lakatta and D. Levy, "Arterial and cardiac aging: major shareholders in cardiovascular disease enterprises," *Circulation*, vol. 107, no. 1, pp. 139–146, 2003.
- [3] C. López-Otín, M. A. Blasco, L. Partridge, M. Serrano, and G. Kroemer, "The hallmarks of aging," *Cell*, vol. 153, no. 6, pp. 1194–1217, 2013.
- [4] L. del Campo, A. Sánchez-López, C. González-Gómez, M. J. Andrés-Manzano, B. Dorado, and V. Andrés, "Vascular smooth muscle cell-specific progerin expression provokes contractile impairment in a mouse model of Hutchinson–Gilford progeria syndrome that is ameliorated by nitrite treatment," *Cell*, vol. 9, no. 3, p. 656, 2020.
- [5] J. C. Kovacic, P. Moreno, E. G. Nabel, V. Hachinski, and V. Fuster, "Cellular senescence, vascular disease, and aging: part 2 of a 2-part review: clinical vascular disease in the elderly," *Circulation*, vol. 123, no. 17, pp. 1900–1910, 2011.
- [6] G. A. Garinis, H. GTJvan der, J. Vijg, and H. JHJ, "DNA damage and ageing: new-age ideas for an age-old problem," *Nature Cell Biology*, vol. 10, no. 11, pp. 1241–1247, 2008.
- [7] P. K. Bautista-Niño, E. Portilla-Fernandez, E. Rubio-Beltrán et al., "Local endothelial DNA repair deficiency causes aging-resembling endothelial-specific dysfunction," *Clinical Science*, vol. 134, no. 7, pp. 727–746, 2020.
- [8] M. J. Yousefzadeh, J. Zhao, C. Bukata et al., "Tissue specificity of senescent cell accumulation during physiologic and accelerated aging of mice," *Aging Cell*, vol. 19, no. 3, article e13094, 2020.
- [9] W. P. Vermeij, J. H. J. Hoeijmakers, and J. Pothof, "Genome integrity in aging: human syndromes, mouse models, and therapeutic options," *Annual Review of Pharmacology and Toxicology*, vol. 56, no. 1, pp. 427–445, 2016.
- [10] A. B. Houtsmuller, S. Rademakers, A. L. Nigg, D. Hoogstraten, J. H. Hoeijmakers, and W. Vermeulen, "Action of DNA repair endonuclease ERCC1/XPF in living cells," *Science*, vol. 284, no. 5416, pp. 958–961, 1999.

- [11] A. Ahmad, A. R. Robinson, A. Duensing et al., "ERCC1-XPF endonuclease facilitates DNA double-strand break repair," *Molecular and Cellular Biology*, vol. 28, no. 16, pp. 5082–5092, 2008.
- [12] D. T. Bergstralh and J. Sekelsky, "Interstrand crosslink repair: can XPF-ERCC1 be let off the hook?," *Trends in Genetics*, vol. 24, no. 2, pp. 70–76, 2008.
- [13] L. J. Niedernhofer, G. A. Garinis, A. Raams et al., "A new progeroid syndrome reveals that genotoxic stress suppresses the somatotroph axis," *Nature*, vol. 444, no. 7122, pp. 1038–1043, 2006.
- [14] W. P. Vermeij, M. E. Dollé, E. Reiling et al., "Restricted diet delays accelerated ageing and genomic stress in DNA-repair-deficient mice," *Nature*, vol. 537, no. 7620, pp. 427–431, 2016.
- [15] H. Wu, B. S. van Thiel, P. K. Bautista-Niño et al., "Dietary restriction but not angiotensin II type 1 receptor blockade improves DNA damage-related vasodilator dysfunction in rapidly aging *Ercc1Δ/−* mice," *Clinical Science*, vol. 131, no. 15, pp. 1941–1953, 2017.
- [16] K. Golshiri, E. Ataei Ataabadi, R. Brandt et al., "Chronic sildenafil treatment improves vasomotor function in a mouse model of accelerated aging," *International Journal of Molecular Sciences*, vol. 21, no. 13, p. 4667, 2020.
- [17] M. Durik, M. Kavousi, I. van der Pluijm et al., "Nucleotide excision DNA repair is associated with age-related vascular dysfunction," *Circulation*, vol. 126, no. 4, pp. 468–478, 2012.
- [18] M. E. Dollé, R. V. Kuiper, M. Roodbergen et al., "Broad segmental progeroid changes in short-lived *Ercc1-Δ7* mice," *Pathobiology of Aging & Age-related Diseases*, vol. 1, no. 1, p. 7219, 2011.
- [19] J. Zhang, W. Zhong, T. Cui et al., "Generation of an adult smooth muscle cell-targeted Cre recombinase mouse model," *Arteriosclerosis, Thrombosis, and Vascular Biology*, vol. 26, no. 3, pp. e23–e24, 2006.
- [20] R. Chakraborty, F. Z. Saddouk, A. C. Carrao, D. S. Krause, D. M. Greif, and K. A. Martin, "Promoters to study vascular smooth muscle," *Arteriosclerosis, Thrombosis, and Vascular Biology*, vol. 39, no. 4, pp. 603–612, 2019.
- [21] J. Doig, C. Anderson, N. Lawrence, J. Selfridge, D. Brownstein, and D. Melton, "Mice with skin-specific DNA repair gene (*Ercc1*) inactivation are hypersensitive to ultraviolet irradiation-induced skin cancer and show more rapid actinic progression," *Oncogene*, vol. 25, no. 47, pp. 6229–6238, 2006.
- [22] N. el-Bizri, C. Guignabert, L. Wang et al., "SM22 α -targeted deletion of bone morphogenetic protein receptor 1A in mice impairs cardiac and vascular development, and influences organogenesis," *Development*, vol. 135, no. 17, pp. 2981–2991, 2008.
- [23] M. Resch, R. Wiest, L. Moleda et al., "Alterations in mechanical properties of mesenteric resistance arteries in experimental portal hypertension," *American Journal of Physiology-Gastrointestinal and Liver Physiology*, vol. 297, no. 4, pp. G849–G857, 2009.
- [24] E. D. van Deel, M. de Boer, D. W. Kuster et al., "Exercise training does not improve cardiac function in compensated or decompensated left ventricular hypertrophy induced by aortic stenosis," *Journal of Molecular and Cellular Cardiology*, vol. 50, no. 6, pp. 1017–1025, 2011.
- [25] L. E. Au-Bridges, C. L. Au-Williams, M. A. Au-Pointer, and E. M. Au-Awumey, "Mesenteric artery contraction and relaxation studies using automated wire myography," *Journal of Visualized Experiments*, vol. 55, article e3119, 2011.
- [26] P. Li, H. Zheng, J. Zhao et al., "Discovery of potent and selective inhibitors of phosphodiesterase 1 for the treatment of cognitive impairment associated with neurodegenerative and neuropsychiatric diseases," *Journal of Medicinal Chemistry*, vol. 59, no. 3, pp. 1149–1164, 2016.
- [27] H. Y. Chung, D. H. Kim, E. K. Lee et al., "Redefining chronic inflammation in aging and age-related diseases: proposal of the senoinflammation concept," *Aging and Disease*, vol. 10, no. 2, pp. 367–382, 2019.
- [28] K. Goto, T. Ohtsubo, and T. Kitazono, "Endothelium-dependent hyperpolarization (EDH) in hypertension: the role of endothelial ion channels," *International Journal of Molecular Sciences*, vol. 19, no. 1, p. 315, 2018.
- [29] P. K. Bautista-Niño, E. Portilla-Fernandez, D. E. Vaughan, A. Danser, and A. J. Roks, "DNA damage: a main determinant of vascular aging," *International Journal of Molecular Sciences*, vol. 17, no. 5, p. 748, 2016.
- [30] P. K. B. Niño, M. Durik, A. H. Danser et al., "Phosphodiesterase 1 regulation is a key mechanism in vascular aging," *Clinical Science*, vol. 129, no. 12, pp. 1061–1075, 2015.
- [31] C. M. Sena, A. Leandro, L. Azul, R. Seíça, and G. Perry, "Vascular Oxidative Stress: Impact and Therapeutic Approaches," *Frontiers in Physiology*, vol. 9, p. 1668, 2018.
- [32] S. P. Didion, "Cellular and oxidative mechanisms associated with interleukin-6 signaling in the vasculature," *International Journal of Molecular Sciences*, vol. 18, no. 12, p. 2563, 2017.
- [33] S. Yang, S. Hua, S. Dominik, S. Peiying, J. L. Patty, and R. G. Daniel, "Aging enhances the basal production of IL-6 and CCL2 in vascular smooth muscle cells," *Arteriosclerosis, Thrombosis, and Vascular Biology*, vol. 32, no. 1, pp. 103–109, 2012.
- [34] M. Park, S. Choi, S. Kim et al., "NF- κ B-responsive miR-155 induces functional impairment of vascular smooth muscle cells by downregulating soluble guanylyl cyclase," *Experimental & Molecular Medicine*, vol. 51, no. 2, pp. 1–12, 2019.
- [35] M. C. de Waard, I. van der Pluijm, N. Zuiderveen Borgesius et al., "Age-related motor neuron degeneration in DNA repair-deficient *Ercc1* mice," *Acta Neuropathologica*, vol. 120, no. 4, pp. 461–475, 2010.
- [36] I. Karakasilioti, I. Kamileri, G. Chatzinikolaou et al., "DNA damage triggers a chronic autoinflammatory response, leading to fat depletion in NER progeria," *Cell Metabolism*, vol. 18, no. 3, pp. 403–415, 2013.
- [37] A. Csiszar, D. Sosnowska, M. Wang, E. G. Lakatta, W. E. Sonntag, and Z. Ungvari, "Age-associated proinflammatory secretory phenotype in vascular smooth muscle cells from the non-human primate *Macaca mulatta*: reversal by resveratrol treatment," *The Journals of Gerontology: Series A*, vol. 67, no. 8, pp. 811–820, 2012.
- [38] D. E. Kim, M. E. T. Dollé, W. P. Vermeij et al., "Deficiency in the DNA repair protein ERCC1 triggers a link between senescence and apoptosis in human fibroblasts and mouse skin," *Aging Cell*, vol. 19, no. 3, article e13072, 2020.
- [39] G. C. Meléndez, J. L. McLarty, S. P. Levick, Y. du, J. S. Janicki, and G. L. Brower, "Interleukin 6 mediates myocardial fibrosis, concentric hypertrophy, and diastolic dysfunction in rats," *Hypertension*, vol. 56, no. 2, pp. 225–231, 2010.
- [40] N. A. Gilotra, A. Devore, A. Hays et al., "Cardiac and hemodynamic effects of acute phosphodiesterase-1 inhibition in human heart failure," *Journal of Cardiac Failure*, vol. 26, no. 10, p. S12, 2020.

Research Article

Gasotransmitter CO Attenuates Bleomycin-Induced Fibroblast Senescence via Induction of Stress Granule Formation

Yingqing Chen ¹, Feng Jiang ¹, Guangyao Kong ¹, Shuo Yuan ², Yuying Cao ¹,
Qinggao Zhang ^{1,2}, Qianqian Wang ¹, and Liping Liu ¹

¹Chronic Disease Research Center, Medical College, Dalian University, Dalian, 116622 Liaoning, China

²Key Laboratory of Natural Medicines of the Changbai Mountain, Ministry of Education, College of Pharmacy, Yanbian University, Yanji, Jilin Province 133002, China

Correspondence should be addressed to Qinggao Zhang; zhangqinggao@dlu.edu.cn, Qianqian Wang; wangqianqian@dlu.edu.cn, and Liping Liu; 1106548638@qq.com

Received 6 March 2021; Revised 19 May 2021; Accepted 29 May 2021; Published 30 June 2021

Academic Editor: T. Michael De Silva

Copyright © 2021 Yingqing Chen et al. This is an open access article distributed under the Creative Commons Attribution License, which permits unrestricted use, distribution, and reproduction in any medium, provided the original work is properly cited.

Cellular senescence is recognized as a phenomenon wherein a proliferative cell undergoes a permanent growth arrest. The accumulation of senescent cells over time can become harmful and result in diseases and physiological decline. Plasminogen activator inhibitor (PAI-1) is considered as a critical marker and mediator of cellular senescence. The formation of stress granules (SGs) could prevent senescence through the sequestration of PAI-1, and we previously suggested that exogenous carbon monoxide (CO) could induce SG assembly via integrated stress response (ISR). Although CO is known to possess anti-inflammatory, antioxidative, and antiapoptotic properties, whether it exerts antisenescent effect is still not well defined. Here, to address whether CO-induced SGs could protect against cellular senescence, we first treated lung fibroblasts with bleomycin (BLM) to establish DNA damage-induced cellular senescence, and observed a significant increase of several hallmarks of senescence through SA- β -gal staining, immunofluorescence, qRT-PCR, and Western blot assay. However, pre- and posttreatment of CO could remarkably attenuate these senescent phenotypes. According to our immunofluorescence results, CO-induced SGs could inhibit BLM-induced cellular senescence via sequestration of PAI-1, while it was abolished after the cotreatment of ISR inhibitor (ISRIB) due to the inhibition of SG assembly. Overall, our results proposed a novel role of CO in suppressing bleomycin-induced lung fibroblast senescence through the assembly of SGs.

1. Introduction

Cellular senescence is a process of permanent cell cycle arrest in response to various physiological and environmental stresses, including radiation (ionizing and UV), multiple anticancer drugs (bleomycin and etoposide), and oxidative stress [1]. Several studies have reported that the accumulation of senescent cells in tissues has both positive and negative consequences. The positive effects of senescent cells include tumor suppression, muscle regeneration, and skin wound healing in young organisms. Conversely, the detrimental effects of senescent cells have been observed in the context of age-related conditions, including cancer, cardiovascular diseases, neurodegeneration, diabetes, sarcopenia, and declining immune function in the elderly [2–4]. Senes-

cent cells typically appear flattened and enlarged and show increased cytoplasmic granularity [1]. In addition, senescent cells also display several other differences from proliferative cells. These differences include the increase of senescence-associated β -galactosidase (SA- β -gal) activity, phosphorylated H2A histone family member X (γ -H2AX) foci, cyclin-dependent kinase inhibitors (CDKIs), such as p21^{CIP1} and p16^{INK4a}, and senescence-associated secretory phenotype (SASP) which consists of growth hormones, proinflammatory cytokines, chemokines, angiogenic factors, and extracellular matrix remodeling proteases [5, 6]. Recent observations have supported that the increased secretion of serine protease inhibitor plasminogen activator inhibitor 1 (PAI-1), a component of SASP, can accelerate the aging in mice, and which is not only a marker but also a critical mediator of cellular

senescence [7]. Furthermore, senescence-inducing signals such as DNA damage response (DDR) and oxidative stress usually enhance the activation of tumor suppressor p53, and which trigger the expression of PAI-1 to interfere cyclin D1-dependent phosphorylation of Rb resulting in the irreversible cell cycle arrest [8].

Due to the role of cellular senescence in diseases such as neurodegeneration, cancer, and aging-related fibrosis, it has been reported to be an attractive therapeutic target. There are mainly two strategies that are under current development [9]. The first approach focuses on identifying compounds that can specifically induce senescent cells to die, and which is termed as senolytics. Given that senescent cells are resistant to apoptosis, the mechanism involved in this resistance is a preferential target of senolytics. The second approach is aimed at reducing the negative effect of SASP. Rapamycin, resveratrol, and metformin have been shown to effectively reduce the expression of SASP through inhibition of the NF- κ B and mTOR signaling pathways [9, 10]. Besides these strategies, more recent studies have showed that hydrogen sulfide (H₂S) and nitric oxide (NO), two kinds of gasotransmitters, can, respectively, delay nicotinamide-induced premature senescence and oxidative stress-induced epithelial cell senescence via reducing ROS production and enhancing SIRT1 activity [11, 12]. However, it is still unclear whether carbon monoxide (CO), one another gasotransmitter, can protect cells against stress-induced premature senescence.

CO is endogenously synthesized by heme oxygenase (HO), which can be induced by various circumstances (HO-1) or constitutively expressed in several organs (HO-2) [13]. Either applying a low concentration of exogenous CO or induction of the endogenous CO by HO-1 activation can exhibit cyto- and tissue-protective effects in various models of cellular and tissue injuries involving anti-inflammatory, antioxidant, and antiapoptotic effects [14]. Our numerous studies have demonstrated that long-term treatment of low-dose CO can protect various pathological conditions, including hepatic ischemia/reperfusion injury [15], acute lung injury [16], sepsis [17], Alzheimer's disease [18], and acetaminophen-induced liver injury [19]. Accumulative studies have reported that CO can generate low levels of mitochondrial reactive oxygen species (mtROS) via inhibition of cytochrome c oxidase, which in turn mediates integrated stress response (ISR) [20, 21]. Recently, we also proved that low levels of mtROS generated by CO could specifically induce the protein kinase R-like endoplasmic reticulum kinase (PERK)/eukaryotic translation initiation factor 2A (eIF2 α) signaling pathway and upregulated sestrin 2 (SESN2) [22], fibroblast growth factor 21 (FGF21) [23], and parkin [19] expression to promote redox homeostasis and enhance cellular survival.

In response to diverse environmental stresses, including heat, hyperosmolarity, and oxidative stresses, eukaryotic cells temporarily turn off the protein synthesis to control energy expenditure for the repair of stress-induced damage [24]. One of the main mechanisms is the formation of stress granule (SG) in the cytoplasm, and the nonmembrane-bounded SGs can arrest mRNAs and several harmful proteins to protect cells from apoptosis [24, 25]. SG biogenesis is recognized

as a conserved stress response and that can be initiated by the oligomerization of Ras GTPase-activating protein-binding protein 1 (G3BP1) and aggregation of RNA-binding proteins, including T cell intracytoplasmic antigen (TIA-1) and TIA1-related protein (TIAR) [26]. Accumulative evidence has depicted that the assembly of SGs can protect cells from apoptosis via minimizing energy expenditure, controlling proteostasis and ribostasis, and improving cell survival under damaging conditions [27]. Furthermore, SG formation can inhibit cellular senescence via the sequestration of PAI-1 into SGs and subsequently enhances the pathway of cyclin D1 to remove cell cycle arrest and delay the senescent state [28]. Intriguingly, our recent study has clearly suggested that exogenous CO can induce the formation of SGs through the induction of ISR, especially through the PERK-eIF2 α signaling pathway [29]. However, whether CO-induced SGs can prevent stress-induced premature senescence is still not well defined.

In this study, to construct DNA damage-induced senescence, we treated human and mouse fibroblasts with bleomycin (BLM) that can cause chromosomal instability, and we found that the administration of CO-releasing molecular (CORM-A1) and exogenous CO gas could effectively inhibit the cellular senescence, and the induction of SGs could sequester PAI-1 to recover the cyclin D1 signaling pathway to ameliorate cell cycle arrest. Moreover, we showed that ISR inhibitor (ISRIB) could abolish the protective effect of CO on BLM-induced premature senescence via suppressing the formation of SGs and enhancing the secretion of PAI-1. Our data indicated a novel mechanism whereby CO could protect against DNA damage-mediated cellular senescence through the induction of SG assembly and sequestration of PAI-1, in the cytoplasm, to delay the process of cellular senescence.

2. Materials and Methods

2.1. Reagents and Chemicals. CO-releasing molecular-A1 (CORM-A1), thapsigargin (Tg), PAI-1 inhibitor (TM5441), and ISR inhibitor (ISRIB) were purchased from Sigma-Aldrich (St. Louis, MO, USA). Bleomycin (BLM) was purchased from MedChemExpress LLC (MCE, Monmouth Junction, NJ).

2.2. Cell Culture. Human Caucasian fibroblast-like fetal lung cells (WI-38 cells) were cultured in Minimum Essential Medium (MEM, Thermo Fisher Scientific, Waltham, MA, USA) with 10% fetal bovine serum (FBS, BI, USA) and 1% penicillin-streptomycin (Gibco, USA) solution at 37°C in a humidified incubator with 5% CO₂. We isolated primary mouse embryonic fibroblasts (MEFs) from 8-week female pregnant C57BL/6 mice and cultured in DMEM (Gibco, Grand Island, NY) medium with 10% fetal bovine serum, 1% penicillin-streptomycin solution, and 1% MEM nonessential amino acid solution (N1250, Solarbio, Beijing, China).

2.3. Transfection of siRNAs. Small interfering RNA (siRNA) against human PA I-1 (siPAI-1, sc-36179) and negative control siRNA (scRNA, sc-37007) were purchased from Santa Cruz Biotechnology, Inc. (Santa Cruz, CA, USA). WI-38 cells

were seeded in a 6-well plate at a concentration of 3×10^5 cells per well, and cells were transfected with siPAI-1 and scRNA, respectively, by utilizing Lipofectamine 2000 (Invitrogen, Carlsbad, USA) in accordance with the manufacturer's protocol. In brief, dilute 100 pmol siRNA oligomer in 250 μ l Opti-MEM (Gibco, USA) without serum and mix gently. Dilute 5 μ l Lipofectamine 2000 in 250 μ l Opti-MEM without serum and mix gently for 5 min at room temperature. After a 5-minute incubation, combine the diluted oligomer with the diluted Lipofectamine 2000. Mix gently and incubate for 20 min at room temperature. Drop the 500 μ l oligomer-Lipofectamine 2000 complexes to each well containing cells and medium. Mix gently by rocking the plate back and forth. After a 36-hour transfection, cells were additionally treated with BLM for 96 h. Then, the cells were collected for SA- β -gal staining, qRT-PCR, and Western blot assay.

2.4. RNA Isolation and Quantitative Real-Time Polymerase Chain Reaction (qRT-PCR). Total RNA was isolated from WI-38 cells and MEFs by utilizing TRIzol reagent (Takara, Otsu, Japan), according to the manufacturer's instructions. In brief, 2 μ g of total RNA was used to generate cDNA using Prime Script™ RT Reagent kit with gDNA Eraser (Takara, Otsu, Japan). The synthesized cDNA was subjected to PCR-based amplification. To perform quantitative real-time PCR (qRT-PCR), the synthesized cDNA was amplified with TB Green Premix EX Taq™ II (Takara, Otsu, Japan) on Bio-Rad CFX Connect™ Real-Time PCR Detection System (Bio-Rad Laboratories). The following primers were human GAPDH (forward 5'-CAA TGA CCC CTT CAT TGA CCT C-3', reverse 5'-AGC ATC GCC CCA CTT GAT T-3'), human p21 (forward 5'-CGA TGG AAC TTC GAC TTT GTC A-3', reverse 5'-GCA CAA GGG TAC AAG ACA GTG-3'), human IL-6 (forward 5'-ACT CAC CTC TTC AGA ACG AAT TG-3', reverse 5'-CCA TCT TTG GAA GGT TCA GGT TG-3'), human TNF- α (forward 5'-GCT GCA CTT TGG AGT GAT CG-3', reverse 5'-GTT TGC TAC AAC ATG GGC TAC AG-3'), human IL-1 β (forward 5'-TTA CAG TGG CAA TGA GGA TGA C-3', reverse 5'-GTC GGA GAT TCG TAG CTG GAT-3'), human PAI-1 (forward 5'-TGA TGG CTC AGA CCA ACA AAG-3', reverse 5'-CAG CAA TGA ACA TGC TGA GG-3'), mouse GAPDH (forward 5'-GGG AAG CCC ATC ACC ATC T-3', reverse 5'-CGG CCT CAC CCC ATT TG-3'), mouse p21 (forward 5'-GTG GCC TTG TCG CTG TCT T-3', reverse 5'-GCG CTT GGA GTG ATA GAA ATC TG-3'), mouse IL-6 (forward 5'-CCA GAG ATA CAA AGA AAT GAT GG-4', reverse 5'-ACT CCA GAA GAC CAG AGG AAA T-3'), mouse TNF- α (forward 5'-AGA CCC TCA CAC TCA GAT CAT CTT C-3', reverse 5'-TTG CTA CGA CGT GGG CTA CA-3'), and mouse IL-1 β (forward 5'-TCG CTC AGG GTC ACA AGA AA-3', reverse 5'-ATC AGA GGC AAG GAG GAA ACA C-3').

2.5. Western Blot. Cell lysates were prepared using protein extraction kit (Solarbio, Beijing, China) containing protease

inhibitor and phosphatase inhibitors. Total protein concentration of the lysates was measured using a BCA protein assay kit (Solarbio, Beijing, China). Proteins were resolved by SDS-PAGE, transferred onto polyvinylidene difluoride (PVDF) membrane (Millipore, Darmstadt, Germany), and probed with appropriate dilutions of the following antibodies: cyclin D1 (1:1000, 2922S, Cell Signaling), Lamin A/C (1:1000, sc-6215, Santa Cruz), TERT (1:500, abs136649, Absin), and β -actin (1:1000, 4967S, Cell Signaling). Then, the membranes were incubated with secondary antibody in the room temperature for 40 min. Antibody binding was visualized with an ECL chemiluminescence system (GE Healthcare Bio-Sciences, Little Chalfont, UK), and chemiluminescence signal was read by Bio-Rad ChemiDoc XRS+ (Bio-Rad Laboratories, Hercules, CA). The relative band density was analyzed by using ImageJ2x software (US National Institutes of Health, Bethesda, USA).

2.6. Nuclear and Cytosolic Fractions. To check the nuclear translocation of cyclin D1, the nuclear and cytoplasmic proteins of cultured WI-38 cells were separated by Nuclear/Cytosol Fraction Kit (BioVision, USA) according to the manufacturer's protocol. In brief, harvested cells were added 100 μ l of cytosol extraction buffer (CEB) containing DTT and protease inhibitors. After vortex and 10 min incubation on ice, the extracts were centrifuged at 16,000 g for 5 min at 4°C and the supernatant was immediately removed to separate the cytoplasmic fraction from the nuclei. The nuclei pellets were then added 50 μ l nuclei extraction buffer (NEB), vortexed briefly, and set on ice every 10 min for a total 40 min. After centrifuging at 16,000 g for 10 min at 4°C, the supernatant nuclear extracts were stored at -80°C for future use.

2.7. SA- β -gal Staining. To observe the senescent cells, WI-38 and MEF cells were treated with bleomycin to construct DNA damage-induced premature cellular senescence. Then, senescence-associated- (SA-) β -galactosidase (gal) staining was performed by utilizing a cellular senescence cell histochemical stain kit (Sigma, CS0030) according to the manufacturer's protocol. For lung tissue staining, the left part of lung tissues was fixed at room temperature for 2 h, with a solution containing 2% formaldehyde and 0.2% glutaraldehyde in PBS, and washed three times with PBS. Then, lung tissues were incubated overnight at 37°C (in the absence of CO₂) with the staining solution containing X-gal in N,N-dimethylformamide (pH 6.0).

2.8. Immunofluorescence. To observe the formation of SGs and the sequestration of PAI-1 and the γ -H2AX foci, WI-38 cells were plated on a 4-well Lab-Tek chambered cover glass (Nunc, Thermo Scientific, Waltham, MA) and pretreated with CORM-A1 (40 μ M) for 6 h followed by the administration of 25 μ g/ml bleomycin for 96 h to construct DNA damage-induced premature cellular senescence. Then, cells were washed in 1 \times PBS, fixed with 4% (v/v) paraformaldehyde in PBS at room temperature for 15 min, and permeabilized with 0.1% (v/v) Triton X-100 in PBS for 5 min. Then, cells were washed three times with PBS before

incubation for 2 h at room temperature with primary antibodies (anti-TIA1, 1:500, ab140595, Abcam; anti-G3BP1, 1:200, sc-365338, Santa Cruz; anti-PAI-1, 1:200, sc-5297, Santa Cruz; and anti- γ -H2AX, 1:200, ab81299, Abcam) diluted in 1% (*w/v*) BSA in PBS. Cells were washed further three times with 1 \times PBS before incubation for 1 h with secondary fluorophore-coupled antibodies (Alexa Fluor 594 goat anti-rabbit IgG, 1:500, Invitrogen and Alexa Fluor 488 rabbit anti-mouse IgG, 1:400, Invitrogen), respectively. Secondary antibodies were diluted in 1% (*w/v*) BSA in 1 \times PBS. After incubation, cells were washed three times with 1 \times PBS and were imaged with an Olympus FV1000 confocal microscope (Olympus, Tokyo, Japan). Quantifications from immunofluorescence images were done by counting cells with TIA1 and G3BP1 colocalized SGs per total number of cells in randomly selected field. Each field contained at least 30 cells, and three images per condition were analyzed.

2.9. Measurement of PAI-1 and Several SASP Secretions. WI-38 cells were pretreated with 40 μ M CORM-A1 for 6 h followed by the administration of 25 μ g/ml for 96 h. During the process of cellular senescence, WI-38 cells were post-treated with 40 μ M CORM-A1 for 6 h every two days. After a 4-day incubation, cultured supernatant was collected, and the concentrations of PAI-1 and several SASPs, including IL-6, TNF- α , and IL-1 β , were measured by human PAI-1 (DuoSet ELISA DY9387-05, BD Biosciences), human IL-6 (Cusabio Biotech, Wuhan, China), human TNF- α (Cusabio Biotech, Wuhan, China), and human IL-1 β (Cusabio Biotech, Wuhan, China) ELISA kit according to the manufacturer's instructions.

2.10. Statistics. For statistical comparison, all values were expressed as the mean \pm SD. Statistical differences between all experimental groups were applied by one-way ANOVA with Tukey's post hoc test, and all statistical analyses were assessed by GraphPad Prism software version 5.03 (San Diego, CA). The statistically significant changes among groups were considered as probability values of $p \leq 0.05$.

3. Results

3.1. CO Inhibits Bleomycin-Induced Cellular Senescence in Human and Mouse Fibroblasts. Bleomycin, a widely used antineoplastic drug, is well known for its side effects on induction of severe interstitial pulmonary fibrosis (IPF). Due to its combination with iron that reduces molecular oxygen to superoxide and hydroxyl radicals, bleomycin can induce DNA injury and further lead to single- and double-stranded breaks [30]. Increasing studies have demonstrated that bleomycin-mediated pulmonary fibrosis is mainly caused by lung epithelial and fibroblast senescence via activating DNA damage response (DDR) [30, 31]. To identify whether exogenous CO exerted inhibitory effect on bleomycin-induced fibroblast senescence, we first checked the cellular toxicity of CO-releasing molecular A1 (CORM-A1) on human fibroblast-like fetal lung cells, WI-38 cells, with various concentrations (0, 10, 20, 40, and 80 μ M) for 6 h. As we expected, low-dose CORM-A1 showed no toxicity

on WI-38 cells (Figure 1(a)). Then, cells were pretreated with CORM-A1 in a dose-dependent manner (0, 20, 40, and 80 μ M) for 6 h followed by the administration of bleomycin (25 μ g/ml) for 96 h. During the challenge of bleomycin, cells were posttreated with CORM-A1 for 6 h every two days. After a 4-day incubation, we found that bleomycin alone significantly increased the number of cells positive for the expression of p21 (Figure 1(b)) and several SASPs, including IL-6, TNF- α , and IL-1 β (Figures 1(c)–1(e)). However, pre- and posttreatment of CORM-A1 could significantly reduce the levels of p21 and SASPs stimulated by bleomycin, indicating that CORM-A1 might possess antisenescent effect on bleomycin-induced premature senescence. As a negative control, herein, we treated cells with inactive CORM-A1 (iCORM-A1) that is incapable of releasing CO and found that iCORM-A1 showed no interference in p21 and SASP levels in the presence of bleomycin (Figures 1(b)–1(e)). Given that 40 μ M CORM-A1 showed optimally to reduce the levels of p21 and SASP, in the following studies, we chose 40 μ M as the appropriate dose to treat cells.

To further assess the antisenescent effect of CORM-A1, we treated WI-38 cells (Figure 1) and primary mouse embryonic fibroblasts (MEFs) (Figure 2) with CORM-A1 in the stimulation of bleomycin and found that the enhanced markers of cellular senescence, including the percentage of senescence-associated (SA)- β -gal-positive cells (Figures 1(f) and 2(b)), γ -H2AX foci (Figures 1(g) and 2(c)), mRNA expression of p21 (Figure 2(d)), IL-6 (Figure 2(e)), TNF- α (Figure 2(f)), and IL-1 β (Figure 2(g)), were all significantly decreased. Due to p21 is a well-known target gene of p53, and which plays a critical role in the process of cellular senescence [1, 5, 6], we next checked the protein levels of p53 and p21 in WI-38 cells. Consistent with the results obtained from the regulation of senescent transcripts, the pretreatment of CORM-A1 could remarkably decrease the protein levels of p53 and p21 in the challenge of bleomycin (Figures S2A–S2C). To further investigate whether exogenous CO gas could also protect against cellular senescence, we next treated WI-38 cells with 250 ppm CO gas for 6 h every two days in the presence or absence of bleomycin (25 μ g/ml) for 96 h. Our results revealed that the exogenous CO gas could remarkably inhibit the corresponding senescence markers induced by bleomycin (Figure S1). According to these results, we clearly demonstrated that low-dose administration of CORM-A1 and CO gas could effectively prevent bleomycin-induced premature senescence.

3.2. PAI-1 Is Involved in Bleomycin-Induced Premature Senescence in WI-38 Cells. Plasminogen activator inhibitor 1 (PAI-1) is a primary inhibitor of tissue-type and urokinase-type plasminogen activators, which can inhibit the conversion of plasminogen into plasmin, and plays a major role in fibrogenesis [32]. Accumulating evidences have suggested that PAI-1 expression is significantly increased in senescent cells, and which might be not only a marker but also a key mediator of cellular senescence and organismal aging [7]. To determine whether PAI-1 was essential for bleomycin-incubated cellular senescence, we first checked the mRNA expression of PAI-1 in WI-38 cells. Our results

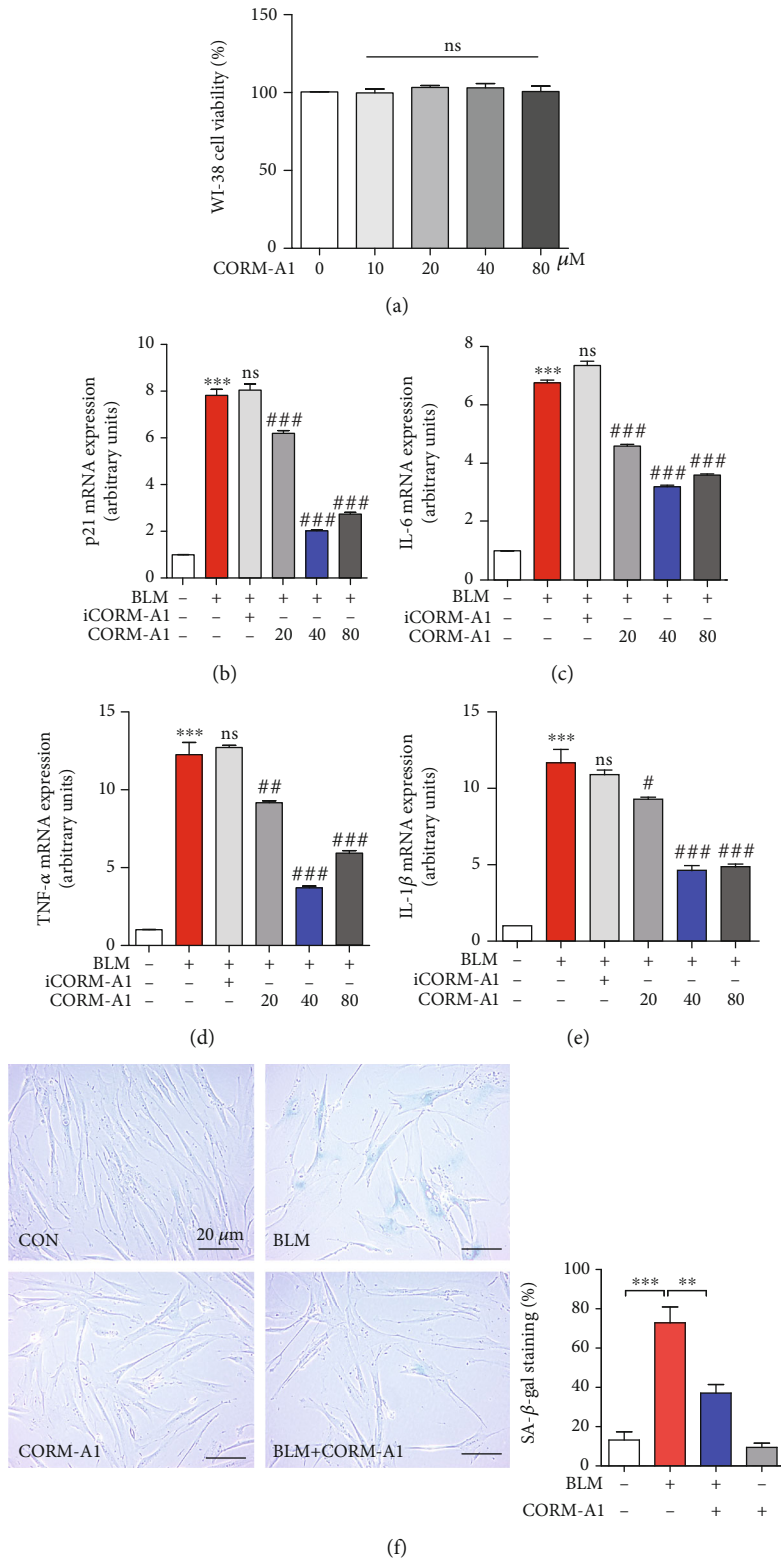
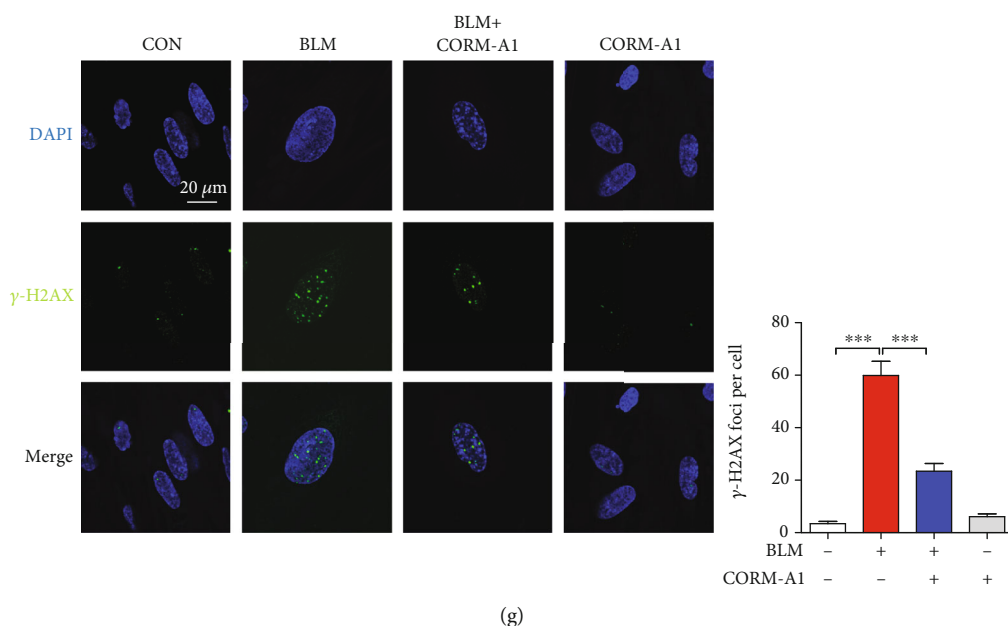


FIGURE 1: Continued.



(g)

FIGURE 1: CORM-A1 inhibits BLM-induced cellular senescence in human diploid lung fibroblasts. (a) WI-38 cells were treated with various concentrations of CORM-A1 (0, 10, 20, 40, and 80 μ M) for 6 h, and MTT assay was performed to assess the cell viability. (b–e) WI-38 cells were pretreated with CORM-A1 (0, 20, 40, and 80 μ M) and iCORM-A1 (40 μ M) for 6 h followed by the challenge of bleomycin (BLM, 25 μ g/ml) for 96 h. During the process of senescence, cells were posttreated with CORM-A1 (0, 20, 40, and 80 μ M) for 6 h every other day. After a 4-day incubation, the mRNA expressions of p21 (b), IL-6 (c), TNF- α (d), and IL-1 β (e) were measured by quantitative real-time- (qRT-) PCR. Quantitative data are expressed as the means \pm SD; $n = 3$. *** $p < 0.001$ vs. the vesicle control group. # $p < 0.05$, ## $p < 0.01$, and ### $p < 0.001$ vs. the BLM-alone treatment group. Then, senescence-associated- (SA-) β -gal staining (f) and immunofluorescence for detecting γ -H2AX foci (g) were applied in the pre- and posttreatment of CORM-A1 (40 μ M). Quantitative data are expressed as the means \pm SD ($n = 3$ determined in three independent experiments). ** $p < 0.01$ and *** $p < 0.001$. ns: not significant.

showed that bleomycin could induce a significant enhancement of PAI-1 (Figures 3(a) and S2D). Next, to evaluate whether increased PAI-1 expression was involved in the bleomycin-induced premature senescence, we transfected cells with siRNA against PAI-1 (Figures 3(b) and S2D), and then cells were stimulated with bleomycin. We found that, in the administration of bleomycin, silencing PAI-1 could dramatically decrease the markers of senescence, including the percentage of SA- β -gal stained cells (Figure 3(c)) and the expression of p21 (Figures 3(d) and S2D), p53 (Figure S2D), IL-6 (Figure 3(e)), TNF- α (Figure 3(f)), and IL-1 β (Figure 3(g)) compared with cells transfected with scramble RNA (scRNA). Furthermore, PAI-1 inhibitor, one small molecule TM5441 [33], also exhibited a significant inhibitory effect on bleomycin-induced cellular senescence. Our data showed that the treatment of TM5441 (10 μ M) in the presence of bleomycin (25 μ g/ml) could significantly decrease SA- β -gal-positive cells (Figure 3(h)) and mRNA expression of several SASPs (Figures 3(i)–3(l)). These data strongly demonstrated that PAI-1 played a critical role in bleomycin-induced premature senescence, and the inhibition of PAI-1 could effectively ameliorate the process of senescence.

3.3. CO-Induced SGs Participate in Reducing Bleomycin-Induced Senescence by PAI-1 Sequestration. One previous study has demonstrated that the assembly of SGs induced by continuous mild oxidative stress can decrease the number

of senescent cells through the sequestration of PAI-1 and subsequently activates the cyclin D1-dependent signaling pathway to maintain proliferative state [28]. Our recent study has reported that low-dose exogenous CO can stimulate SG formation by selective induction of the PERK-eIF2 α signaling pathway, one branch of integrated stress response (ISR) [29]. Based on these reports, we hypothesized that the antisenescence effect of CO might be mediated by SG formation. Here, we first confirmed the beneficial effect of CO on SG assembly by treating WI-38 cells with various concentrations of CORM-A1 (0, 20, 40, and 80 μ M) for 6 h. Immunofluorescence was applied to check the amount of SGs by applying anti-TIA-1 and anti-G3BP1 antibodies. According to our results, 40 μ M and 80 μ M CORM-A1 (Figure 4(a)) could significantly increase the assembly of TIA-1- and G3BP1-positive SGs in the cytoplasm, and iCORM-A1 revealed no benefits on SG assembly (Figure 4(a)), suggesting again that CORM-A1 exerted an inducible effect on SG formation. In further study, we tried to check whether CO could stimulate the sequestration of PAI-1 into SGs in the stimulation of bleomycin. As we expected, the increased number of SGs induced by CORM-A1 could effectively sequester PAI-1 through detecting the coaggregation of TIA-1 and PAI-1 (Figure 4(b)). Simultaneously, we evaluated the secretion of PAI-1 by ELISA assay. Cells treated with bleomycin alone significantly increased the secretion of PAI-1, while CORM-A1 administration could dramatically attenuate the level of PAI-1 in cultured medium (Figure 4(c)). To

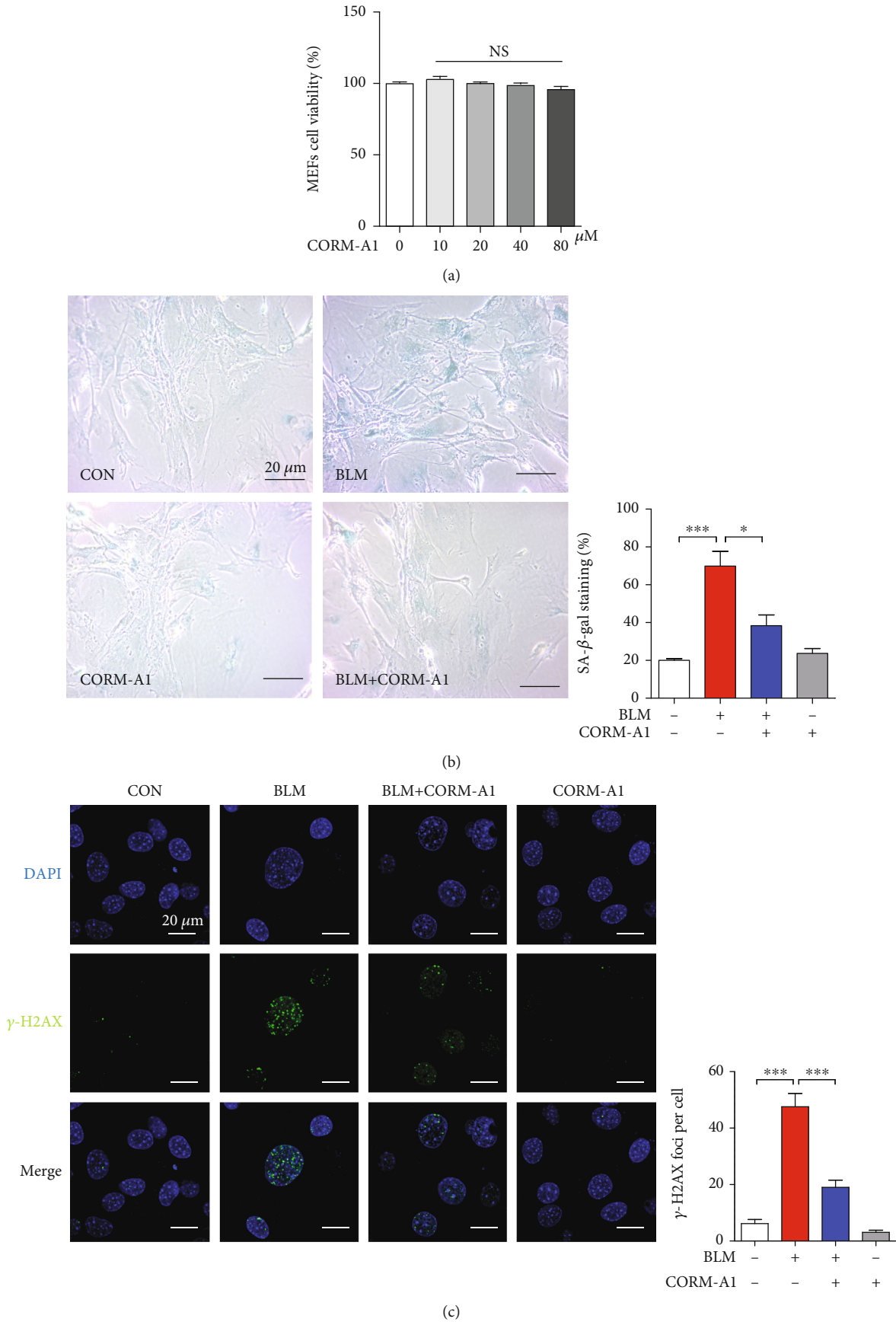


FIGURE 2: Continued.

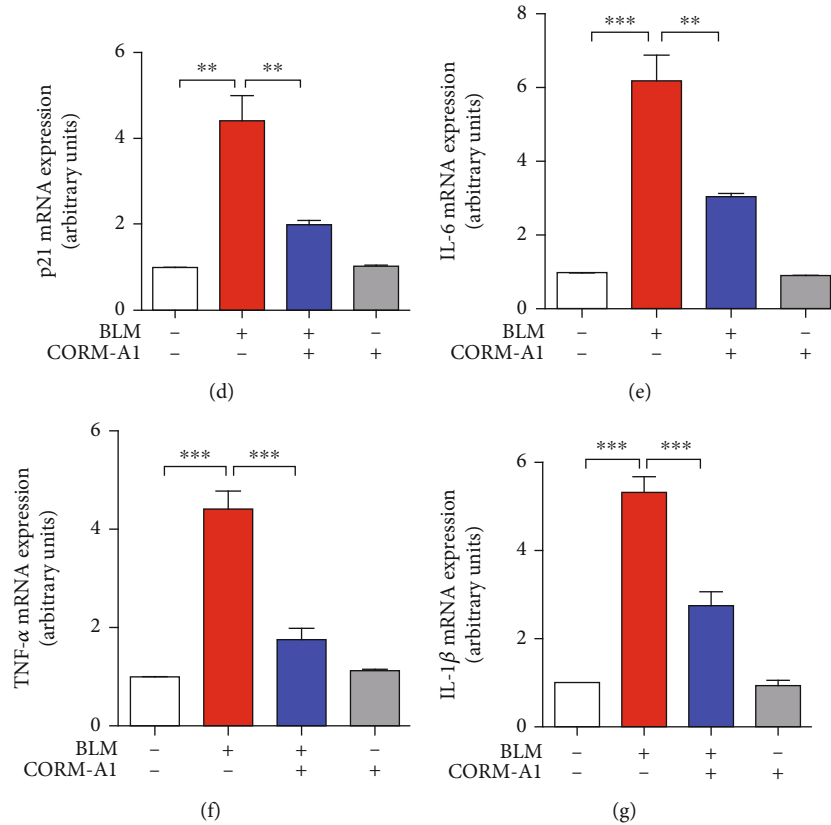


FIGURE 2: CORM-A1 attenuates BLM-induced cellular senescence in mouse embryonic fibroblasts. (a) Mouse embryonic fibroblasts (MEFs) were treated with CORM-A1 in a dose-dependent manner (0, 10, 20, 40, and 80 μM) for 6 h, and MTT assay was performed to assess the cell viability. MEFs were pretreated with CORM-A1 (40 μM) for 6 h prior to the stimulation of BLM (25 $\mu\text{g}/\text{ml}$) for 48 h. Then, SA- β -gal staining (b) and γ -H2AX foci (c) were detected, and the mRNA expressions of p21 (d), IL-6 (e), TNF- α (f), and IL-1 β (g) were detected by qRT-PCR. Quantitative data are expressed as the means \pm SD ($n = 3$ determined in three independent experiments). * $p < 0.05$, ** $p < 0.01$, and *** $p < 0.001$. ns: not significant.

define whether the decreased secretion of PAI-1 was associated with the transcription of PAI-1, we next assessed the mRNA level of PAI-1, and our data showed that CORM-A1 could slightly decreased the transcripts (Figure 4(d)), indicating that the secretion of PAI-1 regulated by CORM-A1 was mainly resulted from the induction of SGs rather than the downregulation of PAI-1 transcription. It has been reported that PAI-1 secretion correlates with the onset of senescence via inhibition of cyclin D1 nuclear translocation and hypophosphorylation of Rb [34]. To check the level of cyclin D1 in the nucleus, we isolated cytosol and nuclear fractions from WI-38 cells and found that the level of cyclin D1 was significantly decreased in bleomycin-treated cells, while it was significantly increased in the fraction of the cytoplasm (Figure 4(e)). In addition, CORM-A1 could positively regulate the nuclear translocation of cyclin D1 (Figure 4(e)), and which is associated with the increase of Rb phosphorylation (Figure 4(f)). Moreover, we also observed that the secretions of SASP, including IL-6 (Figure 4(g)), TNF- α (Figure 4(h)), and IL-1 β (Figure 4(i)), induced by bleomycin were dramatically reduced in the administration of CORM-A1. Our findings demonstrated that CO-mediated downregulation of PAI-1 secretion was associated with the SG formation, and which could enhance the activation of cyclin D1

and hyperphosphorylation of Rb to delay the process of senescence and the secretion of SASP.

3.4. ISRIB Abolishes CO-Induced SG Assembly and Recovers Bleomycin-Mediated Cellular Senescence. According to our recent study, CO-induced SG assembly was dependent on the ISR signaling pathway, and ISR inhibitor, ISRIB, could decrease the formation of SGs in the administration of CORM2 and CO gas [29]. To confirm these reported results, we first cotreated WI-38 cells with CORM-A1 and ISRIB for 6 h and observed that ISRIB could significantly inhibit the formation of SGs by visualizing the coaggregation of TIA-1 and G3BP1 in the cytoplasm (Figure 5(a)). Next, to analyze whether the inhibition of SGs by ISRIB could negatively regulate the antisenescent effect of CORM-A1, we next performed pre- and posttreatment of CORM-A1 in WI-38 cells with or without ISRIB for 6 h followed by the administration of bleomycin for 96 h. After a 4-day incubation, we checked the percentage of SA- β -gal-positive cells (Figure 5(b)) and the number of γ -H2AX foci per cell (Figure 5(c)). In bleomycin-induced senescent cells, the enhanced activity of SA- β -gal and γ -H2AX foci was significantly decreased by CORM-A1, and which was reversed in the cotreatment of ISRIB (Figures 5(b) and 5(c)). Moreover, we also observed that ISRIB

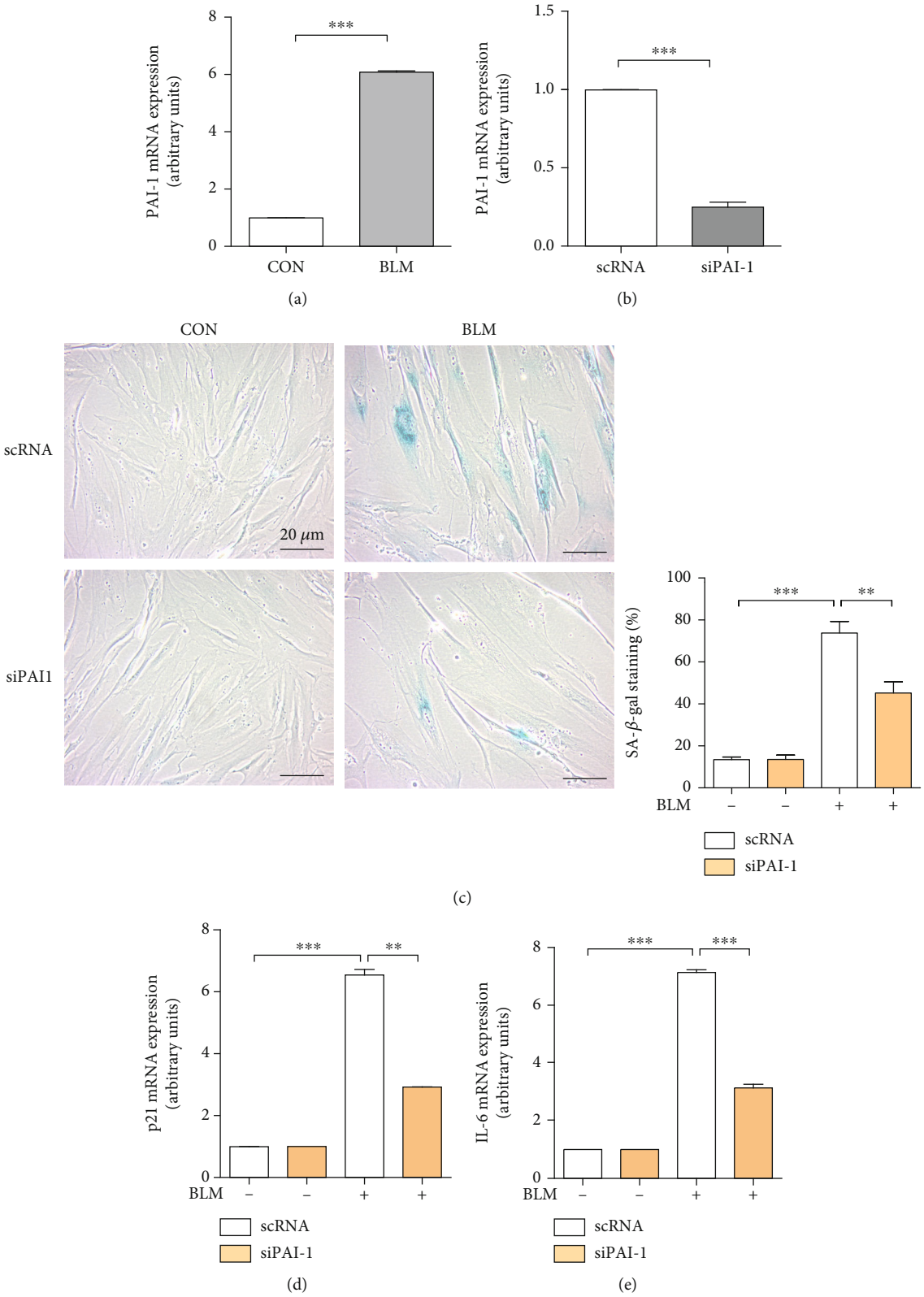


FIGURE 3: Continued.

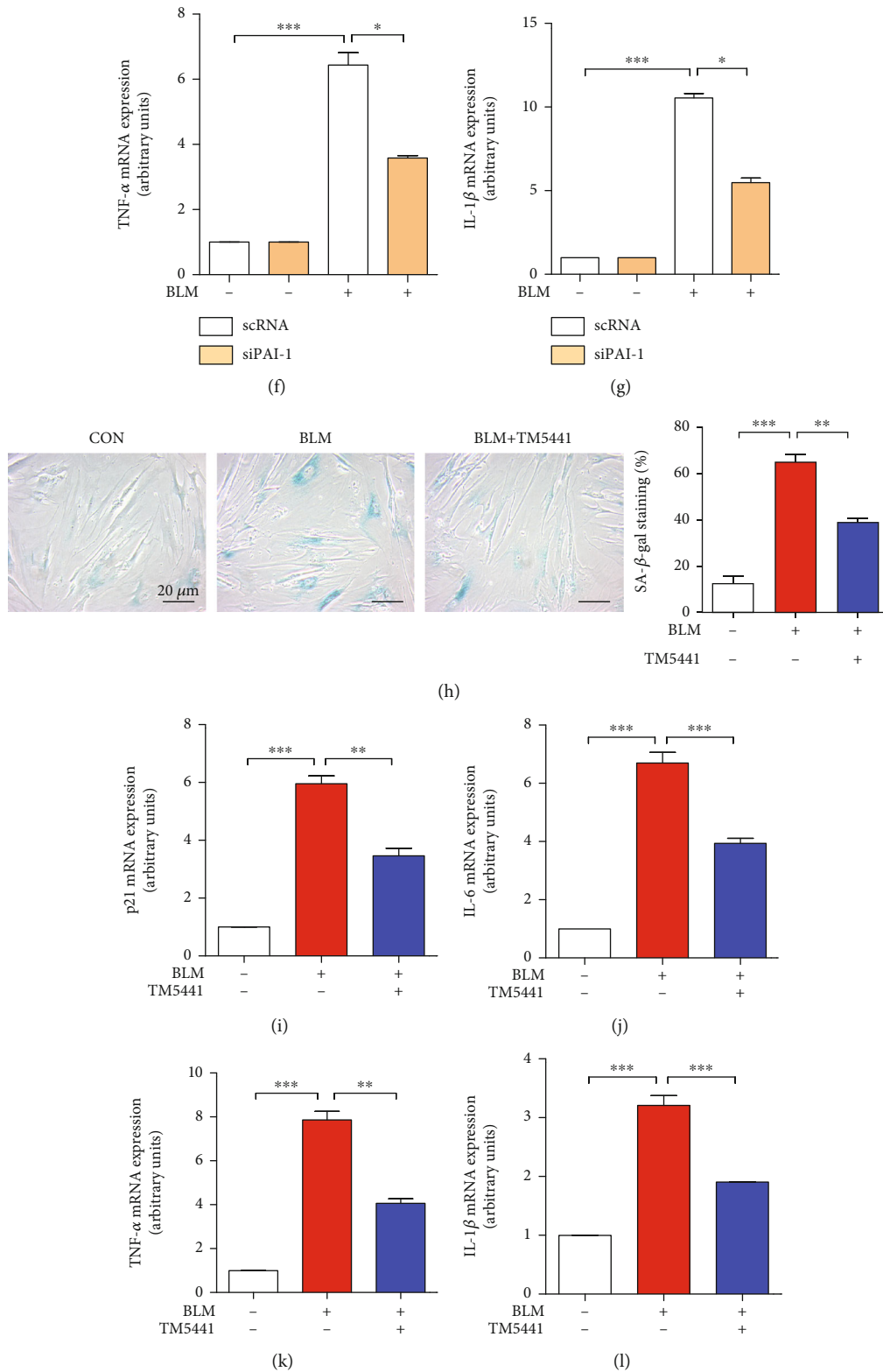
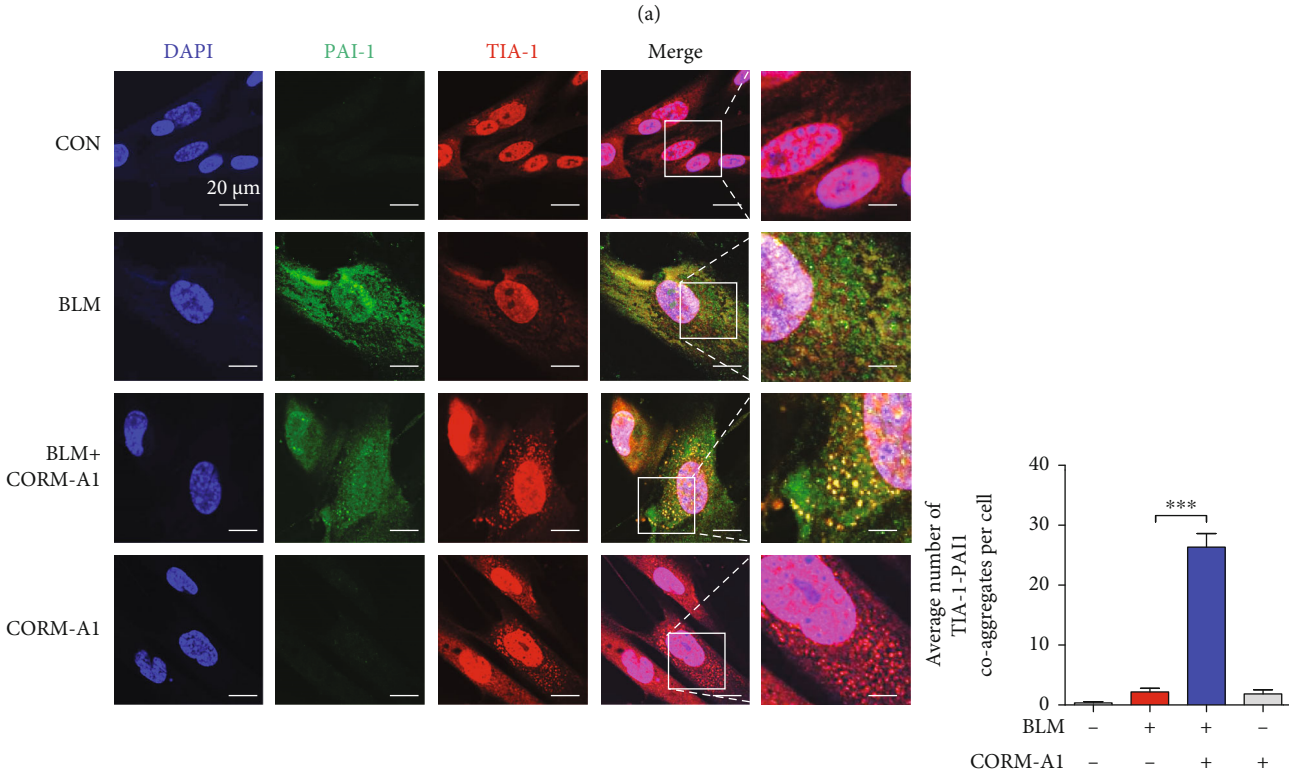
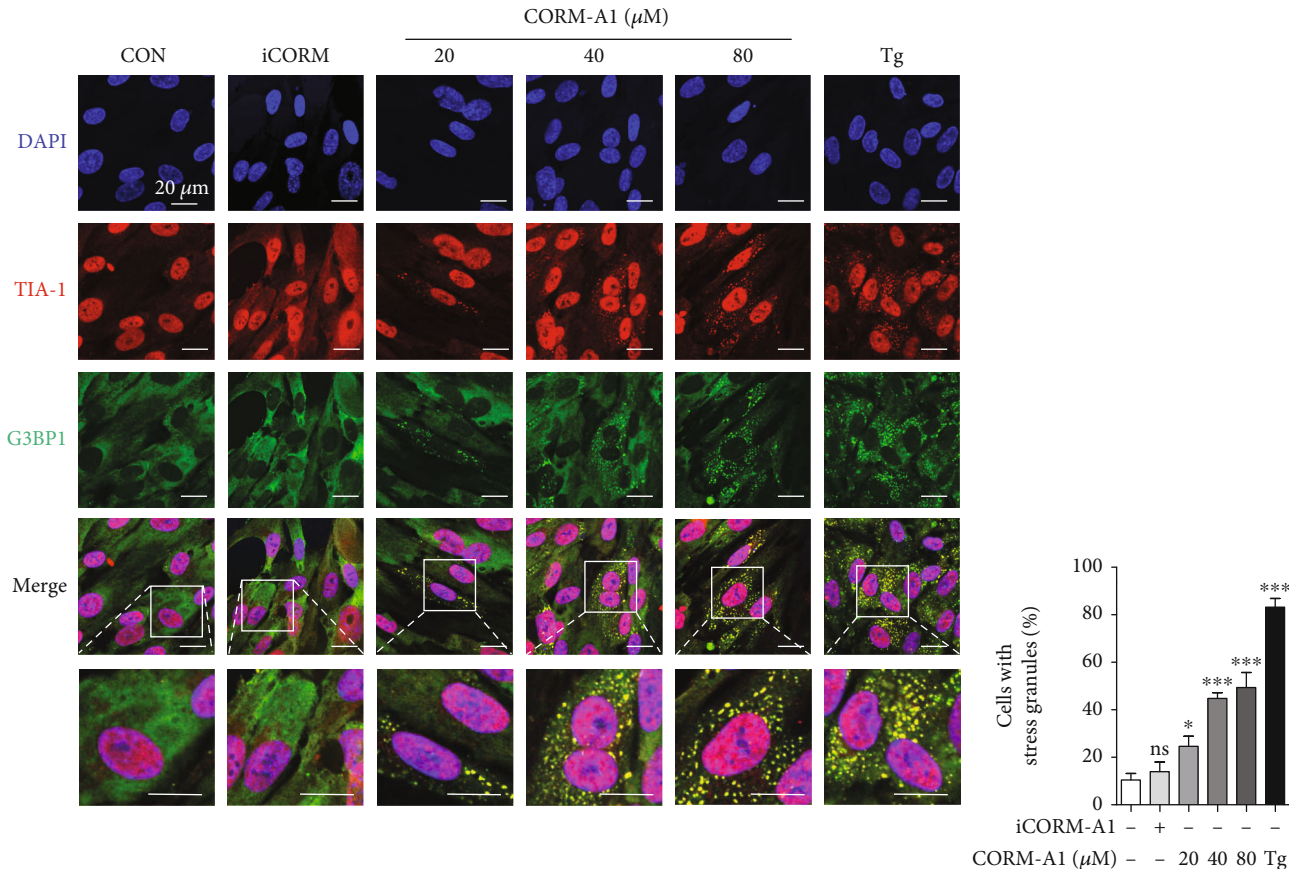


FIGURE 3: PAI-1 is involved in BLM-induced fibroblast senescence. (a) WI-38 cells were treated with BLM (25 μ g/ml) for 96 h, and the mRNA expression of PAI-1 was detected by qRT-PCR. (b) WI-38 cells were transfected with scramble siRNA (scRNA) and siRNA against PAI-1 (siPAI-1) for 36 h, and then, PAI-1 mRNA level was assessed by qRT-PCR. Transfected cells were treated with BLM (25 μ g/ml) for 96 h, and cells were performed SA- β -gal staining (c), and the mRNA expressions of p21 (d), IL-6 (e), TNF- α (f), and IL-1 β (g) were measured by qRT-PCR. WI-38 cells were cotreated with PAI-1 inhibitor, TM5441 (10 μ M), and BLM (25 μ g/ml) for 96 h. Then, SA- β -gal staining (h) and the mRNA expressions of p21 (i), IL-6 (j), TNF- α (k), and IL-1 β (l) were measured by qRT-PCR. Quantitative data are expressed as the means \pm SD ($n = 3$ determined in three independent experiments). * $p < 0.05$, ** $p < 0.01$, and *** $p < 0.001$.



(b)
FIGURE 4: Continued.

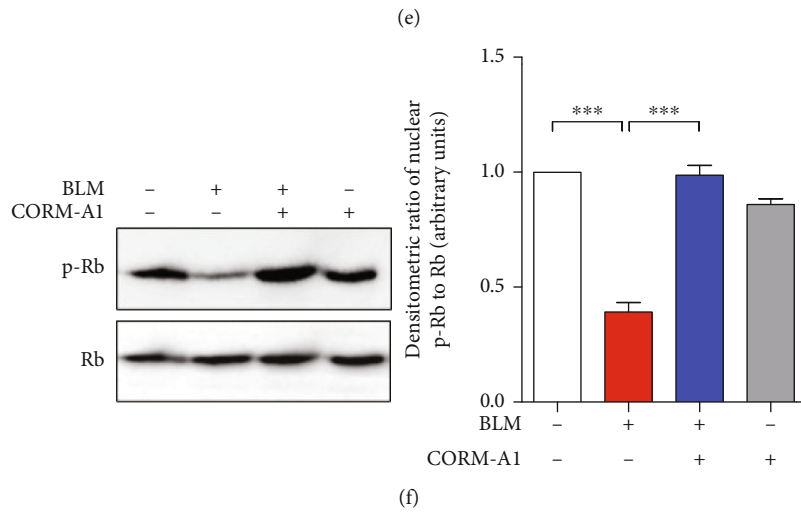
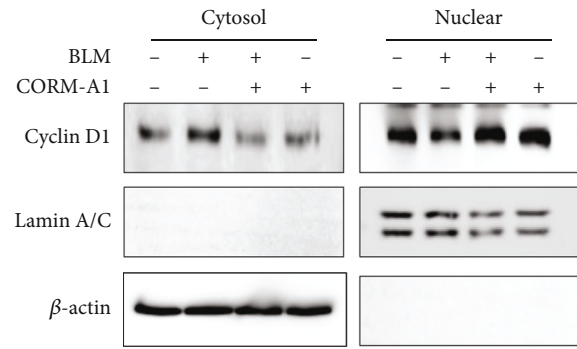
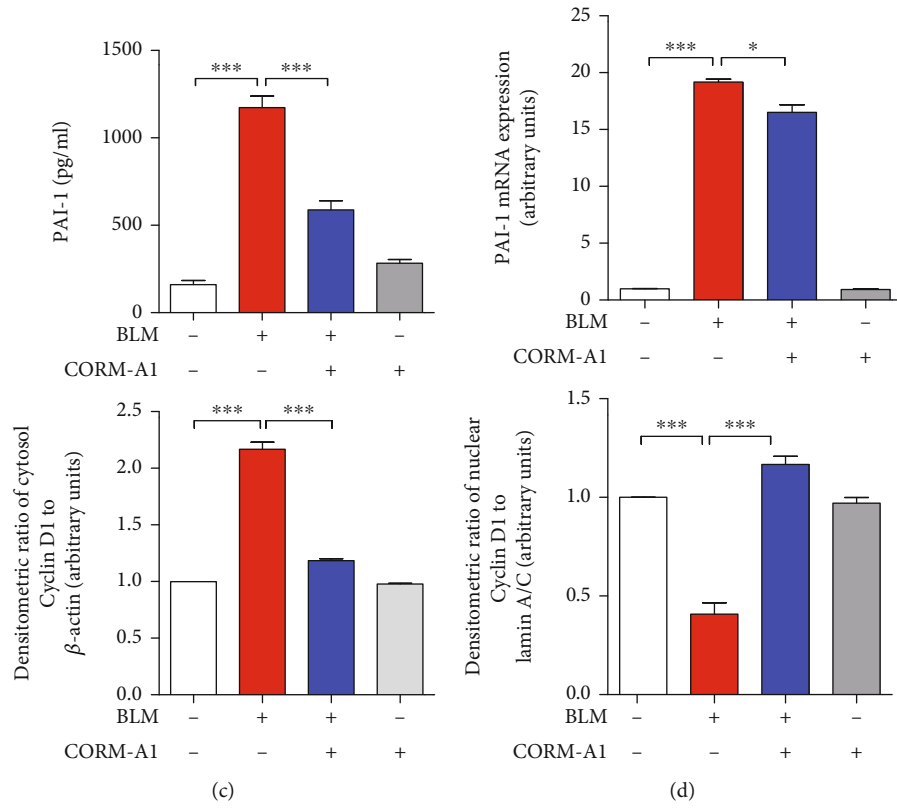


FIGURE 4: Continued.

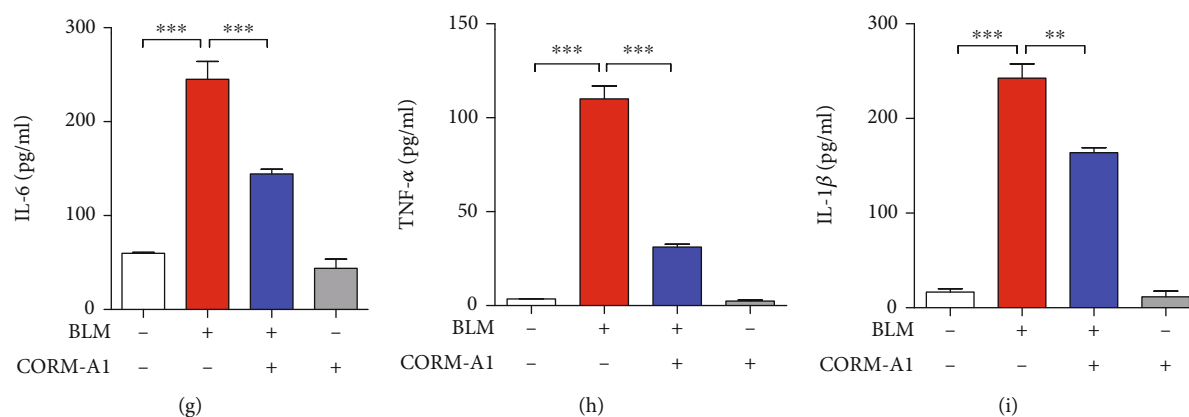


FIGURE 4: CO inhibits secretion of PAI-1 in senescent cells via SG formation. (a) WI-38 cells were treated with CORM-A1 in various concentrations (0, 20, 40, and 80 μM) and iCORM-A1 (40 μM) for 6 h. As a positive control, WI-38 cells were treated with 200 nM thapsigargin (Tg) for 45 min, and then, immunofluorescence assay was performed to detect the formation of SGs by visualizing the colocalization of TIA-1 (red) and G3BP1 (green). (b) WI-38 cells were pretreated with CORM-A1 (40 μM) for 6 h prior to the administration of bleomycin (25 $\mu\text{g}/\text{ml}$) for 96 h. After a 4-day treatment, immunofluorescence assay was performed to detect the TIA-1 (red) and PAI-1 (green) coaggregates. The secretion of PAI-1 was assessed by ELISA (c), and the mRNA expression of PAI-1 was assessed by qRT-PCR (d). (e) Nuclear translocation of cyclin D1 was measured by Western blot assay in cytosol and nuclear fractions. (f) The phosphorylated and total forms of Rb were analyzed by Western blot assay. The secretion of SASP, including IL-6 (g), TNF- α (h), and IL-1 β (i), was measured by ELISA. Quantitative data are expressed as the means \pm SD ($n = 3$ determined in three independent experiments). ** $p < 0.01$ and *** $p < 0.001$. ns: not significant.

strongly inhibits the sequestration of PAI-1 into CO-induced SGs (Figure 5(d)), and for that reason, the inhibitory effect of CORM-A1 on PAI-1 secretion was drastically abolished (Figure 5(i)). Next, we also checked the mRNA expression of p21 (Figure 5(e)), several SASPs (Figures 5(f)–5(h)), and protein levels of p53 (Figure S2E) and p21 (Figure S2E). As we expected, administration of ISRIB could robustly deplete the inhibitory effect of CORM-A1 on downregulation of p53, p21, and SASP expression. Additionally, ISRIB also abrogated the inhibitory effect on the secretion of SASP (Figures 5(i)–5(l)).

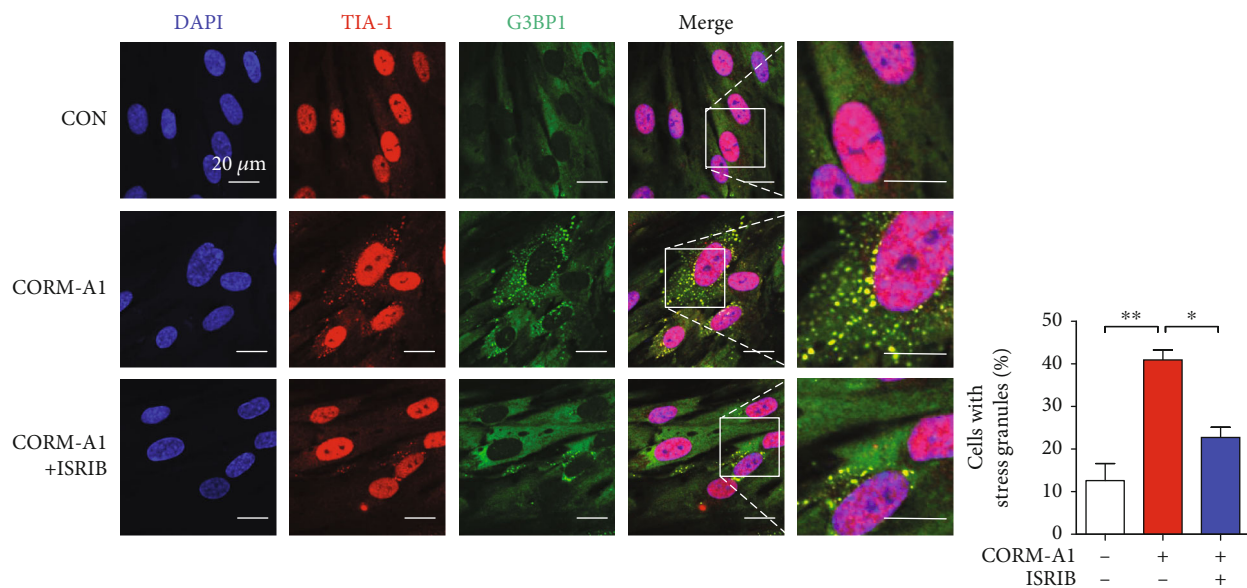
Telomere shortening is an important marker of cellular senescence [1], and bleomycin has been reported to induce telomere shortening and cellular senescence to provoke the development of pulmonary fibrosis [35]. Moreover, several studies have proved that telomerase is a ribonucleoprotein that includes the telomerase reverse transcriptase (TERT) and the telomerase RNA (TERC) [36, 37]. Telomerase inhibition by targeting TERT has been shown to induce cellular senescence, shortening of telomere, and DNA damage [38]. Based on these studies, to verify whether exogenous CO could regulate telomere shortening via induction of SGs, we next checked the protein level of TERT (Figure S2E). Our results showed that bleomycin-mediated cellular senescence could interfere with the protein level of TERT, and CORM-A1 could significantly reverse the change of TERT. However, ISRIB cotreatment remarkably compromises the enhancement of TERT induced by CORM-A1. These results demonstrated that exogenous CO could upregulate TERT expression to control telomere shortening, and which might be associated with the formation of SGs, while the detailed molecular mechanisms should be clarified in further studies.

Taken together, our data clearly indicated that ISRIB could interfere with the antisenescent effect of CO on bleomycin-induced cellular senescence via diminishing SG assembly and sequestration of PAI-1 and influencing telomere shortening.

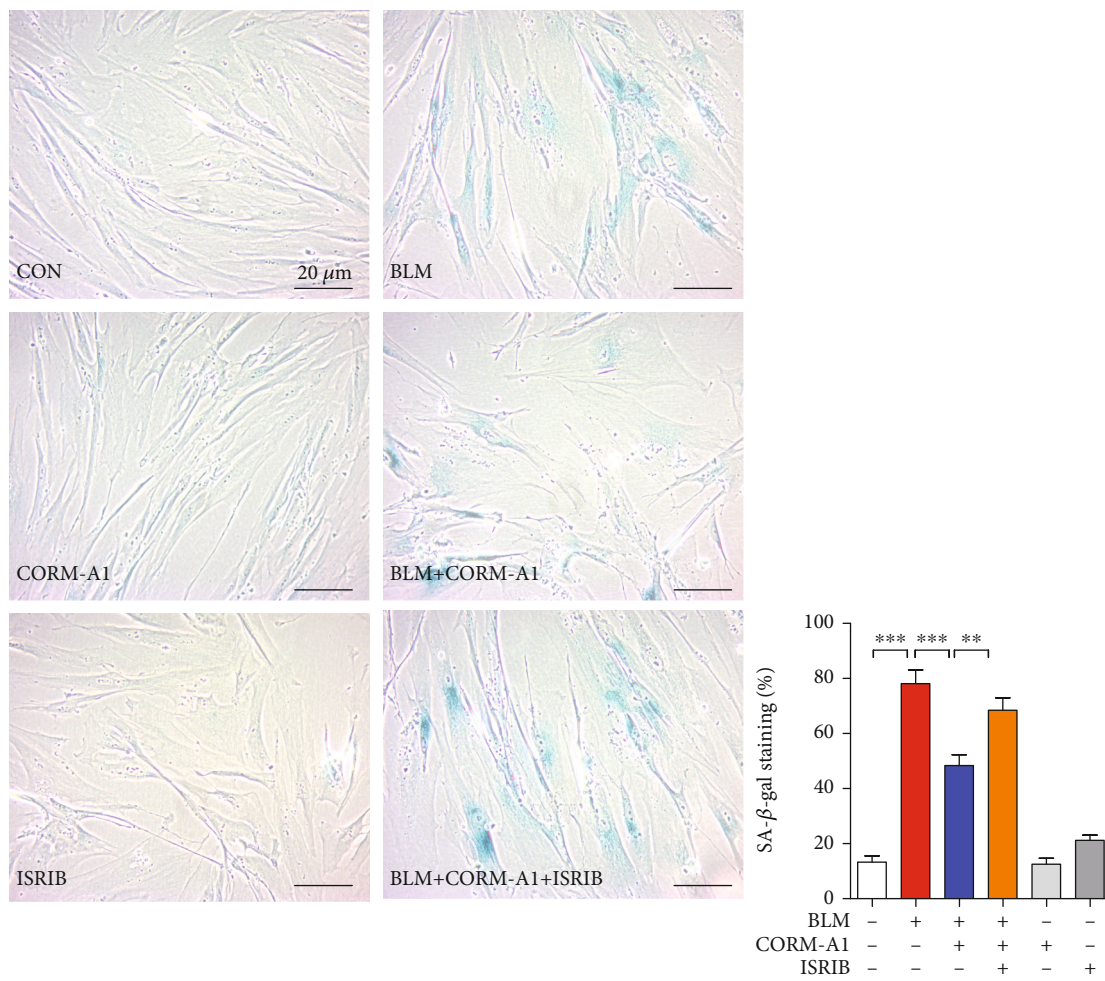
4. Discussion

Cellular senescence can induce both beneficial and deleterious outcomes in a context-dependent manner [4, 39], and these opposing effects mediated by senescent cells are strongly related to the upregulation of SASP, including growth factors, cytokines, and extracellular matrix metalloproteinase [40]. Accumulating evidences have supported that PAI-1, a member of SASP, is a critical marker of cellular senescence associated with aging and aging-related pathologies, such as metabolic syndrome, chronic kidney disease, and multiorgan fibrosis [7, 41]. One previous study has demonstrated that the formation of SGs induced by continuous mild stress can prevent replicative senescence by promoting the localization of PAI-1 into SGs, which can increase the nuclear translocation of cyclin D1 to delay the process of replicative senescence [28]. Recently, we have proved that CO possesses a beneficial effect on SG formation through the induction of ISR [29]. Based on these reports and our results, herein, we demonstrated for the first time that the assembly of SGs mediated by CO could sequester PAI-1, which protects cells against bleomycin-induced premature senescence.

In this study, we treated human diploid fibroblasts WI-38 cells and primary mouse embryonic fibroblasts with bleomycin to establish DNA damage-induced premature senescence. Bleomycin, one mixture of glycopeptide antitumor drug, is

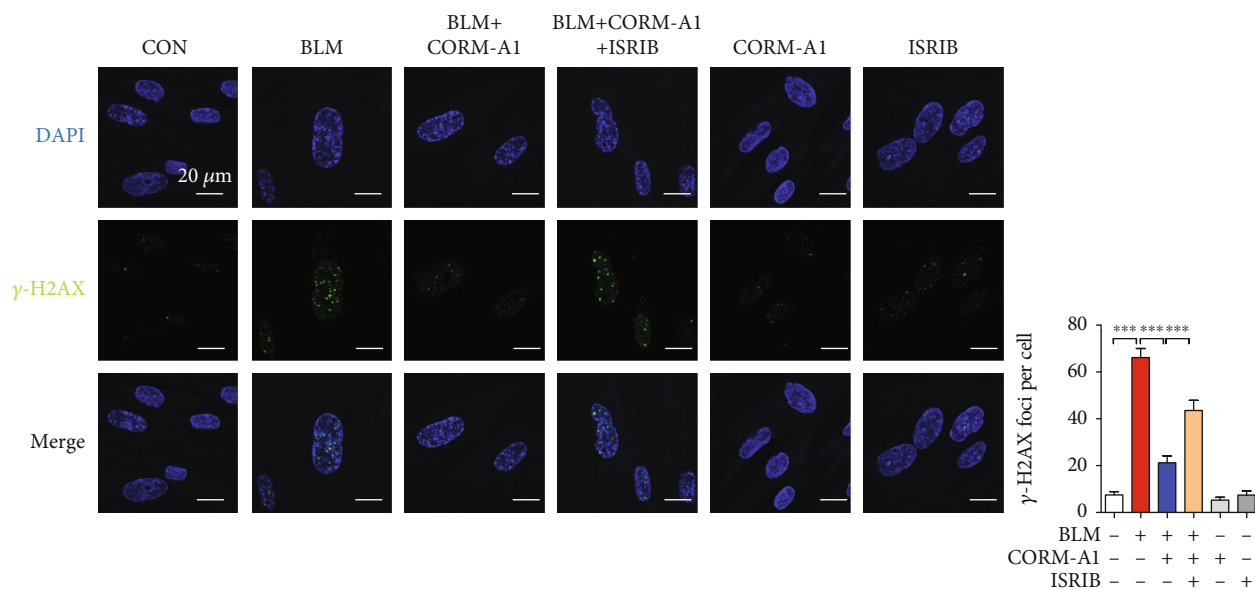


(a)

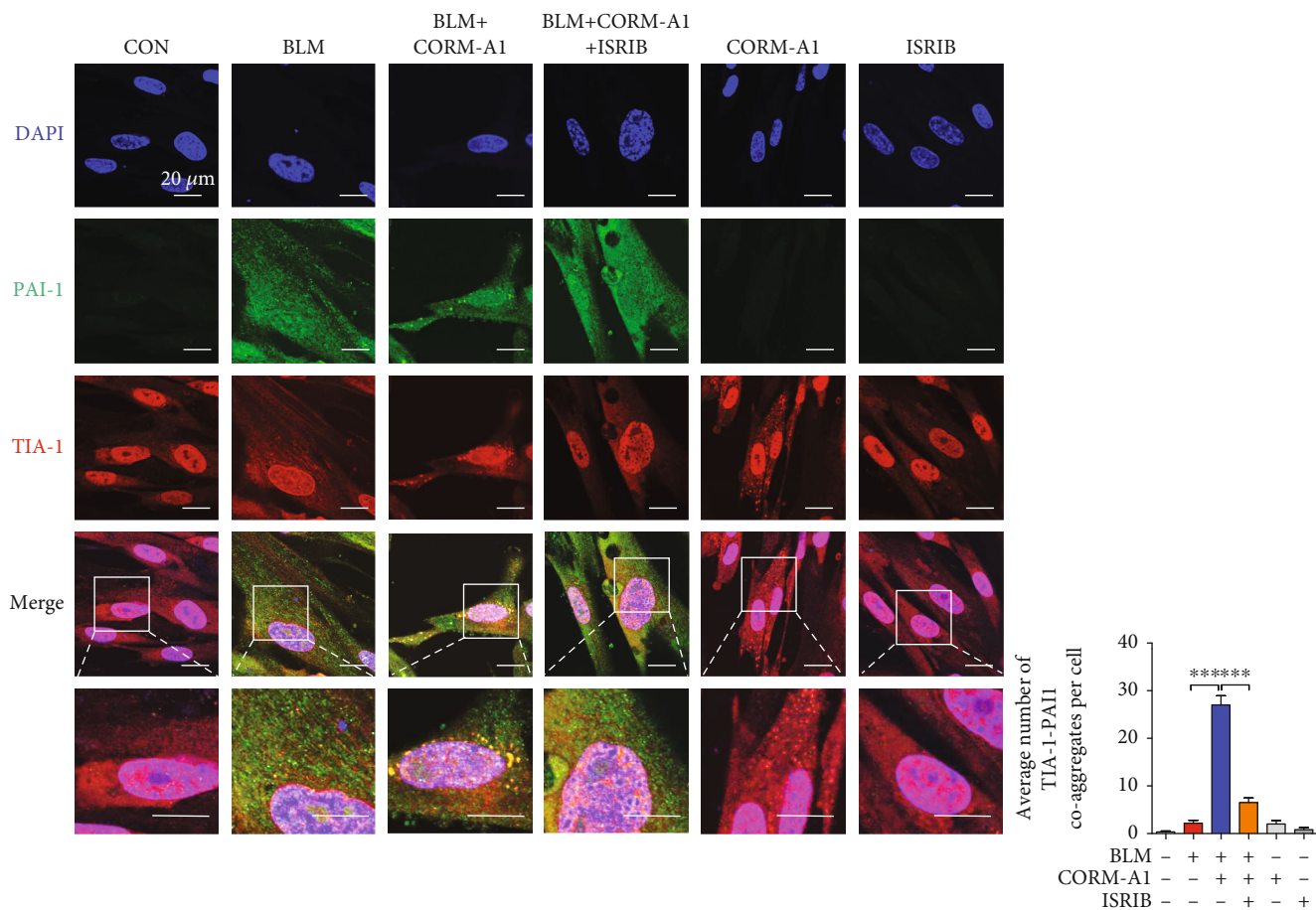


(b)

FIGURE 5: Continued.



(c)



(d)

FIGURE 5: Continued.

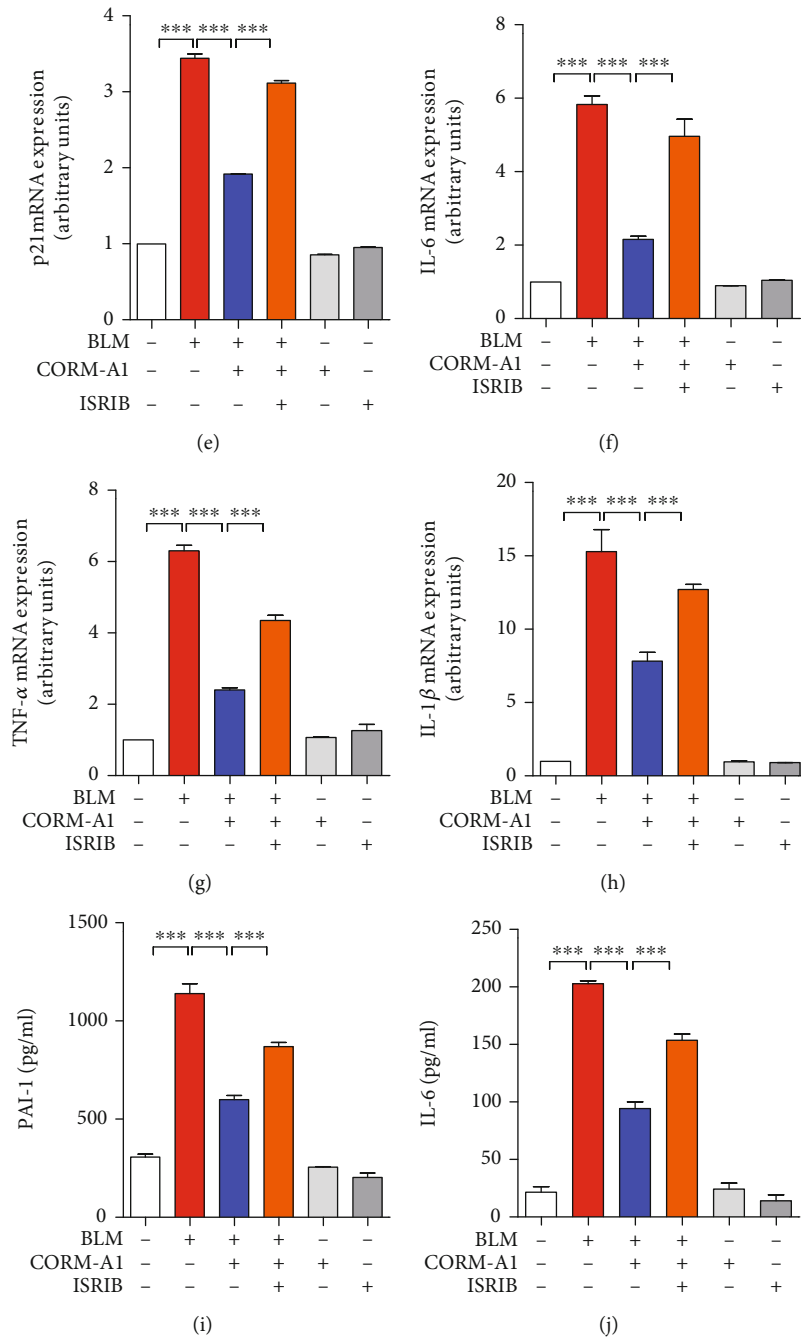


FIGURE 5: Continued.

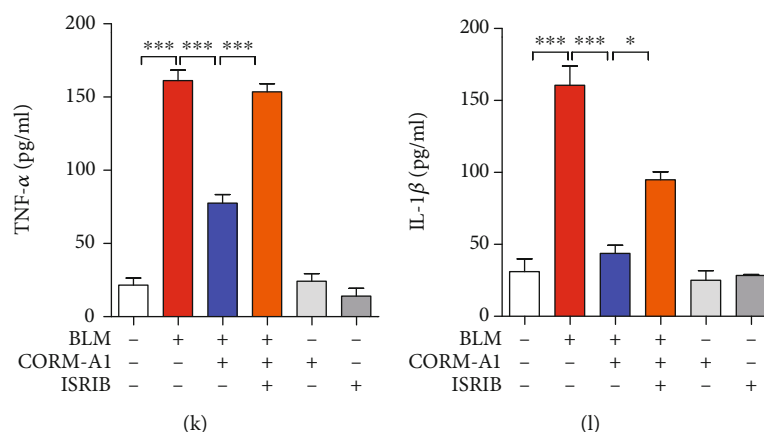


FIGURE 5: ISIRIB abrogates CO-mediated SG formation and recovers BLM-induced cellular senescence. (a) WI-38 cells were treated with 40 μ M CORM-A1 in the presence or absence of ISIRIB (200 nM) for 6 h. Immunofluorescence assay was performed to detect the formation of SGs by visualizing the colocalization of TIA-1 (red) and G3BP1 (green). WI-38 cells were pretreated with CORM-A1 (40 μ M) with or without ISIRIB (200 nM) for 6 h followed by the challenge of bleomycin (25 μ g/ml) for 96 h. Then, SA- β -gal staining (b) and γ -H2AX foci (c) were detected, and immunofluorescence assay (d) was performed to assess the coaggregates of TIA-1 (red) and PAI-1 (green). The mRNA expressions of p21 (e), IL-6 (f), TNF- α (g), and IL-1 β (h) by qRT-PCR. The secretions of PAI-1 (i), IL-6 (j), TNF- α (k), and IL-1 β (l) were detected by ELISA. Quantitative data are expressed as the means \pm SD ($n = 3$ determined in three independent experiments). * $p < 0.05$, ** $p < 0.01$, and *** $p < 0.001$.

widely used for treatment of squamous cell carcinomas, testicular carcinoma, and Hodgkin's and non-Hodgkin's lymphomas [42]. Bleomycin is also one of the most toxic antineoplastic drugs for inducing lung fibrosis, due to epithelial cell injury with reactive hyperplasia, epithelial-mesenchymal transition, differentiation of fibroblasts to myofibroblasts, and the basement membrane and alveolar epithelium injuries [43]. Besides that, accumulating evidence suggested that bleomycin can also induce apoptosis and senescence in lung nonepithelial cells, such as lung fibroblasts, through oxidative stress-induced single- and double-stranded breaks in DNA [30]. To ameliorate these side effects on normal cells, here, we observed that the administration of exogenous CO revealed a strong antisenescent effect on bleomycin-mediated premature senescence. Our results showed that the administration of low-dose CORM-A1 and CO gas could significantly decrease multiple hallmarks of senescence, including the percentage of SA- β -gal-positive cells, DNA damage-associated γ -H2AX foci, cell cycle arrest-associated protein p53, and CDK inhibitor p21, as well as several SASPs (Figures 1 and 2 and S1 and S2). To validate the optimal concentration of CORM-A1, we first pretreated WI-38 cells with CORM-A1 in a dose-dependent manner and found that 40 μ M CORM-A1 showed most effectively to inhibit bleomycin-induced p21 and SASP (Figures 1(b)–1(e)). Moreover, cells treated with CORM-A1 for 6 h showed no cytotoxicity in WI-38 and MEF cells.

Given that PAI-1 is defined as a novel biomarker and a critical mediator of cellular senescence [7, 33, 41], we next evaluated whether PAI-1 was associated with bleomycin-induced lung fibroblast senescence. Consistent with the previous study that chemotherapeutic agent can induce the mRNA expression of PAI-1 in a glioblastoma cell strain [44], we also observed bleomycin-stimulated cells

exerted a significant enhancement of PAI-1 in WI-38 cells (Figures 3(a) and S2D). Next, we silenced the expression of PAI-1 or used PAI-1 inhibitor to explain the crucial role of PAI-1 in bleomycin-induced premature senescence. Our data clearly suggested that, as cells transfected with siRNA against PAI-1 or cotreated with small molecular inhibitor, TM5441, the senescence-associated markers were all dramatically decreased. Consistent with the data reported in previous study [45], PAI-1 could regulate the p53 downstream signaling pathway, and PAI-1 gene silencing could significantly downregulate the protein levels of p53 and p21 to reduce the process of senescence (Figure S2D). These data firmly indicated again that PAI-1 is not only a mediator but also a therapeutic target for the bleomycin-induced lung fibroblast senescence.

In response to diverse environmental stresses, eukaryotic cells will activate defense mechanisms to control energy expenditure for the repair of stress-induced damage, and one of the important mechanisms to promote cell survival is induction of the SG assembly in the cytoplasm [27]. Recently, it has been reported that cellular senescence can interfere the formation of cytoplasmic SGs through the inhibition of SG-nucleating proteins [46]. However, continuous exposure to temperate oxidative stress can induce SG formation, which interferes the process of replicative senescence via sequestration of PAI-1 and then activates the nuclear translocation of cyclin D1 to attenuate cell cycle arrest [28]. CO has been proved as a novel inducer of SG formation via induction of the PERK-eIF2 α signaling pathway, one of the three ISR branches [29]. Based on these reports, herein, we tried to evaluate the relationship between antisenescent effect of CO and its beneficial effect on SG formation (Figure 4). According to our results, in the challenge of bleomycin, CORM-A1 could induce the localization of PAI-1 into SGs through the

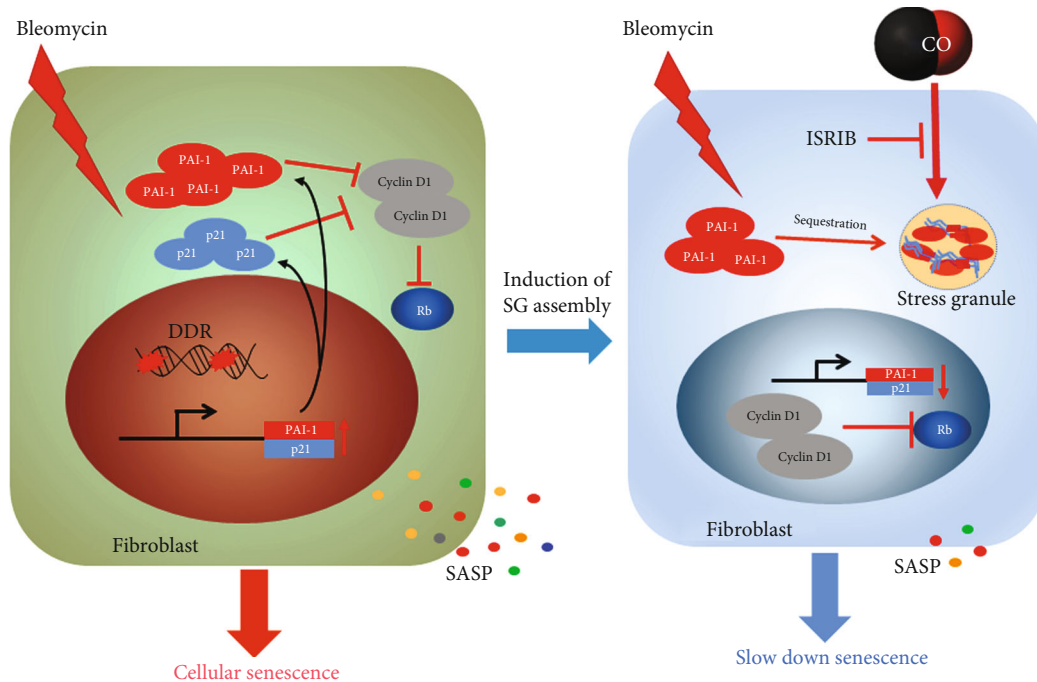


FIGURE 6: The molecular mechanism responsible for CO-mediated SG formation attenuates bleomycin-induced cellular senescence.

aggregation of TIA-1 and PAI-1, which also dramatically reduced the secretion of PAI-1. In addition, our results revealed that CORM-A1 showed a mild inhibitory effect on PAI-1 transcription and that was not a main cause but partially interfere the secretion of PAI-1. Next, to point out the activity of PAI-1, we assessed its downstream signaling pathway and found that CORM-A1 could significantly induce the nuclear translocation of cyclin D1 (Figure 4(d)) and hyperphosphorylation of Rb (Figure 4(e)) in the stimulation of bleomycin. These results are consistent with previous study [28] that the increased formation of SGs by continuous mild stress could sequester PAI-1 and subsequently activates cyclin D1 nuclear translocation and delay the process of replicative senescence.

Integrated stress response (ISR) has been reported to trigger the formation of SGs by the phosphorylation of eIF2 α and reduce the formation of 43S translation preinitiation complexes. However, ISR inhibitor (ISRIB) can block the phosphorylation of eIF2 α and the formation of SGs [47]. To further assess whether ISRIB could abolish the antisenescent effect of CO by compromising SG assembly, we cotreated WI-38 cells with CORM-A1 and ISRIB followed by the challenge of bleomycin and found that ISRIB could significantly abrogate the antisenescent effect of CORM-A1 and recover the bleomycin-induced premature senescence (Figure 5). Moreover, with previous study [28], ISRIB could dramatically inhibit the sequestration of PAI-1 into CO-induced SGs, and the secretion of PAI-1 was reversely increased. All above data proved again that the formation of SGs enhanced by CORM-A1 played a pivotal role in the prevention of bleomycin-induced cellular senescence rather than the control of PAI-1 transcripts and suggested that ISR is important for CO-mediated antisenescent function.

Herein, we also observed that the administration of bleomycin could decrease the protein level of TERT, one critical component of telomerase [36, 37], and which might be associated with telomere shortening during the process of cellular senescence. Interestingly, as cells were pretreated with CORM-A1, the level of TERT showed a significant elevation, while the combinatorial treatment of ISRIB drastically abrogated the beneficial effect of CORM-A1 on TERT expression, suggesting that CO could regulate bleomycin-induced telomere shortening through upregulation of TERT, and which might be related to ISR activation and the SG formation. For the further study, we planned to determine that how CO enhances TERT and what role of CO-induced SGs plays in TERT expression and telomere shortening.

In conclusion, our work strongly demonstrated that the gasotransmitter CO could protect lung fibroblasts against bleomycin-induced premature senescence by inducing SG formation, promoting the sequestration of PAI-1 into SGs, as well as controlling the telomere shortening. These effects could activate cyclin D1 and hyperphosphorylation of Rb to delay the process of cellular senescence (Figure 6). We propose that the utilization of gaseous transmitter, CO, can be a novel therapeutic strategy to prevent bleomycin-mediated cellular senescence and its side effects associated with pathogenesis.

Abbreviations

BLM:	Bleomycin
CDK1:	Cyclin-dependent kinase 1
CO:	Carbon monoxide
CORM-A1:	CO-releasing molecular-A1

DDR:	DNA damage response
eIF2 α :	Eukaryotic translation initiation factor 2A
FGF21:	Fibroblast growth factor 21
G3BP1:	GTPase-activating protein-binding protein 1
γ -H2AX:	Phosphorylated H2A histone family member X
HO:	Heme oxygenase
H ₂ S:	Hydrogen sulfide
IL-6:	Interleukin-6
IL-1 β :	Interleukin-1 beta
ISR:	Integrated stress response
ISRIB:	ISR inhibitor
mTOR:	Target of rapamycin
mtROS:	Mitochondrial reactive oxygen species
NF- κ B:	Nuclear factor-kappa B
NO:	Nitric oxide
PAI-1:	Plasminogen activator inhibitor
PERK:	Protein kinase R-like endoplasmic reticulum kinase
SA- β -gal:	Senescence-associated β -galactosidase
SASP:	Senescence-associated secretory phenotype
SESN2:	Upregulated sestrin 2
SG:	Stress granules
TERT:	Telomerase reverse transcriptase
Tg:	Thapsigargin
TIA-1:	T cell intracytoplasmic antigen
TNF- α :	Tumor necrosis factor alpha.

Data Availability

All data needed to evaluate the conclusions in the paper are present in the paper and/or Supplementary Materials. Additional data related to this paper may be requested from the authors.

Conflicts of Interest

All authors have disclosed that they do not have any conflicts of interest.

Authors' Contributions

Y.C. and L.L. designed the experiments. Y.C., F.J., and G.K. have performed most of the experiments with help from Y.C., S.Y., L.L., Q.W., and Q.Z. Data were analyzed by Y.C., L.L., Q.W., and Q.Z. The manuscript was written by Y.C., L.L., and Q.Z.

Acknowledgments

This work was supported by the National Natural Science Foundation of China (82000074 and 61671098), the Scientific Research Funding Project of Education Department of Liaoning Province (jyt-dldxjc202005), the Natural Science Fund of the Department of Science and Technology of Liaoning Province (No. 20180550388), the Science and Technology Innovation Fund Project of Dalian (2020JJ27SN071), and the Dalian Youth Science and Technology Star Research Project (2020JJ27SN029).

Supplementary Materials

Figure S1: low-dose CO gas ameliorates BLM-induced cellular senescence in WI-38 cells. (A) WI-38 cells were treated with CO gas (250 ppm) in a time-dependent manner (0, 6, 12, and 24 h), and MTT assay was performed to detect cell viability. WI-38 cells were pretreated with CO gas (250 ppm) for 6 h followed by the challenge of BLM (25 μ g/ml) for 48 h. Then, SA- β -gal staining (B) and γ -H2AX foci (C) were detected, and the mRNA expressions of p21 (D), IL-6 (E), TNF- α (F), and IL-1 β (G) were detected by qRT-PCR. Quantitative data are expressed as the means \pm SD ($n = 3$ determined in three independent experiments). * $p < 0.05$, ** $p < 0.01$, and *** $p < 0.001$. Figure S2: protein levels of p53, p21, PAI-1, and TERT in different groups. (A–C) WI-38 cells were pretreated with CORM-A1 (40 μ M) for 6 h followed by the stimulation of BLM (25 μ g/ml) for 96 h. During the process of senescence, cells were posttreated with CORM-A1 (40 μ M) for 6 h every other day. After a 4-day incubation, the protein levels of p53 and p21 were measured by Western blot assay. (D) WI-38 cells were transfected with scramble siRNA (scRNA) and siRNA against PAI-1 (siPAI-1) for 36 h and then treated with BLM (25 μ g/ml) for 96 h. Protein levels of p53, p21, and PAI-1 were detected by Western blot assay. (E–H) WI-38 cells were pretreated with CORM-A1 (40 μ M) with or without ISRIB (200 nM) for 6 h followed by the challenge of bleomycin (25 μ g/ml) for 96 h. Then, protein levels of p53, p21, and TERT were assessed by Western blot. Bar graphs are summary data of normalized densitometric ratios. Quantitative data are expressed as the means \pm SD ($n = 3$ determined in three independent experiments). * $p < 0.05$ and *** $p < 0.001$. (*Supplementary Materials*)

References

- [1] A. Hernandez-Segura, J. Nehme, and M. Demaria, "Hallmarks of cellular senescence," *Trends in Cell Biology*, vol. 28, no. 6, pp. 436–453, 2018.
- [2] A. Freund, A. V. Orjalo, P. Y. Desprez, and J. Campisi, "Inflammatory networks during cellular senescence: causes and consequences," *Trends in Molecular Medicine*, vol. 16, no. 5, pp. 238–246, 2010.
- [3] D. J. Baker, T. Wijshake, T. Tchkonja et al., "Clearance of p16^{Ink4a}-positive senescent cells delays ageing-associated disorders," *Nature*, vol. 479, no. 7372, pp. 232–236, 2011.
- [4] M. Gorospe and K. Abdelmohsen, "MicroRegulators come of age in senescence," *Trends in Genetics*, vol. 27, no. 6, pp. 233–241, 2011.
- [5] M. Serrano, A. W. Lin, M. E. McCurrach, D. Beach, and S. W. Lowe, "Oncogenic ras provokes premature cell senescence associated with accumulation of p53 and p16^{Ink4a}," *Cell*, vol. 88, no. 5, pp. 593–602, 1997.
- [6] M. Narita, V. Krizhanovskiy, S. Nunez et al., "A novel role for high-mobility group a proteins in cellular senescence and heterochromatin formation," *Cell*, vol. 126, no. 3, pp. 503–514, 2006.
- [7] D. E. Vaughan, R. Rai, S. S. Khan, M. Eren, and A. K. Ghosh, "Plasminogen activator inhibitor-1 is a marker and a mediator of senescence," *Arteriosclerosis, Thrombosis, and Vascular Biology*, vol. 37, no. 8, pp. 1446–1452, 2017.

- [8] S. Shetty, P. Shetty, S. Idell, T. Velusamy, Y. P. Bhandary, and R. S. Shetty, "Regulation of plasminogen activator inhibitor-1 expression by tumor suppressor protein p53," *The Journal of Biological Chemistry*, vol. 283, no. 28, pp. 19570–19580, 2008.
- [9] A. Soto-Gamez and M. Demaria, "Therapeutic interventions for aging: the case of cellular senescence," *Drug Discovery Today*, vol. 22, no. 5, pp. 786–795, 2017.
- [10] T. Nacarelli and C. Sell, "Targeting metabolism in cellular senescence, a role for intervention," *Molecular and Cellular Endocrinology*, vol. 455, pp. 83–92, 2017.
- [11] M. Zheng, W. Qiao, J. Cui et al., "Hydrogen sulfide delays nicotinamide-induced premature senescence via upregulation of SIRT1 in human umbilical vein endothelial cells," *Molecular and Cellular Biochemistry*, vol. 393, no. 1-2, pp. 59–67, 2014.
- [12] J. Chao, Y. Guo, and L. Chao, "Protective role of endogenous kallistatin in vascular injury and senescence by inhibiting oxidative stress and inflammation," *Oxidative Medicine and Cellular Longevity*, vol. 2018, Article ID 4138560, 8 pages, 2018.
- [13] T. Seki, D. T. Curiel, M. Naruse, and K. Takano, "HO (heme oxygenase)/CO (carbon monoxide) system," *Nihon Rinsho*, vol. 58, Supplement 1, pp. 188–191, 2000.
- [14] S. W. Ryter and A. M. Choi, "Heme oxygenase-1/carbon monoxide: novel therapeutic strategies in critical care medicine," *Current Drug Targets*, vol. 11, no. 12, pp. 1485–1494, 2010.
- [15] H. J. Kim, Y. Joe, J. K. Yu et al., "Carbon monoxide protects against hepatic ischemia/reperfusion injury by modulating the miR-34a/SIRT1 pathway," *Biochimica et Biophysica Acta*, vol. 1852, no. 7, pp. 1550–1559, 2015.
- [16] S. K. Kim, Y. Joe, Y. Chen et al., "Carbon monoxide decreases interleukin-1 β levels in the lung through the induction of pyrin," *Cellular & Molecular Immunology*, vol. 14, no. 4, pp. 349–359, 2017.
- [17] Y. Joe, Y. Chen, J. Park et al., "Cross-talk between CD38 and TTP is essential for resolution of inflammation during microbial sepsis," *Cell Reports*, vol. 30, no. 4, pp. 1063–1076.e5, 2020.
- [18] H. J. Kim, Y. Joe, Y. Chen, G. H. Park, U. H. Kim, and H. T. Chung, "Carbon monoxide attenuates amyloidogenesis via down-regulation of NF- κ B-mediated BACE1 gene expression," *Aging Cell*, vol. 18, no. 1, article e12864, 2019.
- [19] Y. Chen, H. J. Park, J. Park et al., "Carbon monoxide ameliorates acetaminophen-induced liver injury by increasing hepatic HO-1 and Parkin expression," *FASEB Journal*, vol. 33, no. 12, pp. 13905–13919, 2019.
- [20] B. S. Zuckerbraun, B. Y. Chin, M. Bilban et al., "Carbon monoxide signals via inhibition of cytochrome c oxidase and generation of mitochondrial reactive oxygen species," *FASEB Journal*, vol. 21, no. 4, pp. 1099–1106, 2007.
- [21] L. Liu, D. R. Wise, J. A. Diehl, and M. C. Simon, "Hypoxic Reactive Oxygen Species Regulate the Integrated Stress Response and Cell Survival," *The Journal of Biological Chemistry*, vol. 283, no. 45, pp. 31153–31162, 2008.
- [22] H. J. Kim, Y. Joe, S. K. Kim et al., "Carbon monoxide protects against hepatic steatosis in mice by inducing sestrin-2 via the PERK-eIF2 α -ATF4 pathway," *Free Radical Biology & Medicine*, vol. 110, pp. 81–91, 2017.
- [23] Y. Joe, S. Kim, H. J. Kim et al., "FGF21 induced by carbon monoxide mediates metabolic homeostasis via the PERK/ATF4 pathway," *FASEB Journal*, vol. 32, no. 5, pp. 2630–2643, 2018.
- [24] P. Anderson and N. Kedersha, "RNA granules: post-transcriptional and epigenetic modulators of gene expression," *Nature Reviews: Molecular Cell Biology*, vol. 10, no. 6, pp. 430–436, 2009.
- [25] N. Kedersha, P. Ivanov, and P. Anderson, "Stress granules and cell signaling: more than just a passing phase?," *Trends in Biochemical Sciences*, vol. 38, no. 10, pp. 494–506, 2013.
- [26] N. Gilks, N. Kedersha, M. Ayodele et al., "Stress granule assembly is mediated by prion-like aggregation of TIA-1," *Molecular Biology of the Cell*, vol. 15, no. 12, pp. 5383–5398, 2004.
- [27] M. D. Panas, P. Ivanov, and P. Anderson, "Mechanistic insights into mammalian stress granule dynamics," *The Journal of Cell Biology*, vol. 215, no. 3, pp. 313–323, 2016.
- [28] A. Omer, D. Patel, X. J. Lian et al., "Stress granules counteract senescence by sequestration of PAI-1," *EMBO Reports*, vol. 19, no. 5, 2018.
- [29] Y. Chen, Y. Joe, J. Park, H. C. Song, U. H. Kim, and H. T. Chung, "Carbon monoxide induces the assembly of stress granule through the integrated stress response," *Biochemical and Biophysical Research Communications*, vol. 512, no. 2, pp. 289–294, 2019.
- [30] M. Kasper and K. Barth, "Bleomycin and its role in inducing apoptosis and senescence in lung cells - modulating effects of caveolin-1," *Current Cancer Drug Targets*, vol. 9, no. 3, pp. 341–353, 2009.
- [31] X. Chen, H. Xu, J. Hou et al., "Epithelial cell senescence induces pulmonary fibrosis through Nanog-mediated fibroblast activation," *Aging*, vol. 12, no. 1, pp. 242–259, 2020.
- [32] C. Dellas and D. J. Loskutoff, "Historical analysis of PAI-1 from its discovery to its potential role in cell motility and disease," *Thrombosis and Haemostasis*, vol. 93, no. 4, pp. 631–640, 2005.
- [33] A. E. Boe, M. Eren, S. B. Murphy et al., "Plasminogen activator inhibitor-1 antagonist TM5441 attenuates N ω -nitro-L-arginine methyl ester-induced hypertension and vascular senescence," *Circulation*, vol. 128, no. 21, pp. 2318–2324, 2013.
- [34] R. M. Kortlever, P. J. Higgins, and R. Bernards, "Plasminogen activator inhibitor-1 is a critical downstream target of p53 in the induction of replicative senescence," *Nature Cell Biology*, vol. 8, no. 8, pp. 877–884, 2006.
- [35] Y. Y. Liu, Y. Shi, Y. Liu, X. H. Pan, and K. X. Zhang, "Telomere shortening activates TGF- β /Smads signaling in lungs and enhances both lipopolysaccharide and bleomycin-induced pulmonary fibrosis," *Acta Pharmacologica Sinica*, vol. 39, no. 11, pp. 1735–1745, 2018.
- [36] E. Sahin, S. Colla, M. Liesa et al., "Telomere dysfunction induces metabolic and mitochondrial compromise," *Nature*, vol. 470, no. 7334, pp. 359–365, 2011.
- [37] X. Zhang, V. Mar, W. Zhou, L. Harrington, and M. O. Robinson, "Telomere shortening and apoptosis in telomerase-inhibited human tumor cells," *Genes & Development*, vol. 13, no. 18, pp. 2388–2399, 1999.
- [38] X. Ling, W. Yang, P. Zou et al., "TERT regulates telomere-related senescence and apoptosis through DNA damage response in male germ cells exposed to BPDE *in vitro* and to B[a]P *in vivo*," *Environmental Pollution*, vol. 235, pp. 836–849, 2018.
- [39] N. E. Sharpless and C. J. Sherr, "Forging a signature of *in vivo* senescence," *Nature Reviews Cancer*, vol. 15, no. 7, pp. 397–408, 2015.
- [40] J. P. Coppe, C. K. Patil, F. Rodier et al., "Senescence-associated secretory phenotypes reveal cell-nonautonomous functions of

- oncogenic RAS and the p53 tumor suppressor,” *PLoS Biology*, vol. 6, no. 12, pp. 2853–2868, 2008.
- [41] A. K. Ghosh, R. Rai, K. E. Park, M. Eren, T. Miyata, and L. D. Wilsbacher, “A small molecule inhibitor of PAI-1 protects against doxorubicin-induced cellular senescence,” *Oncotarget*, vol. 7, no. 45, pp. 72443–72457, 2016.
- [42] J. S. Lazo and S. M. Sebti, “Bleomycin,” *Cancer Chemotherapy and Biological Response Modifiers*, vol. 17, pp. 40–45, 1997.
- [43] V. Della Latta, A. Cecchetti, S. Del Ry, and M. A. Morales, “Bleomycin in the setting of lung fibrosis induction: from biological mechanisms to counteractions,” *Pharmacological Research*, vol. 97, pp. 122–130, 2015.
- [44] M. Osmak, I. Vrhovec, and J. Skrk, “Cisplatin resistant glioblastoma cells may have increased concentration of urokinase plasminogen activator and plasminogen activator inhibitor type 1,” *Journal of Neuro-Oncology*, vol. 42, no. 2, pp. 95–102, 1999.
- [45] C. Jiang, G. Liu, T. Luckhardt et al., “Serpine 1 induces alveolar type II cell senescence through activating p53-p21-Rb pathway in fibrotic lung disease,” *Aging Cell*, vol. 16, no. 5, pp. 1114–1124, 2017.
- [46] O. Moujaber, H. Mahboubi, M. Kodiha et al., “Dissecting the molecular mechanisms that impair stress granule formation in aging cells,” *Biochimica et Biophysica Acta (BBA) - Molecular Cell Research*, vol. 1864, no. 3, pp. 475–486, 2017.
- [47] C. Sidrauski, A. M. McGeachy, N. T. Ingolia, and P. Walter, “The small molecule ISRIB reverses the effects of eIF2 α phosphorylation on translation and stress granule assembly,” *eLife*, vol. 4, 2015.

Research Article

Endothelial Cell-Derived SO₂ Controls Endothelial Cell Inflammation, Smooth Muscle Cell Proliferation, and Collagen Synthesis to Inhibit Hypoxic Pulmonary Vascular Remodelling

Xin Liu,¹ Shangyue Zhang,¹ Xiuli Wang,¹ Yuanyuan Wang,¹ Jingyuan Song,¹ Chufan Sun,¹ Guozhen Chen,² Guosheng Yang,³ Yinghong Tao,³ Yongyan Hu,³ Dingfang Bu,⁴ Yaqian Huang ¹, Junbao Du ^{1,5} and Hongfang Jin ¹

¹Department of Pediatrics, Peking University First Hospital, Beijing 100034, China

²Department of Pediatrics, The Affiliated Yantai Yuhuangding Hospital of Qingdao University, Yantai 264000, China

³Laboratory Animal Facility, Peking University First Hospital, Beijing 100034, China

⁴Central Laboratory, Peking University First Hospital, Beijing 100034, China

⁵Key Laboratory of Molecular Cardiology, Ministry of Education, Beijing 100091, China

Correspondence should be addressed to Yaqian Huang; yaqianhuang@126.com, Junbao Du; junbaodu1@126.com, and Hongfang Jin; jinhongfang51@126.com

Received 25 January 2021; Revised 27 March 2021; Accepted 5 April 2021; Published 17 April 2021

Academic Editor: Andrea Berenyiova

Copyright © 2021 Xin Liu et al. This is an open access article distributed under the Creative Commons Attribution License, which permits unrestricted use, distribution, and reproduction in any medium, provided the original work is properly cited.

Hypoxic pulmonary vascular remodelling (PVR) is the major pathological basis of aging-related chronic obstructive pulmonary disease and obstructive sleep apnea syndrome. The pulmonary artery endothelial cell (PAEC) inflammation, and pulmonary artery smooth muscle cell (PASMC) proliferation, hypertrophy and collagen remodelling are the important pathophysiological components of PVR. Endogenous sulfur dioxide (SO₂) was found to be a novel gasotransmitter in the cardiovascular system with its unique biological properties. The study was aimed to investigate the role of endothelial cell- (EC-) derived SO₂ in the progression of PAEC inflammation, PASMC proliferation, hypertrophy and collagen remodelling in PVR and the possible mechanisms. EC-specific aspartic aminotransferase 1 transgenic (EC-AAT1-Tg) mice were constructed *in vivo*. Pulmonary hypertension was induced by hypoxia. Right heart catheterization and echocardiography were used to detect mouse hemodynamic changes. Pathologic analysis was performed in the pulmonary arteries. High-performance liquid chromatography was employed to detect the SO₂ content. Human PAECs (HPAECs) with lentiviruses containing AAT1 cDNA or shRNA and cocultured human PASMCs (HPASMCs) were applied *in vitro*. SO₂ probe and enzyme-linked immunosorbent assay were used to detect the SO₂ content and determine p50 activity, respectively. Hypoxia caused a significant reduction in SO₂ content in the mouse lung and HPAECs and increases in right ventricular systolic pressure, pulmonary artery wall thickness, muscularization, and the expression of PAEC ICAM-1 and MCP-1 and of PASMC Ki-67, collagen I, and α -SMA ($p < 0.05$). However, EC-AAT1-Tg with sufficient SO₂ content prevented the above increases induced by hypoxia ($p < 0.05$). Mechanistically, EC-derived SO₂ deficiency promoted HPAEC ICAM-1 and MCP-1 and the cocultured HPASMC Ki-67 and collagen I expression, which was abolished by andrographolide, an inhibitor of p50 ($p < 0.05$). Meanwhile, EC-derived SO₂ deficiency increased the expression of cocultured HPASMC α -SMA ($p < 0.05$). Taken together, these findings revealed that EC-derived SO₂ inhibited p50 activation to control PAEC inflammation in an autocrine manner and PASMC proliferation, hypertrophy, and collagen synthesis in a paracrine manner, thereby inhibiting hypoxic PVR.

1. Introduction

Aging is an important risk factor for a variety of diseases [1–3]. With the increase of the global elderly population, the incidence of aging and age-related diseases such as chronic obstructive pulmonary disease (COPD) and obstructive sleep apnea syndrome (OSAS) has also been gradually increased [4, 5]. Among them, hypoxic pulmonary hypertension (PH) and pulmonary vascular remodelling (PVR) are the critical pathological basis. PVR includes pulmonary artery endothelial cell (PAEC) dysfunction, and pulmonary artery smooth muscle cell (PASMC) proliferation, hypertrophy, and collagen accumulation [6–9]. Previous studies reported that an imbalance among small vasoactive molecules played a critical role in the progression of PVR. The imbalance among protein-derived bioactive molecules, active lipid mediators, small nucleic acids, and gaseous signalling molecules is predominantly involved in the pulmonary artery structural changes and the abnormal vasoconstriction and vasorelaxation [10–16]. However, the mechanisms underlying the excessive PAEC inflammation, PASMC proliferation, hypertrophy, and collagen remodelling remain unclear.

Recent studies have shown that endothelial cells (ECs) play a critical role in maintaining vascular homeostasis, while EC dysfunction leads to various vascular diseases [17, 18]. For example, Xue et al. observed that the overexpression of EC-derived cyclophilin A caused spontaneous PH by promoting PAEC inflammation and PASMC proliferation [19]. Moreover, EC dysfunction and endothelial-to-mesenchymal cell transition enhanced collagen accumulation in the pathogenesis of human fibrotic diseases [20]. These results suggest that ECs might affect the function of ECs and other neighboring cells (primarily smooth muscle cells [SMCs]) in the vascular walls in an autocrine/paracrine manner, by which ECs play an important role in the development of PVR. However, the mechanisms by which ECs affect the behavior of PAECs and PASMCs to play a role in the development of PVR are complex and have not yet been fully elucidated.

In 2008, the endogenous sulfur dioxide (SO_2)/aspartate aminotransferase (AAT) pathway was found to exist in the vascular ECs of rats [21]. More recently, the production of endogenous SO_2 catalyzed by AAT1 has been identified in human PAECs (HPAECs) [22]. As a gasotransmitter, SO_2 has a series of important advantages, including sustained production, rapid diffusion, and free passage through cell membranes with a short half-life. It exerts a variety of biological functions in the cardiovascular system. For example, *in vivo*, the exogenous SO_2 donor showed a protective role in rat atherosclerosis and sepsis-induced cardiac dysfunction via the inhibition of cellular inflammation [23, 24]. *In vitro*, the deficiency of SO_2 contributed to cellular proliferation and collagen accumulation [25]. Moreover, the deficiency of endogenous SO_2 might be implicated in the pathogenesis of myocardial hypertrophy [26]. These data strongly suggest that EC-derived SO_2 might play a regulatory role in PAEC inflammation in an autocrine manner and in PASMC proliferation, hypertrophy, and collagen deposition in a paracrine manner. As such, in the present study, we further explored whether EC-derived SO_2 might control PAEC inflammation

in an autocrine manner and control PASMC proliferation, hypertrophy, and collagen deposition in a paracrine manner to reveal a new mechanism for PAEC inflammation and PAEC-PASMC communication in the control of PASMC proliferation, hypertrophy, and collagen remodelling by SO_2 .

Recent data have suggested that EC inflammation, SMC proliferation, and collagen synthesis are under the control of nuclear factor- κB (NF- κB) [27, 28]. Briefly, some stimuli, such as tumor necrosis factor α (TNF- α), lead to the activation of the I κB kinase complex, allowing I κB to undergo phosphorylation and degradation, and NF- κB dimers (thought to be p50 heterodimers primarily) to translocate to the nucleus to promote gene transcription [29]. The inhibition of p50 evidently restricted E-selectin expression induced by TNF- α in human umbilical vein ECs, and NF- κB activation triggered bladder SMC collagen biosynthesis and proliferation [30, 31]. But the regulatory mechanisms for p50 are unclear so far. Intriguingly, endogenous SO_2 exhibited a protective effect by repressing NF- κB activation in adipocytes and macrophages.

Based on these evidences, in this study, we aimed to determine the possible role of EC-derived SO_2 in the progression of hypoxic PVR and its possible underlying mechanisms in association with the PAEC inflammatory response, PASMC proliferation, hypertrophy, and collagen production to reveal a new mechanism for PAEC inflammation and PAEC-PASMC communication in the control of PASMC proliferation, hypertrophy, and collagen remodelling by SO_2 .

2. Materials and Methods

2.1. Animal Model. Endothelial cell-specific AAT1 transgenic (EC-AAT1-Tg) and wild-type (WT) littermate mice (C57BL/6J background) were purchased from Cyagen Biosciences (Suzhou, China). Genotype was confirmed using polymerase chain reaction analysis in 10-day-old mice. Male mice aged 10–12 weeks were randomly divided into WT, hypoxic WT (WT+H), EC-AAT1-Tg, and hypoxic EC-AAT1-Tg (EC-AAT1-Tg+H) groups. The mice of the WT and EC-AAT1-Tg groups breathed in room air (21% O_2), whereas hypoxic mice were placed in a small animal hypoxic chamber ($9 \pm 0.5\%$ O_2) (XBS-02B; Hangzhou Aipu Instrument Co., Ltd., China) 8 h daily for 5 weeks to induce hypoxic PH [32]. All institutional and national guidelines for the care and use of animals (fisheries) were followed. The animal experiment was approved by the Laboratory Animal Ethics Committee of Peking University First Hospital (Ethics No. 201526).

2.2. High-Performance Liquid Chromatography (HPLC) Quantitative Detection of SO_2 Content in Mouse Lung Tissue. As mentioned earlier, HPLC (Agilent 1200 series; Agilent Technologies, CA, USA) was used to detect the SO_2 content in mouse lung tissue. Briefly, 100 μL of the standard sodium sulfite and a sample of mouse lung tissue homogenate were mixed with 70 μL of sodium borohydride (0.212 mol/L) in Tris-HCl (0.05 mol/L, pH 8.5). The mixture was then incubated at room temperature for 30 min. Next, 5 μL of monobromobimane (70 mmol/L) in acetonitrile was

mixed with the 170 μL mixture. After the above mixture was incubated at 42°C for 10 min, 40 μL of perchloric acid (1.5 mol/L) was added. To remove the protein precipitates and neutralize the mixture, the mixture was centrifuged (12,400 g) at 25°C for 10 min, and 10 μL of Tris-HCl (2 mol/L, pH 3.0) was added to the supernatant. Finally, the HPLC operation and result analysis were performed as described previously [33].

2.3. Detection of Mouse Right Ventricular Systolic Pressure (RVSP) Changes by Right Heart Catheterization. The RVSP of mice was directly measured by catheterization. The mice were anesthetized by intraperitoneal injection of 0.5% sodium pentobarbital (0.1 ml/10 g). A catheter was inserted through the external jugular vein to reach the right ventricle of the mouse. The BL-420F Biological Function Experimental System (Chengdu Taimeng Instrument Co. Ltd., China) was used to measure the mouse RVSP to predict the changes in pulmonary artery pressure [32].

2.4. Measurement of Mouse Pulmonary Acceleration Time (PAT) and Pulmonary Ejection Time (PET) Using Echocardiography. Echocardiography was performed using the Vevo 2100 high-resolution imaging system (Visualsonics, Toronto, Canada). The mice were initially anesthetized by intraperitoneal injection of 0.5% sodium pentobarbital (0.1 ml/10 g). Pulsed-wave Doppler recording of the pulmonary blood flow was obtained from the parasternal short axis view at the aortic valve level. Samples were positioned at the tip of the pulmonary valve leaflets and aligned to maximize laminar flow as described previously. PAT (defined as the time from the onset of flow to peak velocity by pulsed-wave Doppler recording) and PET (the time from the onset to the termination of pulmonary flow) variables were determined. All measured variables were the average of 3–5 cardiac cycles [34].

2.5. Preparation and Morphological Analysis of Mouse Lung Tissue. The mice were killed by cervical dislocation. Their lungs were removed and rinsed with 4°C phosphate-buffered saline (PBS). The lungs were then fixed in 4% paraformaldehyde solution for 24 h to prepare paraffin-embedded sections or frozen sections of lung tissue. The sections were stained with hematoxylin and eosin (HE) and Hart's method for morphological analysis. As previously reported [35], the degree of muscularization can be determined by the ratio of the number of nonmuscular vessels (NMV), partial muscular arteries (PMA), and muscular arteries (MA). PVR can be quantitatively analyzed by calculating the percentage of 15–50 μm pulmonary arteriole muscularization.

2.6. Immunofluorescence. Frozen sections of lung tissue and cells were rinsed with PBS and fixed with 4% paraformaldehyde solution for 20 min. Tissue sections and cells were blocked with bovine serum albumin and incubated with the primary antibodies at 4°C overnight (vWF: 1:200, Zhongshan Jinqiao Biotechnology Co., Ltd., China; AAT1 1:50, Sigma-Aldrich, USA; p-p50 1:50 and ICAM-1 1:20, Santa Cruz Biotechnology Company, USA; p50 1:100 and Ki-67

1:100, Cell Signaling Technology Company USA; F4/80 1:300, α -SMA 1:300, collagen 1:25 and MCP-1 1:100, Abcam Company, UK). On the second day, the secondary fluorescent antibodies were incubated in the dark. All sections were counterstained with nuclear 4,6-diamino-2-phenylindole (DAPI; Zhongshan Jinqiao Biotechnology Co., Ltd., China). Immunofluorescence imaging was performed using a confocal laser scanning microscope (Leica, Wetzlar, Germany) for observation and comparison.

2.7. Primary HPAEC Culture. Primary HPAECs and primary EC culture system were purchased from PriCells Biomedical Technology Co., Ltd. (Wuhan, China); cells at 4–6 generation were used for experiments. HPAECs were transfected with lentivirus containing AAT1 shRNA or cDNA (Cyagen Biosciences, Suzhou, China) for 2–3 days to induce AAT1 knockdown or overexpression. 1% O₂ was used to induce a hypoxic cell inflammation model.

2.8. Coculture of Primary Human PSMCs (HPASMCs) and HPAECs. Primary HPASMCs and primary SMC culture system were purchased from Lifeline Cell Technology (USA). Transwell plates (Corning, China) were used for the coculture of HPASMCs and HPAECs. We seeded HPASMCs in the lower compartment of the transwell plates by using the SMC culture system. Infected HPAECs were planted in the upper compartment with an EC culture system and were separated from the lower compartments by a microporous membrane. An inhibitor of p50 andrographolide (4 μM , Andro, Selleck, USA) was used for experiments [30].

2.9. SO₂ Probe-Based In Situ Detection of SO₂ Content in HPAECs. The SO₂ fluorescent probe was used to analyze the SO₂ content in HPAECs *in situ* as previously reported [22]. After the unbound SO₂ probe was removed and the nuclei were stained with DAPI, we observed the red fluorescence intensity of the SO₂ probe under a high-resolution confocal laser microscope.

2.10. Western Blot. Lung tissues or cells were lysed in lysis buffer to obtain total protein. Denatured proteins were separated by 10% sodium dodecyl sulfate-polyacrylamide gel electrophoresis and transferred to nitrocellulose membranes (Amersico, USA). The membranes were incubated with specific primary antibodies (GAPDH 1:4000, β -actin 1:4000, AAT1 1:1000, ICAM-1 1:400, MCP-1:1000, Ki-67 1:500, collagen I 1:1000, α -SMA 1:1000 and p-p50 1:1000) and secondary antibodies (1:2000) conjugated with horseradish peroxidase. The FluorChem M MultiFluor System (Protein-simple, USA) was used to scan the protein bands in grayscale. The ImageJ software was used to quantitatively analyze each band, and each protein band was corrected with its own internal reference GAPDH or β -actin grayscale [33].

2.11. p50 DNA-Binding Activity Detected by Active Motif-Enzyme-Linked Immunosorbent Assay (ELISA). Active motif-ELISA (Active Motif, USA) was used to determine the DNA-binding activity of p50 in HPAEC nuclear protein. The nuclear protein extraction steps were initially performed as described earlier [14]. The DNA-binding activity of p50

was then evaluated according to manufacturer's instructions. In short, the binding buffer, the sample diluted with lysate, 1x washing buffer, p50 primary antibody (1:1000, prepared with 1x antibody binding buffer), secondary antibody, and color developing solution were added in turn. We observed the color change during the experiment. The experiment was stopped when the color turned to moderate dark blue by adding stop solution, and then, the color turned yellow. Finally, we measured the absorbance value at 450 nm as soon as possible.

2.12. Adhesion Test of THP-1 Monocyte Cell Line and HPAECs. After inducing the HPAEC inflammatory response, THP-1 mononuclear cells initially stained with the red fluorescent Dil (Beyotime Biotechnology, China) were added to the HPAECs. HPAECs and THP-1 cells were incubated at 37°C for 1 h. PBS was then used to remove unadhered THP-1 cells. Subsequently, we fixed the cells with 4% paraformaldehyde solution for 20 min. Finally, the mounting medium containing DAPI was added, and fluorescence was observed under an immunofluorescence microscope.

2.13. Data Analysis. Statistical analyses were performed with the SPSS 21.0 software (SPSS Inc., USA). Data were expressed as mean \pm SEM and analyzed using one-way ANOVA. p values < 0.05 were considered statistically significant.

3. Results

3.1. Hypoxia Caused Reduction in EC-Derived SO_2 . Immunofluorescence and HPLC showed decreased AAT1 protein expression in PAECs and SO_2 content in the lungs of WT mice under hypoxia compared with control WT mice (Figures 1(a) and 1(b)) ($p < 0.05$). By Western blot analysis and SO_2 fluorescent probe method, we further confirmed that compared with the control vehicle group, the levels of AAT1 protein and SO_2 were downregulated in hypoxic HPAECs, whereas overexpression of AAT1 significantly improved the endogenous SO_2 level in ECs and prevented the decrease in EC-derived SO_2 caused by hypoxia (Figures 1(c) and 1(d)) ($p < 0.05$).

3.2. Increased EC-Derived SO_2 Ameliorated Hypoxia-Induced PVR and PH In Vivo. To reveal the role of EC-derived SO_2 in the pathogenesis of hypoxic PVR, we constructed EC-AAT1-Tg mice to increase SO_2 levels in mouse PAECs (Figure S1a). We found an increased expression of AAT1 protein in PAECs and SO_2 content in the lung of EC-AAT1-Tg mice, compared with the mice in the WT group (Figures 1(a) and 1(b)) ($p < 0.05$). After exposure to intermittent hypoxia for 5 weeks, both the RVSP detected by the right heart catheter and the PAT/PET ratio in this experiment suggested that hypoxic WT (WT+H) mice developed significant PH compared with the control WT mice. We also observed that markers of PVR, the thickness of pulmonary artery walls, and the proportion of muscularized arteries were dramatically enhanced in mice of the WT+H group by HE and Hart's methods. However, compared with mice in EC-AAT1-Tg group with increased EC- SO_2 content, hypoxia did not induce significant PVR and PH in mice of EC-

AAT1-Tg+H group (Figures 1(e)–1(k)) ($p < 0.05$). The above results suggested that the decrease in SO_2 in ECs resulted in increased vascular remodelling and hypoxic PH in mice.

3.3. Increased EC-Derived SO_2 Ameliorated Hypoxia-Induced PAEC Inflammation, PASMCM Proliferation, Hypertrophy, and Collagen Production. We next sought to determine the role of EC-derived SO_2 in PAEC inflammatory reaction, PASMCM proliferation, hypertrophy, and collagen synthesis, which dramatically contribute to PVR. *In vivo*, by immunofluorescence *in situ* detection of ICAM-1 and MCP-1 expression and macrophage infiltration in pulmonary vasculature, we found that compared with WT mice, hypoxia dramatically increased the expression of ICAM-1 and MCP-1, known markers of EC inflammatory process in mouse PAECs, and macrophage infiltration in the pulmonary arteries of WT+H mice. Moreover, Western blot quantitative determination of ICAM-1 protein in mouse lung showed similar results (Figures 2(a) and 2(b), Figure S2a and S2b) ($p < 0.05$). But the treatment with EC-AAT1-Tg to increase SO_2 level successfully repressed hypoxia-induced increases in the protein expression of ICAM-1 and MCP-1, and macrophage infiltration in mouse lung tissue (Figures 2(a) and 2(b), Figure S2a and S2b) ($p < 0.05$). Consistent with the *in vivo* results, we found that AAT1 overexpression to increase the content of EC-derived SO_2 evidently inhibited hypoxia-induced increases in ICAM-1 and MCP-1 in HPAECs and THP-1 cell adhesion to HPAECs *in vitro* (Figure S2c–S2f) ($p < 0.05$). These data suggested that the increase in SO_2 in ECs could inhibit hypoxic vascular inflammation in an autocrine manner.

We then evaluated the effect of EC-derived SO_2 on hypoxic PASMCM proliferation, hypertrophy, and collagen deposition *in vivo*. Compared with the mice in the WT group, immunofluorescence showed enhanced Ki-67 staining in the pulmonary arteries of the WT+H group. While compared with the mice of EC-AAT1-Tg group, no significant increase was found in the expression of Ki-67 induced by hypoxia in the mice of EC-AAT1-Tg+H group (Figure 2(c)). In addition, immunofluorescence showed an increased α -SMA expression, a marker of SMC hypertrophy, in the pulmonary arteries of WT mice under hypoxia compared with WT mice under normoxia, while there was no significant difference in α -SMA expression between EC-AAT1-Tg mice with and without hypoxic exposure (Figures 2(c) and 2(d)). We also observed that the increased collagen I in PASMCMs of mice under hypoxia was successfully repressed in EC-AAT1-Tg mice with sufficient SO_2 (Figure 2(d)). The above results indicated that increased EC-derived SO_2 ameliorated hypoxia-induced PASMCM proliferation, hypertrophy, and collagen accumulation in a paracrine manner.

3.4. EC-Derived SO_2 Deficiency Activated HPAEC Inflammation, HPASMCM Proliferation, Hypertrophy and Collagen Synthesis In Vitro. To directly identify the role of EC-derived SO_2 in HPAEC inflammatory process, HPASMCM proliferation, hypertrophy, and collagen production, we infected HPAECs with lentivirus containing AAT1 shRNA

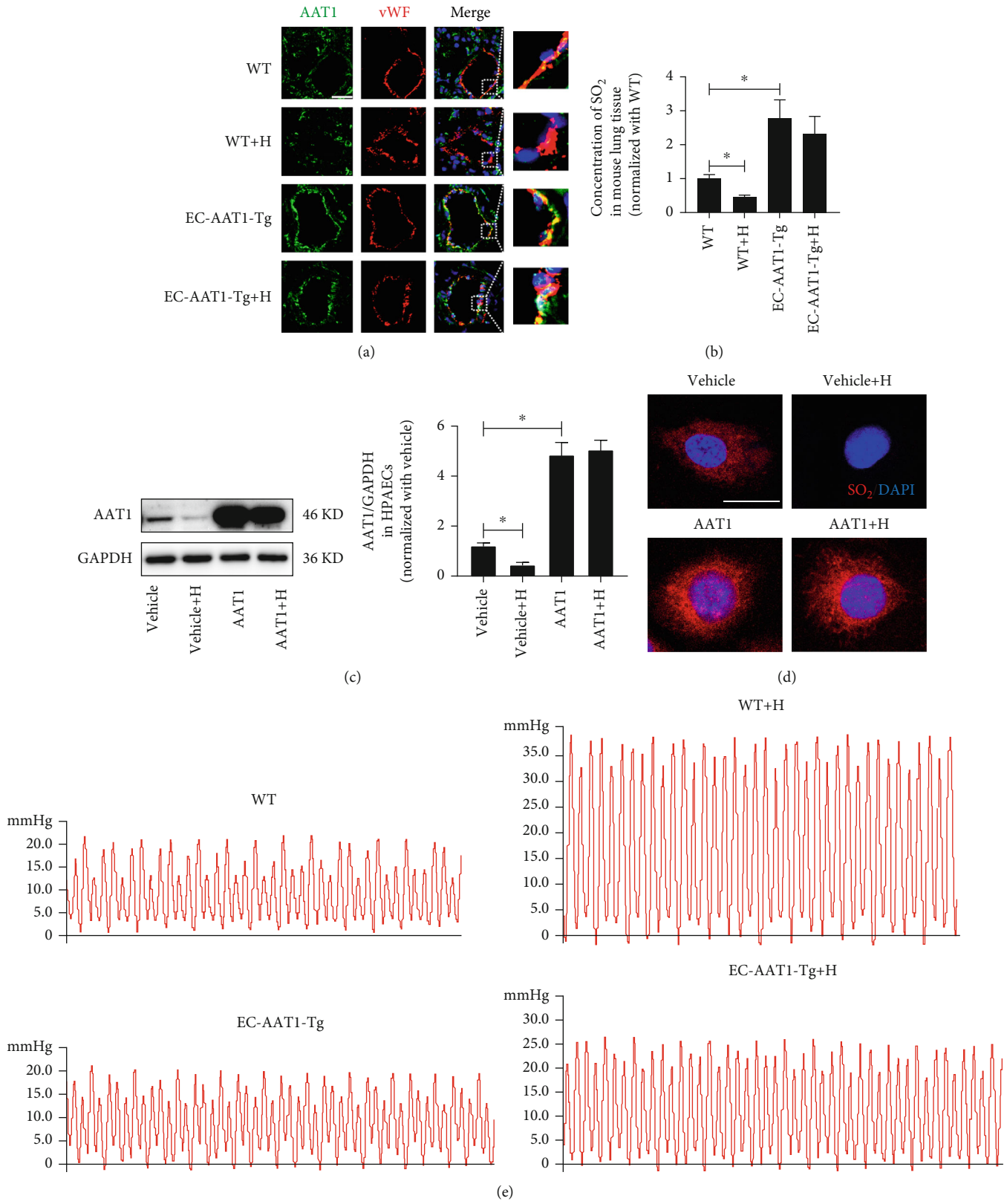


FIGURE 1: Continued.

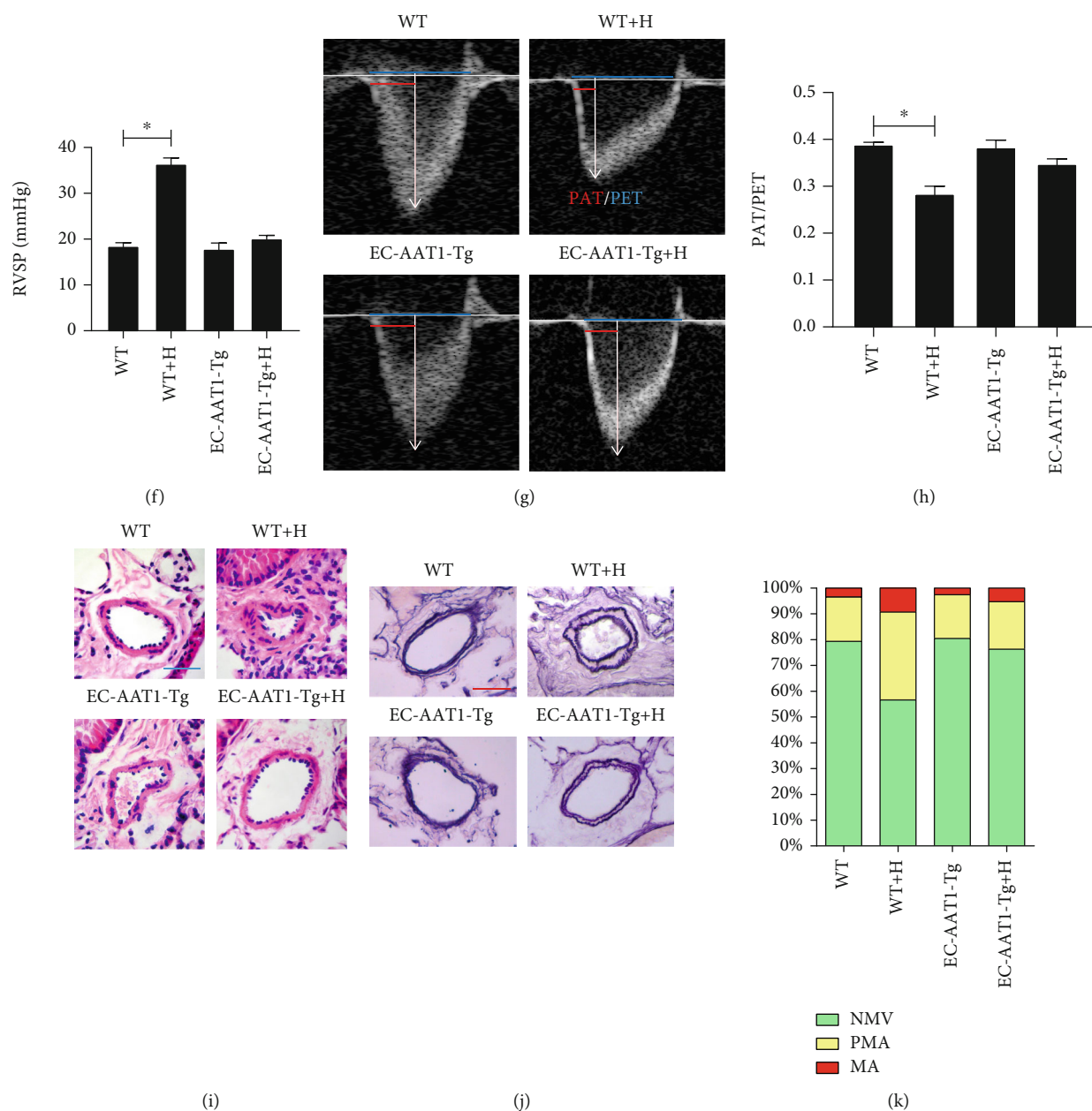


FIGURE 1: Increased EC-derived SO₂ ameliorates hypoxia-induced PH. (a) Immunofluorescence *in situ* detection of AAT1 protein expression in mouse PAECs. Green fluorescence represents AAT1 protein, and red fluorescence represents vWF, a marker for ECs; the nuclei were stained with DAPI. (b) HPLC method was performed to detect SO₂ content in mouse lung tissue ($n = 5 - 17$). (c) Western blot analysis was carried out to detect the expression level of AAT1 protein in HPAECs ($n = 10$). (d) Red SO₂ fluorescent probe method was used to determine the SO₂ level in HPAECs, and the nuclei of HPAECs were stained with DAPI. (e, f) Catheter method was performed to detect mouse right ventricular systolic pressure (RVSP) ($n = 6 - 8$). (g, h) The ratio of pulmonary acceleration time (PAT) to pulmonary ejection time (PET) of the mouse pulmonary artery blood flow was measured using ultrasound ($n = 8$). (i, j) HE and Hart's methods were used to detect PVR in mice. (k) Hart's method was conducted to analyze the degree of muscularization of small pulmonary vessels in mice ($n = 8$); NMV: nonmuscular vessels; PMA: partial muscular arteries; MA: muscular arteries. The data were expressed as mean \pm SEM, $*p < 0.05$, scale bar: 20 μ m.

to reduce the expression of the key enzyme AAT1 for SO₂ production. By Western blot analysis and the SO₂ fluorescent probe method, we confirmed that the AAT1 protein level and SO₂ probe staining significantly decreased in AAT1-knockdown (AAT1 shRNA) HPAECs. However, treatment with SO₂ donor restored SO₂ level in HPAECs (Figures 3(a) and 3(b)) ($p < 0.05$).

Compared with the scramble control group, we further verified that the protein expression of ICAM-1 and MCP-1 and the number of monocyte adhesion to HPAECs in the AAT1 shRNA group all evidently increased. However, supplementation with SO₂ donor successfully inhibited these increases in AAT1 shRNA HPAECs (Figures 3(c)–3(e)) ($p < 0.05$). In addition, HPASMCs cocultured with HPAECs

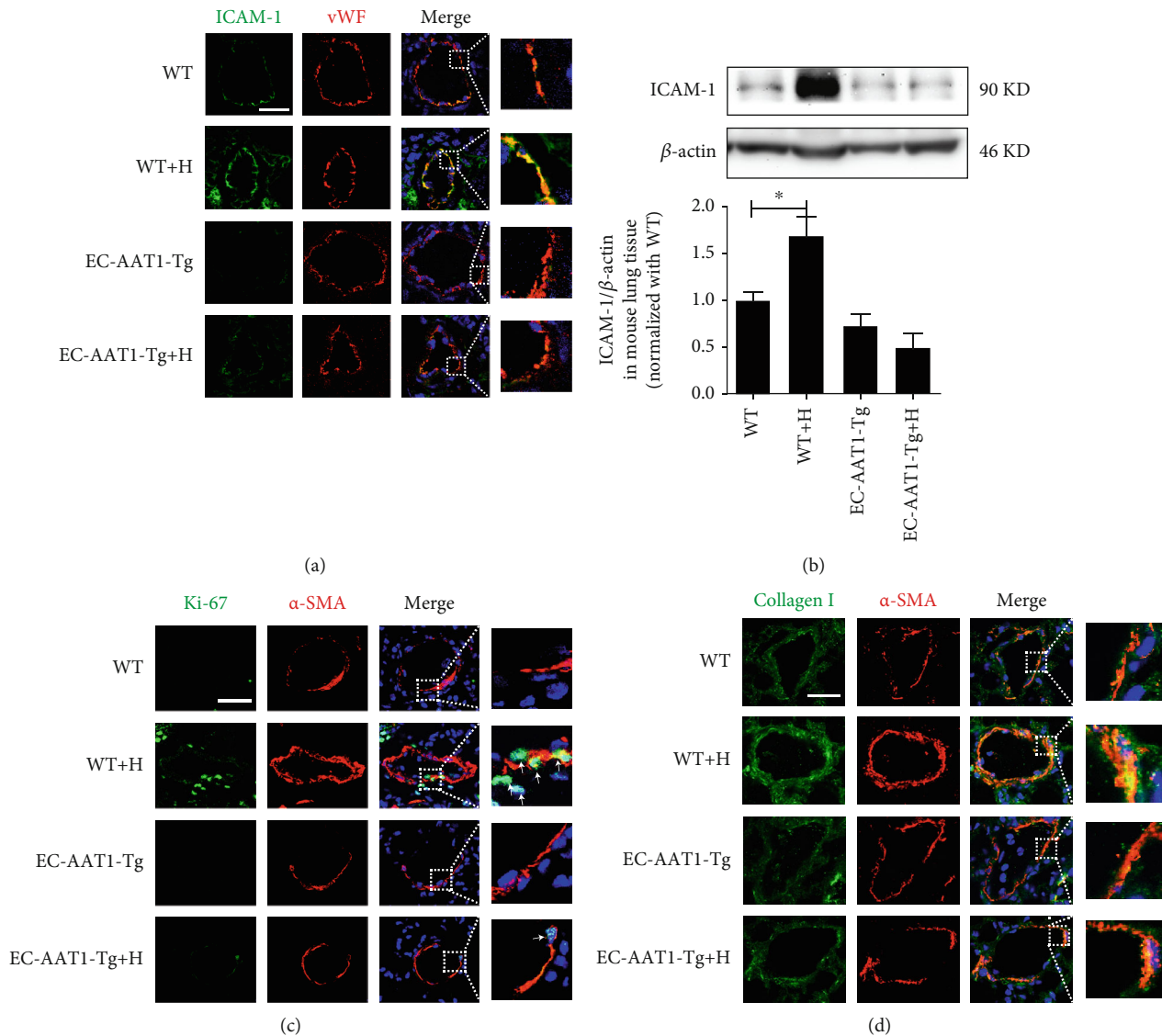


FIGURE 2: Increased EC-derived SO_2 ameliorates hypoxia-induced PAEC inflammation, PASM proliferation, hypertrophy, and collagen production *in vivo*. (a) Immunofluorescence *in situ* detection of ICAM-1 protein expression in mouse PAECs; green fluorescence represents ICAM-1 protein. (b) Western blot analysis was performed to detect the expression level of ICAM-1 protein in mouse lung tissue ($n = 10$). (c, d) Immunofluorescence *in situ* detection of Ki-67, α -SMA, and collagen I protein expression in mouse PSMCs; green fluorescence represents Ki-67 and collagen I protein, and red fluorescence represents α -SMA. The data were expressed as mean \pm SEM, * p < 0.05, scale bar: 20 μ m.

of the AAT1 shRNA group showed increased expression of Ki-67, collagen I, and α -SMA, which were also suppressed by supplementation with SO_2 donor in HPAECs (Figures 3(f) and 3(g), Figure S3a and S3b) ($p < 0.05$). The above studies directly suggested that SO_2 derived from ECs regulated the function of HPAECs and HPASMCs. Moreover, the deficiency of EC-derived SO_2 activated the inflammatory reaction of HPAECs in an autocrine manner, and the proliferation, collagen biosynthesis, and hypertrophy of HPASMCs in a paracrine manner.

3.5. EC-Derived SO_2 Inhibited p50 Activation to Repress PAEC Inflammation, and PASM Proliferation, and

Collagen Deposition. Considering that NF- κ B (particularly p50 heterodimers) plays a critical role in cell inflammation, proliferation, and collagen metabolism, we further observed p50 activation in HPAECs and HPASMCs to reveal the mechanism by which EC-derived SO_2 played a protective effect. The nuclear translocation of p50 was significantly enhanced in HPAECs of the AAT1 shRNA group compared with the scramble group, but this effect was reversed by the treatment with SO_2 donor (Figure 4(a)).

Furthermore, in the hypoxia-induced HPAEC inflammatory response, the phosphorylation, nuclear translocation, and activity of p50 evidently increased in HPAECs of the hypoxic vehicle (vehicle+H) group compared with the

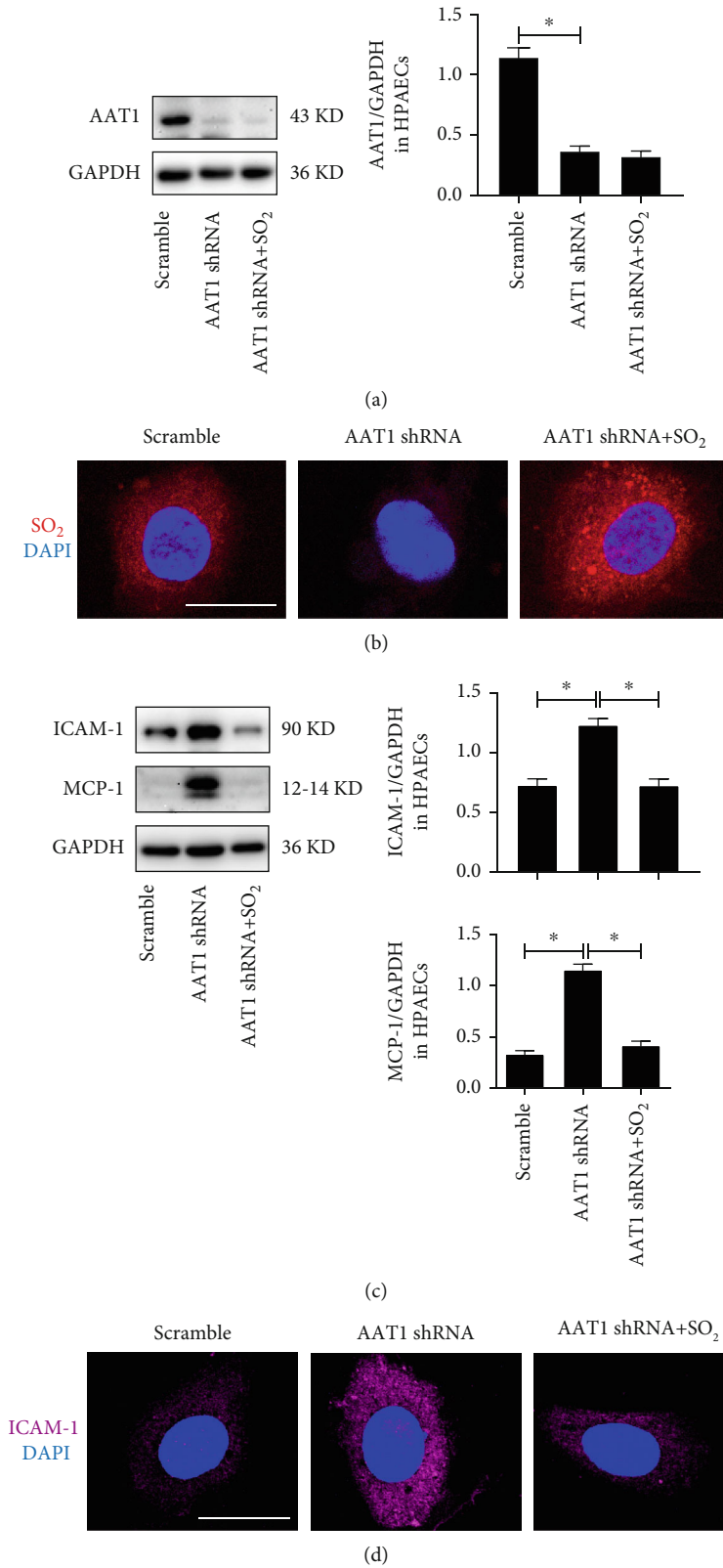


FIGURE 3: Continued.

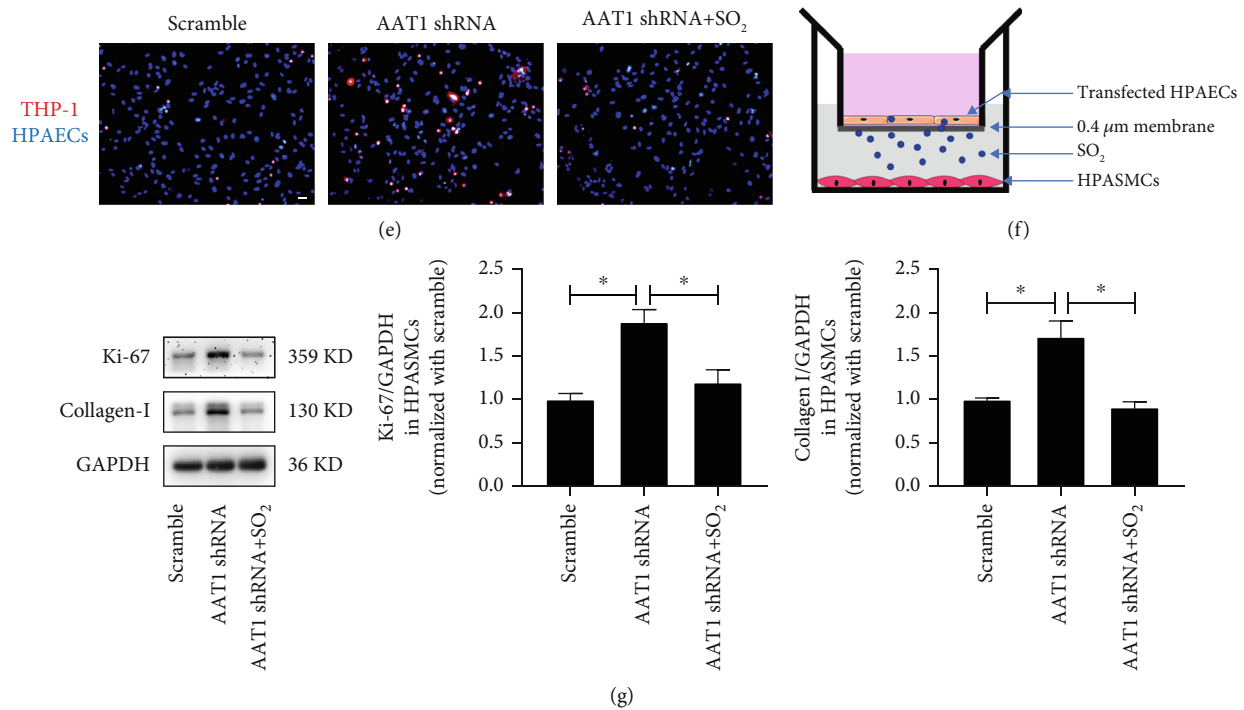


FIGURE 3: EC-derived SO₂ deficiency activates HPAEC inflammation, HPASMC proliferation, and collagen synthesis *in vitro*. (a) Western blot analysis was performed to detect the expression level of AAT1 protein in HPAECs ($n = 12$). (b) The red SO₂ fluorescent probe method was used to detect the SO₂ level in HPAECs; the nuclei were stained with DAPI. (c) Western blot analysis was used to detect the expression level of ICAM-1 and MCP-1 protein in HPAECs ($n = 12$). (d) Immunofluorescence method was used to detect the expression level of ICAM-1 protein in HPAECs *in situ*. Purple fluorescence represents ICAM-1 protein. (e) Fluorescence method was conducted to detect the adhesion of THP-1 cells and HPAECs. The red Dil color marks the THP-1 cells, and the DAPI color marks the nuclei of HPAECs. (f) Diagram of the transwell used for the coculture system *in vitro*. (g) Western blot analysis method to detect the expression level of Ki-67 and collagen I protein in HPASMCs cocultured with HPAECs ($n = 10$). The data were expressed as mean \pm SEM, * $p < 0.05$, scale bar: 20 μ m.

normoxic vehicle group. However, no significant differences were found in AAT1-overexpressed HPAECs between the normoxic and hypoxic treatment groups (Figure S4a-S4c) ($p < 0.05$). Moreover, the *in vivo* EC-AAT1-Tg abolished hypoxia-induced p50 activation (Figure S4d).

Meanwhile, we found that with inhibition of endogenous SO₂ generation in HPAECs, nuclear translocation of p50 in HPASMCs cocultured with HPAECs was activated significantly, which was repressed by the treatment with SO₂ donor as well (Figure 4(b)). These results suggested that p50 may be the molecular target of SO₂.

To investigate whether the inflammatory reaction of HPAECs and the proliferation and collagen accumulation of HPASMCs were mediated by p50, intervention with Andro, an inhibitor of p50, demonstrated that Andro successfully prevented nuclear translocation of p50 induced by the decrease in EC-derived SO₂ in HPAECs and HPASMCs (Figures 4(a) and 4(b)). Meanwhile, the enhanced expression levels of ICAM-1 and MCP-1 in HPAECs of the AAT1shRNA group were significantly inhibited by Andro treatment (Figure 4(c)) ($p < 0.05$). In agreement with the results of HPAECs, the increased expression of Ki-67 and collagen I in HPASMCs cocultured with HPAECs of the AAT1shRNA group was also inhibited

by Andro (Figures 4(d) and 4(e)). The above results indicated that Andro completely blocked the augmentation of HPAEC inflammation, HPASMC proliferation, and collagen production caused by the decrease in EC-derived SO₂ and p50 was a key molecular target for the control of PAEC inflammation, PASM proliferation, and collagen remodeling by SO₂.

4. Discussion

We demonstrated that EC-derived SO₂ was an important endogenous controller of hypoxic PVR. It inhibited PAEC inflammatory process in an autocrine manner and PASM proliferation, hypertrophy, and collagen accumulation in a paracrine manner. NF- κ B p50 signalling might mediate the above effect of EC-derived SO₂.

PVR is the main pathological feature of aging-related COPD and OSAS [6, 7]. The key roles of PAEC inflammation, and PASM proliferation, hypertrophy, and collagen deposition in the pathogenesis of PVR have been suggested by previous studies [8, 9, 11, 25, 36]. However, the mechanisms underlying the endogenous control of PVR have not been identified. Evidence supports that ECs play an important role in the pathogenesis of PVR [18, 19]. However,

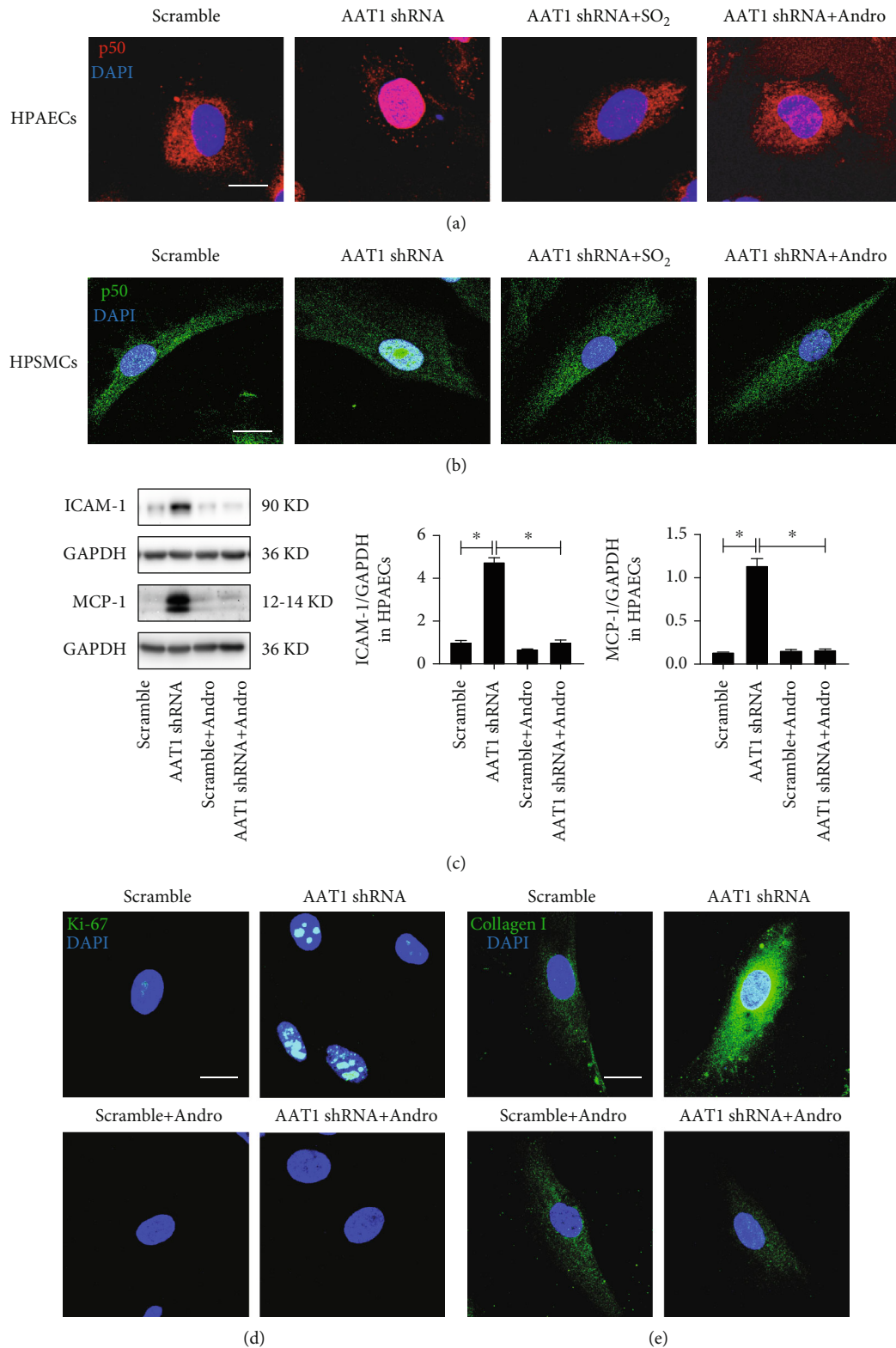


FIGURE 4: EC-derived SO₂ inhibits p50 activation to repress PAEC inflammation, PASMC proliferation, and collagen deposition. (a) Immunofluorescence *in situ* detection of p50 protein distribution in HPAECs. Red fluorescence represents p50 protein, and DAPI staining labels HPAEC nuclei. (b) Immunofluorescence *in situ* detection of p50 protein distribution in HPASMCs cocultured with HPAECs. Green fluorescence represents p50 protein, and DAPI staining labels HPASMC nuclei. (c) Western blot analysis was used to detect the expression level of ICAM-1 and MCP-1 protein in HPAECs ($n = 12$). (d, e) Immunofluorescence *in situ* detection of Ki-67 and collagen I protein expression in HPASMCs cocultured with HPAECs. Green fluorescence represents Ki-67 and collagen I protein. Andro: andrographolide, an inhibitor of p50. Data were expressed as mean \pm SEM, * $p < 0.05$, scale: 20 μ m.

how PAEC inflammation is regulated and whether PASMCM proliferation, hypertrophy, and collagen synthesis are controlled through PAEC-PASMC communication in PVR are not completely clear.

Recently, the gasotransmitter SO_2 with a range of properties, including sustained production, rapid diffusion, and broad functions has been shown to be produced endogenously in HPAECs [21, 22]. Previously, our laboratory and others showed the critical roles of SO_2 donor in controlling cellular collagen metabolism, inflammation, proliferation, and hypertrophy in the pathogenesis of cardiovascular diseases [23–26]. In the present study, we found that the decrease in endogenous SO_2 in hypoxic PH mice with significant PVR and HPAECs, and hypoxic exposure caused the downregulated expression of AAT1 protein in mouse PAECs and HPAECs. This finding indicated that the endogenous SO_2 /AAT1 pathway in ECs was probably associated with hypoxic PH and PVR.

To investigate the regulatory effects of EC-derived SO_2 on the development of hypoxic PH and PVR, and the mechanisms, EC-AAT1-Tg mice with forced expression of AAT1 in ECs were used in the *in vivo* experiment, and AAT1 cDNA was transfected with a lentivirus vector to hold the AAT1 expression in *in vitro* experiment. Unlike WT mice, EC-AAT1-Tg mice did not respond to hypoxic stimulation, demonstrated by the results that hypoxic exposure induced an increase in RVSP and PVR in WT mice, but normoxic EC-AAT1-Tg mice exhibited similar RVSP and vascular structure to EC-AAT1-Tg mice exposed to hypoxia. Furthermore, hypoxia-induced the expression of inflammatory factor ICAM-1 and MCP-1 in the PAECs and macrophage infiltration in the pulmonary arteries were alleviated in EC-AAT1-Tg mice. In accordance with the results *in vivo*, AAT1 overexpression blocked the hypoxia-stimulated expression of ICAM-1 and MCP-1 in HPAECs and monocyte adhesion to HPAECs. It is known that PVR is mainly produced by a thickening of the lamina media due to an increase in PASMCM proliferation, hypertrophy, and collagen deposition [8, 11, 25, 36]. Especially, cell hypertrophy is a well-known cell senescence hallmark [2, 37]. Therefore, we observed the effect of EC-derived SO_2 on the PASMCM behaviors *in vivo*. The data showed that hypoxia stimulated the increased expression of proliferative marker Ki-67, hypertrophy marker α -SMA, and classical collagen I in PASMCMs in WT mice, but not in EC-AAT1-Tg mice. The abovementioned results suggested an important role of EC-derived SO_2 in the regulation of hypoxic PVR.

Conversely, to directly investigate the effect of EC-derived SO_2 on the HPAEC inflammation, and HPASMCM proliferation, hypertrophy, and collagen deposition, HPAECs were transfected with human AAT1 shRNA lentivirus to decrease the level of EC-derived SO_2 , and SO_2 donor was used for rescuing the effect of AAT1 knockdown. As we expected, the deficiency of endogenous SO_2 in HPAECs caused spontaneous overexpression of ICAM-1 and MCP-1 in ECs and monocyte adhesion to HPAECs. Recently, the insufficiency of endogenous SO_2 in adipocytes and macrophages has been found to induce spontaneous inflammatory responses, strengthening the protective role of endogenous SO_2 in the

cardiovascular system [38, 39]. Interestingly, HPASMCMs cocultured with AAT1 shRNA HPAECs presented a PH phenotype characterized by increased Ki-67 and α -SMA expression, and accumulation of collagen I in association with the decreased SO_2 content in HPAECs. These results further supported that EC-derived SO_2 was an important endogenous controller of PVR. EC-derived SO_2 inhibited the PAEC inflammatory process in an autocrine manner, and the coculture of HPAECs and HPASMCMs further verified that EC-derived SO_2 inhibited PASMCM proliferation, hypertrophy, and collagen accumulation in a paracrine manner.

To demonstrate the mechanism by which EC-derived SO_2 controls PAEC inflammation, PASMCM proliferation, and collagen accumulation, the treatment with gene knockdown and SO_2 donor in HPAECs showed that the deficiency of EC-derived SO_2 promoted nuclear translocation of p50 in HPAECs and HPASMCMs with significantly augmented PAEC inflammation, PASMCM proliferation, and collagen remodelling. By contrast, the increase in EC-derived SO_2 by AAT1 overexpression obviously inhibited hypoxia-induced activation of p50 in PAECs, thereby attenuating hypoxic PAEC inflammation, PASMCM proliferation, and collagen remodelling *in vitro* and *in vivo*. More interestingly, the treatment with Andro, a p50 inhibitor, markedly blocked nuclear translocation of p50, and the subsequent PAEC inflammation, PASMCM proliferation, and collagen accumulation induced by the decrease in EC-derived SO_2 in HPAECs and HPASMCMs. Therefore, these findings clarified that EC-derived SO_2 inhibited p50 activation to control the inflammation of PAECs, and PASMCM proliferation, and collagen accumulation.

The mechanism by which SO_2 inhibits p50 activation has not yet been elucidated. The DNA-binding activity of p50 is regulated by the redox reaction, and NO nitrosylates the cysteine sulfhydryl groups of p50 and significantly inhibits its DNA-binding activity [40, 41]. Intriguingly, SO_2 is also implicated in oxidative and reductive modification of proteins, such as AAT1 and p65, to modulate protein function in association with the cysteine sulfhydryl groups [42, 43]. In addition, previous studies also indicated that TGF- β /Smad, Raf-1/MEK-1/Erk/MAPK, AE2, and Dkk1/Wnt signalling pathways were implicated in the regulation of SO_2 on PASMCM proliferation, hypertrophy, and collagen deposition [35, 44–49]. In the future, further investigating the mechanism by which SO_2 regulates p50 and revealing the potential clinical value of application of SO_2 gas for the treatment of hypoxic PH are necessary.

5. Conclusions

The obtained data elucidated that endogenous SO_2 in ECs exerted autocrine and paracrine effects to control PAEC inflammation, and PASMCM proliferation, hypertrophy and collagen remodelling to inhibit PVR induced by hypoxia. The findings revealed a novel PAEC-PASMC communication mechanism in the endogenous control of hypoxic PVR by EC-derived SO_2 . Moreover, this study identified a potential target for the treatment of hypoxic PVR in aging-related cardiopulmonary diseases.

Data Availability

All data needed to evaluate the conclusions in the paper are present in the paper and/or Supplementary Materials. Additional data related to this paper may be requested from the authors.

Conflicts of Interest

The authors declare that there is no conflict of interest regarding the publication of this paper.

Acknowledgments

We thank Dr Pan Huang, Wen Yu, Zhizhou Shen, Mengxiang Sun, Qiang Shen, and Yao Song for their expert technical advice and Editage (<http://www.editage.cn>) for English language editing. This work was supported by the National Natural Science Foundation of China [grant numbers 91439110, 81770422, 82070445].

Supplementary Materials

Supplementary 1. Figure S1: Detection of mouse genotype. The mice numbers are 1-9. Numbers 1, 3, and 7 represent wild-type (WT) mice. Numbers 2, 4-6, and 8-9 represent endothelial cell-specific AAT1 transgenic (EC-AAT1-Tg) mice.

Supplementary 2. Figure S2: Increased EC-derived SO₂ ameliorates hypoxia-induced PAEC inflammation *in vivo* and *in vitro*. (a) Immunofluorescence *in situ* detection of MCP-1 protein expression in mouse PAECs. Red fluorescence represents MCP-1 protein and green fluorescence represents endothelial cell marker CD31. (b) *In situ* detection of macrophage infiltration around the mouse pulmonary arteries by immunofluorescence. Green fluorescence represents mouse macrophage marker F4/80, and red fluorescence represents vascular smooth muscle marker α -SMA. (c, d) Western blot analysis ($n = 9$) and immunofluorescence methods were used to detect the expression level of ICAM-1 protein in HPAECs. Yellow fluorescence represents ICAM-1. (e) Western blot analysis was used to detect the expression level of MCP-1 protein in HPAECs ($n = 9$). (f) Fluorescence method was performed to detect the adhesion of THP-1 cells and HPAECs. Red Dil staining marks THP-1 cells and DAPI color marks the nuclei of HPAECs. The data were expressed as mean \pm SEM, $*p < 0.05$, scale: 20 μ m.

Supplementary 3. Figure S3: EC-derived SO₂ deficiency stimulated HPASMChypertrophy *in vitro*. (a) The expression level of α -SMA protein, a marker of smooth muscle cell hypertrophy, in HPASMCs cocultured with HPAECs was detected by Western blot method ($n = 9$). (b) The expression level of α -SMA protein in HPASMCs cocultured with HPAECs *in situ* was observed by immunofluorescence method. The red fluorescence represents α -SMA protein and blue DAPI color marks the nuclei of HPASMCs. The data were expressed as mean \pm SEM, $*p < 0.05$, scale bar: 20 μ m.

Supplementary 4. Figure S4: AAT1 overexpression inhibits hypoxia-induced activation of p50 in PAECs. (a) Western

blot analysis was used to detect the phosphorylation level of p50 protein in HPAECs ($n = 9$). (b) The distribution of p50 protein in HPAECs was detected by immunofluorescence *in situ*. Green fluorescence represents p50 protein. (c) Active motif-ELISA was performed to detect the DNA-binding activity of p50 in HPAECs ($n = 9$). (d) Immunofluorescence was used to *in situ* detect p-p50 protein expression in mouse PAECs, green fluorescence represents p-p50 protein. The data were expressed as mean \pm SEM, $*p < 0.05$, scale: 20 μ m.

References

- [1] T. M. De Silva, M. L. Modrick, F. Dabertrand, and F. M. Faraci, "Changes in cerebral arteries and parenchymal arterioles with aging: role of rho kinase 2 and impact of genetic background," *Hypertension*, vol. 71, no. 5, pp. 921–927, 2018.
- [2] B. J. North and D. A. Sinclair, "The intersection between aging and cardiovascular disease," *Circulation Research*, vol. 110, no. 8, pp. 1097–1108, 2012.
- [3] S. Laurent, "Defining vascular aging and cardiovascular risk," *Journal of Hypertension*, vol. 30, Suppl, pp. S3–S8, 2012.
- [4] L. Fang, P. Gao, H. Bao et al., "Chronic obstructive pulmonary disease in China: a nationwide prevalence study," *The Lancet Respiratory Medicine*, vol. 6, no. 6, pp. 421–430, 2018.
- [5] L. S. Gaspar, A. R. Álvaro, J. Moita, and C. Cavadas, "Obstructive sleep apnea and hallmarks of aging," *Trends in Molecular Medicine*, vol. 23, no. 8, pp. 675–692, 2017.
- [6] D. Sajkov and R. D. McEvoy, "Obstructive sleep apnea and pulmonary hypertension," *Progress in Cardiovascular Diseases*, vol. 51, no. 5, pp. 363–370, 2009.
- [7] S. Sakao, N. F. Voelkel, and K. Tatsumi, "The vascular bed in COPD: pulmonary hypertension and pulmonary vascular alterations," *European Respiratory Review*, vol. 23, no. 133, pp. 350–355, 2014.
- [8] T. Thenappan, M. L. Ormiston, J. J. Ryan, and S. L. Archer, "Pulmonary arterial hypertension: pathogenesis and clinical management," *BMJ*, vol. 360, article j5492, 2018.
- [9] L. C. Price, S. J. Wort, F. Perros et al., "Inflammation in pulmonary arterial hypertension," *Chest*, vol. 141, no. 1, pp. 210–221, 2012.
- [10] Y. Ban, Y. Liu, Y. Li et al., "S-nitrosation impairs KLF4 activity and instigates endothelial dysfunction in pulmonary arterial hypertension," *Redox Biology*, vol. 21, article 101099, 2019.
- [11] E. Falcetti, S. M. Hall, P. G. Phillips et al., "Smooth muscle proliferation and role of the prostacyclin (IP) receptor in idiopathic pulmonary arterial hypertension," *American Journal of Respiratory and Critical Care Medicine*, vol. 182, no. 9, pp. 1161–1170, 2010.
- [12] L. Deng, F. J. Blanco, H. Stevens et al., "MicroRNA-143 activation regulates smooth muscle and endothelial cell crosstalk in pulmonary arterial hypertension," *Circulation Research*, vol. 117, no. 10, pp. 870–883, 2015.
- [13] D. Zhang, X. L. Wang, S. Y. Chen et al., "Endogenous hydrogen sulfide sulfhydrates IKK β at cysteine 179 to control pulmonary artery endothelial cell inflammation," *Clinical Science (London, England)*, vol. 133, no. 20, pp. 2045–2059, 2019.
- [14] S. S. Feng, S. Y. Chen, W. Yu et al., "H₂S inhibits pulmonary arterial endothelial cell inflammation in rats with monocrotaline-induced pulmonary hypertension," *Laboratory Investigation*, vol. 97, no. 3, pp. 268–278, 2017.

- [15] A. Berenyiova, I. Dovinova, M. Kvandova et al., "The effect of chronic NO synthase inhibition on the vasoactive and structural properties of thoracic aorta, NO synthase activity, and oxidative stress biomarkers in young SHR," *Oxidative Medicine and Cellular Longevity*, vol. 2018, Article ID 2502843, 10 pages, 2018.
- [16] I. Blaha, M. E. López-Oliva, M. P. Martínez et al., "Bladder dysfunction in an obese Zucker rat: the role of TRPA1 channels, oxidative stress, and hydrogen sulfide," *Oxidative Medicine and Cellular Longevity*, vol. 2019, Article ID 5641645, 12 pages, 2019.
- [17] B. W. Wong, E. Marsch, L. Treps, M. Baes, and P. Carmeliet, "Endothelial cell metabolism in health and disease: impact of hypoxia," *The EMBO Journal*, vol. 36, no. 15, pp. 2187–2203, 2017.
- [18] H. J. Sun, Z. Y. Wu, X. W. Nie, and J. S. Bian, "Role of endothelial dysfunction in cardiovascular diseases: the link between inflammation and hydrogen sulfide," *Frontiers in Pharmacology*, vol. 10, p. 1568, 2020.
- [19] C. Xue, M. Sowden, and B. C. Berk, "Extracellular cyclophilin A, especially acetylated, causes pulmonary hypertension by stimulating endothelial apoptosis, redox stress, and inflammation," *Arteriosclerosis, Thrombosis, and Vascular Biology*, vol. 37, no. 6, pp. 1138–1146, 2017.
- [20] S. Piera-Velazquez, F. A. Mendoza, and S. A. Jimenez, "Endothelial to mesenchymal transition (EndoMT) in the pathogenesis of human fibrotic diseases," *Journal of Clinical Medicine*, vol. 5, no. 4, p. 45, 2016.
- [21] S. X. du, H. F. JIN, D. F. BU et al., "Endogenously generated sulfur dioxide and its vasorelaxant effect in rats," *Acta Pharmacologica Sinica*, vol. 29, no. 8, pp. 923–930, 2008.
- [22] X. Liu, D. Zhang, K. Li et al., "Effect of endogenous sulfur dioxide on the apoptosis induced by cobalt chloride in the human pulmonary arterial endothelial cells," *Journal of Applied Clinical Pediatrics*, vol. 13, pp. 999–1003, 2018.
- [23] W. Li, C. S. Tang, H. F. Jin, and J. B. Du, "Regulatory effects of sulfur dioxide on the development of atherosclerotic lesions and vascular hydrogen sulfide in atherosclerotic rats," *Atherosclerosis*, vol. 215, no. 2, pp. 323–330, 2011.
- [24] L. Yang, H. Zhang, and P. Chen, "Sulfur dioxide attenuates sepsis-induced cardiac dysfunction via inhibition of NLRP3 inflammasome activation in rats," *Nitric Oxide*, vol. 81, pp. 11–20, 2018.
- [25] W. Yu, D. Liu, C. Liang et al., "Sulfur dioxide protects against collagen accumulation in pulmonary artery in association with downregulation of the transforming growth factor β 1/smad pathway in pulmonary hypertensive rats," *Journal of the American Heart Association*, vol. 5, no. 10, article e003910, 2016.
- [26] Q. H. Chen, L. L. Zhang, S. Y. Chen et al., "Downregulated endogenous sulfur dioxide/aspartate aminotransferase pathway is involved in angiotensin II-stimulated cardiomyocyte autophagy and myocardial hypertrophy in mice," *International Journal of Cardiology*, vol. 225, pp. 392–401, 2016.
- [27] I. S. Afonina, Z. Zhong, M. Karin, and R. Beyaert, "Limiting inflammation—the negative regulation of NF- κ B and the NLRP3 inflammasome," *Nature Immunology*, vol. 18, no. 8, pp. 861–869, 2017.
- [28] W. Wu, W. Zhang, M. Choi et al., "Vascular smooth muscle-MAPK14 is required for neointimal hyperplasia by suppressing VSMC differentiation and inducing proliferation and inflammation," *Redox Biology*, vol. 22, article 101137, 2019.
- [29] N. D. Perkins, "Integrating cell-signalling pathways with NF- κ B and IKK function," *Nature Reviews. Molecular Cell Biology*, vol. 8, no. 1, pp. 49–62, 2007.
- [30] Y. F. Xia, B. Q. Ye, Y. D. Li et al., "Andrographolide attenuates inflammation by inhibition of NF- κ B activation through covalent modification of reduced cysteine 62 of p50," *Journal of Immunology*, vol. 173, no. 6, pp. 4207–4217, 2004.
- [31] J. Lai, M. Ge, S. Shen et al., "Activation of NF κ B-JMJD3 signaling promotes bladder fibrosis via boosting bladder smooth muscle cell proliferation and collagen accumulation," *Biochimica et Biophysica Acta - Molecular Basis of Disease*, vol. 1865, no. 9, pp. 2403–2410, 2019.
- [32] L. Zhang, Y. Wang, G. Wu et al., "Blockade of JAK2 protects mice against hypoxia-induced pulmonary arterial hypertension by repressing pulmonary arterial smooth muscle cell proliferation," *Cell Proliferation*, vol. 53, no. 2, article e12742, 2020.
- [33] L. L. Zhang, H. F. Jin, Y. J. Song et al., "Endogenous sulfur dioxide is a novel inhibitor of hypoxia-induced mast cell degranulation," *Journal of Advanced Research*, vol. 29, pp. 55–65, 2020.
- [34] H. B. Thibault, B. Kurtz, M. J. Raheer et al., "Noninvasive assessment of murine pulmonary arterial pressure: validation and application to models of pulmonary hypertension," *Circulation. Cardiovascular Imaging*, vol. 3, no. 2, pp. 157–163, 2010.
- [35] Y. Sun, Y. Tian, M. Prabha et al., "Effects of sulfur dioxide on hypoxic pulmonary vascular structural remodeling," *Laboratory Investigation*, vol. 90, no. 1, pp. 68–82, 2010.
- [36] D. Zabini, E. Granton, Y. Hu et al., "Loss of SMAD₃ promotes vascular remodeling in pulmonary arterial hypertension via MRTF disinhibition," *American Journal of Respiratory and Critical Care Medicine*, vol. 197, no. 2, pp. 244–260, 2018.
- [37] Á. Valdés, A. V. Treuer, G. Barrios et al., "NOX inhibition improves β -adrenergic stimulated contractility and intracellular calcium handling in the aged rat heart," *International Journal of Molecular Sciences*, vol. 19, no. 8, article 2404, 2018.
- [38] H. Zhang, Y. Huang, D. Bu et al., "Endogenous sulfur dioxide is a novel adipocyte-derived inflammatory inhibitor," *Scientific Reports*, vol. 6, no. 1, article 27026, 2016.
- [39] Z. Zhu, L. Zhang, Q. Chen et al., "Macrophage-derived sulfur dioxide is a novel inflammation regulator," *Biochemical and Biophysical Research Communications*, vol. 524, no. 4, pp. 916–922, 2020.
- [40] T. Taetzsch, S. Levesque, C. McGraw et al., "Redox regulation of NF- κ B p50 and M1 polarization in microglia," *Glia*, vol. 63, no. 3, pp. 423–440, 2015.
- [41] J. R. Matthews, C. H. Botting, M. Panico, H. R. Morris, and R. T. Hay, "Inhibition of NF- κ B DNA binding by nitric oxide," *Nucleic Acids Research*, vol. 24, no. 12, pp. 2236–2242, 1996.
- [42] Y. Song, H. Peng, D. Bu et al., "Negative auto-regulation of sulfur dioxide generation in vascular endothelial cells: AAT1 S-sulfenylation," *Biochemical and Biophysical Research Communications*, vol. 525, no. 1, pp. 231–237, 2020.
- [43] S. Chen, Y. Huang, Z. Liu et al., "Sulphur dioxide suppresses inflammatory response by sulphenylating NF- κ B p65 at Cys 38 in a rat model of acute lung injury," *Clinical Science (London, England)*, vol. 131, no. 21, pp. 2655–2670, 2017.
- [44] Y. Huang, Z. Shen, Q. Chen et al., "Endogenous sulfur dioxide alleviates collagen remodeling via inhibiting TGF- β /Smad pathway in vascular smooth muscle cells," *Scientific Reports*, vol. 6, no. 1, p. 19503, 2016.

- [45] Y. Wang, X. Wang, S. Chen et al., "Sulfur dioxide activates $\text{Cl}^-/\text{HCO}_3^-$ exchanger via sulphenylating AE2 to reduce intracellular pH in vascular smooth muscle cells," *Frontiers in Pharmacology*, vol. 10, p. 313, 2019.
- [46] H. J. Wu, Y. Q. Huang, Q. H. Chen et al., "Sulfur dioxide inhibits extracellular signal-regulated kinase signaling to attenuate vascular smooth muscle cell proliferation in angiotensin II-induced hypertensive mice," *Chinese Medical Journal*, vol. 129, no. 18, pp. 2226–2232, 2016.
- [47] D. Liu, Y. Huang, D. Bu et al., "Sulfur dioxide inhibits vascular smooth muscle cell proliferation via suppressing the Erk/MAP kinase pathway mediated by cAMP/PKA signaling," *Cell Death & Disease*, vol. 5, no. 5, article e1251, 2014.
- [48] L. Luo, X. Hong, B. Diao, S. Chen, and M. Hei, "Sulfur dioxide attenuates hypoxia-induced pulmonary arteriolar remodeling via Dkk1/Wnt signaling pathway," *Biomedicine & Pharmacotherapy*, vol. 106, pp. 692–698, 2018.
- [49] M. Romero, A. Ortega, A. Izquierdo, P. López-Luna, and R. J. Bosch, "Parathyroid hormone-related protein induces hypertrophy in podocytes via $\text{TGF-}\beta_1$ and p27^{Kip1}: implications for diabetic nephropathy," *Nephrology, Dialysis, Transplantation*, vol. 25, no. 8, pp. 2447–2457, 2010.